Chapter 2
Komatiite-Associated Ni-Cu-(PGE) Deposits

C. Michael Lesher

Mineral Exploration Research Centre, Department of Earth Sciences,
Laurentian University, Sudbury, Ontario P3E2C6 Canada

Stephen J. Barnes

CSIRO Exploration and Mining, 26 Dick Perry Avenue, Kensington 6151 Western Australia

2.1 Introduction

Ni-Cu-(PGE) deposits associated with komatiitic rocks in Archean and Proterozoic volcanic belts (Fig. 2.1) are the most important examples of magmatic mineralization in volcanic rocks. They contain ~20 percent of the world's total identified Ni resources in deposits with ≥0.8 percent Ni and they contain significant amounts of Co and Cu, and minor amounts of PGEs. Sizes of individual mined deposits, measured in terms of contained Ni metal, range from 1×10^4 tons to more than 2.5×10^6 tons (Fig. 2.2) (see review by Barnes, 2006). The largest deposits, such as Thompson, Perseverance and Mt. Keith, rival in size some of the largest nickel deposits of any class in the world.

Komatiites are ultramafic lavas, known from experimental studies to have erupted at very high temperatures. Field relationships indicate that fluid dynamics and physical volcanology strongly influenced ore localization, so komatiite-hosted deposits provide critical information concerning sulfide segregation, metal partitioning, and localization processes in high-temperature volcanic systems.

Komatiite-associated deposits are similar in many respects to magmatic Ni-Cu-(PGE) deposits associated with other rock types. They are normally hosted by the most magnesian units in the sequence, are commonly localized in footwall embayments, commonly occur at or near the bases of the host units, typically grade upwards from massive or semi-massive to disseminated mineralization, and are composed primarily of pyrrhotite, pentlandite, and chalcopyrite with minor pyrite and magnetite and trace platinum group minerals (PGMs). However, they are distinct from other deposit types in being commonly volcanic, in more often exhibiting olivine-sulfide "net" textures, in being derived from magmas that were originally much further from sulfide saturation, and in typically having higher Ni-Co-IPGE[1] contents and lower Cu-PPGE-Au contents.

The geological characteristics of these deposits have been previously reviewed by Groves and Hudson (1981), Marston (1984), Marston *et al.* (1981), Lesher (1989), Lesher and Keays (2002), Lesher and Barnes (2008), Barnes (2006), Naldrett (2004) and Hoatson *et al.* (2006); resource information has been compiled by Hoatson *et al.* (2006), Ross and Travis (1981), Barnes (2006) and Eckstrand and Hulbert (2007); and their exploration geochemistry has been reviewed by Lesher and Stone (1996), Barnes *et al.* (2004) and Barnes (2006). The purpose of this chapter is to amalgamate and update these reviews, to summarize current thinking on geologic, genetic, and exploration models, and to place this class of deposit within the context of other associations within the larger class of magmatic Ni-Cu-(PGE) deposits.

2.1.1 Nomenclature and classification

Nomenclature

Although the Archaean and Proterozoic komatiitic host rocks for these deposits are all metamorphosed to some degree, pseudomorphous and palimpsest textures are locally preserved in almost all deposits, including those that have been strongly deformed and metamorphosed (e.g., Perseverance, Thompson) and are very well preserved in many deposits (e.g., Alexo, Kambalda, Langmuir, Raglan), so igneous nomenclature will be used throughout this chapter.

[1] Platinum-group elements (PGE) are commonly subdivided into platinum-group PGEs (PPGE: Pd, Pt, Rh) and iridium-group PGEs (IPGE: Ru, Ir, Os) based on the different geochemical behaviors of the two groups.

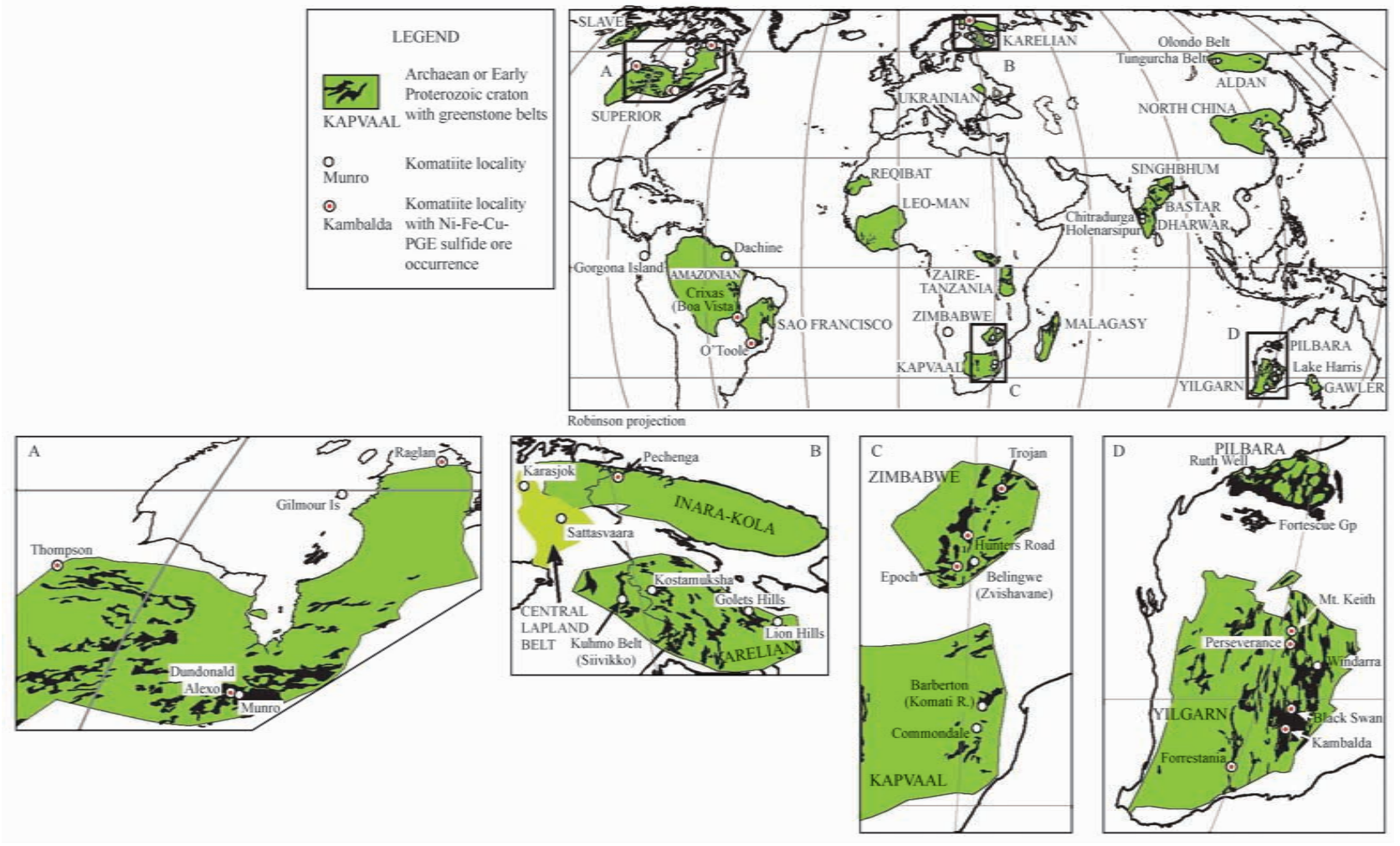

Fig. 2. 1 Locations of major komatiite-associated Ni-Cu-(PGE) deposits (modified from Arndt *et al.* 2008).

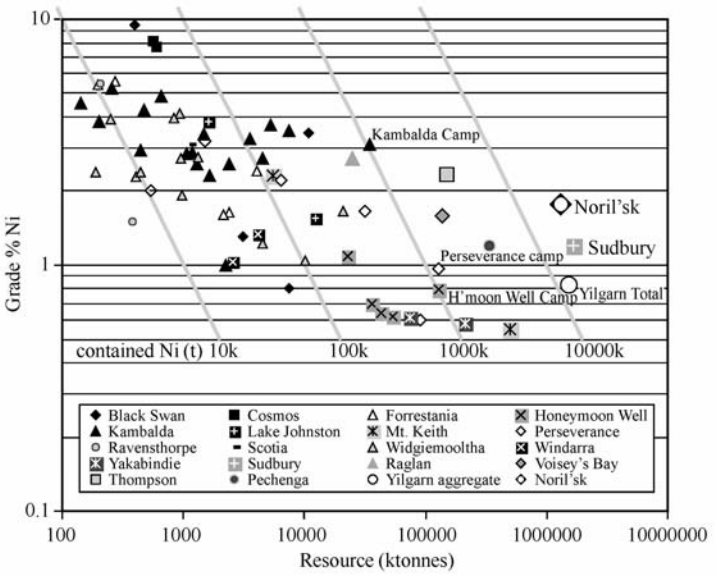

Fig. 2. 2 Grade-tonnage plot, after Barnes (2006).

Komatiite

The IUGS presently defines komatiite as a *volcanic rock with* > 18% *MgO* (*volatile-free*) *and* < 1% TiO_2 (Le Bas, 2000). Kerr and Arndt (2001) and Arndt *et al.* (2008) reviewed the problems with this classification and recommended that komatiite be defined as *a lava with characteristic spinifex-textured olivines, or rocks that can be related directly, using field or petrographic criteria, to lavas with this texture*. The importance of including spinifex (platy skeletal) olivine in the definition is that it excludes olivine porphyritic rocks ("picrites") that form by accumulation of olivine into basaltic liquids. This definition also includes volcanic and subvolcanic rocks related to komatiites, that may not exhibit olivine spinifex textures, intrusive rocks that contain olivine spinifex textures, and spinifex-textured and related rocks previously referred to as "ferropicrites" by Hanski (1992) that formed from very different mantle sources than other komatiites. Thus, komatiites are simply ultramafic volcanic-rocks with a variety of geochemical and petrogenetic subtypes (Al-undepleted, Al-depleted, Al-enriched, Fe-Ti enriched), just as basalts are mafic volcanic rocks with a variety of different geochemical and petrogenetic subtypes (e.g., MORB, OIB, Al-rich, Ti-rich, Fe-rich).

The IUGS currently defines volcanic rocks with 12% – 18% MgO and < 1% TiO_2 as picrites, which would include most but not all komatiitic basalts. We prefer to reserve the term *picrite* for olivine-porphyritic rocks with 10% – 18% MgO and < 1% TiO_2 that do not contain (or are related directly to rocks containing) olivine or pyroxene spinifex textures, and to use the term *komatiitic basalt* for rocks with 10% – 18% MgO that do contain (or are directly related to rocks containing) olivine or pyroxene spinifex textures.

This still leaves us with one of the greatest deficiencies of IUGS terminology, which is that it is genetically-based and defines all coarse-grained mafic-ultramafic rocks (e.g., *gabbro*, *pyroxenite*, *peridotite*, and *dunite*) as plutonic and all fine-grained mafic-ultramafic rocks (e.g., *basalt*, *picrite*, *komatiite*) as volcanic. Because the terms *gabbro*, *pyroxenite*, *wehrlite*, *peridotite*, and *dunite* are so firmly entrenched into the geological literature of these deposits and because we believe that lithological nomenclature should be non-genetic, we will use these terms to refer to cumulate rocks with appropriate mineralogy and textures, but without any implications regarding volcanic or subvolcanic setting. The various lithofacies exhibited by komatiites given in Table 2. 1.

Aphyric komatiites can be subdivided into high-Mg komatiites (34% – 25% MgO), which are saturated in olivine but undersaturated in chromite (Murck and Campbell, 1986), low-Mg komatiites (25% – 18% MgO), which are saturated in olivine and chromite, olivine-phyric komatiitic basalts (15% – 18% MgO), and pyroxene-phyric komatiitic basalts (10% – 15% MgO). The compositions of associated cumulate rocks vary with the MgO content of the liquids and the cumulus minerals that crystallized from them (Table 2. 1).

Mineralization

Deposits of Ni-Cu-(PGE) mineralization in igneous rocks have been referred to as *magmatic Ni-Cu-(PGE) deposits* (referring to metals recovered), *magmatic Fe-Ni-Cu-(PGE) sulfide deposits* (referring to mineralogy and distinguishing them from laterites), or as *magmatic sulfide deposits* (more general). They should not be referred to as *magmatic Ni-Cu-(PGE) sulfide deposits* (Fe is a major component of the sulfides) or *NiS deposits* (millerite is rare to absent).

Magmatic Ni-Cu-(PGE) deposits, including komatiite-associated deposits, can be subdivided into five groups, based on the form of the deposits and the distribution of the

Table 2.1 Komatiite lithofacies (from Lesher, 1989; Lesher, 2007, and Arndt *et al*., 2008).

Lithofacies	Characteristics
Non-cumulate	
Volcaniclastic	Predominantly hydroclastic (e.g., flow-top breccias), occasionally epiclastic, rarely pyroclastic (cg heterolithic or fg tuffaceous) or autoclastic
Aphyric	Glassy to aphanitic, rarely vesicular, with fg quench Ol ± Pyx ± sulfides, < 5% phenocrysts; 10% – 18% MgO in komatiitic basalts, 18% – 25% MgO in low-Mg komatiites, 25% – 34% in high-Mg komatiites
Random Ol spinifex	10% – 25% fg-mg randomly-oriented Ol plates in an aphanitic to glassy matrix with fg "quench" Ol ± Pyx ± sulfides, occasionally vesicular; 12% – 34% MgO
Random Pyx spinifex	10% – 25% fg-mg randomly-oriented Pyx needles in an aphanitic to glassy matrix with fg "quench" Pyx ± sulfides; 10% – 15% MgO
Olivine-phyric	5% – 25% fg-mg skeletal olivine in an aphanitic to glassy matrix with fg-mg Ol ± Pyx ± sulfides, rarely vesicular; 25% – 35% MgO in high-Mg komatiites, 18% – 25% in low-Mg komatiites, 10% – 18% MgO in komatiitic basalts
Pyroxene-phyric	5% – 25% fg-mg polyhedral olivine in an aphanitic to glassy matrix with fg-mg Ol ± Pyx ± sulfides, rarely vesicular; 20% – 25% MgO in high-Mg komatiites, 15% – 20% in low-Mg komatiites, 10% – 15% MgO in komatiitic basalts
Gabbro	fg-cg, equigranular; melanocratic (Cpx-Pl), mesocratic (Pl-Cpx), leucocratic (Pl-Cpx-Qtz), or ferrogabbroic (Pl-Qtz-Cpx-Mag-Ilm)
Crescumulate	
Platy Ol spinifex	cg dendritic networks of platy Ol, interstitial glass with fg quench Ol ± Pyx ± sulfides; 18% – 34% MgO (only in komatiites)
Acicular Pyx spinifex	cg parallel acicular Pyx, interstitial glass with fg quench Ol ± Pyx ± sulfides; 10% – 15% MgO (only in komatiitic basalts)
Ol crescumulate	25% – 75% mg branching Ol ± interstitial Chr in an aphanitic to glassy matrix with fg quench Ol ± Pyx ± sulfides, often vesicular; 20% – 30% in komatiitic basalts, 25% – 35% MgO in low-Mg komatiites, 30% – 40% in high-Mg komatiites
Pyx crescumulate	25% – 75% mg branching Pyx and interstitial Mag-Ilm in a fg gabbroic matrix, typically ferrogabbroic to leuocratic
Cumulate	
Ol-Pyx orthocumulate *komatiitic wehrlite*	10% – 50% fg polyhedral Ol, 10% – 60% vcg oikocrystic Cpx, 10% – 40% interstitial glass; 25% – 30% MgO
Ol orthocumulate *komatiitic peridotite*	50% – 75% fg-mg polyhedral Ol ± interstitial Chr, 25% – 75% interstitial glass with fg quench Ol ± Pyx ± sulfides; 25% – 30% in komatiitic basalts, 30% – 35% MgO in low-Mg komatiites, 35% – 40% in high-Mg komatiites
Ol mesocumulate *komatiitic peridotite*	75% – 90% mg polyhedral Ol ± euhedral-subhedral interstitial Chr, 10% – 25% interstitial glass with fg quench Ol ± Pyx ± sulfides; 30% – 35% in komatiitic basalts, 35% – 40% MgO in low-Mg komatiites, 40% – 45% in high-Mg komatiites
Ol adcumulate *komatiitic dunite*	> 90% cg polyhedral Ol ± euhedral to interstitial Chr, < 10% interstitial glass ± pyroxene ± sulfides; 35% – 40% in komatiitic basalts, 40% – 45% MgO in low-Mg komatiites, 45% – 52% in high-Mg komatiites

Ol = olivine, **Pyx** = pyroxene (normally augite with pigeonite cores), **Pl** = plagioclase, **Chr** = chromite, **Mag-Ilm** = magnetite-ilmentite; **fg** = fine-grained (< 1 mm), **mg** = medium-grained (1 – 2 mm), **cg** = coarse-grained (> 2 mm)

mineralization in the host rocks (Table 2.2). Type I stratiform basal massive to disseminated mineralization occurs in many other associations, but the type examples occur at Kambalda. Type Ib massive magmatic veins are a minor mineralization type associated with Type I komatiite-associated deposits, but is an important ore type in other associations (e.g., Cu-PPGE-rich footwall veins at Sudbury). Type Ⅱ strata-bound internal disseminated to net-textured mineralization is also common in many other associations, but is presently economic only where serpentinization has upgraded Ni tenors[1] (e.g., Mt Keith, Black Swan) or in localities like Jinchuan where it is net-textured. Type Ⅲ (stratiform "reef") is present in almost all highly differentiated units and is almost always subeconomic, but is an important ore type in other associations (e.g., Bushveld, Stillwater). Type Ⅳa Ni-enriched metasediment mineralization occurs in several komatiite-associated deposits where Type I ores are intimately associated with sulfidic metasedimentary rocks, best typified

[1] Ore grade is the abundance of metal in the whole rock/ore sample; ore tenor is the abundance of metal in 100% sulfides.

Table 2.2 Classification of mineralization types in komatiite-associated magmatic Ni-Cu-PGE deposits (modified from Lesher and Keays, 2002).

Origin	Magmatic						Hydrothermal-Metamorphic		Tectonic
Type	I basal/footwall		II strata-bound internal			III reef	IV		V
Subtype	Ia stratiform	Ib footwall vein	IIa coarse disseminated	IIb fine disseminated	IIc very finely disseminated	stratiform	IVa metasediment	IVb vein	offset
Sulfide distribution	at or near the bases of komatiitic peridotite or komatiitic dunite units	veins or stringers in host or wall rocks associated with Type Ia mineralization	"blebby" and "globular" disseminations within komatiitic peridotite or dunite units	interstitial disseminations within komatiitic peridotite or dunite units	"cloudy" disseminations within komatiitic peridotite or dunite units	at or near contact between lower cumulate zones and upper gabbro zones within strongly differentiated units	layers in sulfidic metasediments associated with Type I mineralization	veins in wall rocks associated with Type I mineralization	faults and shear zones within host or wall rocks associated with Type I mineralization
Primary sulfide textures	massive, net-textured, disseminated; sometimes xenolithor xenomelt-bearing	massive	droplet	intercumulus, interstitial or lobate	intercumulus, interstitial	disseminated, rarely net-textured	layered, banded, laminated	massive to disseminated, typically associated with quartz and/or carbonate	brecciated, typically heterolithic; durchbewegung
Ore tenor	typically moderate-low, slightly fractionated	variable, commonly enriched in Cu-PPGE relative to associated contact ores	moderately high, relatively unfractionated	typically high, relatively unfractionated	variable (high to low)	typically high, relatively fractionated	variable, commonly depleted in Cr and Ir relative to associated magmatic ores	variable, commonly depleted in Cr and Ir relative to associated magmatic ores	variable, commonly depleted in Cr, Pt, and Au relative to magmatic ores
Timing and paragenesis	early magmatic, segregated prior to or during emplacement	early or late magmatic, injected during initial emplacement or formed via fractional crystallization of *MSS*	intermediate magmatic, segregated during crystallization of cumulate host rock	intermediate magmatic, segregated during crystallization of cumulate host rock	late magmatic but metamorphically-modified, segregated during crystallization of cumulate host rock	late magmatic, segregated during final stages of crystallization of host rock	late magmatic or syn-metamorphic	syn-metamorphic, mobilized in hydrothermal fluids	syn-tectonic, mobilized from massive or semi-massive sulfides
Examples (see Table 2.3)	Alexo, Kambalda, Langmuir, Raglan, Silver Swan, Windarra	Alexo, Kambalda, Raglan	Black Swan, DambaSilwane, Mariott's prospect, Otter Shoot (Kambalda), parts of Raglan and Silver Swan	David, Goliath, Dumont, Mt. Keith, Perseverance Main, William Lake and parts of Birchtree (Thompson), Yakabindie	Perseverance Main, Raglan	Delta Sill, Romeo Ⅱ Sill, Fred's Flow, Boston Creek Sill, Wiluna	Jan shoot (Kambalda), Langmuir, Perseverance F1A, Redstone, parts of T1-1C-1D (Thompson), Wannaway (Widgiemooltha)	Kambalda, Langmuir, Donaldson West (Raglan)	Birchtree-Bucko-Manibridge-Pipe 2-T1 and parts of 1C-1D (Thompson), Nepean, Perseverance 1A, Harmony, Emily Ann, Maggie Hays, Redross, Redstone, Rocky's Reward, Trojan, Windarra

Table 2.3 List of representative komatiite-associated Ni-Cu-(PGE) deposits summarizing some of their geological characteristics and sources of information.

Country	District/Belt/ Supergroup	Domain/ Assemblage/ Group/Unit	Camp/Area	Deposit (s)	Ore Types						pre-mining resource			Volcanic Setting	Age	Magma Type	Tectonic Setting	General References	Specific References	Note
					I	II	III	IVa	IVb	V	grade % Ni	Ore (mt)	Ni (kt)							
Australia	Yilgarn-EGS, Kalgoorlie Terrane	Agnew-Wiluna	Honeymoon Well	Hannibals, Harrier, Corella, Wedgetail	+	+					0.71	155	1107	P?	NA	AUK	RA?	Donaldson & Bromley (1982); Barnes (2006); Marston (1984)	Gole *et al.* (1998)	
Australia	Yilgarn-EGS, Kalgoorlie Terrane	Agnew-Wiluna	Mt. Clifford	Marriott's, Randall's Find, Mt Newman		+							10	P?	NA	AUK	RA?	Barnes *et al.* (1974); Marston (1984)	Donaldson (1981, 1983)	
Australia	Yilgarn-EGS, Kalgoorlie Terrane	Agnew-Wiluna	Perseverance	Perseverance	+	+				+	0.88	122	1067	P? to SV	NA	AUK	RA?	Hill *et al.* (1995); Barnes (2006)	Billington (1984); Barnes *et al.* (1988a, b, c, 1995); Libby *et al.* (1998), Trofimovs	
Australia	Yilgarn-EGS, Kalgoorlie Terrane	Agnew-Wiluna	Perseverance	Rocky's Reward, Harmony						+	2.41	7.9	190	MD?	NA	AUK	RA?	Barnes (2006)	De-Vitry *et al.* (1998); Duuring *et al.* (2007)	
Australia	Yilgarn-EGS, Kalgoorlie Terrane	Agnew-Wiluna	Mt Keith	Mt Keith MKD5		+					0.55	503	2767	SV	NA	AUK	RA?	Hill *et al.* (1995); Barnes (2006)	Grguric *et al.* (2006); Rosengren *et al.* (2005, 2007); Fiorentini *et al.* (2006, 2007)	
Australia	Yilgarn-EGS, Kalgoorlie Terrane	Agnew-Wiluna	Mt Keith	Cliffs	+						2.3	5.5	127	MD	NA	AUK	RA?	Marston (1984)		
Australia	Yilgarn-EGS, Kalgoorlie Terrane	Agnew-Wiluna	Yakabindie	Six Mile, Goliath		+					0.57	289	1656	P?	NA	AUK	RA?	Naldrett & Turner (1977); Hopf & Head (1998); Marston (1984)	Hill (1982); Groves & Keays (1979); Grguric *et al.* (2006)	
Australia	Yilgarn-EGS, Kalgoorlie Terrane	Agnew-Wiluna	Cosmos	Cosmos, Cosmos Deeps, Tapinos, Prospero, Alec Mairs	+					+	7.91	1.1	92	P? to SV	NA	AUK	RA?	No published data		
Australia	Yilgarn-EGS, Kalgoorlie Terrane	Boorara Domain	Black Swan	Black Swan, Silver Swan, Cygnet	+	+					1.26	10.9	137	P? to SV	NA	AUK	CR	Hicks & Balfe (1998)	Groves *et al.* (1974); Barnes *et al.* (2004); Hill *et al.* (2004); Dowling *et al.* (2004)	
Australia	Yilgarn-EGS, Kalgoorlie Terrane	Kambalda Komatiite, Silver Lake Member	Kambalda-St. Ives-Tramways	Approx 30 distinct deposits including Durkin, Fisher, Gibb, Juan, Hunt, Ken, Long, Lunnon, McMahon, Victor; Jan, Foster; Helmut, Schmidt	+	+		(+)	(+)	(+)	3.08	34	1056	MD-D	NA	AUK	CR	Woodall & Travis (1969); Ross and Hopkins (1975); Gresham & Loftus-Hills (1981); Lesher *et al.* (1984); Lesher (1989); Cowden & Roberts (1990); Stone & Masterman (1998); Stone and Archibald (2004); Stone *et al.* (2005); Marston (1984)	Ewers & Hudson (1972); Keele & Nickel (1974); Keays & Davison (1976); Ross & Keays (1979); Marston & Kay (1980); Keays *et al.* (1981); Woolrich *et al.* (1981); Hudson & Donaldson (1984); Cowden *et al.* (1986); Lesher & Campbell (1993); Cas *et al.* (1999); Cas & Beresford (2001); Beresford & Cas (2001); Beresford *et al.* (2002); Lesher & Burnham (2001)	

Continued

Country	District/Belt/ Supergroup	Domain/ Assemblage/ Group/Unit	Camp/Area	Deposit(s)	Ore Types						pre-mining resource			Volcanic Setting	Age	Magma Type	Tectonic Setting	General References	Specific References	Note
					I	II	III	IVa	IVb	V	grade % Ni	Ore (mt)	Ni (kt)							
Australia	Yilgarn-EGS, Kalgoorlie Terrane	Kambalda Komatiite	Widgie-mooltha	Mt. Edwards, Redross, Wannaway, Widgie 3, Mariner's, Miitel	+			(+)	(+)	+	1.66	21.1	349	D	NA	AUK	CR	McQueen (1981a); Marston (1984)	Heath *et al.* (2001); Seat *et al.* (2004)	
Australia	Yilgarn-EGS, Kalgoorlie Terrane	Kambalda Komatiite	Scotia	Scotia	+						3.07	1.1	35	D	NA	AUK	CR	Marston(1984)	Page & Schmulian (1981); Stolz & Nesbitt (1981)	
Australia	Yilgarn-EGS, Kalgoorlie Terrane	Coolgardie Domain		Nepean	(+)					+	2.3	0.4	9	D?	NA	AUK	CR	Barrett *et al.* (1977); Marston (1984)	Barrett *et al.* (1976); Sanders (1982)	
Australia	Yilgarn-EGS, Youanmi Terrane	Forrestania Greenstone Belt	Forrestania Eastern belt	Cosmic Boy, Digger Rocks	+	+					1.98	8.5	169	P? to SV	NA	ADK	?	Porter & McKay (1981); Perring *et al.* (1995); Frost *et al.* (1998)		
Australia	Yilgarn-EGS, Youanmi Terrane	Forrestania Greenstone Belt	Forrestania Western belt	Flying Fox, New Morning, Spotted Quoll, Lounge	+					(+)	6.0	1.6	99	D?	NA	ADK	?	Perring *et al.* (1995); Frost *et al.* (1998)		
Australia	Yilgarn-EGS, Youanmi Terrane	Lake Johnston Greenstone Belt	Lake Johnston	Maggie Hays, Emily Ann	+					+	1.8	13.9	251	P? to SV	NA	ADK	?	Barnes (2006)	Buck *et al.* (1998)	
Australia	West Pilbara	Karratha-Roeburn Greenstone Belt		Ruth Well	+									D?	MA	ADK	RA?	Nisbet & Chinner (1981); Krapez & Eisenlohr (1998)		
Australia	Yilgarn-EGS, Kurnalpi Terrane		Windarra	Windarra	+			+		+	1.21	6.7	81	D	NA	AUK	CR	Marston (1984)	Schmulian (1984)	
Brazil	Goiás-Tocantins Belt		Crixas	Boa Vista	(+)					+	2.2	6		D?	NA	ADK	?		Costa *et al.* (1997); Ferreira-Filho and Lesher (2001)	
Brazil	Morro do Ferro Belt		Minas Gerais	Fortaleza de Minas (O'Toole)	(+)				+	+	2.55	5.1	130	D?	NA	?	?		Brenner *et al.* (1990); Almeida *et al.* (2007)	
Canada	Abitibi	Kidd-Munro	Dundonald Twp.	Alexo, Dundonald	+					(+)	3.6	0.05	2	MD	NA	AUK	RA	Naldrett (1966); Muir & Comba (1979); Barrie *et al.* (1999); Davis (1999)	Barnes & Naldrett (1986); Houle *et al.* (2008)	
Canada	Abitibi	Kidd-Munro	Munro Twp.	Mickel(Dee's Flow) occurrence	+									D	NA	AUK	RA	Davis (1999)		
Canada	Abitibi	Kidd-Munro	Munro Twp.	Fred's Flow			+							D	NA	AUK	RA	Arndt *et al.* (1977); Arndt (1977)	Stone *et al.* (1996)	

Continued

Country	District/Belt/ Supergroup	Domain/ Assemblage/ Group/Unit	Camp/Area	Deposit(s)	Ore Types						pre-mining resource			Volcanic Setting	Age	Magma Type	Tectonic Setting	General References	Specific References	Note
					I	II	III	IVa	IVb	V	grade % Ni	Ore (mt)	Ni (kt)							
Canada	Abitibi	Malartic	Marbridge	Zones 1-4	(+)					+				D	NA	AUK	RA	Naldrett & Gasparini (1971)		
Canada	Abitibi	Stoughton-Roquemoure	Boston Creek	Boston Creek Unit			+							SV	NA	FP	?	Stone *et al.* (1993)	Houle (2001)	1
Canada	Abitibi	Tisdale	Bartlett Dome	Texmont	+					(+)	1.0	3.8	38	D	NA	AUK	RA	Coad (1979)		
Canada	Abitibi	Tisdale	Halliday Dome	Sothman	+	+					1.0	0.7	7	D	NA	AUK	RA	Coad (1979)	Houle (2001)	
Canada	Abitibi	Tisdale	Shaw Dome	Hart	+					(+)				D	NA	AUK	RA	Coad (1979); Stone & Stone (2000)		
Canada	Abitibi	Tisdale	Shaw Dome	Langmuir	+					(+)	2.1	1.6	33	D	NA	AUK	RA	Coad (1979), Stone & Stone (2000)	Green & Naldrett (1981)	
Canada	Abitibi	Tisdale	Shaw Dome	Redstone	(+)			+		+	2.4	1.2	29	D	NA	AUK	RA	Coad (1979); Stone & Stone (2000)	Robinson & Hutchinson (1982)	
Canada	Abitibi		Dumont	Dumont		+					0.45	175	788	SV	NA	AUK	RA	Duke (1986)	Eckstrand (1975); Brugmann *et al.* (1989)	
Canada	Cape Smith	Chukotat	Raglan Horizon	Cross Lake, C1-2-3, East Lake, Zone 2-3, Katinniq, Zone 5-8, Zone 13-14, West Boundary, Boundary, Donaldson	+	(+)				(+)	2.07	24.7	672	MD-D	PP	KB	RM	Kilburn *et al.* (1969); Lesher (1999); Lesher (2007)	Dillon-Leitch *et al.* (1986); Barnes & Picard (1993); Seabrook *et al.* (2004)	
Canada	Cape Smith	Povungnituk	Delta Horizon	Bravo, Delta, Mequillon	+		(+)							SV	PP	KB	RM	Giovenazzo *et al.* (1989)	Thibert *et al.* (1989); Barnes & Giovenazzo (1990)	2
Canada	Cape Smith	Povungnituk	Delta Horizon	Expo Ungava	+					(+)	6.3	0.86	54	SV	PP	KB	RM	Giovenazzo *et al.* (1989)	Mungall (2007)	2
Canada	Fox River	Fox River Sill			(+)		+							SV	PP	KB	RM	Peck *et al.* (2002)		
Canada	Trans-Hudson	Namew Gneiss		Namew Lake	(+)	+				+				SV	PP	HMB	RM?		Menard *et al.* (1996)	
Canada	Thompson Nickel Belt	Pipe		Bucko, Manibridge, Moak, Pipe I & II, Thompson T1-T2-T3-1C-1D, William Lake	(+)	+		+		+	2.32	150	3487	SV	PP	KB	RM	Peredery *et al.* (1982); Bleeker (1990); LaytonMatthews *et al.* (2007)	Peredery (1979); Hulbert *et al.* (2005)	

Continued

Country	District/Belt/ Supergroup	Domain/ Assemblage/ Group/Unit	Camp/Area	Deposit(s)	Ore Types						pre-mining resource			Volcanic Setting	Age	Magma Type	Tectonic Setting	General References	Specific References	Note
					I	II	III	IVa	IVb	V	grade % Ni	Ore (mt)	Ni (kt)							
Canada	Hearne	Ennadai-Rankin		Rankin Inlet	+						3.3	0.45		SV	NA	KB	?		Hulbert & Gregoire (1993)	
China		Sibao		Dapoling	+									SV	MP	KB	?	Zhou *et al.* (2002)		
Russia	Kolar		Pechenga	Zapolyarninskoe, Zhdanovskoe	(+)	+				+				SV-C-P	PP	FP	RM	Melezhik *et al.* (1994); Green & Melezhik (1999)	Absalov & Both (1997); Brügmann *et al.* (2000); Barnes *et al.* (2001)	
Russia	Kolar		Pechenga	Kaula, Kammikivi, Kotsel'vaara, Semiletka	+					+	1.2	339	4068	SV-C-P	PP	FP	RM			Total Pechenga resource
Vietnam	Song Da Rift			Ban Phuc		+			+		1.26	1.2			P-T		CR	Xinh & Chu (1984)	Glotov *et al.* (2001)	
Zimbabwe	Bulawayan	Reliance	Bindura-Shamva	Trojan	(+)	+				(+)	0.68	20	138	D?	NA	AUK	RM?	Viljoen & Bernasconi (1979); Williams (1979); Hammerbeck (1984); Prendergast (2003)	Chimimba (1984); Maiden *et al.* (1986)	
Zimbabwe	Bulawayan	Reliance	Bubi E	Damba-Silwane		+								P?	NA	AUK	RM?	Williams (1979); Hammerbeck (1984); Prendergast (2003)	Viljoen & Bernasconi (1979)	
Zimbabwe	Bulawayan	Reliance	Filabusi	Epoch		+			(+)		0.60	0.47		C?	NA	AUK	RM?	Viljoen & Bernasconi (1979); Williams (1979); Hammerbeck (1984); Prendergast (2003)		
Zimbabwe	Bulawayan	Reliance	Midlands SE	Hunter's Road		+					0.70	30	210	P?	NA	AUK	RM?	Viljoen & Bernasconi (1979); Williams (1979); Hammerbeck (1984); Prendergast (2003)	Prendergast (2001)	
Zimbabwe	Bulawayan	Reliance	Shangani N	Shangani	(+)	+					0.71	22	138	C	NA	AUK	RM?	Williams (1979); Hammerbeck (1984); Prendergast (2003)	Viljoen *et al.* (1976); Viljoen & Bernasconi (1979)	

Types: I = stratiform basal, II = strata-bound disseminated, III = stratiform "reef", IV = hydrothermal-metamorphic, V = tectonic. Age: P-T = Permo-Triassic, NP = Neoproterozoic, MP = Mesoproterozoic, PP = Paleoproterozoic, NA = Neoarchean, MA = Mesoarchean, PA = Paleoarchean. Tectonic Setting: CR = continental rift, RM = rifted continental margin, RA = rifted arc, OR = orogenic. Volcanic Setting: SV = subvolcanic, C = central, P = "proximal", MD = "mid-distal", D = "distal". Notes: 1 = previously interpreted as a flow, but Houlé *et al.* (2001) report that the upper margin contains xenoliths and has contact metamorphosed overlying basalts, 2 = Chukotat-related sills located in the Povungnituk group. Resource information from Hoatson *et al.* (2005), Barnes (2006), Eckstrand and Hulbert (2007), and other sources listed in Table.

by the Thompson deposit in the Thompson Nickel Belt, but has not been reported in other associations. Type IVb hydrothermal vein mineralization is a relatively minor type in komatiite-associated deposits, but is an important ore type in other associations (e.g., PPGE-Au-Bi-Te rich footwall zones at Sudbury). Type V tectonic offset mineralization occurs at least locally in most Type I deposits, in some cases comprises entire ore bodies, e.g., in the Thompson Nickel Belt (Layton-Matthews *et al*., 2007) and Harmony (Duuring *et al*., 2007) and is also common in most other associations. It is very important to appreciate that the different mineralization types are not mutually exclusive and that many deposits/units contain more than one type.

Representative komatiite-associated Ni-Cu-(PGE) deposits and their principal ore types, interpreted magmatic affinities and tectonic settings, and representative geological references are summarized in Table 2.3. Unless noted otherwise, descriptive data for individual deposits referred to elsewhere in this chapter are taken from these sources.

2.1.2 Age and location

Magmatic Ni-Cu-(PGE) deposits have formed throughout geological time (Fig. 2.3), but except for a few occurrences in the Mesoarchean (Forrestania, Lake Johnson, Windarra, and by a narrow margin, Ruth Well) and one occurrence in the Permo-Triassic (Ban Phuk), most komatiite-associated deposits occur in the Neoarchean and Paleoproterozoic (Table 2.3). This distribution corresponds to spikes in the generation and preservation of high-Mg komatiites at 2.7 Ga and komatiitic basalts at 1.9 Ga (Condie, 2001). The change from high-Mg komatiites to low-Mg komatiites and komatiitic basalts reflects a fundamental change in the thermal and/or compositional structure of the Earth's mantle at the end of the Archean (Campbell and Griffiths, 1990; Lesher and Kamber, 2009) that appears to have also affected their volcanic-subvolcanic settings (see below).

Komatiite-associated Ni-Cu-(PGE) have been identified thus far in Western Australia, Brazil, Finland, Manitoba, New Québec (Ungava), Ontario-Québec, Russia, Viet Nam, and Zimbabwe (Table 2.3; Fig. 2.1). As we shall see there is no reason why they should not form wherever a komatiite lava channel or magma conduit encounters a suitable S source. The East Yilgarn province of Western Australia, the Thompson Nickel Belt in Manitoba, and the Raglan (Cape Smith) belt in Quebec account for more than 90% of the global resource of this class of deposit. Among the Archaean terranes, the East Yilgarn province is overwhelmingly the dominant repository in terms of both number and aggregate size of deposits.

2.1.3 Tectonic settings

Like most other types of magmatic Ni-Cu-(PGE) deposits, komatiite-associated deposits appear to occur primarily in intracratonic rift zones, along rifted continental margins, or in rifted arcs (Table 2.2). Although other types of magmatic Ni-Cu-(PGE) deposits appear to have formed in convergent settings (e.g., Aguablanca: Tornos *et al*., 2005; Kotalahti-Vammala: Makinen and Makkonen, 2004; Peltonen, 1995a, b; Peltonen *et al*., 1995; Råna and Vakkerlien: Papunen, 2003; Wrangelia: Hulbert *et al*., 1997), no equiv-

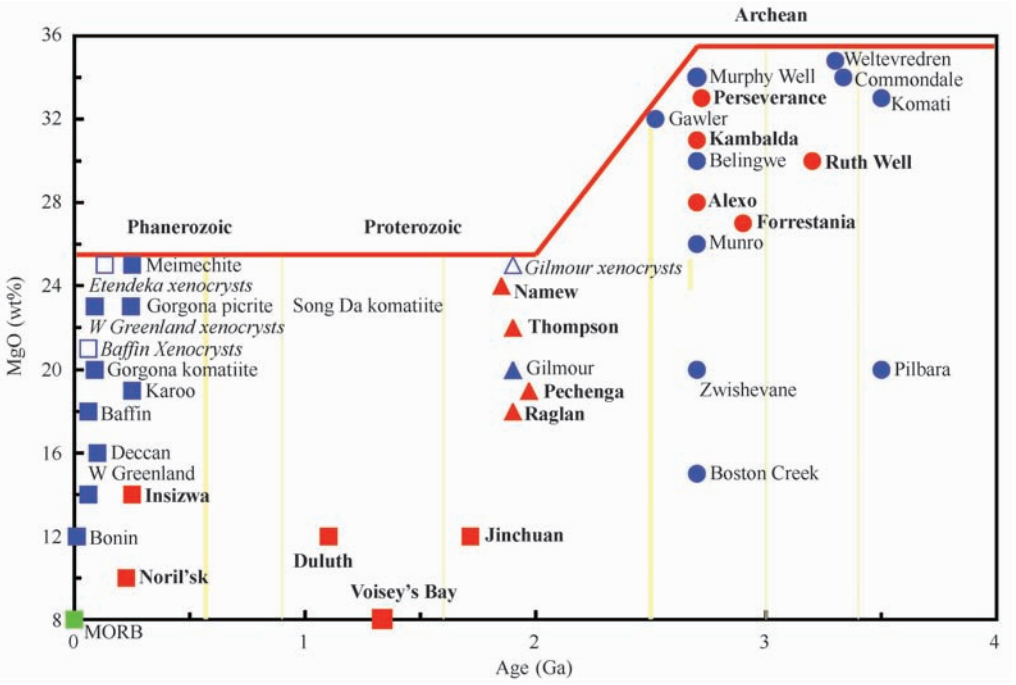

Fig. 2.3 Variation in MgO contents of mantle-derived magmas with time. Data from sources discussed in Arndt *et al*. (2008).

alents have been recognized in Archean greenstone belts.

Groves and Batt (1984) identified two types of greenstone belts in Western Australia: platform-phase greenstones and rift-phase greenstones. Platform-phase greenstones are characterized by a coherent volcanic stratigraphy, abundant komatiitic basalts, and shallow-water volcaniclastic rocks or oxide facies iron-formations, which were interpreted to have formed in relatively shallow water under conditions of low crustal extension. Rift-phase greenstones are characterized by more complex volcanic stratigraphy, abundant komatiites (including komatiitic peridotites and komatiitic dunites), and sulfidic shales or cherts, which were interpreted to have formed in relatively deep water under conditions of high crustal extension. Most komatiite-associated Ni-Cu-(PGE) deposits in Western Australia (e.g., Widgiemooltha, Kambalda-St. Ives-Tramways, Nepean, Mount Keith, Perseverance) occur within rift-phase greenstones, although some occur in platform-phase greenstones (e.g., Forrestania, Lake Johnson, Windarra). Analogous subdivisions have been defined in the Zimbabwe craton (Wilson, 1979), the Abitibi Greenstone Belt (Ludden *et al*., 1986; Chown *et al*., 2002), and the Pilbara Craton (Krapez and Eisenlohr, 1998); in each of these areas komatiite-associated Ni-Cu-(PGE) deposits appear to occur in fault-bounded rift basins superimposed on earlier platformal or arc-related volcanic cycles. Barley *et al*. (2006, 2008) have subdivided the greenstone terranes of the East Yilgarn craton, largely on the basis of the geochemistry of the associated felsic volcanic rocks, into arc sequences and rifted back-arc basins, the latter corresponding to Groves and Batt's rift-phase.

Naldrett (2004, 1989) has shown that many magmatic Ni-Cu-(PGE) deposits were emplaced along or near major crystal faults/lineaments that are interpreted to have provided access for ascent of the host magmas. In the case of komatiite-associated deposits, no structures of that type have been identified at Pechenga, Raglan, or Thompson, but they occur along rifted continental margins and have been thrusted. Gresham and Loftus-Hills (1981) and Beresford *et al*. (2002, 2005) suggested that the Kambalda komatiites were fed by the nearby Boulder-Lefroy Fault, based on thickening of the komatiite stratigraphy towards the fault in the Kambalda-St Ives region, but this is not consistent with facies variations and geochemical trends in the host units (Woolrich *et al*., 1981; Cowden and Roberts, 1990; Gresham and Loftus-Hills, 1981; Lesher and Arndt, 1995; Lesher, 1989) and the basalts (Squire *et al*., 1998), which indicate that that both the basalts and the komatiites flowed parallel to the Lefroy Fault. If the thickening is not structural, it may indicate that the main volcanic pitchline (and perhaps the main locus of mineralization) was further to the east.

Lesher and Keays (2002) noted that the komatiite-associated deposits in the Norseman-Wiluna Belt, several of which have been world-class producers, were emplaced onto much older (colder, more dense) continental crust, whereas those in the Abitibi Greenstone Belt, most of which are subeconomic or have been only minor past producers, were emplaced onto much younger (warmer, less dense) crust (see Fig. 2.9 below). This was interpreted to have influenced the rate of magma ascent and eruption, which as we will see below, appears to be the critical factor influencing the formation of magmatic Ni-Cu-(PGE) deposits in general and komatiite-associated deposits in particular.

2.1.4 Magmatic settings

Magmatic Ni-Cu-(PGE) deposits are associated with almost every mantle-derived mafic-ultramafic magma type, including Al-undepleted and Al-depleted komatiite, komatiitic basalt, ferropicrite, picrite, and high-Mg basalt (Table 2.3). Thus, although the composition of the magma may exert a strong control on the composition of the sulfide ores (see below), the composition of the source and residue, the depth of melting, and the composition of the residue do not appear to affect the fertility of the magmas (Lesher and Groves, 1986; Lesher, 1989; Lesher and Stone, 1996; Sproule *et al*., 2002; Arndt *et al*., 2005). Retention of small amounts of sulfides in the source can markedly influence the abundances of PGE in the magmas because they partition so strongly into sulfide (Keays, 1982; Keays, 1995) (see also Arndt *et al*., 2005), but has only a moderate effect on Cu and a negligible effect on Ni and Co (Barnes *et al*., 1985).

2.1.5 Distribution and stratigraphic setting

Despite structural complications and probable facies variations (see below), mineralized komatiite sequences appear to be correlative over distances of tens to hundreds of kilometres, possibly over entire greenstone provinces. However, they are often heterogeneously distributed on multiple scales.

Craton scale

The deposits in Western Australia occur in the Eastern Goldfields Superterrane and the southern part of the Youanmi Terrane (formerly Southern Cross Province) of the Yilgarn Craton, and there is one small deposit in the West Pilbara, but there are none in the Murchison Province or the northern part of the Youanmi Terrane. Komatiite-associated Ni-Cu-(PGE) deposits in Zimbabwe occur in the Reliance Formation of the Bulawayan Supergroup, but not in the Belingwean or Shamvaian Supergroups (Prendergast, 2003). Komatiites occur in small amounts in most of the greenstone belts in the Superior Province of Ontario-Québec, but komatiite-associated Ni-Cu-(PGE) deposits occur almost exclusively in the Abitibi belt.

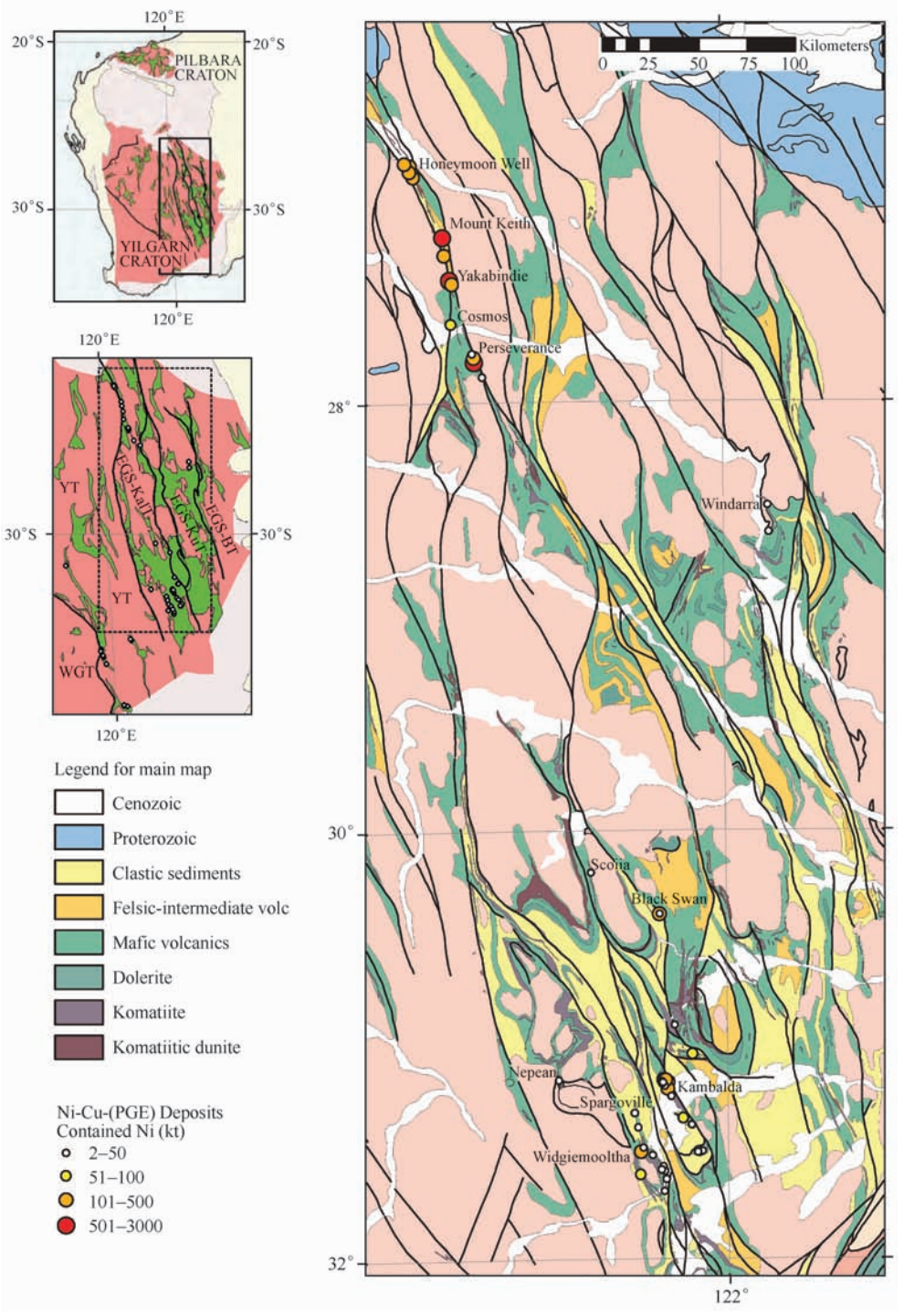

Fig. 2. 4 Simplified map of the Eastern Goldfields Superterrane (from Barnes, 2006) showing the locations of komatiite-associated Ni-Cu-(PGE) deposits.

Regional scale

The dominant repository of deposits hosted by high-MgO komatiites is the Kalgoorlie Terrane (the western portion of what was formerly known as the Norseman-Wiluna Greenstone Belt) of the Eastern Goldfields Superterrane of the Yilgarn Craton (Swager, 1997; Swager *et al*., 1997, 1992) (Fig. 2. 4). Most of the deposits occur in two geographical areas: within the Agnew-Wiluna Belt in the north, where komatiites are intercalated with felsic to intermediate volcanic rocks and sediments, and in the Kambalda-Widgiemooltha region in the south, where komatiites erupted onto a thick pile of tholeiitic basalts. The deposits in the Agnew-Wiluna Belt (including two of the largest deposits of this class in the world, Mt Keith and Perseverance) contain both Type I and Type Ⅱ mineralization, and are localized within or in close proximity to large adcumulate dunite bodies, not found within

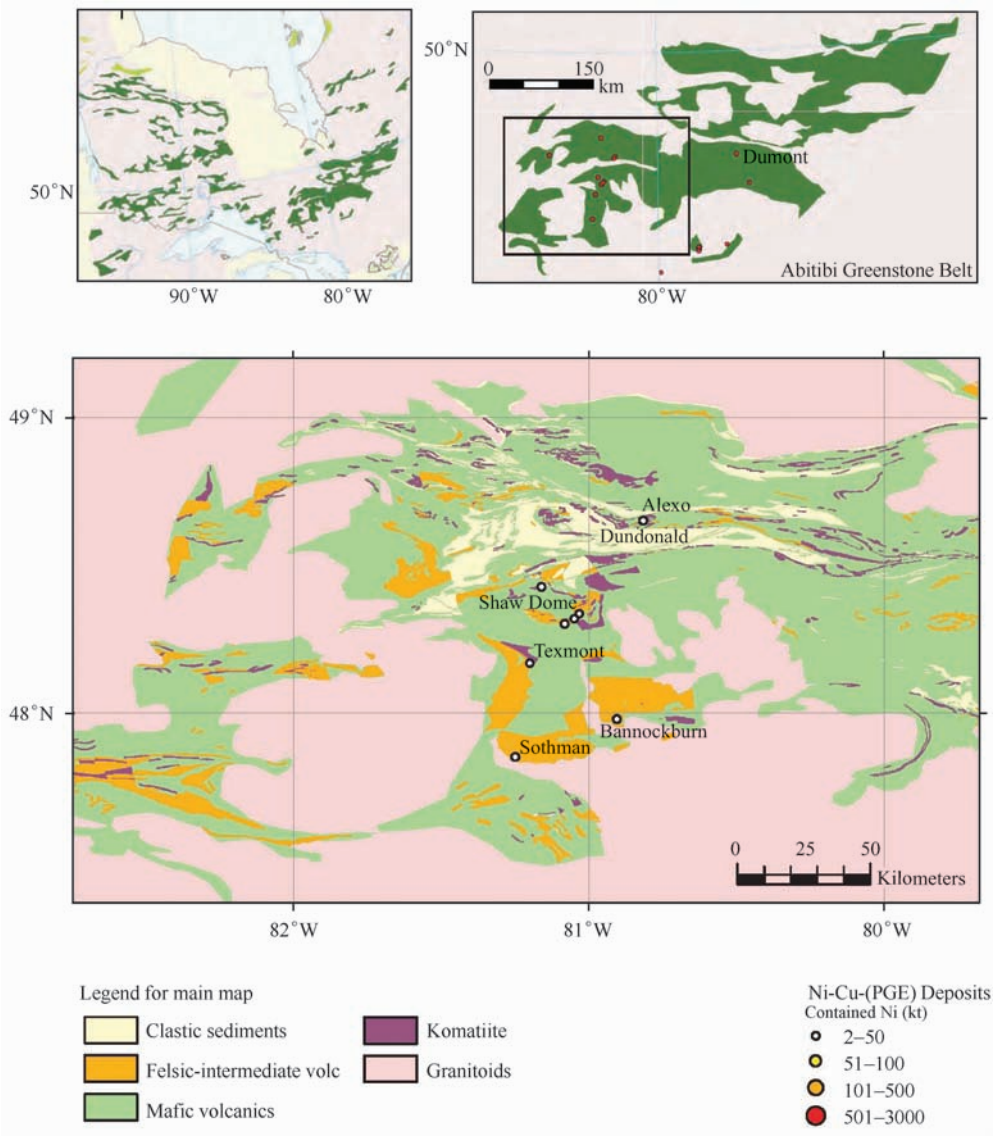

Fig. 2. 5 Simplified map of the Abitibi Greenstone Belt (modified from Barnes, 2006) showing the locations of komatiite-associated Ni-Cu-(PGE) deposits.

the southern portion of the Kalgoorlie Terrane. The deposits in the Abitibi Belt (Fig. 2. 5) occur in the Kidd-Munro and Tisdale assemblages, which contain abundant channelized komatiite units and associated S-bearing country rocks, whereas no deposits have been discovered in the Pacaud and Stoughton-Roquemaure assemblages, which lack those features (Sproule *et al*., 2002). Type I/Ⅱ deposits in Zimbabwe occur as multiple isolated 100 km diameter volcanic-subvolcanic flow-sill complexes of the Reliance formation that can be correlated for ~500 km across the Zimbabwe craton (Prendergast 2003, 2004; Fig. 2. 1). Ni-Cu-(PGE) and PGE-(Cu)-(Ni) deposits in the Cape Smith Belt (Fig. 2. 6) appear to occur at two stratigraphic levels (Giovenazzo *et al*., 1989; St-Onge and Lucas, 1993; Lesher, 2007); all of the Type I/Ⅱ deposits in the Raglan area occur at the base of the Chukotat Group, but there are several subeconomic Type I (Bravo, Expo Ungava, Méquillon) and Type Ⅲ (Delta) deposits in sills in the central part of the Povungnituk Group, which appear to be derived from similar magmas (Mungall, 2007). Type I/Ⅱ deposits in the Pechenga Belt belt occur at or near the same stratigraphic level at or near the top of the suflfide-rich Pilgujärvi metasedimentary formation (AKA "Productive Formation") (Green and Melezhik, 1999; Melezhik *et al*., 1994). Type Ⅳa and Ⅳ (deformed Type I) deposits in the Thompson Nickel Belt were formerly thought to occur at multiple levels in the Ospwagan Group and basement rocks (Bleeker, 1990), but Zwanzig *et al*. (2007) have shown that they are all located in the lower part of the Pipe Formation, which is also where there is the greatest concentration of sulfide-facies banded iron formations (Fig. 2. 7).

Subregional scale

Type I/Ⅱ deposits in the southern Kalgoorlie Terrane

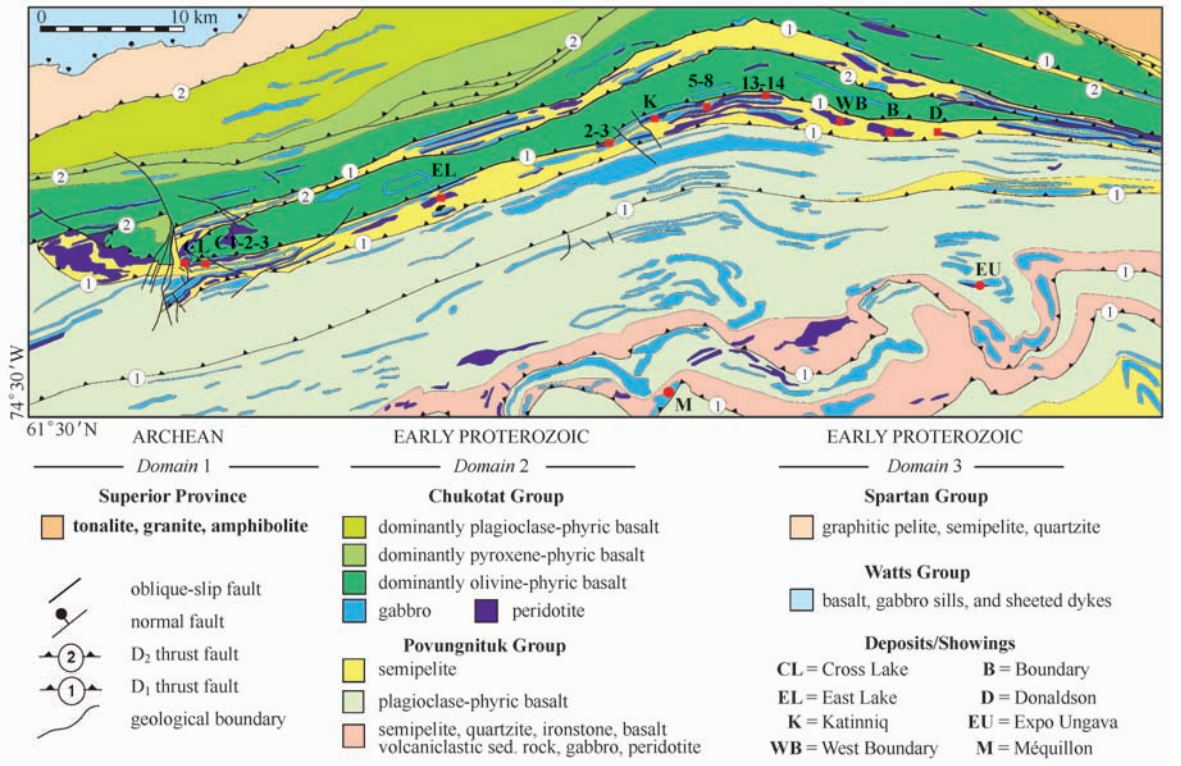

Fig. 2. 6 Map of the eastern part of the Cape Smith Belt (from St-Onge and Lucas, 1993) showing the locations of komatiite-associated Ni-Cu-(PGE) deposits.

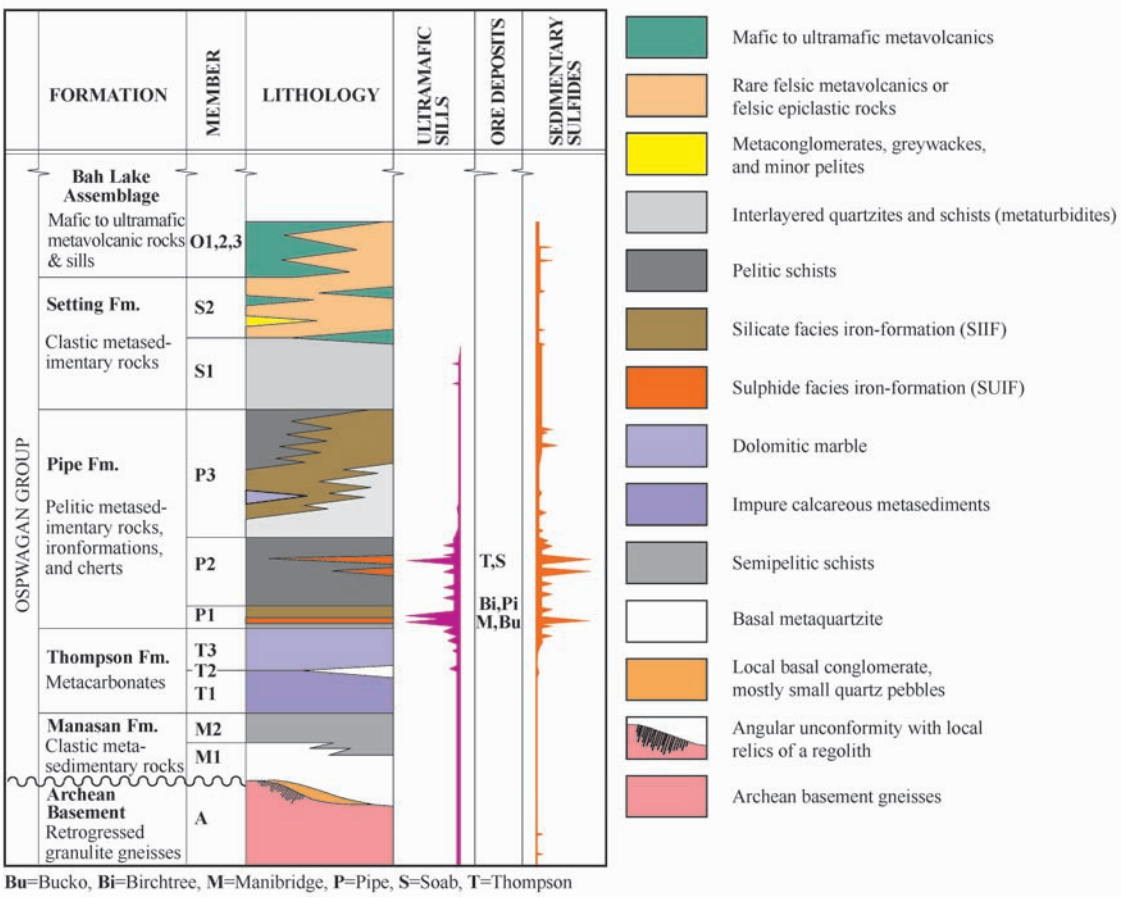

Fig. 2. 7 Stratigraphic column for the Thompson Nickel Belt (from Burnham *et al*., 2003), as modified after Bleeker (1990).

(Fig. 2. 4) and in the Kidd-Munro and Tisdale assemblages of the Abitibi belt (Fig. 2. 5) occur at or near the bases of the komatiite sequences, often in clusters exposed around structural highs (e.g., Kambalda-Tramways-St Ives domes, Shaw-Bartlett-Halliday domes). Type I/Ⅱ deposits in the Raglan formation occur in two stratigraphic members: those in the Cross Lake member appear to represent channelized sheet flows/sills, whereas those in the Raglan member appear to represent deeply erosive lava channels.

The principal footwall lithology varies from district to district, including *basalt* in the Kalgoorlie Terrane (Kambalda-Widgiemooltha, Nepean, and Scotia), *andesite* in the Kidd-Munro assemblage (Alexo-Dundonald, Marbridge), *dacite* in the northern and east-central Kalgoorlie Terrane (Mt. Keith, Perseverance, Cosmos, Black Swan-Silver Swan) and the Tisdale Group (Hart-Langmuir-McWatters-Redstone, Texmont, Sothman, Bannockburn), *banded iron formation* in the Windarra district, and *metapelites* in the Forrestania, Raglan, and Damba-Silwane and Shangani districts. This indicates that these deposits formed in somewhat different tectonic settings, at somewhat different stages in the evolution of greenstone belts, or in somewhat different environments within rift zones.

Most Type I deposits directly overlie or are stratigraphically correlative with S-bearing sediments or volcanic rocks. Most Type Ⅱ deposits also occur in sequences that contain S-bearing country rocks, but stratigraphic relationships are more obscure. The nature and composition of the S-rich rocks varies from sulfidic cherts in the Forrestania, Kambalda, Thompson, Shaw Dome, Trojan, and Windarra areas through sulfidic shales and semi-pelites in the Dundonald, Damba-Silwane, Raglan, and Pechenga areas to localized "massive" sulfides in the Alexo and Namew Lake areas. Although oxide facies iron-formation forms the footwall to several deposits in the Forrestania district, overlying komatiites are intercalated with sulfidic cherts. Ore-sediment relationships vary considerably, even between deposits in the same district. Ores may grade laterally into sediments (e.g., parts of Juan, Lunnon, and Jan shoots at Kambalda, Thompson, and Redstone), directly overlie or lap onto sediments which may be altered, thinned, or discontinuous beneath the ore zone (e.g., Langmuir, Mt. Edwards, Scotia, Trojan, Wannaway, Windarra; Foster, Ken, McMahon, and Cruickshank shoots at Kambalda; Digger Rocks and New Morning at Forrestania), or occur along strike from sediments, separated by a zone of barren contact (e.g., Nepean, Miriam, Widgiemooltha 3; and many shoots at Kambalda). Sediments have been a locus for deformation in many areas, but these variations also exist in least-deformed areas. Although these rocks are a potential source of S (see below), ores may segregate and accumulate downstream from the S source (Lesher *et al*., 1984; Lesher, 1989; Lesher and Campbell, 1993), so they are not always present and not always locally absent.

Type I ores typically occur at or near the bases of the lowermost komatiite flow units ("contact ores") and/or sometimes at the bases of overlying komatiite flow units ("hanging wall ores"). At Kambalda (Gresham and Loftus-Hills, 1981) and Scotia (Stolz and Nesbitt, 1981) they occur within elongate prisms of rock oriented parallel to and overlying the linear ore shoots in which individual flows are thicker, more magnesian, and less stratigraphically-continuous than those flanking the ore environments, indicating a strong volcanic control on ore localization (Gresham and Loftus-Hills, 1981). This has been attributed by some workers to ponding of lavas above or adjacent to proximal feeding fissures (Ross and Hopkins, 1975; Gresham and Loftus-Hills, 1981; Brown *et al*., 1999), but no komatiite feeders have been identified at Kambalda. Stone and Archibald (2004) and Gresham (1986) and Beresford *et al*. (2002) before them suggest that the thinning of the Kambalda Komatiite across the Kambalda Dome indicates the possibility of an east-to-west flow direction, but this contradicts all of the NNW-oriented stratigraphic, petrological, geochemical, and isotopic trends NNW or SSE (see e.g., Woolrich and Giorgetta, 1978; Gresham and Loftus-Hills, 1981; Lesher *et al*., 1984; Lesher, 1989; Cowden and Roberts, 1990; Lesher and Arndt, 1995; Lesher *et al*., 2001). The best interpretation is that they represent channelization of flows from a more distal eruptive site to the NNW (most likely) or SSE (less likely) (Lesher *et al*., 1984; Cowden and Roberts, 1990).

A similar stratigraphic model can be applied to the thicker and more complex ultramafic complexes that host Type Ⅱ deposits (e.g., Mt. Keith, Perseverance, Raglan), which are interpreted to comprise multiple, overlapping thick adcumulate-mesocumulate lava channels that grade laterally into adjacent orthocumulate, porphyritic, and spinifex-textured komatiites (Barnes *et al*., 1988b; Lesher, 1989; Lesher, 2007). They are interpreted to represent more proximal channels associated with similar scales of eruptions or mid-distal to distal channels associated with more voluminous eruptions.

The morphology and size of the komatiite flow field will depend on the volume of lava erupted and the topography of the underlying units. Sequences erupted onto a regionally extensive basalt (e.g., southern Norseman-Wiluna belt: Gresham and Loftus-Hills, 1981) or sediment (e.g., Cape Smith belt: St-Onge and Lucas, 1993; Zimbabwe: Prendergast, 2003) unit will have less topographic relief, will be less likely to become ponded, and will be more likely to form broad flow fields (Hill, 2001; Hill *et al*., 1995; Hill *et al*., 1990) than sequences erupted into a setting containing multiple felsic volcanic centres (Barrie, 1999; Houle *et al*., 2008; Dostal and Mueller, 1997; Davis, 1999).

2.1.6 Volcanic-subvolcanic settings

Most host komatiite sequences are underlain and/or overlain by pillow lavas and contain intercalations of plane-laminated sulfidic shales, sulfidic cherts, or sulfide-facies iron-formation, suggesting emplacement into a relatively deep subaqueous environment.

Many mineralized komatiite sequences appear to grade systematically upwards from thick, komatiitic peridotites or komatiitic dunites at the base through thinner, aphyric and spinifex-textured komatiite flows to massive or pillowed komatiitic basalt flows at the top (e.g., Kambalda, Alexo-Dundonald, Langmuir, Perseverance, Mt. Keith, Scotia, Damba-Silwane, and Raglan). Some mineralized units (e.g., Kambalda-Tramways-St Ives-Widgiemooltha, Scotia, Raglan) are separated by interflow sediments, except near ore zones. Thus, the thicknesses of komatiite flows, time between eruptions, degree of olivine enrichment, and magnesium content of liquids often appear to decrease upwards. This likely reflects a change from more voluminous, episodic eruptions to less voluminous, more continuous eruptions (Lesher, 1989) leading to a regression in lava facies and emplacement of "distal" lava lobe facies on top of "mid-distal" channelized sheet flow facies (Lesher and Arndt, 1995).

There are also variations in the composition and texture of komatiitic lavas across most mineralized volcanic piles (e.g., Kambalda, Scotia, Perseverance, Raglan, Windarra). Komatiitic peridotites grade laterally into porphyritic komatiites, komatiitic dunites grade laterally into komatiitic peridotites, and barren komatiites overlying ore zones may contain more cumulate flows and may be better compositionally and texturally differentiated than those further from mineralization. At Kambalda, these stratigraphic variations define elongate prisms of rock parallel to and overlying linear ore shoots, indicating a strong volcanic control on ore localization (Fig. 2.8). This has been attributed previously to ponding of lavas adjacent to proximal feeding fissures (Ross and Hopkins, 1975; Gresham and Loftus-Hills, 1981; Gresham, 1986), but the absence of feeders and other petrographic and geochemical constraints suggest that it represents channelization of flows erupted from a distal eruptive site along the volcanic pitchline (Lesher *et al.*, 1981, 1984; Cowden and Roberts, 1990). Stone and Archibald (2004) suggested that the thickness of the basal host units at Kambalda were such that they would have formed topographic ridges and suggested that subsequent flows should not flow along the top of a ridge, but after removal of superimposed deformation the upper contact of the basal host units at most shoots are more or less planar (see below) and any doming would simply result in overlapping lens-shaped units, as observed by Lesher (1983, 1989) and Beresford *et al.* (2002).

In contrast, barren komatiite sequences in Barberton, South Africa (Viljoen and Viljoen, 1969, 1982), Belingwe, Zimbabwe (Nisbet *et al.*, 1977, 1982), and Munro Township, Ontario (Arndt *et al.*, 1977) contain few komatiitic peridotites or dunites, and commonly comprise interlayered komatiite and basaltic komatiite. They represent less voluminous eruptions and/or more distal portions of komatiite lava piles (Lesher, 1989; Barnes, 2008; Arndt *et al.*, 2008).

Type I and Ⅱ mineralization is hosted by cumulate lava

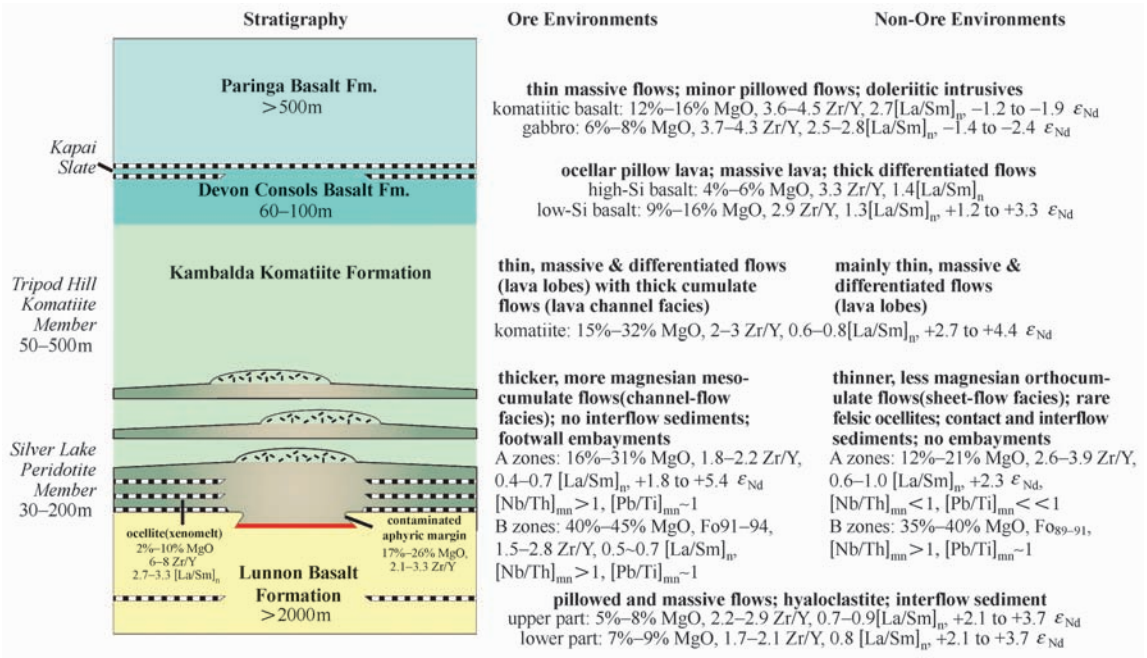

Fig. 2.8 Stratigraphic column summarizing lithological and geochemical variations at Kambalda (summarized from Gresham and Loftus-Hills, 1981; Lesher *et al.*, 1984; Lesher and Arndt, 1995; Lesher *et al.*, 2001).

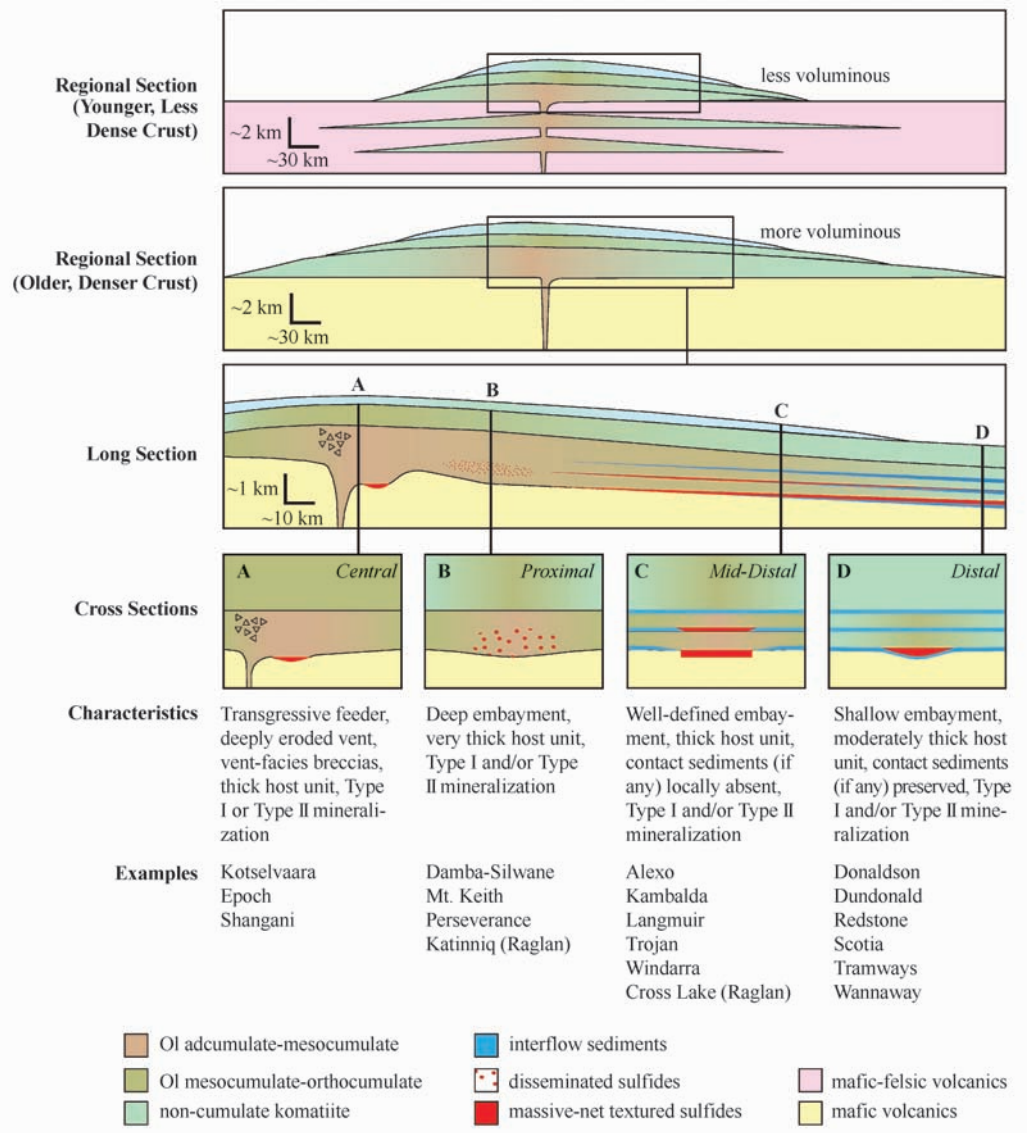

Fig. 2. 9 Volcanic facies of komatiite-associated Ni-Cu-(PGE) deposits (modified from Lesher, 1989; Lesher and Keays, 2002).

channels, subvolcanic feeder sills, or magma conduits. They occur in a widerange of volcanic and subvolcanic environments (Table 2. 3), including subvolcanic, central volcanic, proximal, mid-distal, and distal[1] settings (Fig. 2. 9).

Extrusive Type I komatiite-associated Ni-Cu-(PGE) deposits typically occur at or near the bases of volcanic cycles in which the lower komatiite flows are thicker, more magnesian, more channelized, and commonly intercalated with metasedimentary rocks. Overlying komatiite flows are often thinner, less magnesian, less channelized, and contain few if any interflow metasedimentary rocks (Western Australia: Groves and Hudson, 1981; Gresham and Loftus-Hills, 1981; Marston, 1984; Lesher, 1989; Raglan: Lesher, 2007; Abitibi: Houlé *et al*., 2008; Zimbabwe: Prendergast, 2003). The vertical variations are interpreted to represent a regression in lava facies accompanying a change from more voluminous and more episodic eruptions to less voluminous and more continuous eruptions (Lesher, 1989).

The presence of only lavas, only sills, or both appears to depend on the thickness, rheology, and density of the underlying crust. For example, in the southern part of the Kalgoorlie Terrane in Western Australia, where no komatiite sills have been identified, the supracrustal rocks are underlain by older granitic crust (2. 9 – 3. 2 Ga) (Champion and Cassidy,

[1] The lateral parts and flow fronts of lava flow fields may have distal volcanic characteristics (Lesher, 1989; Hill *et al*., 1990; Prendergast, 2003; see Fig. 2. 9), so the inferred volcanic settings are relative.

2007; Chauvel *et al*., 1985) and the komatiite sequence is underlain by a > 2000 km-thick sequence of dense tholeiitic basalts (Gresham and Loftus-Hills, 1981). In contrast, in the Abitibi greenstone belt, Cape Smith Belt, Thompson Nickel Belt, and in Zimbabwe, where komatiitic lavas are commonly underlain by komatiitic sills, they are underlain by much younger crust (Abitibi: Machado *et al*., 1986) and/or thick sequences of low-density metasedimentary rocks (Zimbabwe: Williams, 1979; Prendergast, 2003, 2004; Cape Smith Belt: St-Onge *et al*., 1993). The age relationships between the komatiite sills and lavas are not clear in most cases, but emplacement of the sills may have dehydrated the sediments and increased the bulk density of the crust, permitting the lavas to erupt (Lesher and Keays, 2002; Houlé *et al*., 2008).

The criteria for distinguishing the environments of emplacement of komatiites have been reviewed by Dann *et al*. (2001), Arndt *et al*. (2004), Lesher (2007), and Houlé *et al*. (2008), and are summarized in Table 2.4. Proximity to eruptive sites may be inferred from proximity to volcanic feeders, physical volcanology of lavas, and stratigraphic relationships with associated volcanic and sedimentary rocks (Table 2.5). Although the precise settings are not always clear, resulting from incomplete exposure and/or ambiguous stratigraphic relationships, interdeposit comparisons suggest a continuum of volcanic environments ranging from subvolcanic through central and proximal volcanic to distal volcanic (Fig. 2.9, Table 2.3).

Table 2.4 Criteria for identifying the mode of emplacement of komatiites (modified from Lesher, 2007)

Feature	Lava Flow or Pond	Deeply Erosive Lava Conduit	Invasive Flow	High-Level Sill
Contact metamorphosed upper contacts*	−	−	+	+
Peperites along upper and/or lateral margins	−	+	+	+
Conformable upper contact	+	+	~	~
Transgressive upper contact	−	−	~	~
Flow-top breccias and polyhedral joints	+	+	~	−
Columnar joints in upper and lower parts	+	+	+	+
Rapidly-cooled mesostases and high-Ca olivine	+	+	~	~
Transgressive lower contact	~	+	+	−
Contact metamorphosed lower contacts*	+	+	+	+
Linear form (subregional scale)	−	+	+	−
Linear ore shoots (local scale)	−	+	+	−
Consistent stratigraphic location	+	+	+	~

+ consistent, ~ possible, − inconsistent; * depends on degree of channelization, magma flux, time, and nature of wall rocks.

Table 2.5 Criteria for identifying the volcanic settings* of mineralized komatiites

Feature	Central Volcanic	Proximal	Mid-Distal	Distal
Vent facies pyroclastic breccias	+	~	−	−
Transgressive feeders	+	~	−	−
Subvolcanic sills	+	+	~	~
Thicker, more magnesian lava channels		+	~	−
Thinner, less magnesian lava channels			+	~
Thermal erosion (channels)**	+ + +	+ +	+	~
Contact metamorphism (channels)**	+ + +	+ +	+	~
Lava lobes (massive or differentiated)	−	~	+	+
Pillow lava	−	−	~	+
Distal pyroclastic deposits	~	~	~	+
Type I mineralization	~	~	+	+
Type Ⅱ mineralization	+	+	~	~

+ consistent, ~ possible, − inconsistent; * Lava facies vary with effusion rate, so all settings and features are relative. ** Varies with the nature of the substrate (consolidated vs. unconsolidated, mafic vs. felsic) and the geometry of the unit.

Table 2.6 Criteria to distinguish between primary and secondary embayments.

	Primary Constructional Embayments	Primary Destructional Embayments	Primary Syn-Volcanic Grabens	Secondary Structural "Embayments"
Geometry	Consistently shallow (2－30m), flat-floored, and commonly (but not always) re-entrant over basaltic substrates; should be modified by thermomechanical erosion over sedimentary and intermediate-felsic volcanic substrates	Shallow to deep (depending on erodability of substrate); concave (if lava fills channel) or re-entrant (if lava does not fill channel), normally irregular on small scale especially where sulfides are present	Variable rather than consistent depths; flat-floored with steep sides; normally highly elongate; should be modified by thermomechanical erosion over sedimentary and intermediate-felsic volcanic substrates	Faults or folds that offset or deform the ore zones, host rocks, and the stratigraphy in the footwall rocks and host rocks
Orientation	Controlled by volcanic pitchline; elongate subparallel to the shoots, but may be elliptical; may also be subparallel to flow directions in footwall rocks	Controlled by volcanic pitchline; elongate subparallel to ore shoots, sediment-free contact zones, and possibly (but not necessarily) flow directions in footwall rocks; petrologically-distinctive host units (which will show only local evidence of contamination)	Elongate subparallel to the ore shoots, but lava flow may not necessarily have been parallel to grabens; no sediment-free zones unless removed by thermomechanical or mechanical erosion	May be subparallel to the same trends if localized on pre-existing volcanic trends, but normally moderately discordant on the larger scale and always markedly discordant on the smaller scale
Transgression	None unless modified by thermomechanical erosion	Ores and host units transgressive to stratigraphy in footwall rocks	None unless modified by thermomechanical erosion	None except that produced tectonically
Basal Komatiite Unit	Unit within embayment is normally thicker (15－100m, ave 50m) and more magnesian (45%－40% MgO) with lower Cr-Al-Ti, formed from more magnesian olivine (Fo_{94-91}) and more magnesian magma (up to 31% MgO), and is characterized by mesocumulate with lesser orthocumulate and crescumulate textures. Unit outside embayment is normally thinner (5－30m, ave 20m) and less magnesian (40%－35% MgO) with higher Cr-Al-Ti, formed from less magnesian olivine (Fo_{91-89}) and less magnesian magma (up to 26% MgO), and is characterized by orthocumulate and crescumulate textures. There may also be distinctive contamination and PGE depletion signatures.			Basal unit will be faulted or folded and will be more or less identical inside and outside the embayment (if embayment is completely structural)
Ore Horizon	Localized in embayment unless there has been some "spill over"	More likely to be completely localized in embayment, but some may spill over	Localized in embayment unless there has been some "spill over"	Extends beyond embayment unless there was a pre-existing embayment
Interflow Sediments	May be present if no thermomechanical erosion (distal)	More likely to be completely eroded	May be present if no thermomechanical erosion (distal)	Extends within embayment (if embayment is completely structural)
Lateral and Footwall Rocks	Lava facies commonly (but not necessarily) different; younging indicators face in the same direction as the rest of the stratigraphic section	Lava facies similar unless erosion localized on specific lithologies (less consolidated, more felsic) or discontinuities	Lava facies similar except by accident	Lava facies similar; younging indicators face upward for faults but outward/downward for folds
Lateral Margin	Aphyric rocks with random spinifex or thermally recrystallized decussate textures and geochemical compositions similar to the upper and lower chilled margins of the same units			Metasomatized cumulate komatiites characterized by schistose fabrics, more Si-rich mineral assemblages (e.g., talc-tremolite vs. serpentine-chlorite or talc-chlorite), but same low Al-Ti contents as cumulate komatiites
Ore "Pinchout"	Decorated with skeletal ferrichromites, identical to those on other primary contacts and produced experimentally			Fault or thrust, no ferrichromites
Contact Metamorphism	Varies with thickness of host unit; minimal in basalts, minor in coherent andesites and dacites, more significant in unconsolidated sediments			
Unmodified to Slightly Modified Examples	Durkin Main, Ken Far East, Juan East, Juan B, Lunnon, Victor shoots at Kambalda	Alexo, Raglan, Silver Swan, Sothman	No unequivocal examples	parts of many shoots in the Kambalda district
Modified Examples	Most other shoots in the Kamblada district (e.g., Fisher, Gibb, Hunt, Long)	Mt. Keith, Perseverance, Windarra		

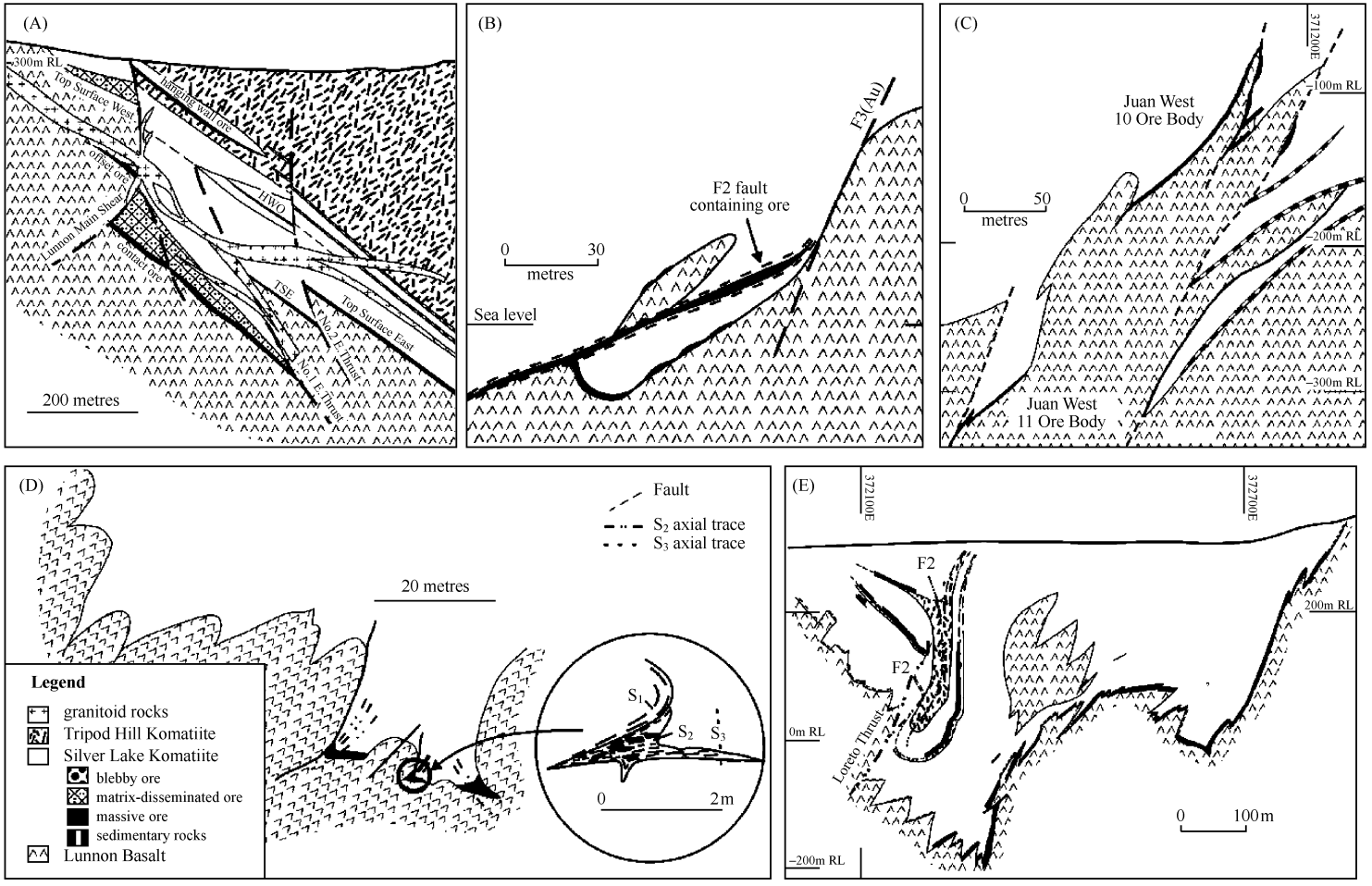

Fig 2. 10 Modified primary embayment (A) and primarily structural embayments (B-E) at Kambalda. (A) E-W cross-section 546250N (looking N) through Lunnon shoot on the southeast flank of the Kambalda Dome (from Stone and Archibald, 2004 as modified from Cowden and Roberts, 1990). Compare with Fig 2. 32 and see discussion below. (B) E-W cross-section #44 through Hunt shoot on the southern flank of the Kambalda Dome, showing thrusting of "Hood Basalt", 14C ore horizon (above basalt slice), and 08F ore horizon (under basalt slice) into the komatiite sequence and folding of underlying 02C ore horizon (from Stone and Archibald, 2004 as modified from Cowden and Roberts, 1990). (C) E-W cross-section 551420N (looking N) through the western part of the Juan complex on the north flank of Kambalda Dome, showing of the Juan West 10C and 11C ore horizons by major reverse-thrust faults (from Stone and Archibald, 2004 as modified from Cowden and Roberts, 1990). (D) E-W cross-section 84 through Hunt D Zone Deeps showing D_2 mesoscopic folds and related massive ore fabrics (from Stone and Archibald, 2004 as modified from Cowden and Archibald, 1987). (E) SW-NE cross-section (looking NW) through Fisher shoot on the western flank of Kambalda Dome, showing a series of very complex structural embayments (from Stone and Archibald, 2004 as modified from a WMC Internal Report).

2.1.7 Ore-localizing embayments

Like Type I deposits in other associations (e.g., Duluth, Noril'sk, Sudbury), most Type I komatiite-associated deposits are localized in or over embayments in the footwall. The only exceptions appear to be extremely deformed deposits (e.g., Harmony, Nepean, Redross, Rocky's Reward, Trojan, Thompson) where the nature of any primary ore-localizing feature has been obliterated and small deposits (e.g., Bannockburn) or smaller parts of larger deposits (e.g., Top Surface West at Lunnon shoot; see below). The geometries of the ore-localizing features vary considerably from deposit to deposit, including: (1) broad concave depressions of various depths (e.g., Alexo, Digger Rocks, Langmuir, Perseverance, Scotia, Silver Swan), Wannaway, Windarra, many shoots in the St. Ives and Tramways areas at Kambalda, and the first-order embayments at Raglan); (2) re-entrant, flat-floored troughs (e.g., most shoots at the Kambalda Dome), and more rarely; (3) deep, narrow troughs that are markedly transgressive to the footwall stratigraphy (e.g., Mickel, several shoots at the Kambalda Dome).

Some embayments are elongate parallel to the length of the ore shoots and host units (e.g., most shoots at Kambalda), some are more irregular (e.g., Langmuir, second-order embayments at Raglan), and some are elliptical (e.g., Ken Far East and Juan East at Kambalda; see Lesher, 1989). Some embayments are quite complex, comprising multiple orders of nested embayments (e.g., Alexo, Raglan). Those overlying sedimentary, felsic, or coarse-grained mafic substrates are transgressive to the footwall stratigraphy (e.g., Alexo, Digger Rocks, Raglan, Sothman, Windarra), but those overlying basalts are only locally slightly transgressive (e.g., Kamblada). Type Ⅱ deposits are also commonly localized over embayments in the footwall (e.g., Damba-Silwane, Hunter's Road, Mt Keith), although they are generally much broader.

Before proceeding further it is important to distinguish between primary and secondary embayments. Cas and Beresford (2001) suggested that "structural trough" should be used for fault-bounded depressions and that these should be distinguished from erosionally-formed "volcanic channels", but the geometries of both vary considerably. Not all structural or volcanic embayments are linear troughs or channels, and thermomechanical erosion can also be a modifying process. We will refer to features that clearly deform the ores, host rocks, and footwall rocks without any evidence of a primary embayment as *secondary* embayments and those that are undeformed or represent deformed syn-volcanic features as *primary* embayments. We will refer to primary embayments formed by constructive volcanic processes as *topographic embayments*, those formed by destructive volcanic processes as *erosional embayments*, and those formed by syn-volcanic faulting as *syn-volcanic grabens*. Criteria for distinguishing between the various types of embayments are given in Table 2.6.

Secondary embayments

There are a variety of tectonically-generated structures that mimick to varying degrees the geometries of primary ore-localiz embayments. The best examples are at Kambalda where Gresham and Loftus-Hills (1981) and subsequently Stone and Archibald (2004) and Stone *et al.* (2005) have shown that most of the larger-scale (>30m) relief on the komatiite/basalt contact at Kambalda is structural. The examples from Hunt, Juan West, and Fisher shoots (Fig. 2.10B-E) shown by Stone and Archibald (2004) are from some of the most deformed areas at Kambalda and most of the irregularities are structural, however, the examples from Lunnon, Victor, and Durkin shoots (Fig. 2.9A and Fig. 2.11A-B) are less deformed and less clearly entirely structural. Lunnon will be discussed in more detail below as an example of a modified topographic embayment, but the sections for Victor and Durkin both show 5 −30m "fault" offsets in the upper contact of the footwall basalt that are not reflected in the overlying komatiite sequence and the contacts are not all stratigraphically equivalent, making a purely structural origin unlikely. The "faults" bounding the western margin of the Victor West Trough (Fig. 2.11A), in particular, are purely interpretive and have been interpreted as high-angle normal faults by Stone and Archibald (2004) but as low-angle thrusts by Beresford *et al.* (2002). They could equally be interpreted as topographic embayments or syn-volcanic grabens. We will discuss this in more detail below, but first, we will examine several structurally-generated embayment margins, so that we will be able to distinguish them from primary or modified primary embayment margins.

One of the best examples of a structural embayment margin (Fig. 2.12A) was described by Frost and Groves (1989) at Foster Shoot in the St. Ives area of the Kambalda District. The NW margin of the ore horizon in the area they mapped was truncated by a fault that thrust pillow basalts over the ore horizon and some of the host cumulate komatiite. The cumulate komatiite was sheared into a foliated talc-carbonate-chlorite schist, there was no aphyric "chilled" komatiite margin, the pillows in the basalts were sheared, and ductile sulfides were thrust into brittle basalts. However, the lower contact of the ore horizon immediately adjacent to this was delicately scalloped and decorated by skeletal ferrichromites, the net-textured and weakly-mineralized cumulate komatiites were undeformed, and the ores contained subspherical to ameboidal komatiite inclusions (Fig. 2.12B, Fig. 2.13A-B). This highlights the extremely heterogeneous nature of the deformation at Kambalda.

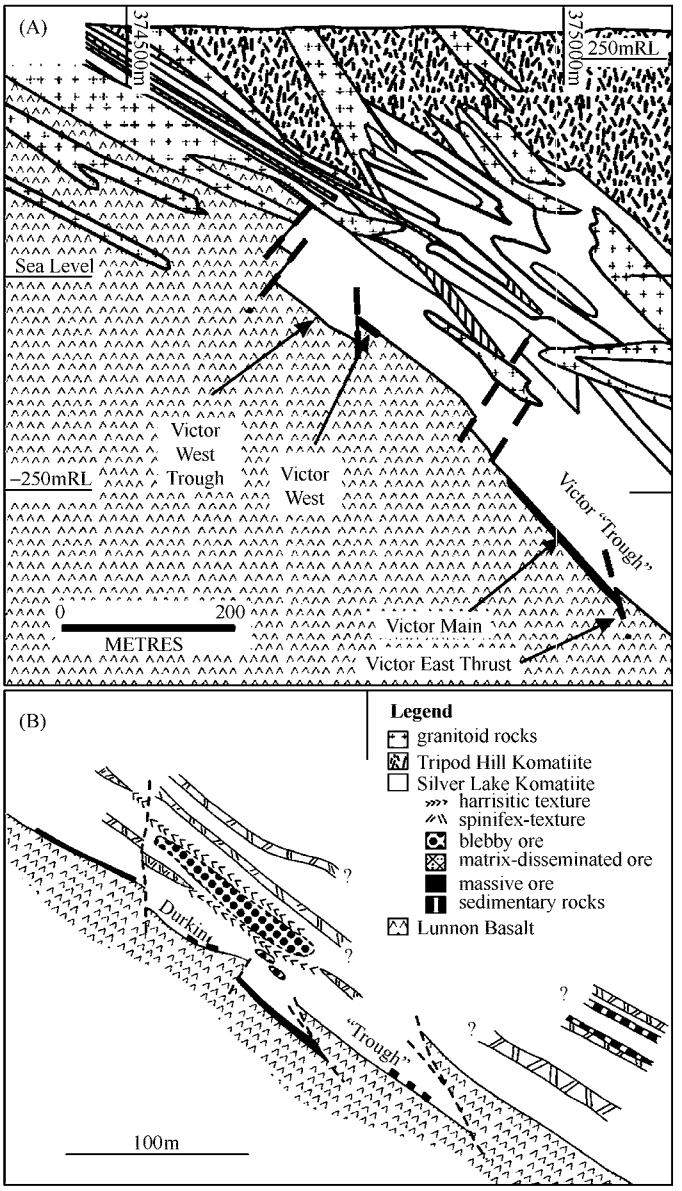

Fig. 2. 11 (A) E-W cross section at 547925N (looking N) through the Victor shoot on the east flank of Kambalda Dome (from Stone and Archibald, 2004 as modified from Middleton and Levy, 1977). Note absence of any offset in the hanging-wall stratigraphy above the Victor West Trough. (B) N-S cross section 372927E (looking W) through the Durkin shoot on the northeast flank of the Kambalda Dome (from Stone and Archibald, 2004 as modified from Cowden, 1988). Note absence of offset on the two features that define the northern ore horizon, absence of mineralization and presence of inter-flow sediments on the flanking margins, and the very coherent. stratigraphy in the koomatiite sequence

Other probable structural embayment margins have been described at D Zone Deeps at Hunt Shoot (Fig. 2. 10D) by Cowden and Archibald (1987) and in the Juan West 1210 area (Fig. 2. 14) by Stone and Archibald (2004). The ore horizon in the D Zone Deeps area was deformed by a series of cuspate folds, mobilizing the ores into several basalt-basalt pinchouts. Most of the present geometry is almost certainly structural, but we cannot be completely sure because the stratigraphy and volcanic facies in the basalts and komatiites were not mapped. If these features are entirely structural, the stratigraphy in the basalts and in the overlying komatiite sequence must also be deformed. The pinchout in the Juan West 1210 area exhibits more of the criteria of a structural pinchout, including the absence of a lateral aphyric "chilled" margin and ferrichromites.

Primary embayments

The geometries of primary embayments vary considerably from deposit to deposit, reflecting the different sizes of lava/magma conduits, different types of footwall rocks, and the modifying effects of superimposed deformation. *Basalts* will be less susceptible to thermomechanical erosion (Williams *et al*., 1998, 1999), more likely to exhibit small scale (2 −

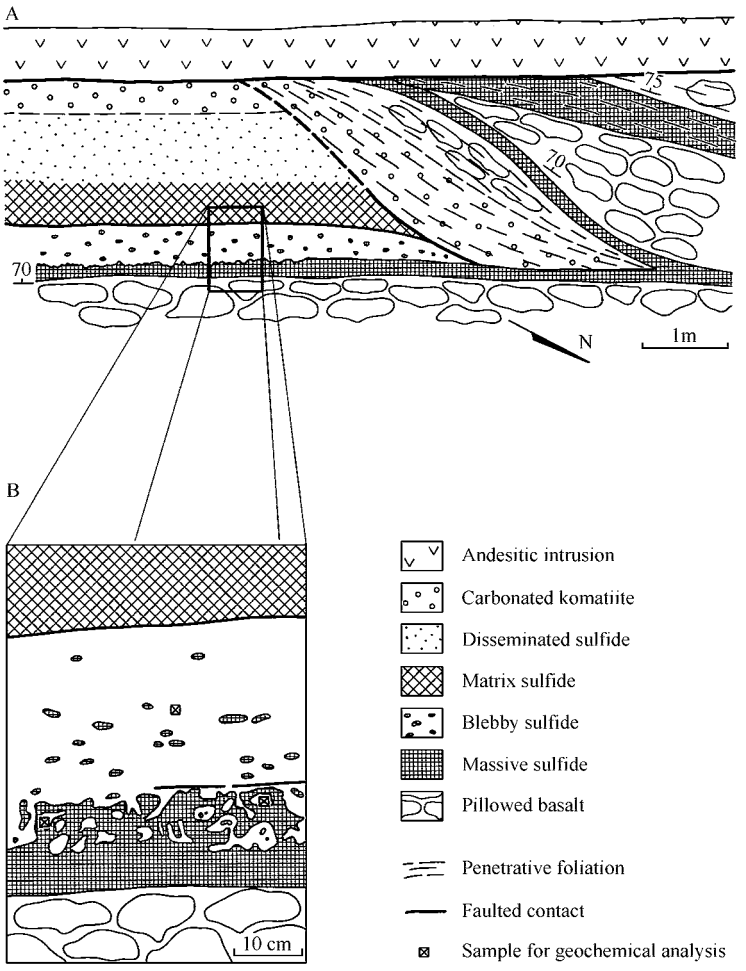

Fig. 2. 12 Structural embayment margin in the contact ore horizon 10 level, Foster shoot, Kambalda (Frost and Groves, 1989). Note presence of pillows above and below ore pinchout and the absence of an aphyric "chilled" margin between the cumulate komatiite and basalt, and the thrust mobilization of sulfides into the basalt.

30m) topographic relief (Lesher, 1989; Squire *et al*., 1998), and less likely to exhibit large-scale (> 100m) topographic relief. *Andesites and dacites* will be more susceptible to thermomechanical erosion (Williams *et al*., 1998; Williams *et al*., 2001), and more likely to exhibit significant amounts of relief on both local and regional scales (Davis, 1999; Cas and Beresford, 2001). Unconsolidated sediments and distal volcaniclastic rocks will be most susceptible to thermomechanical erosion (Williams *et al*., 1998; Williams *et al*., 1999), but least likely to exhibit significant amounts of relief on local or regional scales. With all else equal, larger lava/magma conduits (e.g., Mt. Keith, Perseverance) will erode more of the footwall rocks than intermediate (e.g., Pechenga, Raglan) or smaller (e.g., Kambalda) conduits.

Importantly, all Type I deposits in undeformed to only very slightly deformed areas (e.g., Alexo, Raglan, Sudbury, Noril'sk) are localized in embayments, most volcanic terrains exhibit 2－30m of topographic relief, there are very obvious physical reasons why dense sulfide melts would be localized in embayments and why many substrates would be susceptible to thermomechanical erosion, so it seems unlikely that any of the embayments in komatiite-associated deposits are entirely structural.

Syn-volcanic grabens

Ross and Hopkins (1975), Gresham and Loftus-Hills (1981), and Brown *et al*. (1999) suggested that the embayments at Kambalda were grabens bordered by feeding fissures, whereas Gresham (1986) suggested that they were grabens filled by lavas emplaced from the east. Some degree of faulting is expected in an intracratonic rift zone and some of the sharp discontinuities along the basal ore contacts at Kambalda (Fig. 2. 15C and E below; see also Marston, 1984) are not reflected in the overlying stratigraphy and have long been interpreted to be syn-volcanic, but synvolcanic structural activity cannot explain the differences in the facies of the basalts that form the embayments or the absence of syn-volcanic faults in their predicted locations along the margins of the embayments (Fig. 2. 15 A-E). Some of the "grabens" shown on sections (e.g., Fletcher Trough at Kambalda: Fig. 2b in Stone *et al*., 2005) are 25-year-old interpretations (cf. Fig. 3 in Gresham

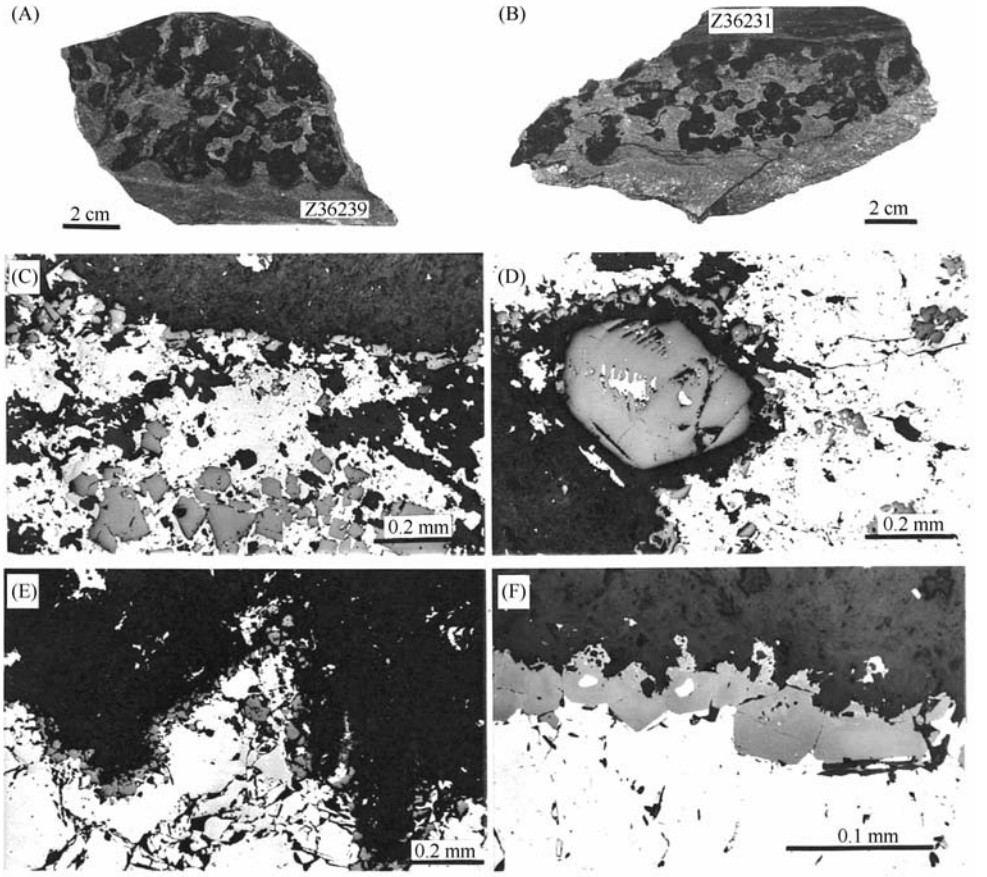

Fig. 2. 13 Textures at the contact between massive sulfide and blebby sulfide zone on the 10 level at Foster shoot, Kambalda (Frost and Groves, 1989a). (A) and (B) Spherical and amoeboid silicate inclusions (komatiite composition) in the upper 5 – 10 cm of a 15 – 40 cm thick massive sulfide layer. (C) Euhedral sulfide-associated spinels (medium gray) in massive pyrrhotite-pentlandite-chalcopyrite. Finer grained spinels are concentrated along the contact of a silicate inclusion (black) and massive sulfides. (D) Large euhedral and slightly skeletal spinel completely enclosed in a silicate inclusion in (A). A semicontinuous rim of spinel separates sulfide and silicate zones. Fine-grained spines are scattered throughout the sulfides. (E) A continuous layer of fine-grained spinel euhedra at the contact of silicate inclusions and the massive sulfide matrix in (A). (F) Close-up of contact-associated spinel in (E). Euhedral faces are well developed in sulfide, but grain margins with silicates are ragged and embayed. Spinels are zoned from dark gray cores (ferrochromite) to light gray Cr-rich magnetite rims.

and Loftus-Hills, 1981) in areas that have not been mined or mapped, and could easily represent topographic embayments. Despite virtually 100% exposure of the footwall during mining, there is no evidence of any volcanic feeders at Kambalda (Gresham and Loftus-Hills, 1981; Lesher, 1989) nor any of the transgressive komatiites, thermo-mechanical erosion features, and vent-facies breccias that characterize the central volcanic environments at Shangani and Kotselvaara (Pechenga). Although we can expect that some komatiite-associated Ni-Cu-(PGE) deposits emplaced into areas undergoing active extension may be localized in volcanic grabens, there are as yet no clear examples.

Erosional embayments

Nisbet (1982) noted that komatiites were very hot (up to 1640℃), very dense (~2900 km · m^{-3}), and very fluid (0. 1 – 1 g-cm · sec^{-1}), and suggested that they might have flowed turbulently and been capable of eroding their substrates and wall rocks. This process was modeled experimentally and numerically by Huppert *et al.* (1984), Huppert and Sparks (1985), and Jarvis (1995), who suggested that the re-entrant embayments at Kambalda could have formed by thermal erosion[1].

[1] We follow Williams *et al.* (1999) and define thermal erosion as the process that involves the breakup and removal of substrate by hot flowing lava, which may include both thermal ablation (i.e., melting) of consolidated and unconsolidated substrate due to heating by the lava and physical degradation (i.e., mechanical erosion) of unconsolidated or partly consolidated material and melt due to shearing or plucking by the moving lava, followed by partial or complete assimilation of melted substrate into the liquid lava.

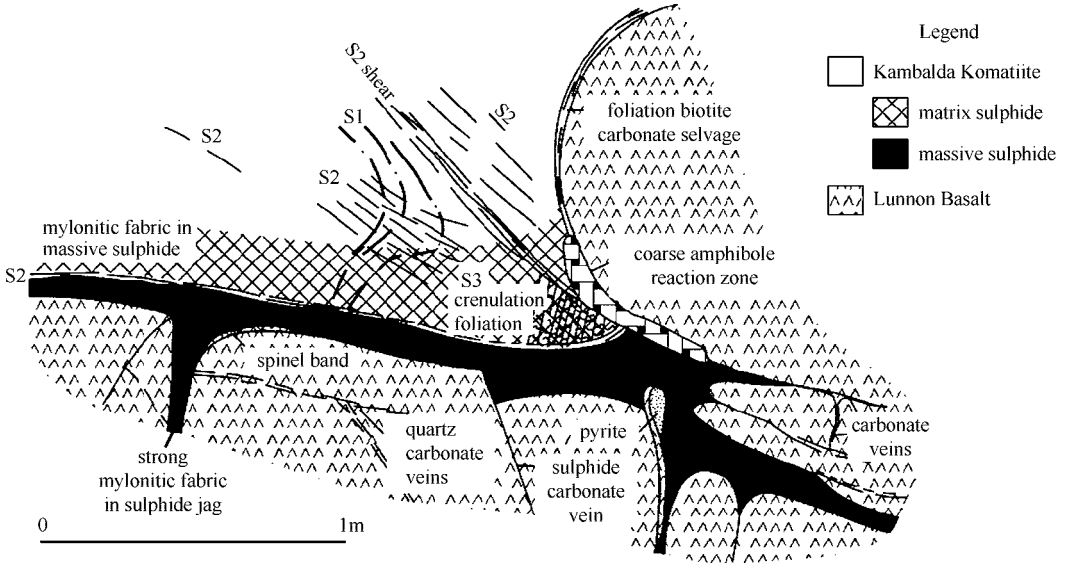

Fig. 2. 14 Map of a structural embayment margin formed by an F_2 fold-thrust couplet, Juan 1210/1-2 stope, east wall, south ore pinchout (from Stone and Archibald, 2004). Note that the basalt above and below the ore pinchout is massive, the margin of the embayment is bordered by a metasomatic reaction zone not an aphyric komatiite, and that there are no ferrichromites along the margins of the ore pinchout.

Kambalda

Although there is evidence for local erosion of basalt at Kambalda (see below), the flat floors of most of the primary and modified primary embayments at the Kambalda Dome are very different from the concave bases of the channels generated in analog experiments of thermo-mechanical erosion (Huppert *et al*., 1984; Huppert and Sparks, 1985) (e.g., Huppert *et al*., 1985; Huppert and Sparks, 1985; Jarvis, 1995; Kerr, 2001). Lesher *et al*. (1984) and Lesher (1989) argued that the flat-floored geometries and stratigraphic relationships of the footwall embayments at Kambalda indicate that they were not generated by thermo-mechanical erosion, but suggested that interflow sediments were completely eroded and that basalts appeared to have been locally eroded. Sediment erosion will be discussed below, but there is evidence for local thermal erosion of basalt by sulfides along the lateral margins of the ore zones (see below), for selective thermal erosion of the basaltic glass component of spinifex-textured komatiite by massive sulfides (see below), and for local mechanical erosion of basalt by sulfides along the base of the ore zones (see Frost and Groves, 1989; Squire *et al*., 1998; see discussion by Cas and Beresford, 2001). These features led Groves *et al*. (1986) to suggest that the re-entrant geometries of the embayments, including the elliptical embayments, might reflect local, selective thermal erosion by highly thermally conductive massive sulfides. The latter interpretation was criticized by Arndt (1986), who argued that a basal sulfide layer would have acted as a lower temperature boundary layer, but he assumed that the lower thermal boundary layer would be the same thickness as the sulfide layer, when it is likely (for the same reason that Arndt argued that the lower thermal boundary layer of the komatiite would have been relatively thin) to have been an order of magnitude thinner. Lesher (1983) and Arndt (1986) considered the possibility that the basal host unit might have eroded through the upper unit of basalt, explaining the absence of flow-top breccias, which are rarely present underneath the ores zones but commonly present on the tops of the penultimate basalt flows outside of the embayments, but Lesher (1989) concluded that this would be too fortuitous and favored a modified topographic origin, but it is possible that the sulfides eroded the flow-top breccias of many penultimate flows, explaining why they are so commonly present in the flanking sequence and not underneath the ore horizon. Williams *et al*. (1998) made many improvements to the Huppert and Sparks (1985) model used by Arndt (1986) and showed that significant erosion of basalt would likely occur only for longer eruptions at shorter distances from the eruptive site and that the amount of erosion would decrease much more rapidly for shorter eruptions and longer distances from the eruptive site than in the Huppert and Sparks models. However, there is much evidence at Kambalda for local thermo-mechanical erosion.

The best example of local thermo-mechanical erosion was that below the Lunnon 806 hanging-wall ore horizon described by Groves *et al*. (1986), where sulfides appear to have eroded an interflow sediment horizon and the upper flow top and random spinifex-textured zone of the underlying flow, infiltrated into the matrix of the platy spinifex-textured zone, melting the interstitial basaltic matrix, forming basaltic domes (Fig. 2. 16). Cas and Beresford (2001) suggested that such

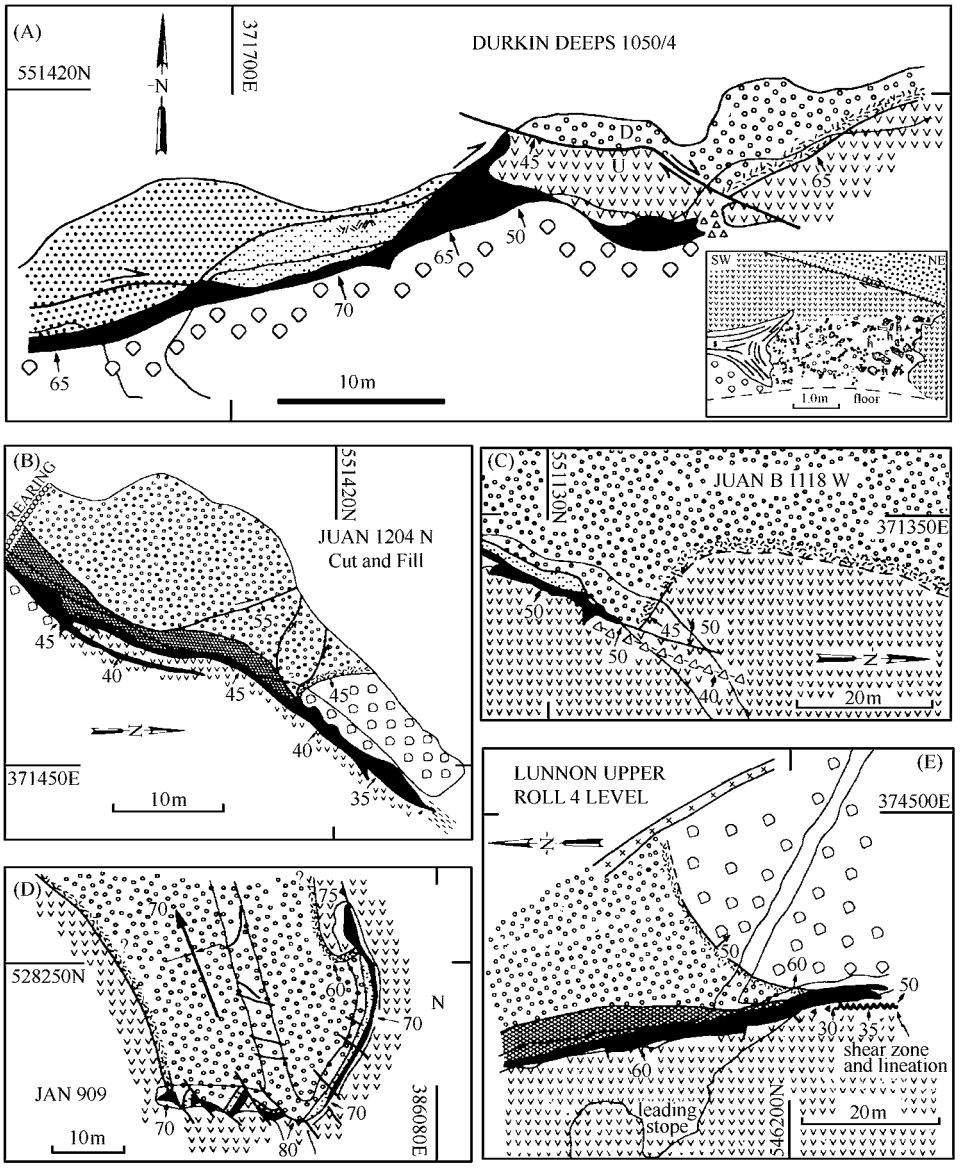

Fig. 2. 15 Maps of modified primary embayment margins at Kambalda. (A) Sublevel plan of Durkin Deeps 1050/4 (mapping by H. Paterson and CML). Ore pinchout is deformed, but terminates in a brecciated lava toe (see inset and Fig. 2. 35 below). After removal of the fault that displaces the outside flanking contact, it is evident that the basalt below the ore horizon is pillowed but that forming the margin of the embayment is massive and bordered by an aphyric lower "chilled" komatiite margin. (B) Plan Juan 1204N cut and fill (mapping by H. L. Paterson and CML). Ore pinchout is sheared parallel to contact, but basalt below ore horizon is massive, basalt above pinchout is pillowed and faces upward, and embayment margin is unsheared and bordered by aphyric komatiite. (C) Level plan of Juan B 1118W drive (mapping by B. D. Kay and D. N. Harley). Ore horizon is overlain by a fault, but correlates with a broken-pillow flow-top breccia and the margin of embayment is unsheared and bordered by aphyric komatiite. (D) Jan 909 drive (mapping by W. Bannister and CML). Ore horizon is deformed by a steeply plunging D2 fold and locally offset by faults subparallel to the axial plane of the fold, but the NE pinchout (see Fig. 2. 18 below) is oblique to the orientation of the deformation and both the NE and S enbayment margins are unfaulted and bordered by unsheared aphyric komatiite. (E) Lunnon Upper Roll 407 drive-419 crosscut area (mapping in leading stope by WMC, remainder by CML). Pinchout is sheared subparallel to contact, but basalt below ore horizon is massive, that above pinchout is pillowed and youngs upwards, and embayment margin is bordered by random spinifex-textured komatiite (see Fig. 2. 32, Fig. 2. 33A-C below). Lithologies: massive basalt ("v" pattern), pillowed basalt and younging direction (pillow symbol), aphyric komatiite (random dashes), cumulate komatiite (random circles), disseminated ore (dots), net-textured ore (cross-hatch), massive ore (black). All faults and shears are indicated; rocks are otherwise unfoliated. Solid lines are mine openings; all mapping projected to breast height.

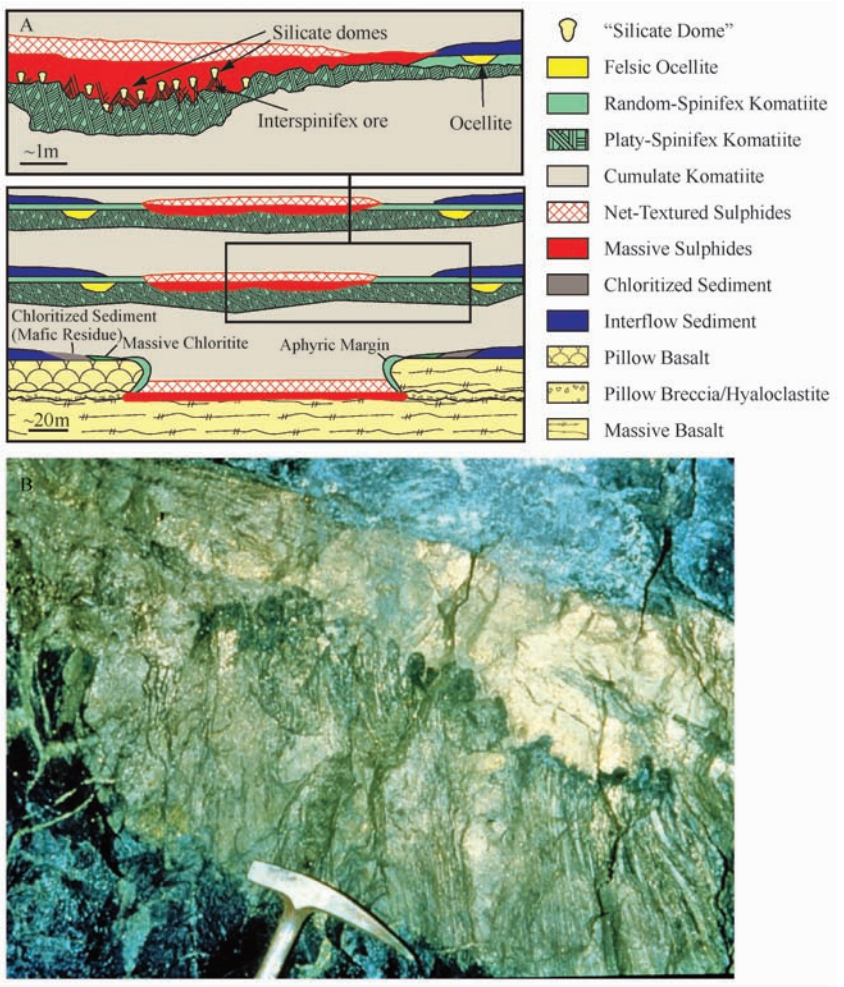

Fig. 2. 16 A. Schematic section of the Lunnon 628 hangingwall ore horizon (modified after Groves *et al*., 1986). B. Photograph of massive ore, silicate domes, and spinifex-textured ore from the same area (photo by M. J. Donaldson).

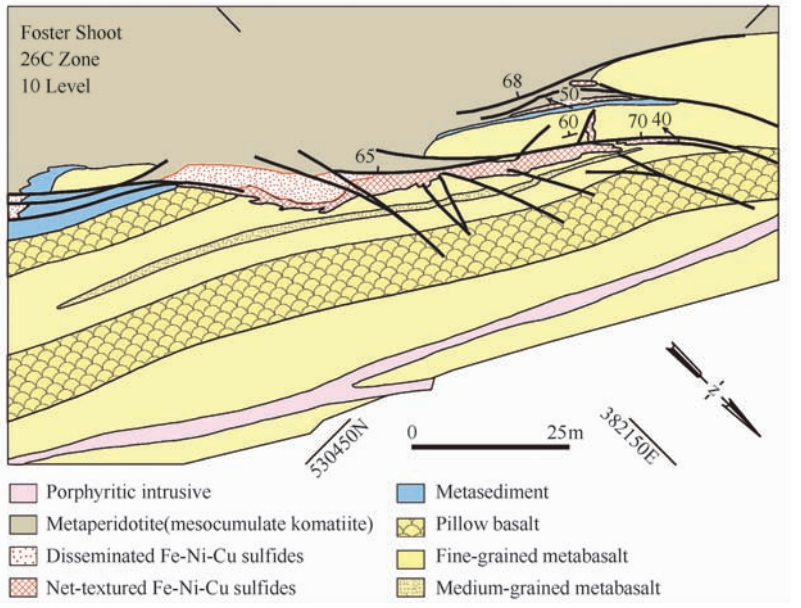

Fig. 2. 17 Map of part of the 26C ore horizon on the 10 level of Foster shoot in the St. Ives area of the Kambalda District (from Evans *et al*., 1989). NW end of embayment is faulted, but basalt flanking embayment is massive, whereas that below ore horizon is pillowed. Ore contact is delicately scalloped (see Fig. 2. 12), not faulted, but transgressive to stratigraphy in underlying basalts, consistent with thermomechanical erosion.

ores formed during metamorphism and Stone and Archibald (2004) suggested that they formed by folding, but neither of these explains the missing sediments, chilled upper margin, and random spinifex-textured zone, the almost perfect preservation of spinifex texture, and the transitions from sulfides to the mesostasis adjacent to pseudomorphs after olivine plates, the similarity of chemical compositions (Ni, Cu, Co, PGE) of spinifex-textured ore and overlying massive ore (Woolrich *et al.* 1981), the occurrence of magmatic ferrochromites in spinifex-textured ores and chromite zones on silicate-sulphide interfaces as in magmatic ores (Groves *et al.*, 1977), the randomly-buckled orientations of the olivine blades, consistent with emplacement of hot sulfide liquid between them, and the occurrence of small chromite-rimmed, silicate-rich domes, consistent with the composition of interpreted segregations of displaced silicate liquid (Groves *et al.*, 1986). Stone and Archibald (2004) argued that the domes were not contact metamorphosed, but they should not be contact metamorphosed if magmatic.

A good example of local thermomechanical erosion of basalt was described at Foster Shoot (Fig. 2. 17) by Evans *et al.* (1989). Stone and Archibald (2004) used this as an example of where detailed structural analysis indicated that 3D polyphase deformation can explain trough formation from a roughly planar contact. However, Evans *et al.* showed that the ore pinchout was faulted (as in the example above) but that tectonic movement could not account for the observed embayment and that floor of the embayment clearly transgressed the underlying basalts in a manner that they considered to be most consistent with thermomechanical erosion. Evans *et al.* considered the depth of the primary embayment to be 5m, but it clearly cuts through the upper pillowed division and half of the lower massive division of the uppermost basalt flow unit. After correction for dip, the thickness appears to be closer to 15m (see Fig. 2. 17).

Basalt-basalt ore pinchouts at Kambalda are commonly sheared (Fig. 2. 15B, C, and E), as ductile sulfides have been a locus for deformation, but there are many other occurrences where they are undeformed and clearly transgressive to the enclosing basalts (e.g., Fig. 2. 15A and D, Fig. 2. 18A-D, Fig. 2. 19A).

Even where deformed, the ores in the pinchouts are only

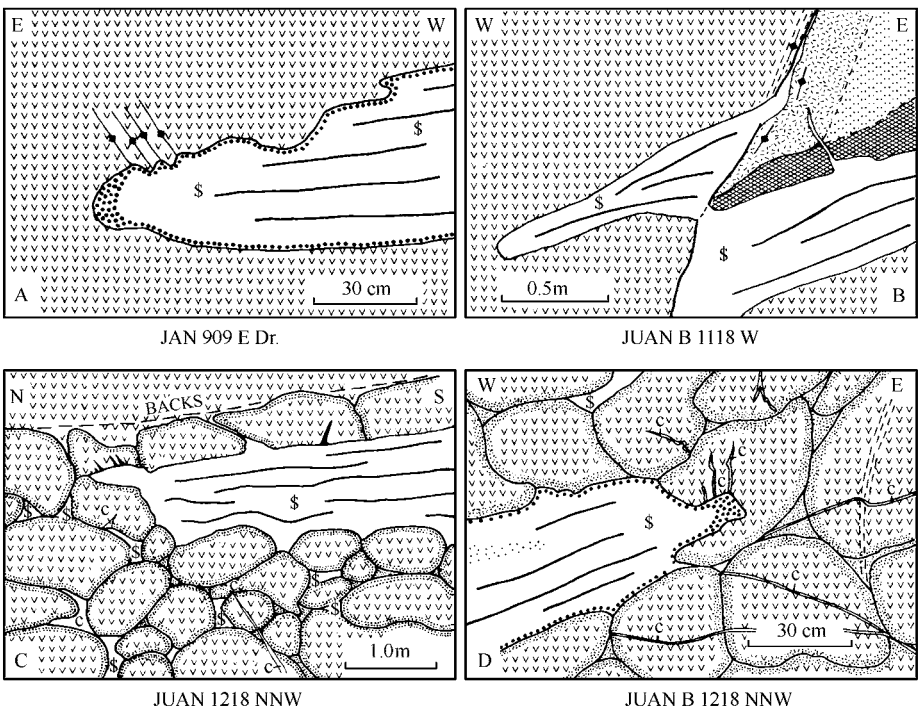

Fig. 2. 18 Face sketches of primary ore pinchouts at Kambalda. A. Northeast end of Jan 909 level. Basalt at end of pinchout is foliated parallel to the axial plane of the D_2 fold structure that deforms the ore horizon, but not ot the trend of the pinchout (see Fig. 2. 15A) and is unfoliated, unfaulted, and decorated with ferrichromites. B. Northwest margin of Juan B 1118W open stope (see Fig. 2. 19 below). Contact between basalt and komatiite is sheared parallel to contact and ore horizon is offset by a fault, but the pinchout is unfaulted and decorated with skeletal ferrichromites (see Fig. 2. 19B-C). C. NW margin of Juan B 1218 NNW ore body. Lower contact conforms to underlying pillow basalt surfaces and upper contact is transgressive to pillows, but ore pinchout is unfaulted. Interpillow spaces around pinchout are mineralized (see Lesher and Keays, 1984). D. N margin of Juan B 1218 NNW ore body. Ore transgresses pillow basalt, but is unfaulted and basalts are unfoliated. *Lithologies*: massive unfoliated basalt ("v" pattern), pillowed basalt and younging direction (pillow symbol), spinifex-textured komatiite (random dashes), cumulate komatiite (random circles), disseminated sulfides in cumulate komatiite (dots), nett-extured sulfides (cross-hatch), massive sulfides (white with Po-Pn layering indicated).

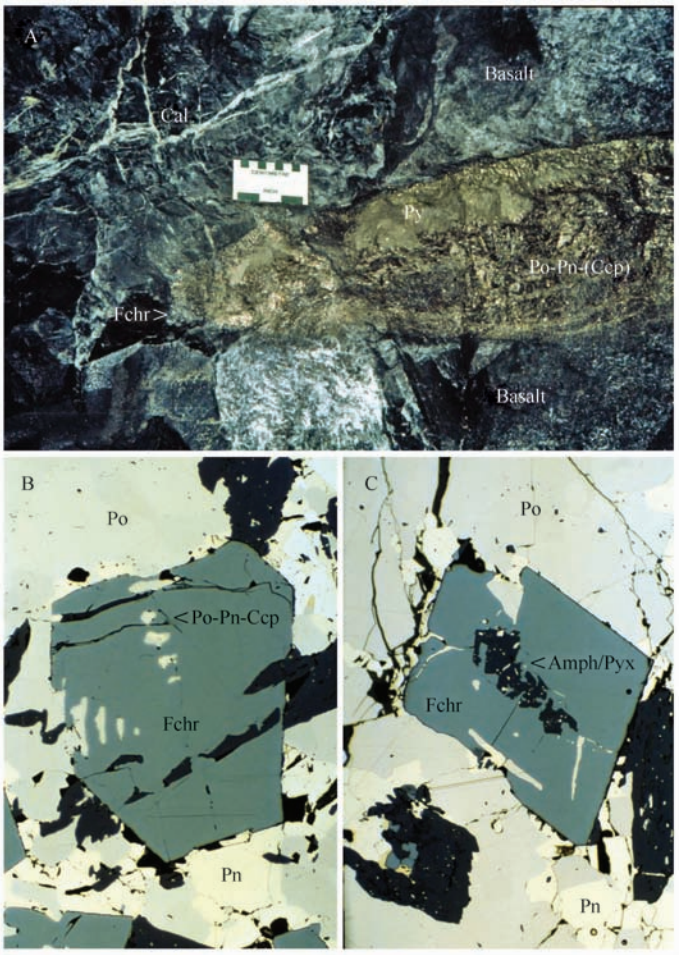

Fig. 2. 19 A. Basalt-basalt ore pinchout at Juan B 1108 stope. There is a carbonate-filled shear above the pinchout, but the basalt around the pinchout is massive and unfoliated (lighter areas are calcite-covered fractures, darker areas are chlorite-filled fractures). B. Skeletal ferrichromite from nose of pinchout containing inclusions of a magmatic pyrrhotite-pentlandite-(chalcopyrite) assemblage. C. Skeletal ferrichromite from same location containing a plumose amphibole (after pyroxene?) crystal.

very rarely enriched in chalcopyrite, which is much more ductile than pyrrhotite and pentlandite (see discussion by Barrett *et al*., 1977; McQueen, 1987). This suggests that most ore pinchouts, especially those that are unfaulted but including those that have been sheared, have not formed tectonically. This leaves several possible origins, none of which are mutually exclusive and all of which may have been important in different areas: (1) Molten sulfide melts may have laterally infiltrated the contact between flanking basalt flows. Molten sulfides are very dense and preferentially wet silicates (see discussion by Ebel and Naldrett, 1997), so they could have very easily been drawn in along lateral contacts. (2) Sulfide melts may have selectively melted basaltic flow-top breccias. Sulfide melts would have been superheated by the komatiite lava and have very high thermal conductivities, so it is possible that they may have selectively melted unconsolidated flow-top breccias (e.g., Fig. 2. 15A) or massive or pillowed basalt (e.g., Fig. 2. 18A-D). This may explain the re-entrant geometries of elliptical shoots like Ken Far East (fig. 5. 15 in Lesher, 1989) or Juan Far East, which may have originated as collapse features (see Fig. 2. 36D below). As discussed by Marston (1984), this is much more plausible than generative them via a "cone thrusting process". (3) Sulfides may have been mobilized along basalt contacts during metamorphism (see discussion by Barrett *et al*., 1977 and McQueen, 1987). However, the ductilities during metamorphism are chalcopyrite ≫ pyrrhotite/monosulfide solid solution (*mss*) > pentlandite ~ pyrite > chromite, so even if all of the Cu and Ni were dissolved in *mss* this cannot explain any of the pinchouts that are decorated by skeletal ferrichromites. None of these requires dislocation of the contact, explaining why the contact is so well preserved in so many localities (Ewers and Hudson, 1972; Evans *et al*., 1989; Frost and Groves, 1989; Lesher, 1989).

The floors of the embayments at the Kambalda Dome commonly correlate with thin (normally 0. 2 – 2m) flow-top breccias that define unit boundaries in the enclosing basalts (Fig. 2. 15A and C; see Fig. 2. 32 and Fig. 2. 35B-D below);

additional examples in Lesher, 1989), but ores only rarely overlie flow-top breccias. Where they do overlie flow-top breccias, the breccia matrix has been replaced by sulfides (Fig. 2. 35E). Although spinifex blades are interconnected and difficult to thermally or mechanically erode, pillow fragments are isolated and should be easily buoyed up and mechanically eroded by dense sulfide melt. This and the low Cr contents of such mineralization led Lesher and Keays (1984) to suggest that interbreccia sulfides had been mobilized into the breccias during metamorphism and deformation, rather than percolated in during ore emplacement. In any case, the absence of flow-top breccias underlying the embayments in areas where one is present in the flanking stratigraphy suggests that they may have been thermomechanically eroded.

Notwithstanding the paucity of evidence for generation of embayments by erosion of basalt at Kambalda, there is a large and growing body of physical and geochemical evidence for selective thermal erosion of komatiite, local thermomechanical erosion of basalt, moderate thermomechanical erosion of gabbro, andesite, and dacite, and significant thermomechanical erosion of unconsolidated sediments in many komatiite-associated Ni-Cu-(PGE) deposits (Table 2. 7).

Table 2. 7 Summary of evidence for wholesale, partial, or incongruent melting at selected Type I magmatic Ni-Cu-(PGE) sulfide deposits (modified from Lesher and Burnham, 2001).

Deposit	Physical Evidence	Geochemical Evidence
Komatiitic		
Alexo	Transgressive embayment, footwall dikes/sills/protrusions, rare xenoliths	*Local* HILE enrichment and Nb-Ta depletion in host rocks
Bannockburn	No embayment, lower contact is altered/hornfelsed	*Local* HILE enrichment and Nb-Ta depletion in host rocks
Dundonald South	Transgressive embayment?	
Forrestania	Transgressive embayments; rare xenoliths	*Local* HILE enrichment in host rocks
Kambalda	Sediments missing under and adjacent to ores, grade laterally into decomposed sediments; ores locally transgress sediment, basalt, and komatiite; rare xenomelts, very rare xenoliths	Non-magmatic S and Pb isotopes and S/Se in ores, *local* HILE enrichment, anomalous Nb-Ta, and anomalous Nd isotopes in host rocks, *local* chalcophile element depletion in host rocks
Langmuir	Transgressive embayment	Non-magmatic S isotopes and S/Se
Namew Lake	Local orbicular textures	Anomalous Cu-Zn-Pb abundances and Pb isotopes in ores; HILE enrichment in host rocks
Pechenga	Transgressive embayments, contact metamorphosed wall rocks, xenoliths	Anomalous S and Os isotopes in ores
Perseverance	Transgressive embayment	*Local* HILE enrichment and Nb-Ta depletion, and chalcophile element depletion in host rocks
Raglan	Transgressive embayments, contact metamorphosed footwall rocks	Non-magmatic S isotopes and S/Se in ores; *local* HILE enrichment in host rocks
Black Swan, Silver Swan, and Gosling	Partially molten and recrystallised footwall xenoliths	
Thompson	Local transgressive relationships between ores and SUIF	Non-magmatic S isotopes and S/Se; *local* HILE enrichment and Nb-Ta depletion in host rocks
Windarra	Ores transgress underlying SUIF	Non-magmatic S isotopes and S/Se
Picritic/Basaltic		
Duluth	Transgressive embayments, contact metamorphosed wall rocks, xenoliths	Non-magmatic S, Os, Pb isotopes, and S/Se in ores, anomalous Cu-Zn-Pb abundances in ores, *locally* anomalous H-C-O-S-Os-Pb isotopes in host rocks
Noril'sk	Xenoliths, contaminated varitextured "taxitic" gabbros, extensive contact metamorphism	Non-magmatic S isotopes in ores, *local* HILE enrichment, local chalcophile element depletion, anomalous Sr-Nd isotopes in host rocks
Voisey's Bay	Abundant xenoliths	Non-magmatic S and Os isotopes in ores, non-magmatic O isotopes in host rocks; *minor* non-magmatic Nd-Sm-Pb isotopes in host rocks; *local* chalcophile element depletion in host rocks
Crust-Dominated		
Sudbury	Transgressive embayments, extensive breccia zones, abundant xenoliths	Non-magmatic Os isotopes in ores; *wholesale* HILE enrichment, and crustal Sr and Nd isotopes in host rocks

* Enrichment in U-Th-LREE relative to Nb-Ta and sometimes also MREE-HREE relative to Ti.

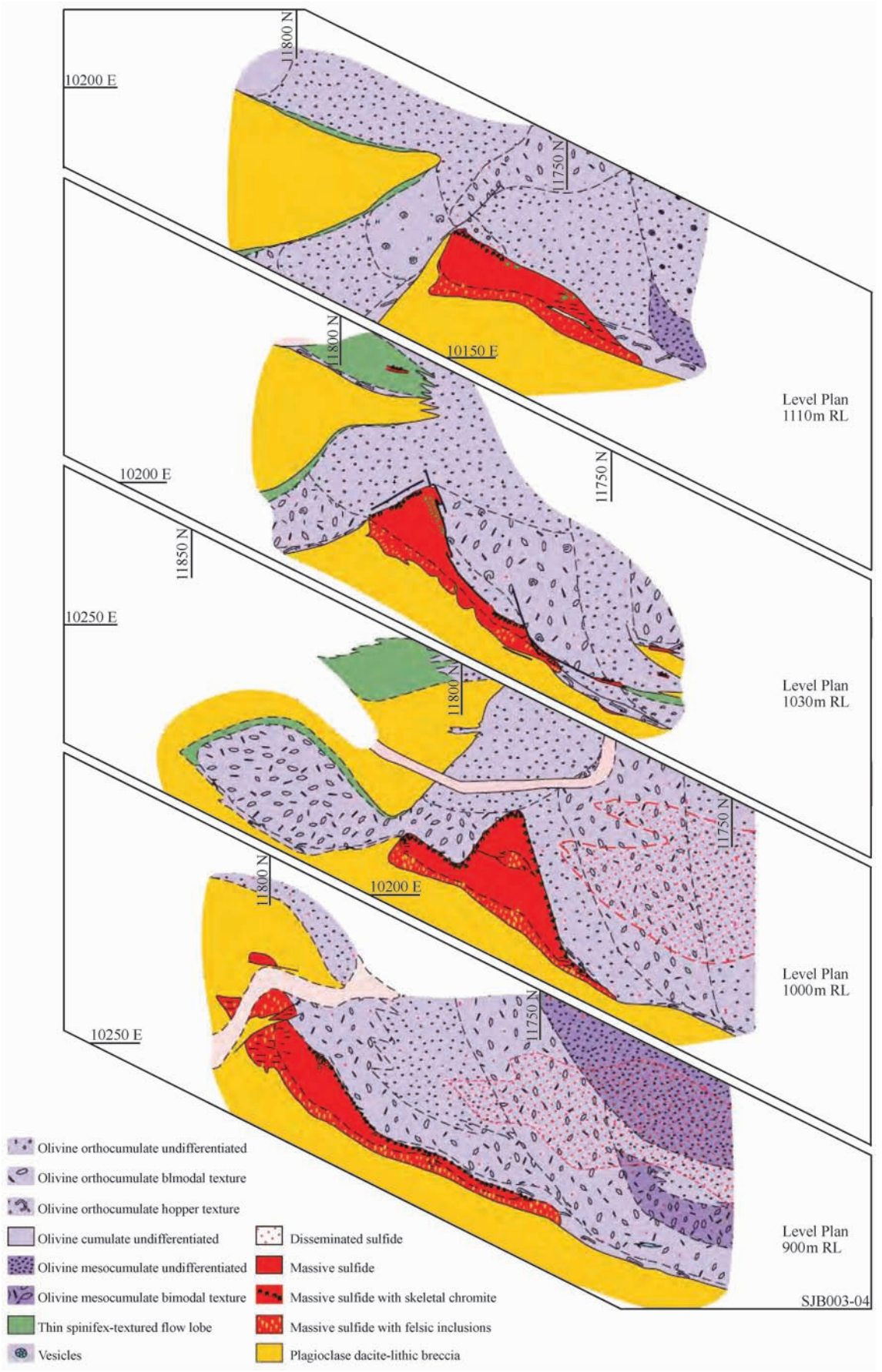

Fig. 2. 20 Level plans of the Silver Swan orebody (Dowling *et al*., 2004).

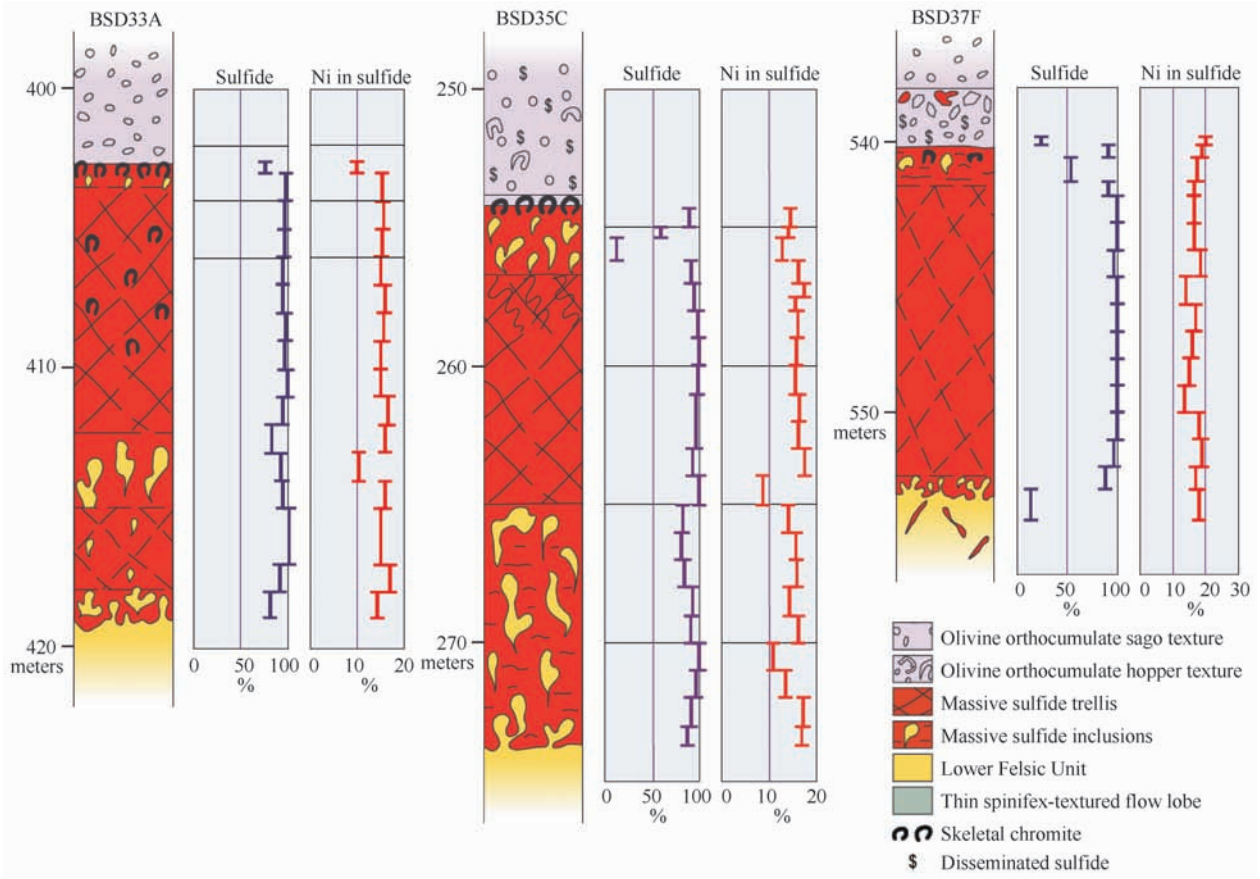

Fig. 2. 21 Silver Swan drill hole profiles (Dowling *et al*., 2004).

Silver Swan

The ores at Silver Swan (Dowling *et al*., 2004; Hill *et al*., 2004) (Fig. 2. 20) exhibit some of the best-preserved magmatic textures observed in any komatiite-associated Ni-Cu-(PGE) deposit, including delicately scalloped contacts between massive ores and underlying dacites (Fig. 2. 20), plumes of melted dacite (Fig. 2. 21, Fig. 2. 22) and other field and geochemical evidence of contamination of komatiite by dacite, and skeletal ferrichromites along all contacts with massive sulfides (Fig. 2. 22E and F). The dacite plumes are analogous to those produced experimentally (Kerr submitted to JGR). The basal contact with the felsic footwall is very irregular (Fig. 2. 20), generally unsheared, and topographic highs correspond to presence of relatively coherent dacite, so it has been interpreted as primary (Hill *et al*., 2004). However, the evidence for local incorporation of fragmental dacite leaves no doubt that the original topography was modified by thermo-mechanical erosion.

Alexo

The broad shallow embayment at Alexo (Fig. 2. 23, Fig. 2. 24) was exposed on a spectacular glacially-polished outcrop that was mechanically-stripped and hydraulically-cleaned of glacial overburden providing continuous exposure of the mineralized basal contact between the komatiite and andesitic footwall rocks. The ores were localized in a series of nested embayments on scales from 100s of meters to a few centimeters with morphologies that varied from concave to re-entrant. The basal contact was very sharp but scalloped and clearly transgressed the footwall rocks without any evidence of a regolith, shearing, or folding. The footwall pillowed andesites were bleached and altered along the entire length of the contact, but the degree of alteration appeared to be thicker and more intense around embayments. Xenoliths of andesite were more common within embayments, komatiitic dikes penetrated downward into the host andesites primarily along the lateral margins of embayments, and komatiitic protrusions into the footwall extended laterally as thin (<2 cm) sills, capturing the last stages of the thermomechanical erosion process (Houlé and Lesher, submitted to *Mineralium Deposita*).

Katinniq (Raglan)

The broad deep embayment at Katinniq (Fig. 2. 25) transgresses underlying sediments and gabbro sills, and underlying semi-pelitic sediments have been metamorphosed to biotite zone (Williams *et al*., 1999; Lesher, 2007). The ores locally contain gabbro inclusions (Fig. 2. 26). The embayment has been interpreted as an thermomechanical erosional depression along the base of a subvolcanic sill (Barnes *et al*., 1982), as a lava pond (Barnes and Barnes, 1990), or as a

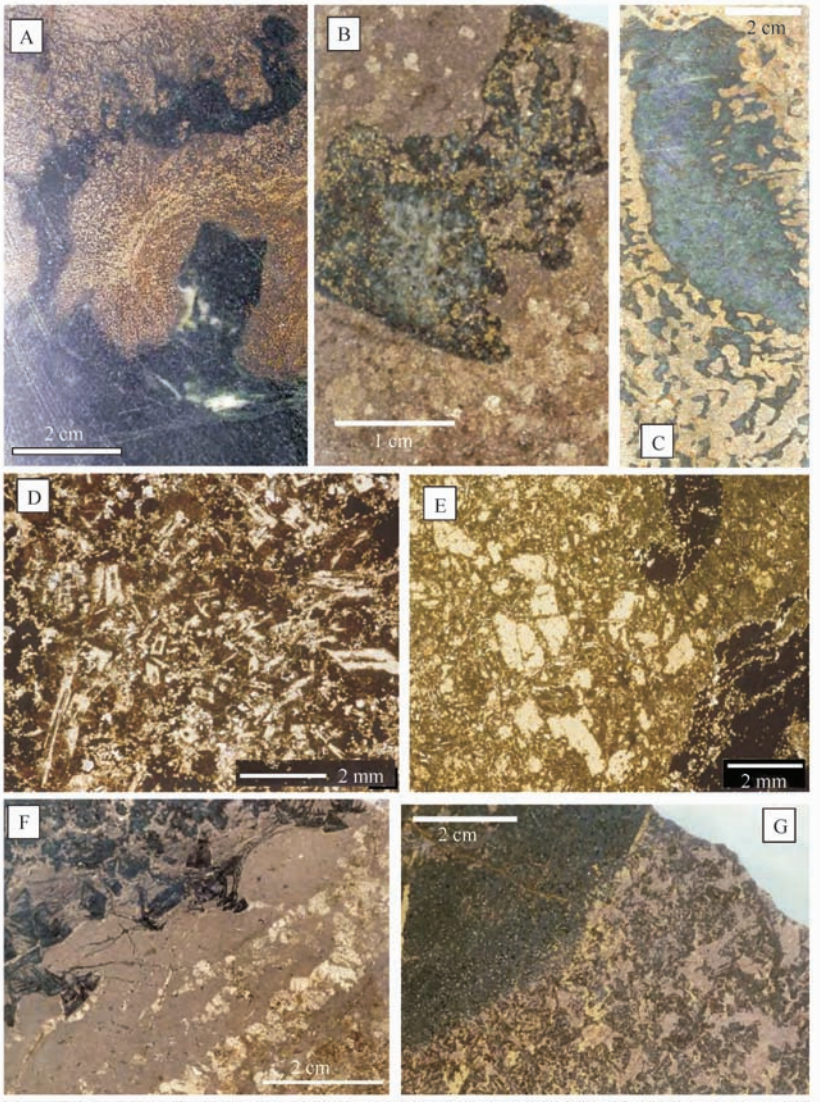

Fig. 2. 22 Silver Swan ores (modified from Dowling *et al*., 2004 and Barnes, 2006). A. Basal contact showing "plume" of partially molten dacite ascending into the sulfide pool. B. Dacite inclusion in massive ore showing unmelted core and remelted margin. C. Partially disaggregated dacite inclusion (xenomelt). D. (photomicrograph) Margin of dacite inclusion showing textures indicative of remelting and rapid cooling producing skeletal swallow-tail plagioclase. E. (photomicrograph) Unmelted dacite inclusion core. F, G. Skeletal ferrian chromite developed within massive sulfide at top contact with komatiite. Reflected light on core slabs except where stated.

deeply erosive lava channel (Lesher, 1999; Lesher, 2007). The latter interpretation seems more likely based on the asymmetric contact metamorphism (Lesher, 2007), the linear nature of the host unit in the subsurface (Osmond and Watts, 1999), and the linear trends of higher and lower tenor ore pods (Gillies, 1993). The second-order embayments that host the ore zones at Katinniq have been cut by faults in some areas, but those in the relatively undeformed eastern end are steep-sided irregular features with locally re-entrant geometries (Chisholm, 2002; Chisholm *et al*., 1999), some of which contain xenoliths of gabbro (see Lesher, 2007).

Perseverance

The deep broad embayment at Perseverance (Fig. 2. 27) was interpreted to overlie metamorphosed dacites and to be thermomechanical erosional (Barnes *et al*., 1988b; Williams *et al*., 2001), but has since been reinterpreted to overlie pelitic sediments intruded by quartz-feldspar porphyries (Trofimovs *et al*., 2003) and to be more structurally modified than originally appreciated (Libby *et al*., 1998). However, a purely structural interpretation does not explain the asymmetric upward and lateral gradations from adcumulate dunite to orthocumulate and aphyric komatiites and the contamination and chalcophile element signatures that accompany those variations (Barnes *et al*., 1988, 1995). The Libby *et al*. (1998) reconstruction retains most of the present geometry with both the host unit and the mineralization being confined to a broad

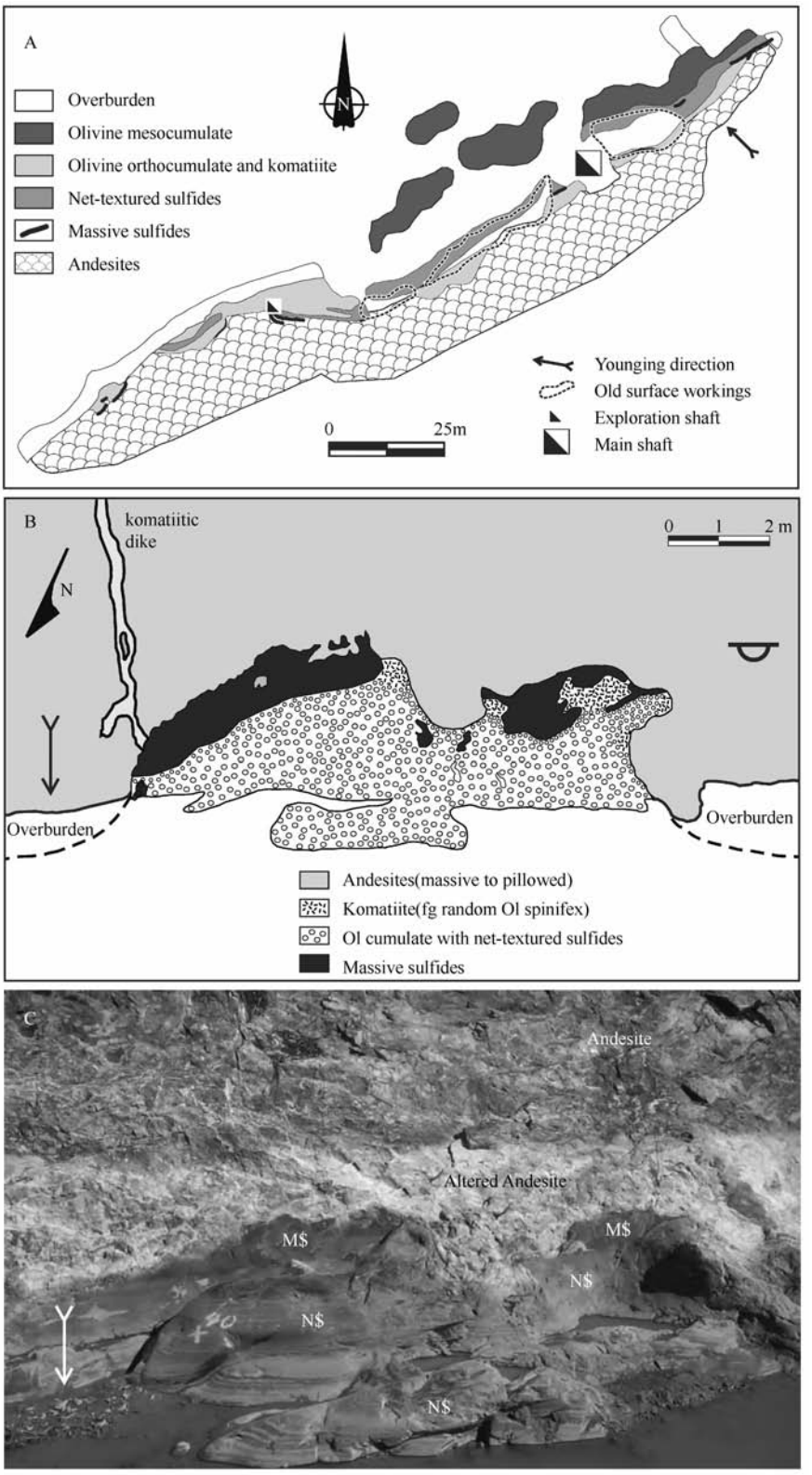

Fig. 2. 23 A. Simplified map of the Alexo mine area showing old surface workings and newly-stripped outcrops (from Houlé *et al*., 2002b, based on mapping by K. Montgomery and M. G. Houlé). Note the highly irregular and transgressive nature of the contact between komatiitic rocks and footwall andesites, which define a broad first-order embayment and several smaller second-order embayments. B. Map of second-order embayment at the SW end of outcrop in A, looking SE (mapping by M. G. Houlé). Note the highly irregular nature of the contact between the ores and footwall andesites. C. Photograph of the area shown in B (photograph by M. G. Houlé). Note the silicification of the andesites adjacent to contact and the komatiitic dyke extending downward into the andesites. M $ = massive sulfides; N $ = net-textured sulfides.

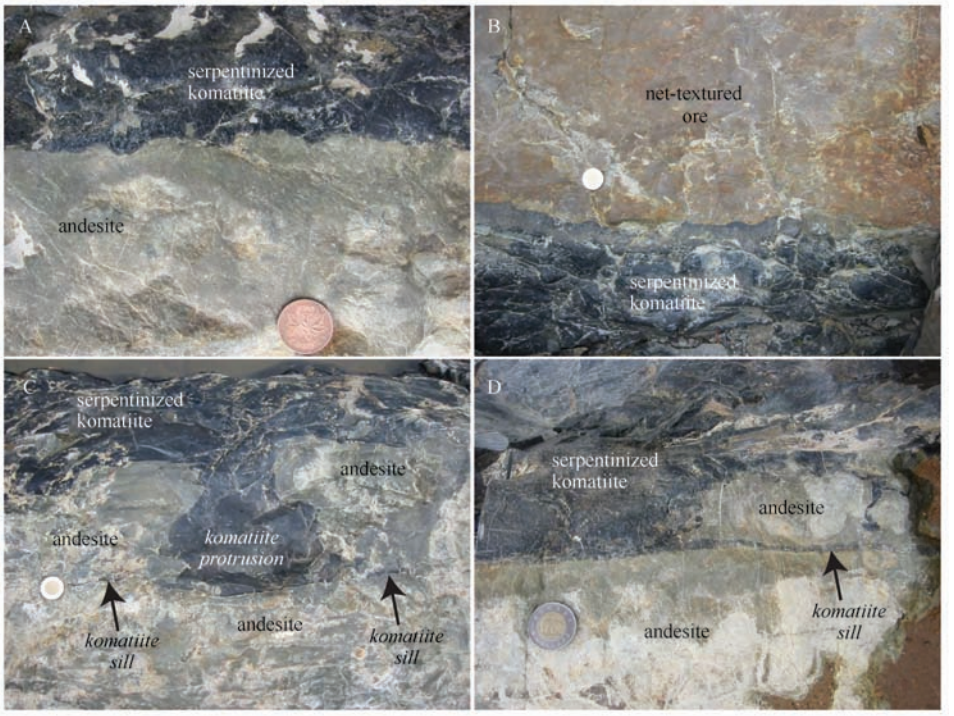

Fig. 2. 24 Photographs of komatiite/andesite contact in the northeast part of the Alexo area shown in Fig. 2. 23. A. Delicately scalloped contact between serpentinized komatiite and bleached andesite. B. Delicately scalloped contact between net-textured ore and serpentinzed komatiite. C. Protrusion of komatiite (slightly contaminated) into and extending laterally as sills into underlying andesite. D. Irregular contact between komatiite and andesite with komatiite sill extending laterally into andesite.

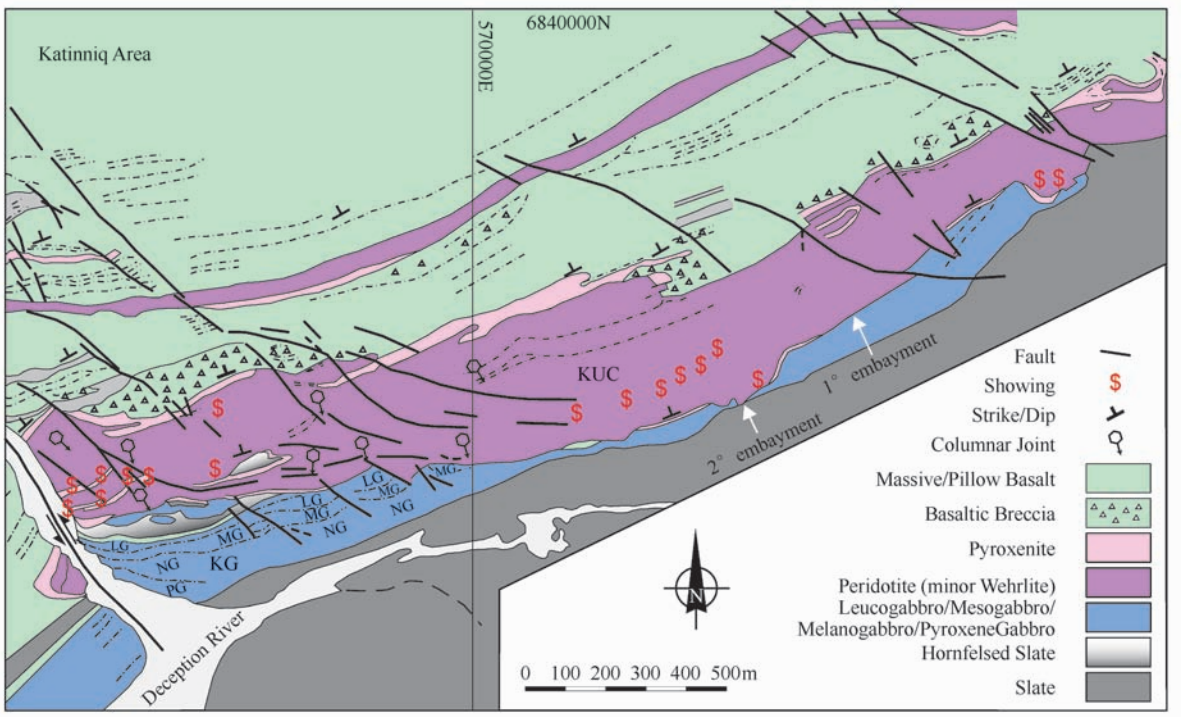

Fig. 2. 25 Simplified map of the Katinniq Ultramafic Complex, Raglan area (based on 1∶2000 mapping by Lesher, 2007). The complex is transgressive to underlying sediments and layered gabbro sill forming a broad first-order concave embayment and several smaller second order embayments. Underlying rocks are contact metamorphosed to biotite zone within 5 – 10m of the contact, but overlying rocks are not contact metamorphosed and reflect lower greenschist facies regional metamorphism. LC = lecogabbro, MG = mafic gabbro, NG = mesogabbro.

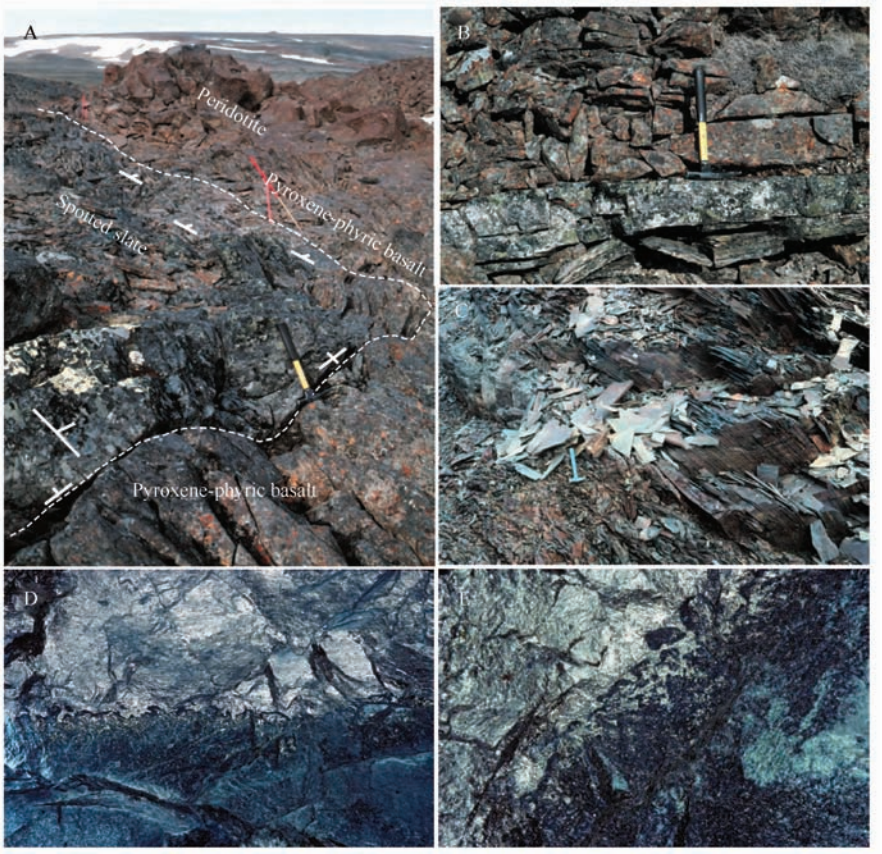

Fig. 2. 26 Photographs of contact relationships in the Katinniq Ultramafic Complex (from Lesher, 2007). A. Photograph of lower contact of ultramafic complex cross-cutting bedding in contact metamorphosed semi-pelite. Contact dips northward (toward upper right) in the upper part of the photo, vertical in the right part of the photo, and westward in the lower left part of the photo. The komatiitic basalt along the contact is contaminated (enriched in HILE relative to MILE with negative Nb-Ta anomaly) and contains pryoxene (not olivine) phenocrysts like most of the rest of the complex. B. Same contact further west showing highly devolatilized (no S or C) and silicified semipelite along contact and underlying spotted hornfelsed semipelite. C. Unhornfelsed graphitic slates 10m further from the contact. D. Delicately-scalloped contact between massive ore (top) and underlying gabbro (bottom). E. Gabbro inclusions along contact between massive sulfides (upper left) and footwall gabbro.

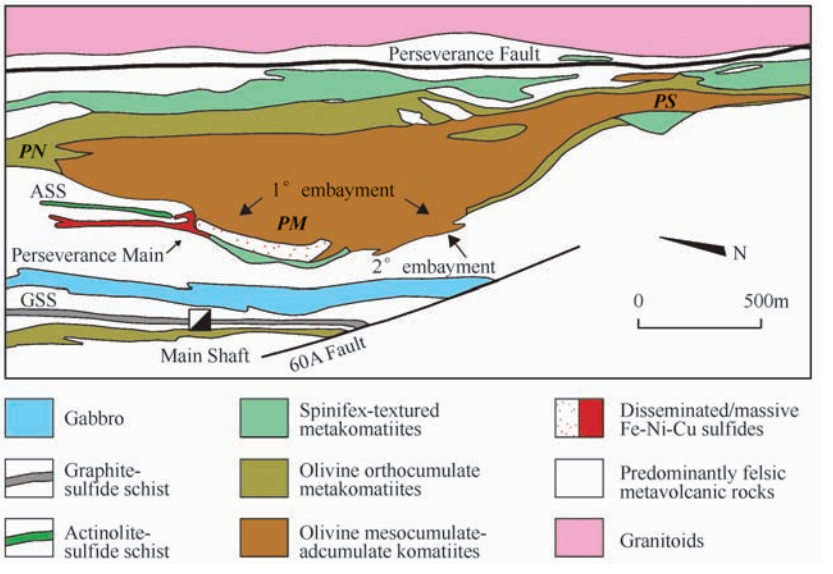

Fig. 2. 27 Map of the Perseverance Ultramafic Complex (modified from Barnes *et al*., 1988).

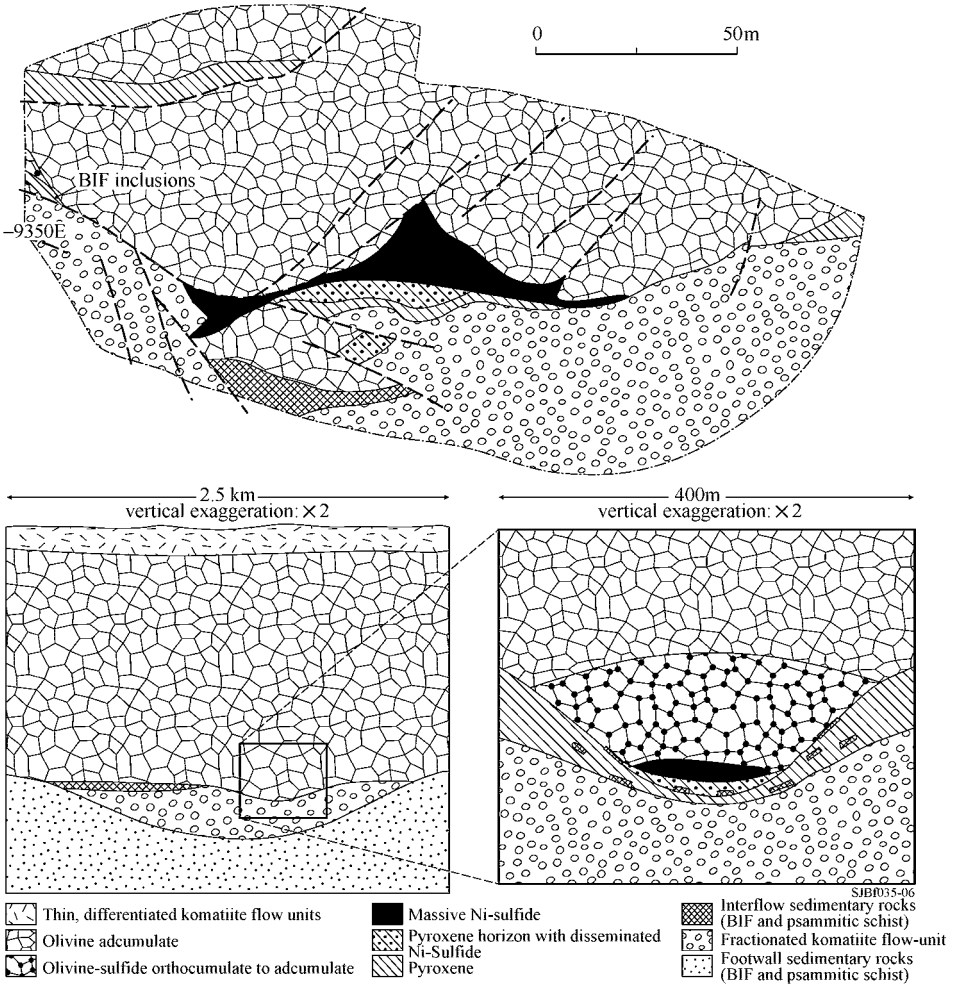

Fig. 2. 28 Map of the Digger Rocks deposit (modified from Perring *et al*., 1995) in the Forrestania Belt of the Southern Cross Province of Western Australia. Showing transgressive relationship to footwall rocks.

deep embayment. Trofimovs *et al*. (2003) have argued against thermomechanical erosion based on the model of Cas *et al*. (1999) for unchannelized flows, but the uniformly high Fo contents of the olivines require a very hot continuously-replenished magma and pelitic sediments would be as erodable if not more erodable than dacites, so it seems unlikely that most or all of the present geometry can be attributable to thermomechanical erosion.

Digger Rocks and Windarra

The Digger Rocks deposit in the Forrestania Belt (Fig. 2. 28) (Perring *et al*., 1995) and the Windarra deposits in the northeastern part of the East Yilgarn (Marston, 1984) (Fig. 2. 29) transgress underlying banded iron formations.

Fortaleza de Minas

Fortaleza de Minas (Brenner *et al*., 1990) is more deformed, but reconstructions indicate that the ores and host rocks were localized in a broad deep embayment overlying and transgressing underlying banded iron formations (Fig. 2. 30).

Theoretical models

Rice and Moore (2001) argued against komatiites being even capable of thermomechanical erosion, citing results from a fluid dynamic model and a wide range of natural and industrial examples. However, they provide almost no details on the parameterization of their model and the examples they cite (wax flowing down a candle, slowly-moving flood basalt and pahoehoe flows, short duration wax model experiments, etc.) are not analogous to the processes that would have occurred beneath thick, hot, dense, fluid, rapidly-moving komatiite channels flowing for very long periods of time over water-bearing unconsolidated sediments or volcaniclastic rocks. Their arguments conflict with the carefully parameterized and completely derived theoretical models and carefully prepared analog models of Huppert *et al*. (1984), Huppert and Sparks (1985), Jarvis (1995), and Kerr (2001), the carefully parameterized and completely-derived theoretical models of Williams *et al*. (1998, 1999, 2002), the thermomechanical erosion rates of ~10 cm per day that have been *directly* measured beneath much smaller and much cooler Hawaiian basalt lava tubes by Kauahikaua *et al*. (1998), and the long list of natural examples of thermomechanical erosion

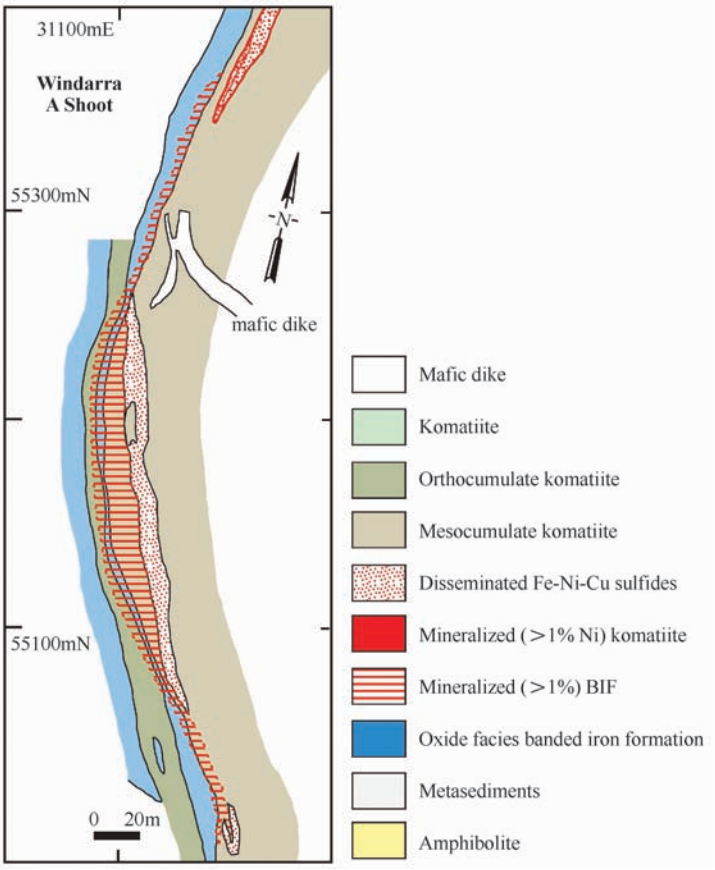

Fig. 2. 29 Plan of the Windarra A Shoot (from Marston, 1984) in the northeastern part of the East Yilgarn Province of Western Australia. The host units are transgressive to the footwall rocks.

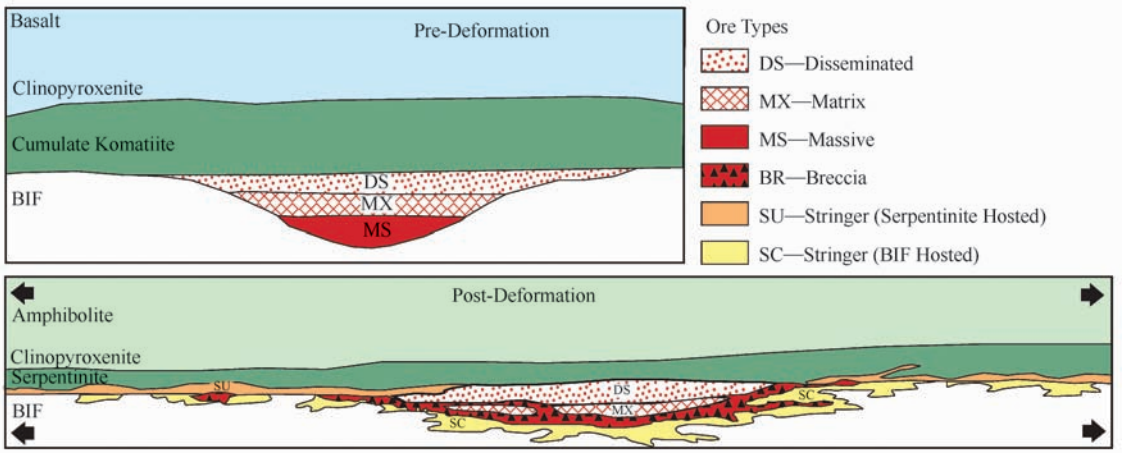

Fig. 2. 30 Schematic map and reconstruction of the Fortaleza de Minas deposit (Brenner *et al.*, 1990).

compiled by Greeley *et al.* (1998). Some of the assumptions they have made (e.g., , presence of olivine primocrysts) are clearly incorrect (see below).

Mechanical vs. thermomechanical erosion

Beresford and Cas (2001) and Cas and Beresford (2001) suggested that the sediments at Kambalda were mechanically rather than thermomechanically eroded and suggested that the contamination reported by Lesher and Arndt (1995) could have been produced by alteration. However, their work was on flow lobes and sheet flow facies not channel-flow facies, they provide no reasonable alternatives for the similar S isotopic compositions of the sediments and ores (Groves *et al.*, 1979; Seccombe *et al.*, 1981), the lateral gradations from unmodified cherty sediments to devolatilized chloritic sediments with identical trace element signatures (Bavinton, 1979; Bavinton, 1981), the presence of xenomelts with precisely the same compositions as the sediments except for being strongly depleted in S, Ni, Cu, and Co (McNaughton

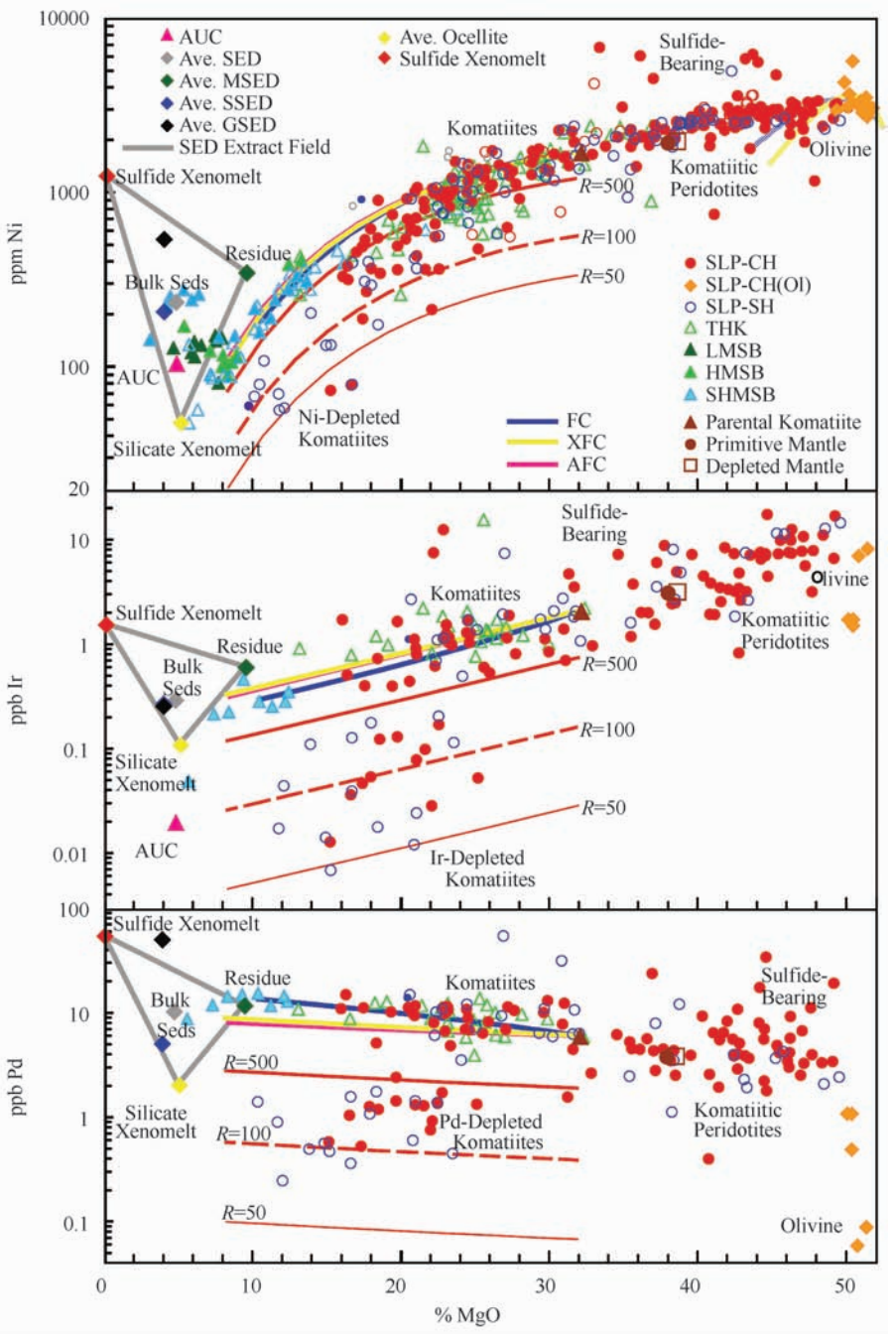

Fig. 2. 31 Ni-Ir-Pd vs. MgO for Kambalda komatiites, unmodified siliceous/graphitic sediments, devolatilized chloritic sediments, felsic ocellar xenomelts, and other lithologies. Bulk sediment compositions lie within a triangle represented by compositions of average silicate xenomelt (felsic ocellites), residue (chloritized sediments), and sulfide xenomelt (sulfide component of sediment prior to enrichment by reaction with komatiite). The enrichment of sulfide xenomelt to form ores with much higher Ni, Ir, and is balanced by chalcophile element depletion in the komatiites (preserved only in the flanking basalt units for reasons discussed by Cowden, 1988, Lesher and Arndt, 1995, and Lesher *et al*., 2001). All other chalcophile and all least-mobile lithophile elements exhibit the same topology. AUC = average Archean Upper Crust (Tayor and McLennan, 1985), SED/MSED/SSED/GSED = average sediment/mafic sediment/siliceous sediment/graphitic sediment (Bavinton and Keays, 1978; Bavinton and Taylor, 1980; Bavinton, 1981), ocellite = average felsic ocellar rock (Frost and Groves, 1989), SLP-CH and SLP-CH (Ol) = Silver Lake Peridotite Member Channel-Flow Facies and Olivine and SLP-SH = Silver Lake Peridotite Member Sheet-Flow Facies (Lesher *et al*., 2001), THK = Tripod Hill Komatiite Member (Lesher and Arndt, 1995), LMSB/HMSB/SHMSB = Paringa and Devon Consuls Basalts (Arndt and Jenner, 1986; Redman and Keays, 1986), primitive mantle from McDonough and Sun (1995), depleted mantle (komatiite source) estimated.

et al., 1988; Frost and Groves, 1989b), or any evidence that Nb and Th were mobile during metamorphism. As discussed by Lesher and Campbell (1993), Lesher and Arndt (1995), Lesher and Burnham (2001), and Lesher *et al*. (2001) the stratigraphic, geological, and geochemical relationships suggests that the sediments beneath the channel-flow facies were thermomechanically eroded and that the silicate and sulfide components decoupled: the silicate component was miscible and was normally assimilated (but rarely preserved as xenomelts) and diluted in the komatiite lava, but the sulfide component was immiscible and remained at the base of the channels forming the sulfide ores. This is supported not only by the field observations but also by the geochemical data, which highlight the decoupling of the components (Fig. 2. 31).

Contact metamorphism/metasomatism

The amount of contact metamorphism beneath and adjacent to embayments has not been studied systematically, but varies from area to area depending on the size of the lava/magma conduit, the nature of the footwall rocks (volcanic vs. unconsolidated sediments), and the degree of superimposed regional metamorphism. For example, massive, pillowed, and volcaniclastic basalts underlying the Kambalda deposits are not noticeably metamorphosed, pillowed andesites underlying the Alexo deposit are silicified within 2m of the contact (Fig. 2. 24C), massive dacites underlying the Bannockburn deposit are chloritized within 20 – 30 cm of the contact (Taranovic *et al*., 2008), and semipelites underlying the Katinniq deposit are strongly devolatilized and recrystallized within 20 cm of the contact (Fig. 2. 25, Fig. 2. 26B) and metamorphosed to biotite facies within 5 – 10m of the contact (Fig. 2. 26A). In all of these areas, these features are present beneath and adjacent to embayments, but not on barren contacts. Stone and Archibald (2004) used the absence of apparent contact metamorphism at Kambalda to argue against thermal erosion, but the rocks at Kambalda have been regionally metamorphosed to lower amphibolite facies (510 ± 20℃ at 2. 5 ± 1 kb; Bavinton, 1981) which would have erased most of the evidence for contact metamorphism. The temperature beneath the much larger embayment at Katinniq, for example, would have been 380 – 460℃ based on presence of biotite and absence of cordierite, andalusite, garnet, or sillimanite. Pelitic rocks are also much more likely to exhibit visible changes than a basalt. Stone and Archibald (2004) noted that the paucity of contact metamorphism contrasts with the strong "contact metamorphism" produced by the felsic intrusion on the east flank of the Kambalda dome, but granitic intrusions contain orders of magnitude more volatiles and alkalis than komatiites, so most of the "contact metamorphism" is metasomatism not thermal metamorphism.

Constructional embayments

Some topographic relief is expected in volcanic terrains (e.g., Alexo, Kambalda-St Ives-tramways-Widgiemooltha, Langmuir, Silver Swan), but less so in areas underlain by thick sequences of regionally-extensive fine-grained sedimentary or volcaniclastic rocks (e.g., Damba-Silwane, Forrestania, Raglan, Perseverance). Because the latter lithologies are also much more susceptible to thermomechanical erosion, we should expect to see less evidence of original topography than in areas underlain by relatively refractory rocks like basalts.

Stone and Archibald (2004) used Lunnon Shoot an example where detailed structural analysis indicated that 3D polyphase deformation can explain trough formation from a roughly planar contact, referencing Cowden (1988). However, Cowden did not show how this could be done and the section shown by Stone and Archibald (Fig. 2. 10A) incorrectly labels the ore horizon on the Upper Roll, which exhibited a complete profile of massive/net-textured/disseminated mineralization (see Fig. 2. 15E), as "offset ore" and it does not include important geological information reported by Middleton (unpubl. WMC report), Lesher (1983, 1989), and Paterson *et al*. (1984). When the stratigraphic, volcanological, lithological, petrographic, and geochemical information reported in those studies is included, a very different picture emerges (Fig. 2. 32):

1) Upper Roll, Main Contact, and Top Surface East are strongly mineralized, underlain by massive basalt, and overlain by mesocumulate komatiite. They are separated by the Lunnon Fault and #1 East Thrust, which clearly offset the stratigraphy in the overlying komatiite sequence. Removal of dip-slip movement on the Lunnon Fault and removal of oblique reverse/sinistral movement on #1 East Thrust restores the hangingwall stratigraphy but leaves a flat-floored embayment bounded by the Upper Roll basalt on the west and the Eastern Step/Top Top Surface East basalts on the east.

2) Top Surface West is only weakly and sporadically mineralized (Middleton unpubl. WMC report) and the underlying Upper Roll basalts are pillowed and young upwards even along the westward-dipping contact with cumulate komatiite (see Fig. 2. 15E).

3) The contact between the Upper Roll basalt and underlying cumulate komatiites is sheared, but bordered by a fine random spinifex-textured aphyric "chilled" margin that is mineralogically, texturally, and geochemically identical to the lower chilled margins of other komatiite flows (Fig. 2. 33A-C) but completely different from the metasomatized talc-tremolite schists underneath the #1 East Thrust (Fig. 2. 33D). If this were a fault, as suggested by stone and Archibald (2004), it should be sheared metasomatized cumulate komatiite like that below #1 East Thrust, not aphyric komatiite.

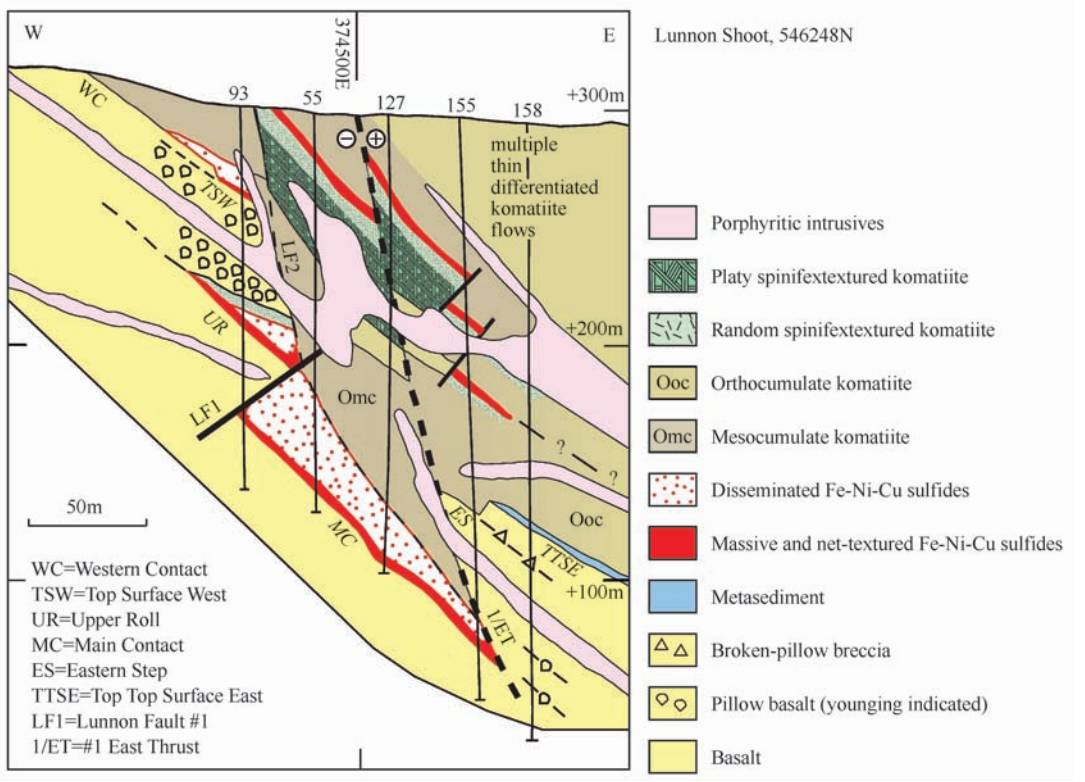

Fig. 2. 32 Section 546248N through the Lunnon shoot (modified from Middleton unpubl. WMC report and Lesher, 1989).

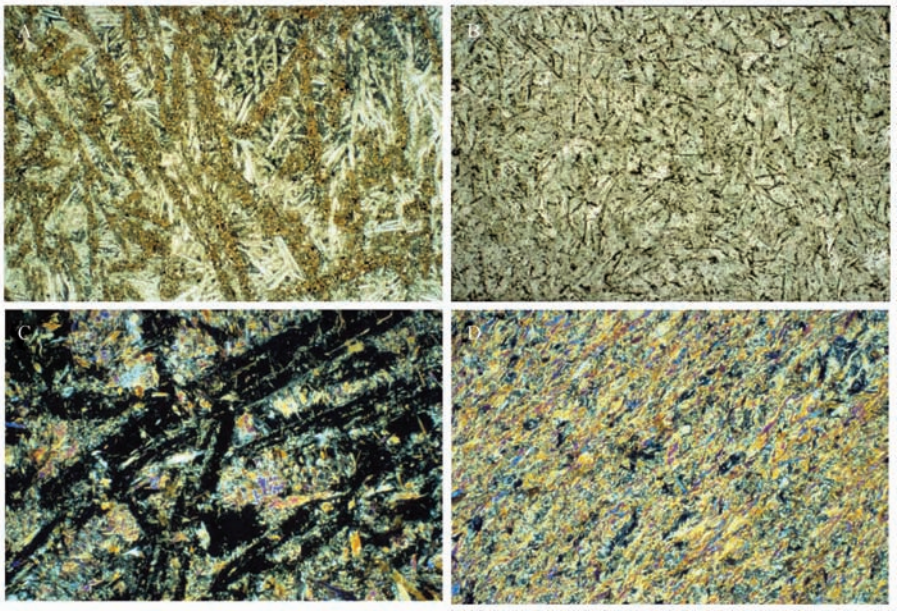

Fig. 2. 33 Photomicrographs of primary and secondary embayment margins at Lunnon Shoot. A. Random spinifex-textured metasomatized komatiite (KD93/258. 2', 91863) comprising random oriented domains of phlogopite-chlorite (brown) after olivine and actinolite (colorless) after clinopyroxene. Plane polarized light. B. Fine random spinifex-textured metasomatized komatiite (KD56/335. 2', 91854) comprising magnetite-carbonate (high relief) pseudomorphs after olivine or pyroxene in a matrix of actinolite-chlorite (both colorless and indistinguishable). Plane polarized light. C. Random spinifex-textured metasomatized komatiite from Lunnon Upper Roll 4 level crosscut (LU4LXC-428) comprising chlorite (dark) after olivine in a matrix of tremolite-actinolite (acicular). Doubly polarized light. D. Schistose metasomatized cumulate komatiite immediately beneath Lunnon #1 East Thrust comprising talc-tremolite and only very minor chlorite. Doubly polarized light. A, B, and C are primary volcanic contacts, indicating that the embayment margins in these locations are unfaulted, whereas D is a tectonic contact.

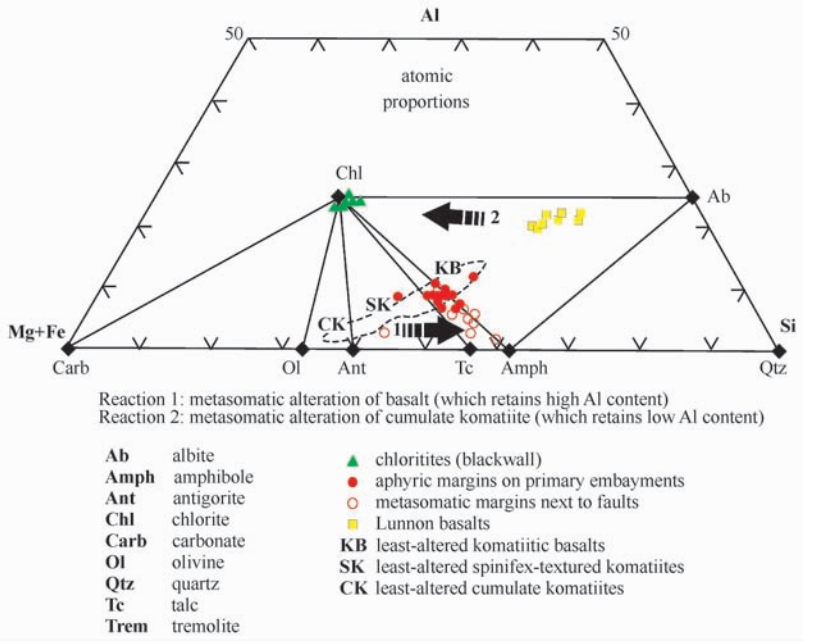

Fig. 2. 34 Al-(Fe + Mg)-Si projection showing the compositions of 13 slightly altered aphyric and spinifex-textured "chilled" margins, 8 strongly-altered cumulate komatiites, 8 Lunnon basalts, and 6 chlorite-rich metasomatic reaction zones from Kambalda. Also shown is the compositional range of 75 least-altered komatiites (Lesher, 1989). Tie lines connect co-existing phases. Arrows indicate projected metasomatic reaction trends.

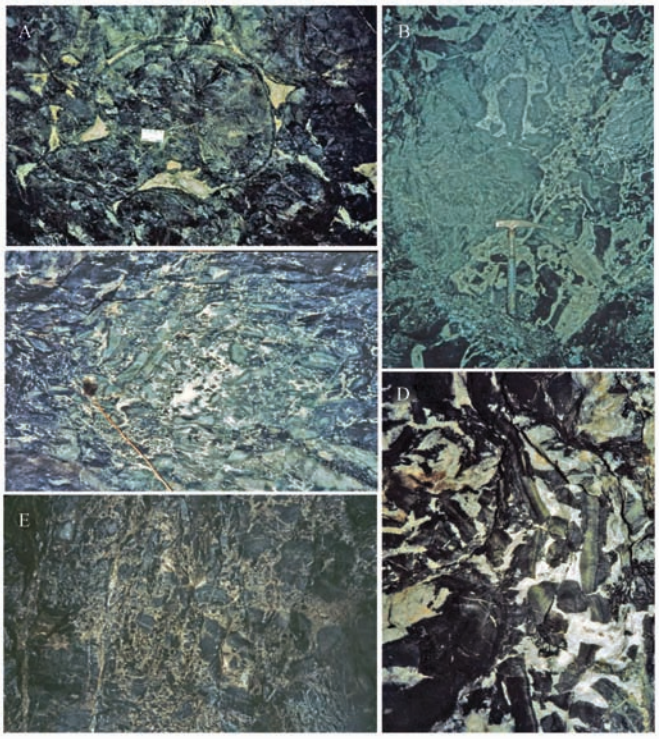

Fig. 2. 35 Well-preserved volcanic structures at Kambalda. A. Pillow basalt below ore horizon, Juan B 1218 NNW stope. Scale is 9 cm wide. B. Brecciated front of lava toe opposite ore pinchout, Durkin Deeps 1050/4 cut and fill stope. Breccia is mineralized adjacent to the pinchout (see Lesher and Keays, 1984). Hammer is ~40 cm long. C. Broken pillow breccia, Lunnon 803 drive, in the proposed location of the #2 East "Thrust" (compare Fig. 2. 10A and Fig. 2. 32). Steel rod is ~2 cm in diameter. D. Broken-pillow breccia opposite northwest ore pinchout, Juan East 412/1 open stope, one of the elliptical ore shoots that is terminated along the entire periphery by basalt-basalt pinchouts (see Lesher, 1989). E. Mineralized flow-top breccia directly beneath contact ore horizon, Juan Main 1104 open stope. Fragments exhibit same broken pillow textures as unmineralized breccias.

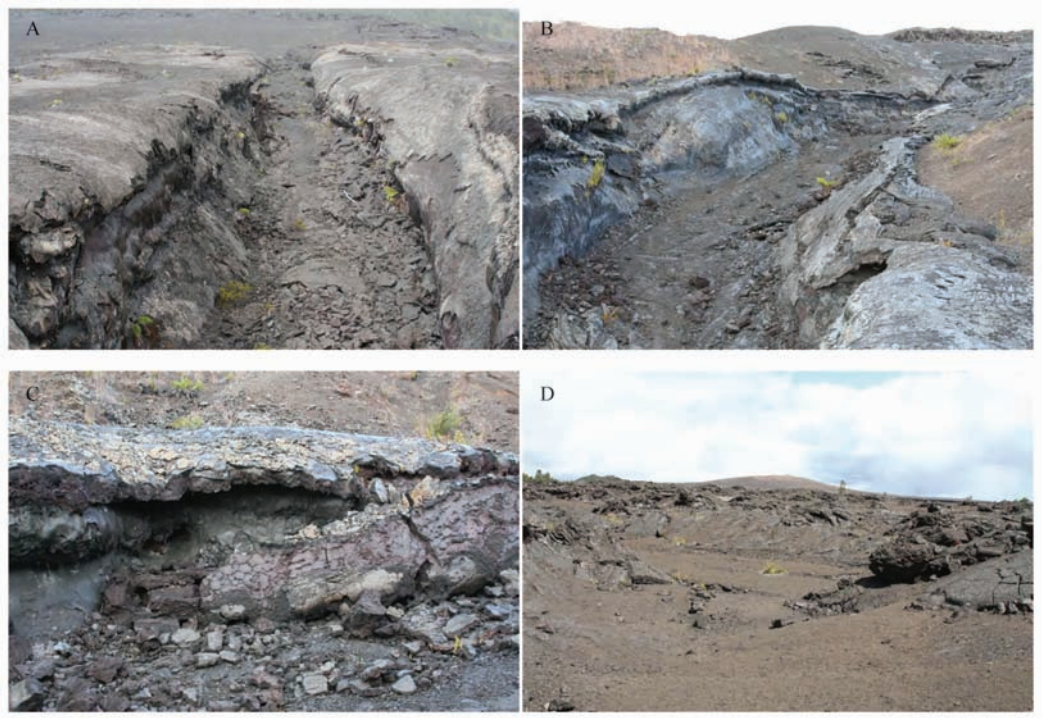

Fig. 2. 36 Volcanic topographic features on the southeast flank of Mauna Loa, Hawaii. A. 4m deep × 6m wide lava channel near Mauna Ulu. B. 3m deep × 9m wide lava channel near Keanakako'i Crater with one steep and locally reentrant margin and one sloping margin. C. close up of collapsed re-entrant margin of lava channel in part of the channel shown in B. D. ~25m diameter collapsed tumulus near Puhimau crater.

4) Top Surface East is strongly mineralized, Eastern Step is barren, and Top Top Surface East is weakly mineralized (Middleton unpubl. WMC report), so they are not stratigraphically or structurally equivalent.

5) The #2 East "Thrust" was exposed in the Lunnon 701, 803, and 903 areas and is represented by a very well preserved flow-top broken pillow breccia (Middleton unpubl. WMC report; Lesher, 1989; Paterson *et al*., 1984) containing small pillows, broken pillows, lava crusts with dark amhibole-rich rims, and fragments of basalt in a matrix of white calcite and lesser quartz (Fig. 2. 35C). Thus, the topography between Eastern Step and Top Top Surface East is a volcanic topographic feature, not a fault.

These observations contradict any suggestions that the ore-localizing embayment at Lunnon Shoot formed entirely by deformation and highlight the need to consider the stratigraphy and facies variations in the footwall rocks and hangingwall rocks when interpreting the origins of ore-localizing embayments.

Detailed mapping of volcanic facies and pillow polarities in the enclosing basalts other areas at Kambalda, including Juan East, Juan B, Juan Main, Durkin Deeps, Ken Far East, and Foster shoots (Lesher, 1989; Evans, 1989; Squire *et al*., 1998) indicates that the embayments in those areas also correlate with stratigraphic contacts in the enclosing basalts (e.g., Fig. 2. 15A-E) and/or are bounded by different basalt facies (e.g., Fig. 2. 17) and were therefore not generated by syn-volcanic faulting, thermomechanical erosion, or post-volcanic folding or faulting.

Although some constructional volcanic features (e.g., drained lava channels) are reentrant in geometry (Fig. 2. 36), all of the unfaulted ore pinchouts studied by Lesher (1983, 1989) locally were transgressive to pillow margins and massive basalts (e.g., Fig. 2. 18) and decorated with skeletal ferrichromites (Fig. 2. 19) with compositions identical to those produced experimentally (Ewers *et al*., 1976) and observed on most undeformed ore-wall rock contacts in deposits of this type (Alexo, Bannockburn, Langmuir, Raglan, Silver Swan). This suggests that at least part of the re-entrant geometry of the primary embayments at Kambalda was produced by thermochemical erosion by massive sulfides (Lesher, 1989). The best interpretation is that primary embayments at Kambalda represented 2 – 30m topographic features that were modified by thermo-mechanical erosion and deformation (Lesher *et al*., 1984; Lesher, 1989; Squire *et al*., 1998; Beresford *et al*., 2002).

The relief on Archean basaltic lava fields has been shown to be up to 20m (e.g., Dimroth *et al*., 1978; Hargreaves and Ayers, 1979), which is similar to that in modern basaltic flow fields and the thicknesses of the flows mapped by Lesher

(1983, 1989), Evans *et al.* (1988), and Squire *et al.* (1998) at Kambalda. As discussed by Squire *et al.* (1998) there are many volcanic topographic features with geometries similar to the embayments. Some are linear and re-entrant (e.g., drained lava channels: Fig. 2. 36A-B, collapsed lava tubes, fissures flanked by spatter) and some are elliptical (deflated tumuli: Fig. 2. 36D). Some are asymmetric with re-entrant margins (Fig. 2. 36C). The scales are different but of the same order of magnitude as some of the smaller embayments at Kambalda, and they formed subaerially, but features even more similar to those at Kambalda are present in submarine flow fields (Soule *et al.*, 2005; Fornari, 1986).

In summary, many of the embayments that host komatiite-associated Ni-Cu-(PGE) ores have been modified by deformation, but there is evidence in most localities that most were primary. Those overlying basalts are more likely to be topographic and less modified by thermo-mechanical erosion, whereas those overlying felsic volcaniclastic rocks or sediments are more likely to be erosional.

2. 2 Host units

The host rocks in many ore deposits play a passive role in ore genesis, by contributing ore metals or a favorable environment for accumulation, but the rocks that host magmatic Ni-Cu-(PGE) deposits, in general, and komatiite-associated Ni-Cu-(PGE) deposits, in particular, played an active role in the genesis of the sulfide ores. They exhibit a number of characteristics that distinguish them from unmineralized komatiites and provide important constraints on ore genetic models.

2. 2. 1 Size and form

The komatiitic peridotites and dunites that host most Type I deposits are anomalously thick, highly magnesian components of komatiite sequences (Fig. 2. 37), but are texturally and compositionally gradational with overlying and adjacent orthocumulate, porphyritic, and spinifex-textured komatiites in almost all localities. Some are lens-shaped and confined to a large degree within footwall embayments (e.g., Zone 2, Zone 3, Katinniq, Zone 6, Zone 8, and Boundary complexes at Raglan) and appear to represent lava channels or deeply erosive lava conduits, whereas others appear to be more sheet-like in form with thicker central parts that appear to represent channelized sheet flows (e.g., Cross Lake complex at Raglan, most Kambalda deposits).

The komatiitic peridotites and dunites that host most Type Ⅱ deposits are lenticular in cross-section; thicker and more magnesian in central parts, thinner and less magnesian at margins, but Dumont is much more differentiated with a gabbroic upper zone. Those at Dumont and Thompson are almost certainly sills, but those in Western Australia typically occupy thickened zones at or very near the base of komatiite sequences, grade along strike into komatiitic peridotites and komatiites, and are conformable with overlying komatiites, komatiitic basalts, and tholeiitic basalts. They were originally

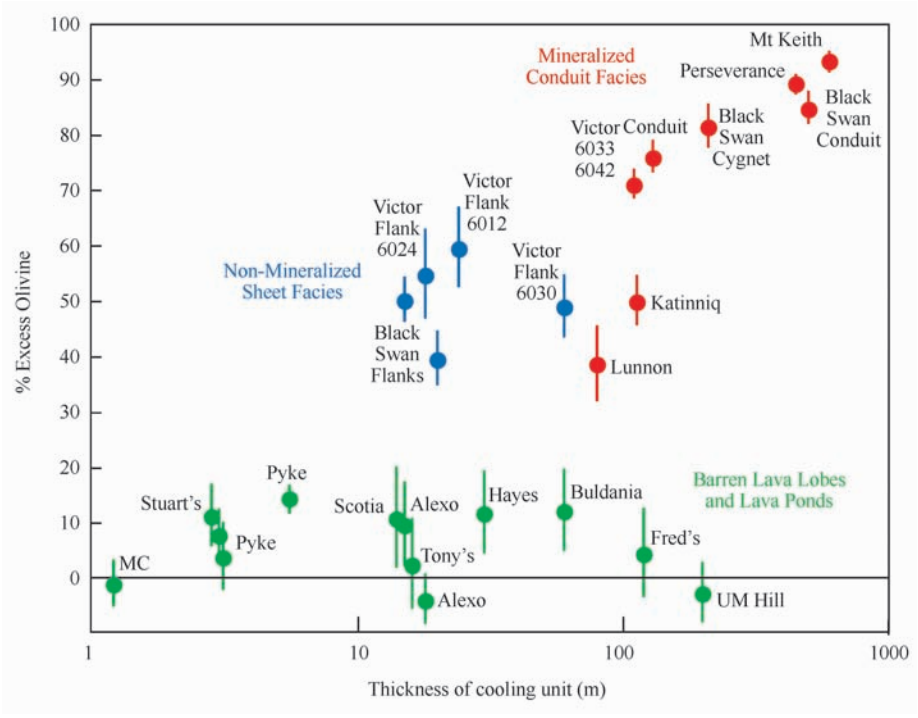

Fig. 2. 37 Plot of excess olivine vs flow thickness. Excess olivine is an estimate of the proportion of accumulated olivine in the flow unit based on a comparison of the bulk MgO content of the entire profile compared with the estimated MgO content of the komatiite liquid component, following Arndt *et al.* (2008).

interpreted as dikes (Binns *et al*., 1977) or subvolcanic sills (Naldrett and Turner, 1977) then as dynamic lava channels (Donaldson *et al*., 1986; Hill *et al*., 1989; Barnes *et al*., 1988b). In a detailed study of the Mt Keith dunite body, Rosengren *et al*. (2005) documented injections and apophyses of komatiite magma as irregular sills and dykes extending from the top and bottom of the dunite body into country rock dacite, indicating that the Mt Keith complex is a subvolcanic sill. However, other komatiitic dunite bodies, notable that at Murrin Murrin east of Leonora (Barnes, 2006), show lateral and vertical transitions into differentiated komatiite flows, strongly supporting an extrusive origin. It is likely that komatiitic dunites formed in both extrusive and shallow intrusive environments, and may also be invasive bodies with characteristics of both (Barnes and Lesher, 2008).

Some correlate with a single unit along strike; others appear to correlate with multiple units along strike (e.g., Lunnon and Durkin shoots at Kambalda). Some have flow-top breccias (e.g., Kambalda, Langmuir, Scotia) and are clearly extrusive, some have flow-top breccias but have peperites along their lateral margins (e.g., Raglan) and appear to be deeply erosive (downward burrowing) to invasive (laterally burrowing), and some are clearly intrusive (e.g., Thompson, most parts of Pechenga). In the Alexo-Dundonald area, deposits appear to have formed in both volcanic and subvolcanic settings (Fig. 2.38). The Bannockburn deposit in Ontario is hosted by komatiitic peridotite in some parts and by a heterolithic apparently autoclastic breccia in other parts (Taranovic *et al*., 2008).

Stone and Archibald (2004) and Stone *et al*. (2005) have attributed the greater thickness of the basal host units at Kambalda compared to barren flanking units to ductile flow of the komatiite during $D_1 - D_2$ deformation. It is difficult to completely discount this process in every situation, but as noted by Woolrich and Giorgetta (1978), Gresham and Loftus-Hills (1981), Lesher and Groves (1984), Lesher (1989), Arndt and Lesher (1995), and Lesher *et al*. (2001), the basal host units at Kambalda are not only thicker, they are also normally not separated by interflow sediments, they are more magnesian and have lower Cr contents, they are capped by more magnesian spinifex-textured rocks, the olivines are more magnesian, they are less contaminated, and they are undepleted in chalcophile elements. In contrast, barren flanking basal units are not only thinner, they are commonly underlain and overlain by relatively planar interflow metasediments, they are less magnesian and have higher Cr contents, they are capped by less magnesian spinifex-textured rocks, they olivines are less magnesian and more often crescumulate, they are more contaminated, and the spinifex-textured rocks are strongly depleted in chalcophile elements. It would be impossible to produce these relationships by deformation.

The units that host subeconomic Type Ⅲ mineralization are typically differentiated flows (e.g., Fred's flow) or sills (i.e., Boston Creek sill, Delta sill).

2.2.2 Internal structure and composition

Komatiitic lava flows and sills vary considerably in terms of internal composition and structure, depending on the degrees of olivine accumulation and differentiation in situ (Fig. 2.39). Most Type Ⅰ and Ⅱ deposits, regardless of whether extrusive or intrusive, are hosted by undifferentiated to poorly-differentiated cumulate[1] units, whereas most Type Ⅲ deposits are hosted by differentiated non-cumulate units. However, there are exceptions even within camps.

The komatiitic peridotite units that host Type Ⅰ mineralization at Kambalda, Silver Swan, are characterized by thick lower cumulate zones and thin upper aphyric and spinifex-textured zones. Several textural/mineralogical/compositional zones can normally be distinguished, but their thicknesses vary considerably and not all zones are present in all units. Some of the host units at Kambalda have only very thin upper spinifex-textured zone and ponded later, whereas others have very thick spinifex-textured zones and ponded earlier. Stratigraphically equivalent, barren flanking units are thinner, less magnesian, and crystallized from less magnesian magmas. Parts of the chilled upper margins of many basal host units at Kambalda are missing and may have been thermally eroded by overlying flows. The basal host unit at Scotia lacks any liquid-rich upper division, but it is overlain by a shear zone and may have been tectonically beheaded. Cumulate zones typically contain granular or polyhedral ortho-mesocumulate olivine (see below), but some contain in situ-crystallized branching crescumulate olivine, in the center and near their bases (e.g., Victor and Durkin shoots, Kambalda). This precludes models involving emplacement of olivine-liquid mushes or ponding/riffling of intratelluric olivine.

The komatiitic peridotite units that host Type Ⅰ/Ⅱ mineralization in the Raglan belt are composed of multiple overlapping units of olivine mesocumulate and orthocumulate komatiitic peridotite with lower pyroxene-phyric "chilled" margins and upper flow-top breccias and/or aphyric chilled margins. In contrast, the units that host mineralization in the remarkably similar Pechenga belt are systematically differentiated from peridotite through pyroxenite to gabbro.

[1] Cumulate units are enriched in olivine and have integrated bulk compositions that are considerably more magnesian than their chilled margins. Non-cumulate units may contain cumulate rocks, but have differentiated in situ and do not contain an excess cumulate component.

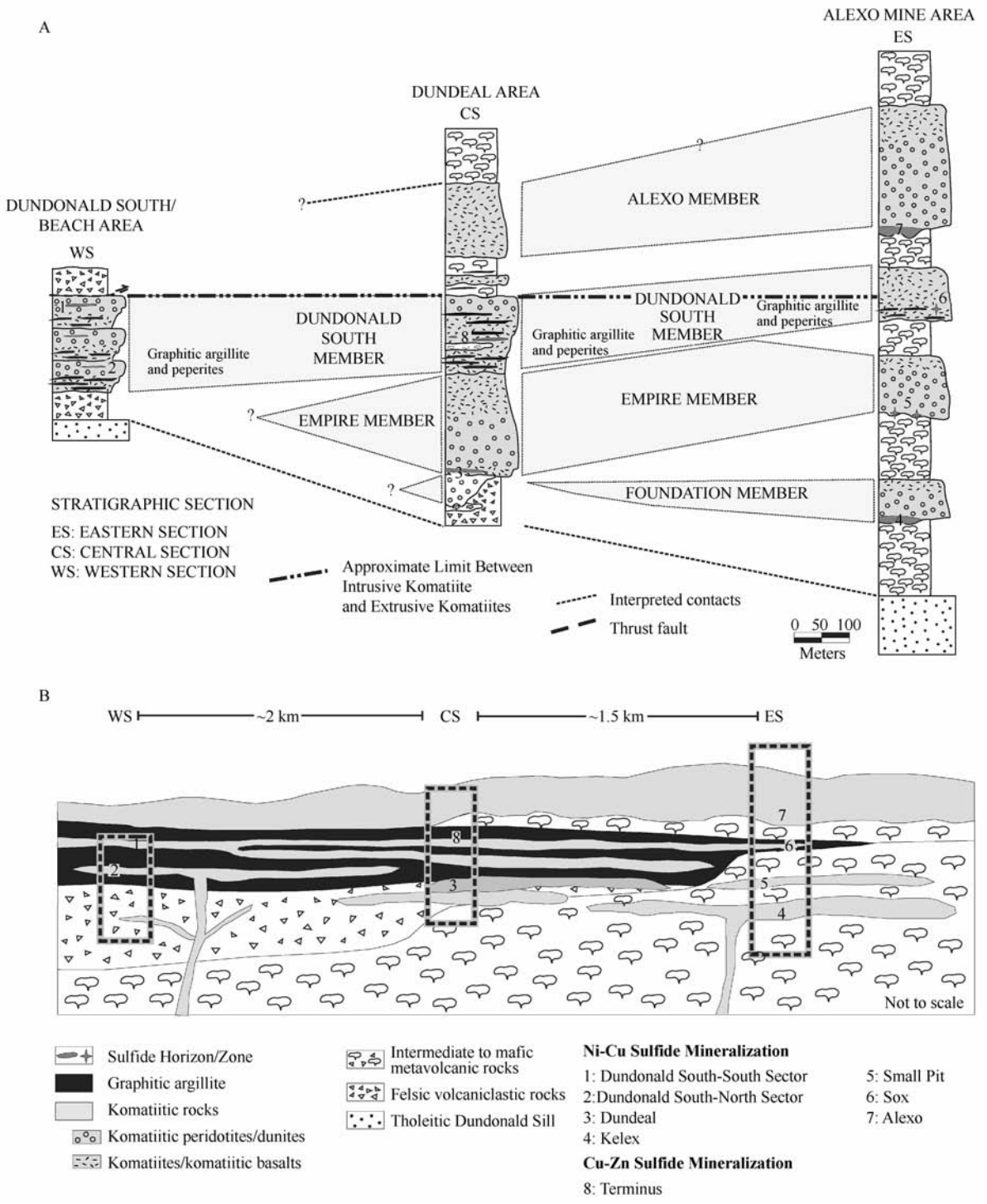

Fig. 2. 38 Stratigraphic section for Dundonald Township, showing the locations of komatiite-associated Ni-Cu-(PGE) mineralization at several levels in the sequence (Houlé *et al.* 2008).

The komatiitic dunite units that hosted (prior to dislocation during deformation) Type IVa and V mineralization at Thompson commonly exhibit an asymmetric variation in cumulus olivine and whole-rock MgO contents characterized by a thin pyroxenitic basal zone that grades into a thicker lower zone of olivine-(chomite) mesocumulate peridotites and adcumulate dunites that become progressively less olivine-rich and grade upward into a thinner pyroxenitic upper zone (Layton-Matthews *et al.*, 2007).

The komatiitic dunite units that host Type Ⅱ mineralization at Mt. Keith and Yakabindie, and Type I mineralization at Perseverance, are typically adcumulate to mesocumulate and undifferentiated. Barren analogs at Marshall Pool and Mt. Clifford exhibit thin chilled margins (Donaldson *et al.*, 1986), but most mineralized bodies simply grade to olivine orthocumulate at their margins (Hill *et al.*, 1989). The Du-

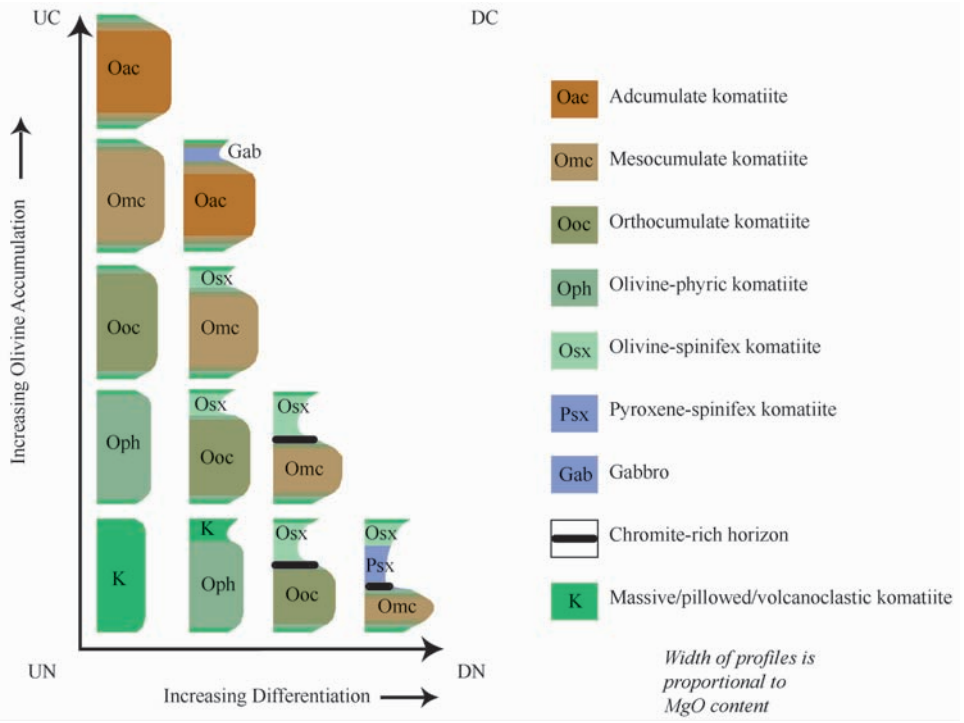

Fig. 2. 39 Facies variations in komatiites based on degree of olivine accumulation and in situ differentiation (modified after Lesher *et al*., 1984). Komatiitic basalts exhibit similar variations (see Lesher and Keays, 2002).

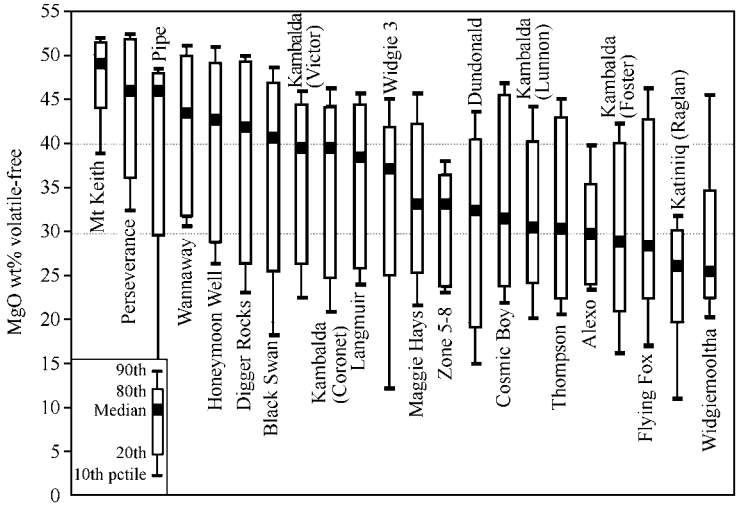

Fig. 2. 40 MgO contents (recalculated volatile-free) for host rock sequences to major komatiite-associated Ni-Cu-(PGE) deposits expressed as box and whisker plots showing 10th, 20th, 50th, 80th, and 90th percentiles (after Barnes *et al*., 2007).

mont dunite is significantly different from other mineralized komatiitic dunites in that it is overlain by Fe-rich tholeiitic basalts, not komatiites, and contains a thick upper zone of gabbroic differentiates.

Excluding Dumont, both types of host units are texturally and compositionally gradational with overlying komatiite flows and are interpreted to be integral parts of the extrusive lava sequence. Most that have been studied in detail exhibit systematic variations in olivine texture, olivine composition, and/or whole-rock composition with stratigraphic height (Ross and Hopkins, 1975; Naldrett and Turner, 1977; Lesher *et al*., 1984; Donaldson *et al*., 1986; Hill *et al*., 1987; Cowden, 1988; Lesher, 1989; Hill *et al*., 1995; Lesher, 2007; Barnes and Lesher, 2008).

MgO contents of host units to selected type 1 and 2 deposits in the East Yilgarn and Abitibi are summarized in Fig. 2. 40. Broadly speaking, the highest tonnage deposits (Perseverance and Mt Keith) are associated with the most

Mg-rich host rocks, these being the adcumulate dunite bodies. The Katinniq deposit is clearly distinct from the others, reflecting the substantially lower MgO content of the parent magma.

2.2.3 Mineralogy

Komatiitic peridotites and dunites originally comprised olivine-clinopyroxene-glass-chromite and olivine-chromite-clinopyroxene ± glass assemblages, respectively. However, all have been metamorphosed to some degree and most have been variably hydrated or carbonated. The present mineralogy of these rocks is therefore a function of metamorphic grade, bulk composition, and degree of hydration and carbonation (Barrett *et al*., 1976; Binns and Groves, 1976; Jolly, 1982; Gole *et al*., 1987; Barnes and Hill, 2000).

Komatiitic peridotites now comprise lizardite-chlorite-chromite-magnetite-clay ± albite ± clinopyroxene (very low grade), antigorite-tremolite-chlorite-ferrichromite-magnetite ± clinopyroxene (low-medium grade, hydrated), talc-magnesite-chlorite-magnetite (low-medium grade, carbonated), metamorphic olivine-talc-tremolite-chlorite-ferricrhomite ± olivine (medium-high grade, hydrated), and metamorphic olivine-chlorite-magnetite ± anthophyllite ± enstatite (medium-high grade, carbonated) assemblages.

Komatiitic dunites now comprise lizardite-brucite-magnetite-chlorite-chromite (very low grade), antigorite-brucite-ferrichromite-magnetite-tremolite-chlorite ± clinopyroxene (low-medium grade, hydrated), talc-magnesite-chromite-magnetite-chlorite (low-medium grade, carbonated), metamorphic olivine-talc-ferrichromite-tremolite-chlorite ± olivine (medium-high grade, hydrated), and metamorphic olivine ± anthophyllite ± enstatite (medium-high grade, carbonated) assemblages.

Olivine

Relict igneous olivine is only very locally preserved in mineralized komatiitic peridotites at Wannaway, Scotia, Kambalda, Perseverance, Raglan, Thompson and a few other localities. Forsterite (Fo) contents typically vary with stratigraphic height and are normally higher than that in stratigraphically equivalent barren flanking units. Igneous olivine in amphibolite facies environments is typically brownish in color, owing to microscopic inclusions of chromite that exsolved during metamorphism, and typically contains 0.10% – 0.29% CaO, 0.05% – 0.23% MnO, 0.11% – 0.24% Cr_2O_3, and 0.36% – 0.57% NiO, similar to that in unmineralized komatiites (see Lesher, 1989). The lower values in these ranges are attributed to loss during metamorphism; altered igneous olivines and olivines regenerated during metamorphism are colorless and contain negligible amounts of the same minor elements. The high Cr, Ca, and Mn contents of the igneous olivines are attributable to the high temperature and low viscosity of komatiitic liquids, together with little opportunity for subsolidus exsolution during rapid cooling. The high Ni contents indicate that much of the olivine did not equilibrate with large amounts of sulfide liquid (Duke and Naldrett, 1978). Olivine at Victor shoot, Kambalda also contains 0.09 – 1.1 ppb Pd, 1.5 – 8.4 ppb Ir, and 0.10 – 0.46 ppb Au (Keays *et al*., 1981), as well as 0.011% ± 0.004% V_2O_3, 0.022% ± 0.006% CoO, < 0.019% Cu, < 0.019% Zn, and < 0.013% Pb (Lesher, 1989). Incorporation of Ir in olivine has been attributed to (i) crystallographic substitution (Brügmann *et al*., 1987), (ii) nucleation of olivine on Ir-rich alloys (Keays, 1982; Barnes *et al*., 1985), or (iii) preferential non-structural incorporation of labile Ir during rapid crystallization (S-J Barnes, pers. comm. to CML, 1988). Barnes and Fiorentini (2008) showed that the relationship between Ir and MgO content in komatiitic cumulates is closely analogous to that of Cr, and inferred temperature-dependent saturation of komatiite magma with Ir-rich alloy at concentrations in the melt in the low ppb range. On this basis the high Ir content of some dunites is attributed to incorporation of cumulus alloy grains, probably as inclusions in olivine.

Relict igneous olivine is only locally preserved at Kambalda, but it is more magnesian (Fo_{94-91}) in the mineralized host units than in barren flanking units (Fo_{91-89}). Olivine in the host unit at Victor shoot is unzoned except for very narrow less magnesian rims and exhibits systematic variations in texture (orthocumulate-crescumulate-mesocumulate) and composition (Fo_{94-91}) with stratigraphic height (Lesher, 1989), indicating that it crystallized *in situ* and was not transported as intratelluric phenocrysts.

Relict igneous olivine (Fo_{95-86}) is preserved in mineralized komatiitic dunite at Perseverance, Betheno, and Dumont, and exhibits similar variations in composition with stratigraphic height. It typically has lower minor element contents than that in komatiitic peridotites, probably reflecting slower cooling rates (Donaldson *et al*., 1986). Ni contents of olivines in the mineralized zones at Dumont are systematically lower (min. 1200 ppm Ni) than those in unmineralized zones (min. 2700 ppm Ni) at equivalent forsterite contents ($Fo_{91-93.5}$), probably reflecting *in situ* separation and equilibration with sulfides (Duke, 1986). Olivines in sulfide-bearing cumulates at Perseverance are strongly depleted in Ni (Barnes *et al*., 1988), and whole rock compositions of sulfide-free adcumulate dunites at persevance also show evidence of olivine depletion as much as 1 km away from the ore zone (see below).

Relict igneous olivine is only preserved in the lower third of the host unit at Katinniq, but exhibits an overall upwards increase in maximum Fo content and mostly reverse zoning, with local reversals to lower Fo and normal zoning (Lévesque

et al., 2002; Lesher, 2007). High Ca (up to 0.29% CaO) and Mn (up to 0.24% MnO) contents indicate rapid cooling. The variations in maximum Fo contents do not correlate with trapped liquid contents, indicating that the olivines crystallized *in situ* and were not transported as intratelluric phenocrysts. The increase in Fo content with stratigraphic height, combined with the reverse zoning of the crystals, is consistent with a model involving progressive magma replenishment in a channelized flow or sill. The Fo contents (Fo_{88-85}) suggest that the composition of the magma ranged ~11%－14% MgO, depending on FeO content, which is much less than the 18% MgO composition of the parental magma inferred from Fe-Mg trends of cumulates and the compositions of chilled margins and associated lavas, but consistent with trace element geochemical studies, which indicate that these rocks have been contaminated by upper crustal rocks, most likely *via* thermomechanical erosion of underlying and adjacent semi-pelites and gabbros (Lesher *et al*., 2001; Lesher, 2007).

Chromite

Chromite is an ubiquitous cumulus-intercumulus accessory phase in komatiites and komatiitic dunites (Barnes, 1998). Most grains exhibit magnetite rims that increase in width and Cr content with increasing metamorphic grade (Donaldson, 1983; Barnes, 2000). Chromites in mineralized komatiite sequences contain 71－74 mole% $R^{2+}Cr_2O_4$, 21－24 mole % $R^{2+}Al_2O_4$, and 4－5 mole % $R^{2+}Fe_2O_4$, and 0.6－2.2 atomic % Zn (see summaries by Lesher, 1989; Barnes, 2000). Chromites in komatiitic dunites show a wider range in composition, down to essentially zero ferric iron, anomalously low Cr/Al ratios, and Zn contents up to 2% (Fig. 2.41). They also show a range in morphology, closely corresponding to the composition of the associated olivine. Chromite in dunites with Fo_{92-93} olivines commonly shows poikilitic interstitial morphologies, frequently misinterpreted as "intercumulus"-these morphologies are actually evidence of in-situ simultaneous growth of chromite and olivine, with rapid relative growth rates of chromite causing molding around olivine grains (Barnes and Hill, 1995). Chromites in mineralized komatiite sequences from amphibolite facies metamorphic environments have high Zn contents, irrespective of the stratigraphic position of the ultramafic flow in which they occur (Groves *et al*., 1977; Lesher and Groves, 1984), although there is evidence that Zn in chromites varies with stratigraphic height within individual units (Donaldson, 1981; Lesher, 1989). Chromites from greenschist or sub-greenschist environments very rarely have elevated Zn. Barnes (2000) argued on the basis of this observation and detailed grain mapping that elevated Zn contents were largely secondary in origin.

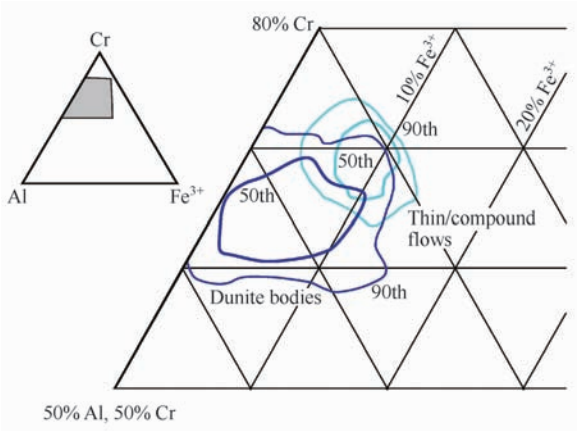

Fig. 2.41 Compositions of chromites from low-metamorphic grade komatiites, subdivided into dunite host rocks, and thin differentiated or compound flow environments. Fields show 50th and 90th percentile contours on data density.

2.3 Lithogeochemistry

Regional metamorphism, including serpentinization and commonly talc-carbonation, has chemically modified all komatiites to some degree (see review by Arndt *et al*., 2008). Alkalic (Cs, Rb, K, Na) and calc-alkalic elements (Ba, Sr, Ca, Eu^{2+}) were most mobile, especially in cumulate rocks where there are few metamorphic phases capable of housing those elements (see discussion by Lesher and Stone, 1996 and Barnes *et al*., 2004). However, Si, Al, Mg, trivalent transition metals (Sc, Ti, V, Cr), some divalent transition metals (Fe, Co, Ni), and most rare-earth elements (REE) and high field-strength elements (Y, Zr, Nb, Ta) appear to have remained relatively immobile (Lesher and Stone, 1996; Barnes *et al*., 2004). At Thompson La was more mobile during recrystallization of serpentine than the other REE (Layton-Matthews *et al*., 2007).

2.3.1 Major element geochemistry

Major element geochemical variations in all areas are consistent with fractional crystallization and accumulation of olivine (e.g., Lesher, 1989; Barnes *et al*., 1988, 2004, 2007; Lesher and Arndt, 1995; Perring *et al*., 1996; Sproule *et al*., 2002; Burnham *et al*., 2003; Lesher, 2007). The compositions of initial liquids deduced from the compositions of upper chilled margins or fine-grained random spinifex-textured zones of the host units (coarse platy spinifex-textured rocks have accumulated olivine), calculated from the compositions of cumulus olivine using experimentally-determined partition coefficients, and inferred from the compositions of conformably overlying lavas are consistent. The initial liquids for these deposits appear to range from an apparent maximum near 32% MgO for most Archean deposits through a maximum of ~22%－24% MgO for Thompson and Namew Lake to a maximum 18% MgO for Raglan (Fig. 2.3), and as noted

above, include Al-undepleted (most deposits), Al-depleted (Forrestania, Ruth Well), and Fe-Ti-rich (Pechenga) types (Table 2.3).

Host units are typically more magnesian than stratigraphically equivalent barren flanking units (e.g., Gresham and Loftus-Hills, 1981; Lesher and Groves, 1984; Hill *et al*., 1995; Perring *et al*., 1995; Beresford *et al*., 2002; Lesher, 2007). At Kambalda, for example, the basal host units are significantly enriched in Mg and Ni, and depleted in Ti, Al, Cr, Fe and Zn relative to adjacent barren flanking units, contain more forsteritic olivine (Fo_{94-91}), and crystallized from more magnesian liquids (28% – 31% MgO) than the barren flanking units (< 26% MgO and Fo_{91-89}, respectively). Analogous variations are observed at Perseverance (Barnes *et al*., 1988) and Raglan (Lesher, 2007). These variations preclude models involving accumulation of intratelluric olivine (e.g., Naldrett and Campbell, 1982).

High-Mg komatiites are undersaturated in chromite (Arndt, 1975; Murck and Campbell, 1986) and Cr occurs in only minor amounts in olivine, so Cr contents decrease with increasing Mg. However, low-Mg komatiites and komatiitic basalts are saturated in chromite, so Cr contents increase with increasing Mg (Lesher and Stone, 1996; Barnes and Brand, 1999).

2.3.2 Lithophile trace element geochemistry

The trace element geochemical variations in most areas are also consistent with fractional crystallization and accumulation of olivine. Elements that are housed in olivine or housed in phases included in olivine (e.g., , Ni, Co) increase with increasing Mg and elements that are not housed in olivine (U-Th-Nb-Ta-Zr-Y-REE) decrease with increasing Mg. Most mineralized Al-depleted komatiites are depleted in HILE[1] relative to MILE and, where analyzed, exhibit positive ε_{Nd} values consistent with derivation from a long-term depleted (normal) mantle source. However, HILE are *locally* enriched with accompanying negative Nb-Ta-(Ti) anomalies, which suggests that they were contaminated at or near the site of emplacement (e.g., Lesher and Arndt, 1995; Lesher *et al*., 2001; Sproule *et al*., 2002; Barnes *et al*., 2004, 2007).

2.3.3 Chalcophile trace element geochemistry

The chalcophile element geochemical variations of most of the komatiites in most areas are also consistent with fractional crystallization and accumulation of olivine. Elements that are housed in olivine or housed in phases included in olivine (e.g., Ni, Co, Ir) increase with increasing Mg and elements that are not housed in olivine (Pd and Pt) decrease with increasing Mg. Cu is typically scattered and appears to have been mobile. This indicates that most of the komatiites did not equilibrate with sulfides in the source or during ascent and emplacement. However, PGE are locally depleted, which suggests that they equilibrated with sulfides at or near the site of emplacement (e.g., Lesher *et al*., 2001; Sproule *et al*., 2005; Barnes *et al*., 2004, 2007).

2.4 Exploration geochemistry

Several geochemical and mineralogical methods of discrimination have been used to distinguish between mineralized and unmineralized komatiites (see reviews by Lesher, 1989, Lesher and Stone, 1996; Lesher *et al*., 1999, 2001; Barnes *et al*., 2004), including Fe-Mg and Ni-Cr in whole rocks, HILE/MILE and Nb/Th ratios in whole rocks, Ni in olivine, Zn in chromian spinel, and trace sulfide contents. This section describes general principles and relationships. Some specific discriminant diagrams, employing these principles and designed for use in exploration programs, are discussed in more detail below under the heading "Applications".

2.4.1 Background

Whole-rock Fe-Mg and Ni-Cr trends

Whole-rock Fe-Mg (Lesher and Groves, 1984; Lesher, 1989; Barnes *et al*.,2004, 2008) and Cr-Ni (Woolrich and Giorgetta, 1978; Lesher and Stone, 1996; Barnes and Brand, 1999) may aid in the identification of channel-flow facies that are more likely to host Ni-Cu-(PGE) mineralization than sheet-flow, lava-pond, or lava-lobe facies. This is because channel-flow facies rocks normally crystallize from more magnesian lavas or from magmas that, if komatiitic, are more likely to (a) be undersaturated in magnesiochromite, (b) crystallize more magnesian olivine, and (c) accumulate larger amounts of olivine, than those in sheet-flow, lava-pond, or lava-lobe facies. However, these processes are not directly related to ore genesis; not all high-Mg, low-Cr cumulate rocks are mineralized, and any mafic magma more evolved than ~20% MgO will be saturated in chromian spinel (Murck and Campbell, 1986) and will produce Cr-rich cumulate rocks (see discussion by Lesher and Stone, 1996). A further complication is that high-Mg channel-flow facies as a group exhibit a wide range of Cr contents that reflects the kinetics of crystallization of the chromian spinel (Barnes, 1998) and/or accumulation of olivine then olivine + chromian spinel from lavas that fractionated and became saturated in ch-

[1] HILE – highly-incompatible lithophile elements (e.g., U-Th-Nb-Ta-LREE); MILE – moderately incompatible lithophile elements (e.g., Zr-MREE-Ti-HREE).

romian spinel during crystallization (Lesher and Stone, 1986). These complications have been discussed by Barnes and Brand (1999), who showed that mineralized komatiite sequences on average have substantially lower Cr contents and Cr∶Ni ratios than unmineralized sequences, this difference being largely due to a combination of magma composition and volcanic facies, but that there is no systematic difference between barren and mineralized units from the same volcanic facies.

Trace element geochemistry

Although crustal contamination of komatiites does not necessarily bring them to sulfide saturation in the absence of a high S content in the contaminant (Lesher and Groves, 1986; Lesher and Arndt, 1995), magma conduits and lava channels are more likely to erode their wall rocks than sheet flows or lava lobes. If this contaminant is upper continental crust or sediments derived from upper continental crust, which are enriched in HILE relative to MILE and depleted in Nb-Ta relative to the other HILE and in Ti relative to the other MILE, then the komatiites, which are normally depleted in HILE relative to MILE, will become enriched in HILE and will exhibit negative Nb-Ta-(Ti) anomalies. Ratios such as La/Sm or La/Yb, Zr/Ti, and Nb/Th or Nb/Yb are particularly useful indicators of contamination, as they are incompatible in olivine, chromite, and sulfides, and because komatiites are high degree partial melts, any departures from mantle ratios can only be due either to contamination or to alteration. Discriminating between these two processes is critical because some elements, notably La and probably Zr, are sufficiently mobile that ratios may be significantly perturbed in rocks with low concentrations, specifically olivine-rich cumulates (Barnes *et al*., 2004b). As long as sample sets are restricted to liquid-rich komatiite lithologies then ratios involving all these elements can be used as reasonably reliable contamination indicators. Care must be taken to obtain high precision analyses, as errors are multiplied when comparing ratios. Lesher and Arndt (1995), Barnes *et al*. (1995), Perring *et al*. (1996), and Lesher *et al*. (2001) have shown that mineralized units at Forrestania, Perseverance, Raglan, and Thompson are contaminated relative to unmineralized units, but that the unmineralized barren flanking units at Kamblada are contaminated relative to mineralized units. The differences are attributable to differences in the thickness of the contaminant: the contaminant at Kambalda was a thin (average 1m) sediment overlying refractory basalt, whereas the contaminants at Forrestania, Perseverance, Raglan, and Thompson were much thicker. However, it is also important to appreciate that contamination is strongly influenced by the amount of magma being processed by the system; contamination will increase rapidly as the flow reaches turbulent conditions, peak at a point close to where the lava/magma flows most turbulently, and then decline as the flow rate (and dilution) increase (see Lesher *et al*., 2001). What is most important is that the contamination be local; if all of the units in a sequence are contaminated, it may reflect contamination at depth or during ascent.

Whole-rock chalcophile element depletion

Chalcophile elements such as Ni, Co, Cu, and PGE partition preferentially into the sulfide phase relative to olivine or silicate magma. Thus, the abundances of these elements in derivative silicate liquids should be strongly influenced by the proportions of fractionated olivine and sulfide that equilibrate in a magma (Duke and Naldrett, 1978; Campbell and Naldrett, 1979; Duke, 1979; Campbell and Barnes, 1984) and should be a sensitive test of magmas that have equilibrated with sulfides. Lesher *et al*. (1981) showed that spinifex-textured komatiites from barren sequences (e.g., Barberton), barren sequences that correlate with mineralized sequences (e.g., Belingwe, Munro), barren flows overlying Type Ⅱ deposits (e.g., Yakabindie), or flows that are associated with only weak disseminated mineralization (e.g., Mt. Clifford) plot along trends expected for olivine-only fractionation. In contrast, spinifex-textured komatiites from mineralized sequences at Kambalda, Scotia, and possibly Widgiemooltha are slightly, but significantly depleted in Ni (and Co, not shown) relative to barren komatiites and trends expected for olivine-only fractionation. Spinifex-textured rocks from thin flow units above Lunnon and Long shoots (Keays *et al*., 1981) are similarly depleted. Cu (and Zn) scatter owing to mobility during alteration and metamorphism. Lesher *et al*. (1981) found no systematic variations between degree of Ni depletion and type of alteration (serpentinization vs. carbonation), proximity to sulfide mineralization (mineralized vs. unmineralized flows), or stratigraphic position (lower vs. upper member), and attributed the depletion at Kambalda to scavenging of chalcophile elements by sulfides prior to eruption. They noted, however, that dispersion in the data required involvement of more than one petrogenetic process. Lesher and Arndt (1995) and Lesher *et al*. (2001) subsequently showed that the olivine spinifex-textured and cumulate rocks overlying the host units and the cumulate rocks in the barren flanking units at Victor shoot and Lunnon shoot at Kambalda are much less contaminated and much less depleted in Ni, Cu, and PGE than pyroxene spinifex-textured and pyroxene cumulate rocks in the barren flanking units, which they attributed to replenishment of the host units and the cores of the barren flanking units after ore emplacement.

PGE have much higher sulfide/silicate partition coefficients of the order of 10^5 (see reviews by Lesher and Stone, 1996; Barnes and Lightfoot, 2005), and should be more sensitive to sulfide separation than Ni, Cu, or Co, but are more difficult to sample and analyze because of their low abundances in silicate rocks. Initial comparisons of data from

Alexo (Brügmann *et al*., 1987), Long, Lunnon, and Victor shoots, Kambalda (Keays *et al*., 1981), Pyke Hill, Munro Township (Crocket and MacRae, 1986), and Mt. Clifford (Keays, 1982) indicated that PGE variations are much more complex. Although Pd-MgO variations were too disperse to infer any differences attributable to sulfide separation, the analysed Kambalda samples were not depleted in Pd relative to the other suites and most of the variation was broadly consistent with olivine fractionation (Pd is relatively incompatible in olivine). Why Kambalda lavas appear to be depleted in Ni, but not Pd was not explained. The solution came from the study of Lesher *et al*. (2001), which showed that the upper spinifex-textured zones capping the barren flanking basal units at Lunnon and Victor shoots are strongly depleted in PGE compared to the upper spinifex-textured zones capping the mineralized basal units, also consistent with the mineralized units being replenished. Interestingly, the cumulate zones in the barren flanking units are not depleted, indicating that they were replenished underneath a depleted crust. This suggests that the flanking sheet-flow facies formed crusts prior to the lava channel facies, consistent with the former having flowed laminarly and the latter having formed turbulently (Lesher *et al*., 1984; Frost and Groves, 1989; Lesher, 1989; Cowden and Roberts, 1990; Williams *et al*., 1998; Cas and Beresford, 2001; Beresford *et al*., 2002).

Ni depletion in olivine

Ni depletion in olivine occurs as part of the chalcophile-element depletion process affecting the whole rock (Duke and Naldrett, 1978; Lesher and Burnham, 1999, 2001) and may be a useful tool for exploration in areas where it is preserved. Although olivine is susceptible susceptible to post-cumulus or metamorphic modification and is commonly pervasively serpentinized, Ni is relatively immobile on the hand-sample scale in olivine cumulate rocks (Donaldson, 1981). The level of Ni in olivine can therefore also be estimated from whole-rock analytical data. For example, an extensive Ni depletion halo was identified in the lower part of the Perseverance dunite body, both in modified igneous olivine compositions and in whole rock elemental data (Barnes *et al*., 1988). Such haloes are a feature of large mineralized flow systems at low magma: sulfide ratios (*R* factors).

Zn enrichment in chromite

Zn enrichment in chromian spinel (e.g., Groves *et al*., 1977) may be a useful tool for exploration in areas where the contaminant is enriched in Zn relative to the magma and where metamorphic grades are low. However, not all contaminants are enriched in Zn, chromian spinel commonly re-equilibrates with the intercumulus liquid during cooling, and Zn has been mobile in many cases during metamorphism. For example, H. Papunen (pers. comm. 1996), Baird (1999), and Barnes (2000) have shown that Zn is commonly added to chromian spinel during low-temperature alteration and further concentrated in the core of grains during prograde metamorphism. Thus, the highly Zn-enriched chromian spinel Widgiemooltha and Kambalda may therefore result from proximity to sedimentary Zn sources during metamorphism and may not necessarily result from igneous processes (see discussion by Barnes, 2000).

Trace sulfides

The presence of sulfides is a very reliable indicator of sulfide saturation, but many sulfide-saturated cumulate rocks are non-economic, and the absence of sulfides does not necessarily indicate that the unit did not form an ore deposit. Although lavas or magmas that have achieved sulfide saturation will normally continue to exsolve a sulfide liquid as they cool, crystallize, and oxidize (see review by Naldrett, 1989, 2004), continued flowage though the lava channels may drive the lava or magma away from sulfide saturation, leaving essentially barren cumulate rocks over the ore zones. For example, at Kambalda (Lesher *et al*., 1984; Lesher, 1989), Perseverance (Barnes *et al*., 1988, 1995), and Digger Rocks (Perring *et al*., 1995), sulfide-bearing cumulates are overlain by sulfide-free cumulates in the same lava channel, indicating that the lava evolved from sulfide-saturated to sulfide-undersaturated during the eruption. The later lavas flowed over a bed of early-formed cumulates and flushed out the earlier sulfide-saturated, contaminated lavas. The resulting cumulates retain no trace of the mineralizing processes. Thus in some areas, contaminated lavas may be preserved in close proximity to the ores (Perseverance: Barnes *et al*., 1995; Lesher *et al*., 2001; Digger Rocks, Perring *et al*., 1995; Raglan and parts of Thompson: Lesher *et al*., 2001), in some areas they may only be preserved in lateral flanking facies (e.g., Kambalda: Lesher and Arndt, 1995), and in some areas they may not be preserved at all (e.g., parts of Thompson: Lesher *et al*., 2001). These complexities must be considered when interpreting komatiite geochemistry, which must always be viewed from the standpoint of physical volcanology.

2.4.2 Application

This section applies the principles outlined above to practical exploration problems, drawing on a large training set of empirical data on well-studied ore-bearing and unmineralized komatiite units from around the world. The data summarized here are from an updated version of the comprehensive database of Archean and Proterozoic komatiite compositions compiled by Barnes et al. (2007). The samples have been subdivided into dunitic conduit (DC), compound sheet flow (CSF), lava lakes and sills (LLS), and thin differentiated lobe (TDL) facies. A "mineralization score" (1 – 5) has been assigned to each unit:

1 = units containing major (>50 k-ton Ni) mineralization (e.g., Kambalda, Mt. Keith, Perseverance, Raglan, Thompson).

2 = units containing minor (<50 k-ton Ni) mineralization (e.g., Dundonald, Alexo).

3 = barren units in close proximity to known mineralization (e.g., Tripod Hill Member at Kambalda) and weakly mineralized units from otherwise barren belts (e.g., Acra locality, East Yilgarn).

4 = barren units in sparsely mineralized greenstone belts (e.g., Murphy Well, Western Australia; Pyke Hill, Ontario).

5 = barren units in completely barren greenstone belts (e.g., Gabanintha, Western Australia).

"Units" are defined as coherent stratigraphic packages of multiple komatiite flows and/or intrusions separated by non-komatiitic rocks on a scale of tens of meters.

The designation of "unmineralized" versus "mineralized" sequences is, of course, not rigorous. We can never be sure that any sequence flagged as "unmineralized" might not host, or have hosted, undiscovered or eroded mineralization. The best that can be done within an individual framework is to limit the "unmineralized" designation to relatively well explored sequences, bearing in mind that there may be many false negatives.

The "training" data set shown in the following figures has been filtered to remove samples that do not contain obviously recognizable magmatic sulfides, using filters based on the S content, and also the MgO-Ni relationship discussed further below. We also eliminated samples showing evidence for extensive metasomatic alteration.

Identifying favorable volcanic facies

Almost all known deposits of any significance occur within lava channels/conduits or channel/conduit-flow facies of channelized sheet flows (Lesher, 1989; Hill and Gole, 1990; Barnes, 2006; Arndt *et al*., 2008). So, it is crucial to be able to distinguish such units and their internal facies at an early stage in an exploration program, and to be able to determine vectors towards pathways within them.

This section describes distinctly different patterns of distribution within the various volcanic facies Fig. 2. 9 and Fig. 2. 39) of elements such as Mg, Fe, and Ni which are compatible in olivine, elements such as Al and Ti which are incompatible, and Cr which is concentrated in chromite but behaves incompatibly in high-MgO chromite-undersaturated liquids (Lesher and Stone, 1996; Barnes, 1998). These patterns are the result of several superimposed factors: (1) crystallization kinetics, which determine the nucleation, morphology, and degree of segregation of olivine and chromite, (2) the extent of crystal/liquid fractionation, which is enhanced by physical ponding of lava and in situ crystallization, (3) processes of inflation and lobe front propagation, which ultimately give rise to formation of long-lived lava pathways, and (4) fluid dynamic processes governing the transport and segregation of crystals from flowing liquid-crystal suspensions.

MgO-FeO

MgO and FeO relationships define the degree of concentration or fractionation of olivine, and also the composition of that olivine. Distinctions between the various facies categories are shown as data density plots in Fig. 2. 42.

The data sets plotted in Fig. 2. 42 draw on the complete database, after filtering for alteration as described above. Trends are interpreted as the result of mixing between komatiite (18 – 30 wt% MgO) and komatiitic basalt (10 – 18 wt% MgO) liquids and olivine of variable composition. Data for dunitic conduit (DC) facies cluster near the pure olivine line, indicating a prevalence of olivine adcumulate and mesocumulate rocks with a relatively restricted range of compositions (mostly Fo_{91}-Fo_{94}). This limited range is a function of extensive flow-through of hot, primitive lava in long-lived pathways, with limited ponding and internal differentiation. Lava lakes and sills (LLS) are also dominated by adcumulate and mesocumulate rocks, but show a much wider range of olivine compositions (mainly Fo_{87}-Fo_{93}). This wider range is a function of localized ponding and fractionation. A further consequence of this is the presence of a linear trend of fractionated liquid compositions with 10% – 15% MgO and 5% – 14% FeO; the low FeO compositions are a hallmark of liquid that has been buffered by reaction with large volumes of relatively Fe-rich olivine. Compound sheet flow (CSF) and thin differentiated lobe (TDL) facies both show extended linear mixtures of a wide range of olivine and liquid compositions, the CSF category having a higher proportion of very olivine-rich rocks (mainly Fo_{91}-Fo_{93}) and a lower proportion of liquid-rich compositions. The fields for mineralized units closely match the combination of fields for dunitic conduits and channelized sheet flows. Finally, a comparison of channel vs. flank environments at Kambalda reveals a similar overall spread of data points at the 80th percentile level, but a considerably tighter cluster of data towards the olivine-rich end of the trend and a more dominant component of very olivine-rich mesocumulates in the channels, as noted by Lesher and Groves (1984).

Ni/Ti-Ni/Cr

Ni and Cr are used to distinguish olivine-rich, chromite-poor mineralized lava channel/conduit facies from less olivine-rich, more chromite-rich unmineralized sheet-flow facies. The most useful strategy is to ratio these elements with Ti or Al, as ratios of these elements, all of which are relatively immobile except during very intense alteration or weathering, are unlikely to be significantly fractionated during metamorphism and/or mild weathering. Inter-element ratios are particularly useful in cheaply-accessible sample materials such as bottom-hole samples from percussion drilling, where Mg is almost

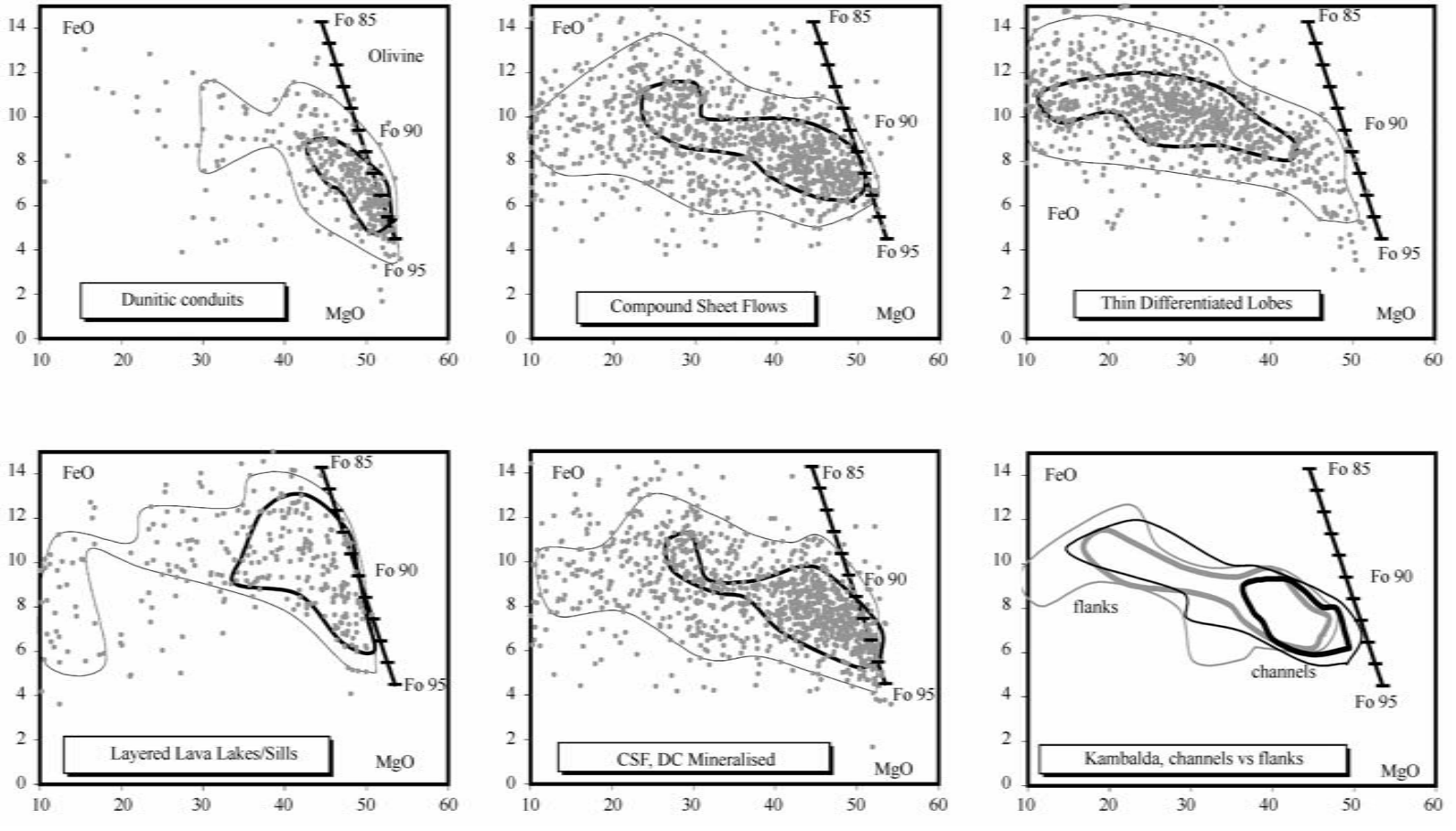

Fig. 2. 42 Data density plots showing FeO-MgO variations in the global komatiite database, subdivided by facies. Contours are 50th and 80th percentiles on data density for each grouping.

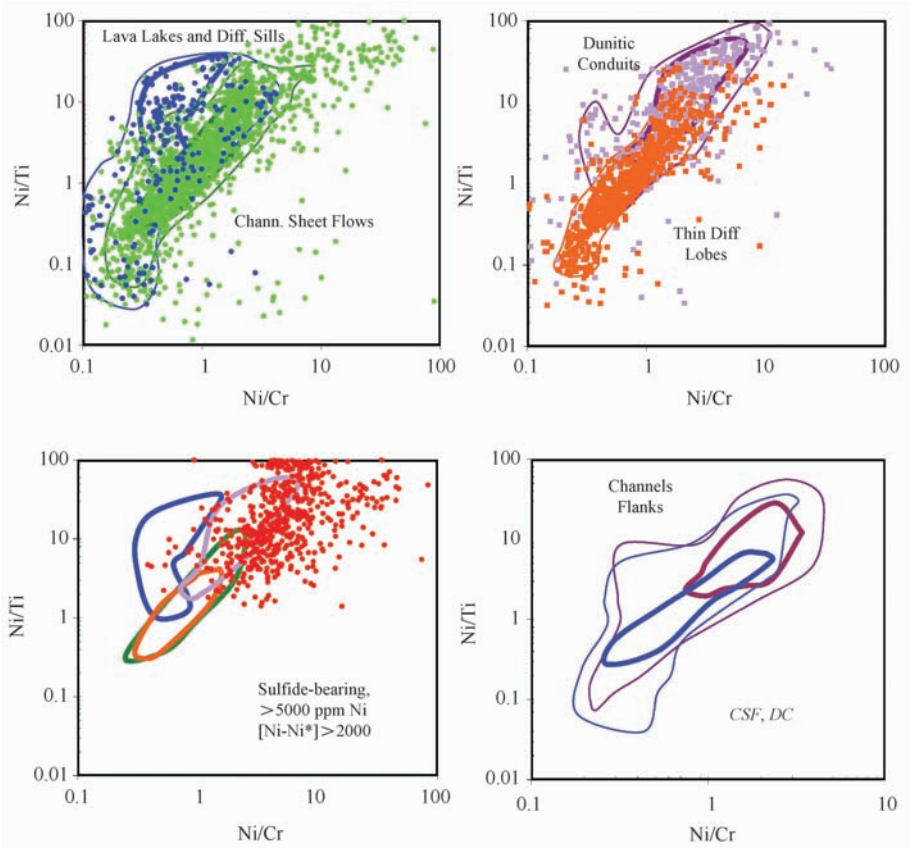

Fig. 2. 43 Plots of weight ratio of Ni/Ti vs. Ni/Cr showing characteristic fields for different volcanic facies (50th and 80th percentiles, upper diagrams), comparison of 50th percentile facies fields for data on disseminated sulfide-bearing rocks; and comparison of channel and flanking facies within the Kambalda compound flow sequence.

certain to have been leached. Ti is preferable to Al, so that both Al-depleted and undepleted suites can be included. Importantly, reliable analyses of Ti, Ni, and Cr within the concentration ranges of interest can now be obtained using portable XRF analysers on drill core or percussion drill spoil eliminating the expense of obtaining research-quality whole rock analyses of fresh rocks. Ni/Ti and Ni/Cr (Fig. 2. 43) distinguish lava lake/sill (LLS) sequences (high Ni/Ti, low Ni/Cr) and dunitic conduits (DC) (high Ni/Ti, high Ni/Cr) from thin differentiated lobe (TDL) and channelized sheet flow (CSF) sequences. Samples containing small amounts of accumulated Ni-rich sulfides define a distinct trend related to the tendency for some sulfide-bearing samples to contain anomalously low Cr, and increasing Ni sulfide content moves data points rapidly towards the top right end of the diagram and out of the defined fields for host rocks. Within compound flow facies, this plot also demonstrates a clear contrast between relatively Ni-rich, olivine-rich rocks in pathways compared with the less olivine-rich flanks, even where sulfide-bearing samples are excluded. This approach is expected to become progressively more useful as the quality of portable XRF instrumentation improves.

Identifying contamination

La/Sm or La/Yb (or Ce/Sm or Ce/Yb if La has been shown to be mobile), Zr/Ti, and Th/Nb or Th/Yb are used to identify contamination, remembering that these elements are more mobile and are determined with lower precision in olivine-rich rocks than in olivine-poor rocks.

Mineralized vs. unmineralized sequences

Fig. 2. 44 shows data density fields for various trace element ratio combinations, comparing mineralized vs barren komatiite units over the known range of greenstone terranes, including the Proterozoic Raglan and Thompson belts. Data are plotted after random exclusion of samples from over-represented localities, as described by Barnes *et al.* (2007). Although the data sets are largely indistinguishable at the 50th percentile level, with the exception of Th/Nb, at the 80th percentile level mineralized units clearly show wider ranges, and distinct evidence for crustal contamination, relative to unmineralized units. The positive correlation between these ratios, and particularly the correlation between Th/Nb and Ce/Sm, is predicted consequence of contamination, as opposed to other mantle-related sources of variability in these elements.

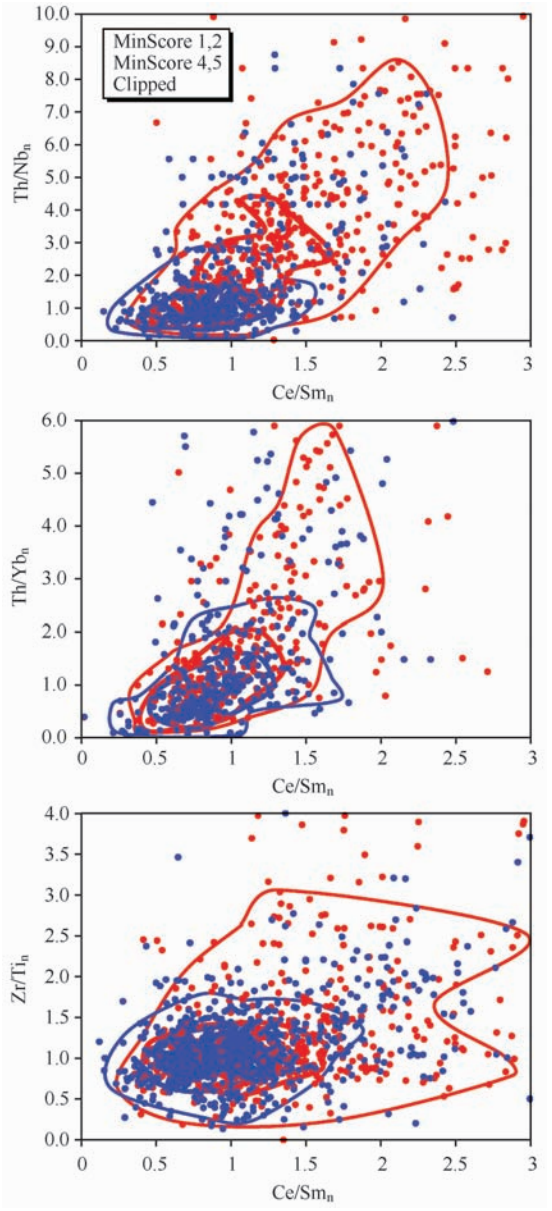

Fig. 2. 44 Lithophile trace element ratio contamination indices-mineralized vs. unmineralised komatiite sequences, 50th and 80th percentils. Data set clipped to compensate for overrepresented localities.

Mineralized vs. unmineralized terranes

A contrast in contamination indicators is clearly evident at terrane scale (Fig. 2. 45), where the Abitibi Belt, the terrane with the lowest endowment of nickel sulfides, shows the tightest cluster of data with predominantly primitive to depleted ratios of Th: Nb and Ce: Sm. Barnes *et al.* (2007) further showed that the most highly mineralized segment of the Abitibi belt, the Shaw Dome region, is characterized by the most contaminated trace element signatures in the komatiites.

In summary, HILE enrichment and negative Nb-Ta-(Ti) anomalies may indicate crustal contamination and may therefore be an indirect guide to mineralization if the contamination process involved incorporation of S, but because contamination alone does not normally bring a komatiite to saturation in sulfide (e.g., Paringa Basalt at Kambalda: Redman and Keays, 1985; Lesher and Arndt, 1995). Contamination signatures are therefore unreliable in the absence of other geological and volcanological evidence, but they may be useful in regional targeting, especially if the contamination is localized.

Identifying sulfide accumulation and fractionation

Ni-MgO

One of the intrinsic challenges in exploring for Ni in komatiites is the high background of unmineralized host rocks, particularly where these rocks are olivine-rich cumulates. Fortunately the background Ni contents of the can be predicted with some confidence from MgO content (Fig. 2. 46). Rocks containing excess sulfide nickel, even where (as is often the case) S has been lost during alteration, will have Ni contents greater than

$$Ni^{*} = 1.1(0.19MgO^{2} + 74MgO - 493)$$

which is based on a polynomial best fit to the Ni-MgO data set in komatiites from unmineralized belts and domains (Fig. 2. 46). This line is a very good fit to the 80th (and 90th) percentile data density contour.

Samples falling well below the unmineralized Ni-MgO trend may well be identifiable as favorable host rocks by virtue of being depleted in Ni owing to prior equilbration with magmatic sulfides. However, on the whole it appears that there is little systematic difference between mineralized (groups 1 and 2) and barren (groups 4 and 5) komatiite sequences worldwide, over and above the difference due to the much higher proportion of extremely olivine enriched cumulates in the former (Fig. 2. 46). This arises from the wide range in liquid compositions and corresponding olivine compositions represented in the data set, the fact that mineralized systems may be replenished erasing any evidence of Ni depletion (Lesher and Arndt, 1995; Lesher *et al.*, 2001), and the fact that magmas depleted in Ni but containing sulfides may form rocks with less depleted or undepleted signatures.

A clearer picture emerges from whole rock data on olivine adcumulates and mesocumulates, where the whole-rock composition is a close approximation to the original olivine composition. Fig. 2. 47 shows data from sulfide-free host rocks from three mineralized cumulate-rich complexes, all from the east Yilgarn: Perseverance, Mt Keith, and Black Swan. Data are plotted against $Mg^{\#}$, as a proxy for the forsterite content of the olivine component. Samples from Perseverance and Mt Keith, which both host extremely large ore bodies, are distinctly depleted in Ni compared with analyzed olivine compositions from typical unmineralized komatiite flows worldwide, although not as depleted in Ni as olivines from the disseminated sulfide ore zones of komatiite cumulate complexes (including Perseverance). In contrast, the Black Swan complex, which hosts a much smaller deposit, shows

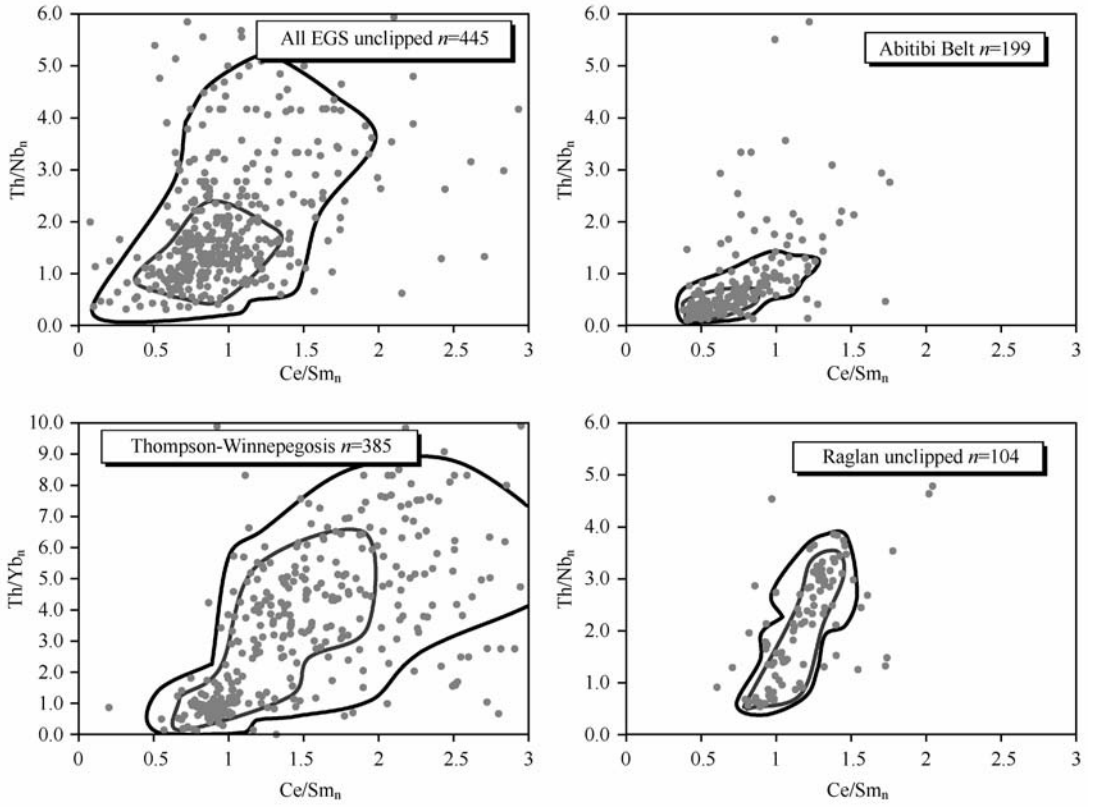

Fig. 2. 45 Lithophile trace element ratio contamination indices-50th and 80th percentiles on data from the eastern Goldfields Superterrane, Abitibi Belt, Thompson and Raglan belts. Data set clipped to compensate for overrepresented localities contamination indices-location.

a whole rock trend in mesocumulates exactly corresponding to that of olivines from "barren" flows. To complicate matters further, a number of sheeted dunite complexes in the East Yilgarn (represented within the "barren units in mineralized domains" set in Fig. 2. 47) show whole rock trends very similar to those of Perseverance despite containing no known sulfide accumulations. For all of these reasons, Ni depletion in olivine-rich rocks appears to be an imperfect although potentially useful discriminator of prospectivity.

PGE in low-S rocks

Platinum group elements (PGE) are extremely sensitive to sulfide liquid extraction owing to their extremely high partition coefficients into sulfide liquids (see review by Barnes and Lightfoot, 2005). Evidence of PGE depletion might therefore be expected in low-S rocks from mineralized komatiite sequences. Pd or Pt are normally used because although all PGE have high sulfide: silicate partition coefficients, IPGE are also compatible in olivine and chromite. Pd/Ti or Pt/Ti ratios are normally used because although the absolute abundances of Pd and Pt will change with fractionation or accumulation of olivine, Pd, Pt, and Ti are all incompatible in olivine, so Pd/Ti and Pd/Ti ratios will not change with fractionation or accumulation of olivine. Finally, in order to compare the Pd/Ti or Pt/Ti ratios with those of the source, we have normalized them to the ratio in the komatiite source mantle (Puchtel *et al*., 2004), using the formula

$$(Pt/Ti)_{kn} = (ppb\ Pt / \%\ TiO_2) / 30$$

The komatiite mantle source value is considered more appropriate than other estimates of mantle PGE contents. Komatiite source compositions for komatiites younger than about 2. 9 Ga appear to be remarkably consistent (Maier, Barnes and Fiorentini, unpublished data), while estimates of primitive mantle PGE contents from analyses of mantle nodules are the subject of vigorous debate and widely varying estimates, probably due to a combination of sampling biases and variance due to metasomatic processes (Lorand *et al*., 2008a, 2008b; Becker *et al*., 2006).

Fig. 2. 48 shows $(Pt/Ti)_{kn}$ vs. MgO in low-S rocks from a range of localities in the East Yilgarn, Abitibi, Raglan, and Thompson belts. $(Pt/Ti)_{kn}$ values close 1 indicate that Pt and Ti have not been fractionated from one another at any point between segregation from the mantle source and emplacement, consistent with previous interpretations that komatiites were undersaturated in sulfides in the source and remained undersaturated during ascent and emplacement (Keays, 1982, 1995; Barnes *et al*., 1985; Lesher and Stone, 1996). Values significantly below unity are expected in mineralized komatiite systems where the magmas have equilibrated with sulfide liquid

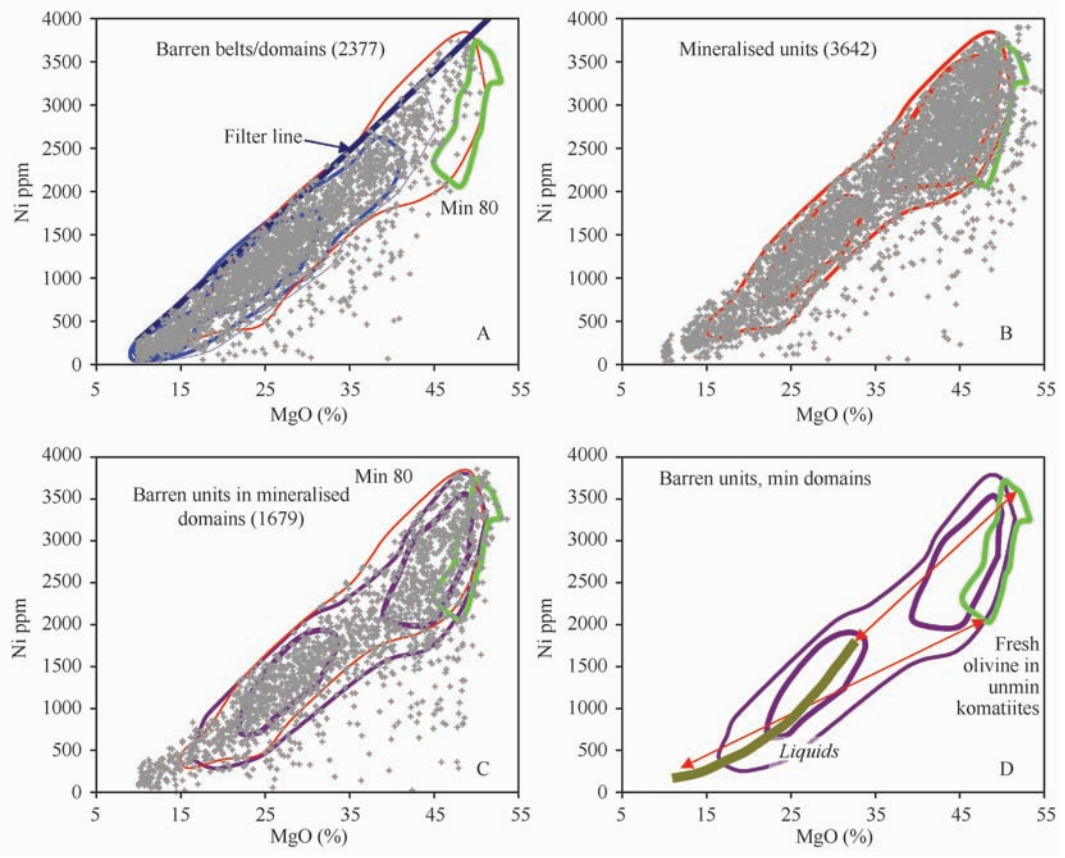

Fig. 2. 46 Plots of Ni (wt ppm) vs. MgO (anhydrous wt%) in all komatiitic rocks in the global database (clipped for over-represented localities), subdivided by various measures of association with mineralization. "Filter Line" is an empirical cut-off for samples containing excess sulfide nickel. Fields are 50th and 80th percentiles on data density. 80th percentile line for mineralised units is shown for reference on all plots. Green outline contains 80% of all data on measured fresh olivine compositions in komatiites, data from Arndt *et al.* (2008) and other unpublished sources. A. Data from unmineralised belts and domains. B. Mineralized belts and domains. C. Unmineralized units within mineralized belts and domains. D. Mixing lines between model liquids and equilibrium olivines.

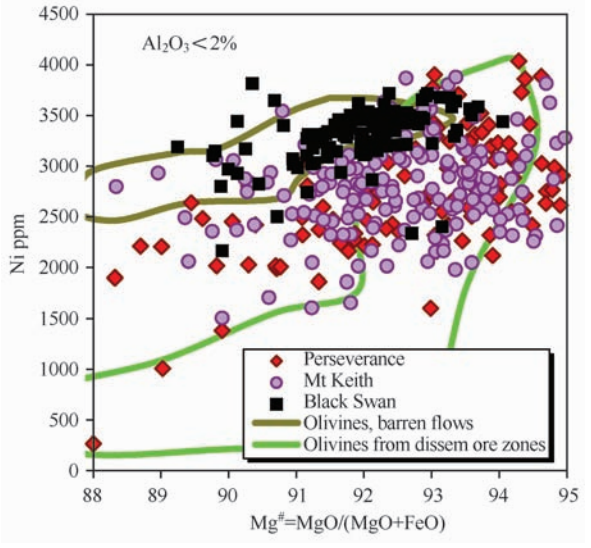

Fig. 2. 47 Plot of whole-rock Ni (ppm) vs molar $Mg^{\#}$ for dunites (low Al olivine cumulates) from the east Yilgarn, compared with fields for microprobe data on fresh olivines from mineralized and barren dunite units.

and values above unity indicate the presence of accumulated sulfide liquid. The data set in Fig. 2. 48 shows a clear contrast between the mostly barren komatiites of the Abitibi Belt (with a few exceptions from mineralized localities) and the much more erratic sulfide-influenced signals of the strongly mineralized Kalgoorlie terrane of the east Yilgarn (particularly the Kambalda Dome) and both the Thompson and Raglan (Cape Smith) Belts. While a high proportion of samples from mineralized belts shows no detectable signal, this discriminator clearly has value where data sets are sufficiently large.

2. 4. 3 Conclusions-applicability of lithogeochemistry

This analysis, using methods likely to be employed during regional exploration, indicates that there is no single geochemical smoking gun for komatiite-associated Ni-Cu-(PGE) deposits. This is not surprising if we bear in mind that mineralizing systems in komatiites (and in most other magmatic sulfide occurrences) are very dynamic systems, involving prolonged flow-through of large volumes of magma. In many cases, the magma which produced a sulfide ore body may be

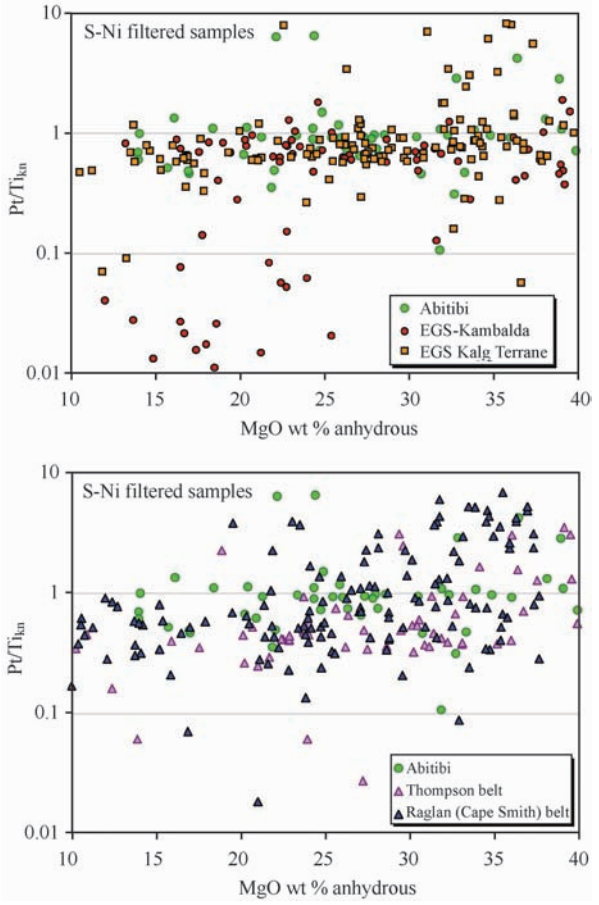

Fig. 2. 48 Plot of Pt/Ti, normalized to best estimate of komatiite source composition at 2. 7 Ga, vs MgO for various greenstone terranes. Data from Lesher *et al.* (2001), Burnham and Lesher(unpublished), Sproule *et al.* (2005), and Barnes and Fiorentini(2008 and unpublished).

very substantially decoupled from it by the time it solidifies, and a mineralized pathway is likely to be flushed out by new magma unrelated to the mineralizing event. As pointed out by Lesher and Arndt (1995), Lesher *et al.* (2001), and Hill (2001), the distribution of contaminated material in lava flow fields will therefore be a complex function of the flow history and the erodability of the substrate, which itself may be strongly influenced by its degree of consolidation (Williams *et al.*, 2001). This distribution may then be further overprinted and confused by metasomatic alteration.

Nevertheless, many of these lithogeochemical indicators are potentially useful in exploration, especially in combination with one another, at scales ranging from regional terrane evaluation to prospect-scale vectoring. By far the best geochemical indicator of prospectivity is, of course, the presence of Ni-enriched sulfides. However, recognition of such anomalies is complicated by high Ni backgrounds in the host rocks, coupled with the high degree of hydrothermal mobility of S. Use of the Ni-MgO background and of Ni-Cr-Ti ratios in weathered and altered rocks, is recommended to improve the detectability of such anomalies. All of these indicators are of greatest value when applied in a volcanological context.

2. 5 Mineralization

2. 5. 1 Distribution

Mineralization in komatiite-associated Ni-Cu-(PGE) deposits varies from stratiform, massive/net-textured/disseminated sulfides in Type I to strata-bound, disseminated to net-textured sulfides in Type Ⅱ. Stratiform mineralization occurs at or near the base of the basal host unit and is normally referred to as contact ore. Stratiform mineralization at the base of overlying flow units is locally referred to as hanging wall ore. Strata-bound, coarse disseminated spheroidal Type Ⅱ sulfides, termed "blebby", "globular", or "droplet" ore, occur centrally disposed within some komatiitic peridotite host units, isolated from contact ores (e.g., Otter shoot, Black Swan, parts of Raglan and many other deposits). Isolated zones of very fine disseminated Type Ⅱ sulfides have been termed "cloud" sulfides.

Some deposits contain only Type I or Type Ⅱ mineralization, but some contain both (Table 2. 3), indicating multiple stages of ore emplacement. Many Type I deposits (e.g., Kambalda) exhibit a contact ore profile comprising a thin, discontinuous layer of massive sulfides (< 20% gangue) directly overlying footwall rock and overlain successively by a thick, more continuous layer of net-textured (matrix) sulfides (20% – 60% gangue), disseminated sulfides (60% – 90% gangue), and barren host rocks. The zoning has been attributed to gravitational segregation-the "Billiard-Ball Model of Naldrett (1973), dynamic flow segregation (Hudson, 1972), dynamic remelting (Lesher and Campbell, 1993), and to density segregation and capillary infiltration (Bazilevskaya and Lesher, unpubl. data) after emplacement. However, some deposits (e.g., Alexo, Raglan) exhibit much more complex ore profiles (Houlé and Lesher, submitled to *Mineralium Deposita*; Chisholm *et al.*, 1999; Bazilevskaya and Lesher, unpubl. data.), which require multi-stage ore emplacement. The proportion of massive ore in some deposits appears to increase with shoot size (Marston *et al.*, 1981), but there are important exceptions (e.g., Perseverance) and massive ore thicknesses are influenced to a very large degree by deformation (see below).

Although the contact ore zone at Lunnon shoot (Ross and Hopkins, 1975) and many of the ore zones at Raglan (Lesher, 2007) are directly overlain by a very thick zones of low-grade disseminated mineralization, most ore zones at Kambalda and those at Alexo and other Type I deposits are overlain by only thin zones of low-grade mineralization. Some deposits, notably the Silver Swan deposit in the Black Swan camp and the Flying Fox deposit in the Forrestania belt, have

essentially no overlying disseminated or matrix ores, a relationship not explicable by tectonism in either case. This is probably related to the accessibility of S upstream from the site of deposition, the rate of magma replenishment, and the timing of ponding in the lava channels (Lesher *et al*., 2001).

Type Ⅱ deposits are typically relatively uniform in grade on a scale of tens of metres, but display centimeter-scale clumping or layering of sulfide abundance. Sulfide abundance commonly correlates on a centimetre scale with olivine grainsize fluctuations, implying that sulfide liquid and olivine accumulated simultaneously *in situ*, rather than by percolation of sulfide through a porous crystal mush. Typically, mineralized dunites grade into sulfide-free dunite, so ore boundaries are arbitrarily defined by cut-off grades.

2.5.2 Ore textures

Most studies of magmatic Ni-Cu-(PGE) deposits describe the textures of the ores, but there have been no systematic comparisons of the various textures. However, the primary (Fig. 2.49, Fig. 2.50), deuteric, and secondary textures of komatiite-associated Fe-Ni-Cu sulfide ores are similar to those in many other associations (Tables 2.8A and B). Of the primary textures (Table 2.8B), several are found more often in komatiite-associated deposits (net texture) and some are found only in komatiite associated deposits (spinifex-textured). The disseminated and net-textured ores associ-

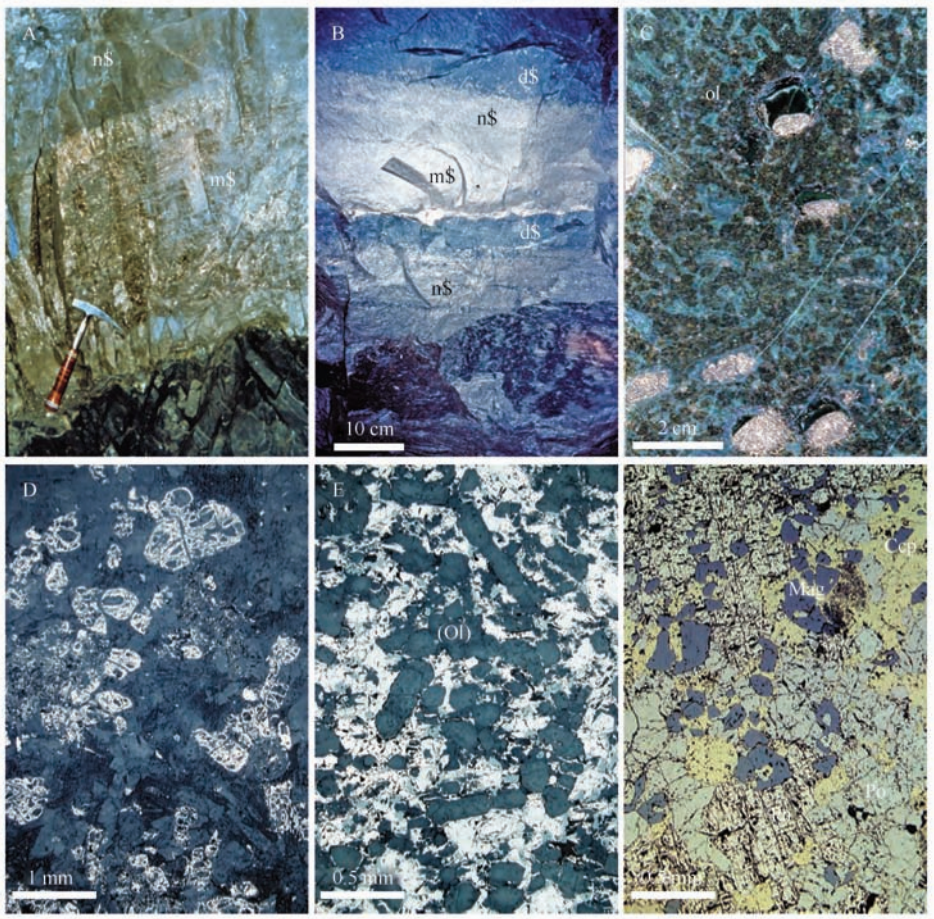

Fig. 2.49 Ore textures in komatiite-associated Ni-Cu-PGE deposits. A. Photograph of typical massive/net-textured/disseminated ore segregation profile overlying massive metabasalt, Juan Main 1204 stope, Kambalda. Banding in massive layer is due to exsolution of pentlandite from MSS during retrograde metamorphism. Pyrite-rich later (to right of hammer) is due to late-stage introduction of S. B. Photograph of complex ore profile in C-1400-3 stope, Katinniq mine, comprising net-textured Fe-Ni-Cu sulfides (lowermost part is joint surface), disseminated sulfides (dark green band in centre, ~5 cm thick), massive sulfides (bright metallic, upper centre), and disseminated sulfides (dark green, top). All contacts are gradational or sharp and delicately scalloped. C. Photograph of coarse disseminated mineralization, Black Swan (from Dowling *et al*., 2004). Sulfides occur at the bases of composite sulfide-silicate segregation vesicles. Plain light. D. Photomicrograph of reverse-net textured sulfides, Katinniq (from Lesher, 2007). Sulfides have replaced olivine, serpentinized olivine, or magnetite derived by serpentinization of olivine (see discussion in text). E. Photomicrograph of net-textured sulfides, Katinniq (from Lesher, 2007). Elongate olivines in a matrix of pyrrhotite-pentlandite (both light yellow) and magnetite (grey). Incident light. F. Photomicrograph of low-tenor massive ore, Katinniq (from Lesher, 2007) containing pyrrhotite (light yellowish grey), pentlandite (light yellow, more pronounced partings), chalcopyrite (yellow), and magnetite (grey). Incident light.

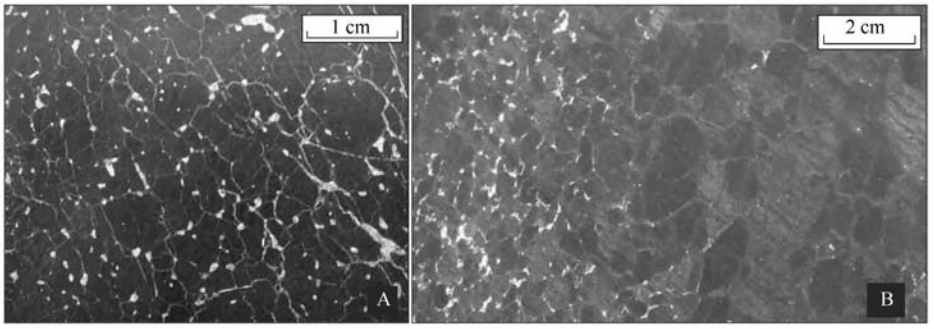

Fig. 2. 50 Photographs of typical sulfide textures in Type IIa ores. Photographs of polished slabs of drill core: (A) typical Mt Keith ore showing sulfide blebs (light color) interstitial to serpentinized olivine (black) in well-developed adcumulate texture; (B) Alternating sulfide-rich and sulfide-poor layers in fresh olivine adcumulate, Perseverance. Olivine grain size is substantially coarser in the sulfide-poor layer.

Table 2. 8A Textures in magmatic Fe-Ni-Cu sulfide ores formed during ore segregation and emplacement, and crystallization (primary), subsolidus equilibration (deuteric), and metamorphism and deformation (secondary) (after Bazilevskaya and Lesher, unpubl.).

Stage	Process	Textures
Primary	Ore segregation and emplacement	Fine interstitial and coarse (blebby/globular/droplet) disseminations, net textures, leopard textures, spinifex textures, sulfide melt-silicate liquid emulsion textures, xenoliths/xenocrysts/xenomelts in massive sulfides, magmatic veins
	Ore crystallization	Mag-Sul and Fchr-Sul intergrowths in Cu-poor ores; Pn 'rosettes" in Cu-rich ores
Deuteric	Subsolidus reequilibration	Most Ccp/Cb textures and all PGM textures, Pn flames and 'eyes' in Po, Pn loops around Po grains, reverse net textures
Secondary	Metamorphism and deformation	Banding and brecciation (durchbewegung) in massive ores, foliations in semi-massive ores, disruption of disseminated and net-textured sulfides by metamorphic Srp, metamorphism of serpentinized net-textured ore to form 'jackstraw' texture (intergrowth of sulfide with non-dendritic platy metamorphic olivine), cloudy disseminated textures, secondary (post-serpentine) sulfides forming loops around serpentinized olivine and replacing clinopyroxene

Mineral Abbreviations: **Ccp** chalcopyrite, **Cb** cubanite, **Mag** magnetite, **Fchr** ferrochromite, **Ol** olivine, **PGM** platinum-group minerals, **Po** pyrrhotite, **Pn** pentlandite, **Srp** serpentine, **Sul** sulfide.

Table 2. 8B Primary magmatic textures in Fe-Ni-Cu sulfide ores (after Bazilevskaya and Lesher, unpubl.)

% Sulfide + Oxide	First Order Textures	Second-Order Textures	Description
1%–30%	**d $** fine disseminated **b $** coarse disseminated	**pd $** patchy (**ld $** leopard) disseminated	widely-dispersed interstitial sulfides within orthocumulate to adcumulate rocks (dunite-peridotite-gabbro); fine in orthocumulate-adcumulate rocks but coarse only in orthocumulate rocks; more uniform in olivine and pyroxene-plagioclase cumulate rocks but less uniform (patchy) in olivine-pyroxene cumulate rocks
30%–65%	**sx $** spinifex-textured **n $** net-textured (olivine cumulates) **mx $** matrix (pyroxene-plagioclase cumulates)	**pn $** patchy net-textured	sulfide networks to platy olivine (sx $), polyhedral olivine (n $), pyroxene-olivine oikocrysts (ln $), or olivine-pyroxene-plagioclase (mx $); sx $ is only present in high-Mg komatiitic rocks
65%–90%	**inm $** inclusion semi-massive		sulfides with abundant mineral or rock inclusions
>90%	**m $** massive		equigranular massive sulfides, Po-rich varieties often contain embayed magnetites, komatiitic ores often contain ferrochromites (along ore/silicate contacts); may contain inclusions of footwall rocks

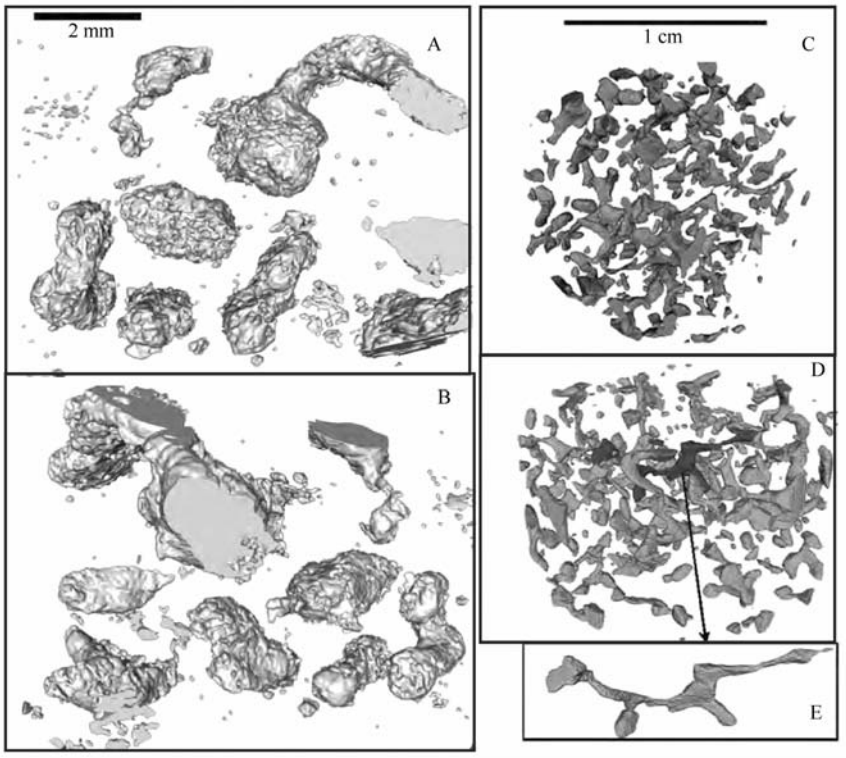

Fig. 2. 51 Rotated views of 3D X-ray computed tomograms of sulfide blebs from Black Swan orthocumulate (left) and Mt Keith adcumulate (right).

ated with high-Mg komatiites are typically more uniformly distributed than those associated with komatiitic basalts (e.g., Raglan, Kingash) which are typically much more patchy because of the presence of oikocrystic pyroxene (Bazilevskaya and Lesher, unpubl. data).

The morphology of magmatic sulfides in igneous rocks is controlled by the wetting properties of sulfide liquids against silicates. Textural studies (Bazilevskaya and Lesher, unpubl. data; Tonnelier *et al*., 2009), experimental studies (Rose and Brenan, 2001; Mungall and Su, 2005), and three-dimensional X-ray tomographic images of sulfide aggregates in komatiitic olivine cumulates (Barnes *et al*., 2008) indicate that sulfide liquids wet olivine crystals and form interconnected networks only in the absence of silicate melt. Consequently, the ability of sulfide liquids to migrate through the pore spaces of olivine cumulates is limited. Disseminated sulfide greater than ~1% in komatiites must have formed by in situ fractional accumulation of olivine-sulfide with additional physical accumulation of transported sulfide droplets a few mm in size (see below) and that they accumulated more or less in the proportions in which they are now found, rather than by percolation through cumulate pore spaces.

Barnes *et al*. (2008) collected three-dimensional X-ray tomograms of samples of fine interstitial sulfides in olivine adcumulate rocks from Mt. Keith and coarse sub-spherical aggregates in olivine orthocumulate rocks from Black Swan, and found that the interstitial sulfides formed well-connected branching tubes or channels along olivine triple grain boundaries even at sulfide abundances as low as ~3%, whereas the subspherical sulfides formed discrete entities with no interconnectivity (Fig. 2. 51). The correlations with the textures of the rocks are consistent with experimental results of Mungall and Su (2005) on the ability of sulfide liquid to wet olivine in the absence of silicate melt (adcumulates) but not in the presence of silicate melt (orthocumulates).

This interpretation provides an explanation for the textural difference between coarse disseminated, fine disseminated, and net-textured mineralization. Coarse disseminated sulfides can form only within orthocumulates where they are wetted by silicate liquid, net-textured sulfides can only form in mesocumulates where they can wet olivine, but fine disseminated sulfides can form in orthocumulates, mesocumulates, or adcumulates. The spherical morphology of sulfide droplets in some coarse disseminated ores may represent incorporation into vesicles, but in other ores is may reflect the inability of the droplets to wet olivine when surrounded by silicate liquid in unconsolidated orthocumulates. Excellent natural examples occur in the Cygnet and Black Swan disseminated ores in Western Australia, which show a transition between the two types (Barnes *et al*., 2009).

Some examples of coarse disseminated sulfides are associated with vesicular komatiites, and in this setting commonly contain caps of altered silicate glass (Fig. 2. 49C). These have been interpreted as segregation vesicles (see Beresford and

Cas, 2001), although it is not clear what mechanism could cause complete incorporation of sulfide into vesicles without leaving any residue in the remaining interstitial silicate melt. Prichard *et al.* (2004) interpreted similar features as settled droplets.

Cas and Beresford (2001) noted that spinifex-textured ores also occur "isolated" within spinifex zones, below the bases of komatiites that are not mineralized, and that in places spinifex and equant [olivine] crystals have been replaced by sulfide, and suggested that sulfide had been metamorphically mobilized, but provide no explanation for the absence of the interflow sediment, aphyric flow-top, and fine-grained random olivine spinifex-textured zone or for the origin of the silicate domes. They provide no photos or comparisons between the occurrences they studied and those studied by Groves et al. (1986), but sulfides are orders of magnitude more mobile and much more reactive at the magmatic stage and the normal Cr contents of the spinifex ores that have been analyzed (Paterson *et al.*, 1984) suggest that they are magmatic (see discussion by Lesher and Keays, 1984).

2.5.3 Mineralogy

Primary (i.e., non-supergene) Type I sulfides have a relatively simple mineralogy dominated by pyrrhotite-pentlandite-pyrite, lesser pentlandite-pyrite, and rarer pentlandite-pyrite-millerite sulfide assemblages. Chalcopyrite, magnetite, and ferritchromite are ubiquitous minor phases. Magnetite is commonly more abundant in matrix and disseminated ores, whereas pyrite is commonly more abundant in massive ores (Cowden and Archibald, 1987). Hudson and Donaldson (1984) and Dillon-Leitch *et al.* (1986) provide comprehensive lists of rarer native elements, oxides, sulfides, tellurides, arsenides, and antimonides at Kambalda and Donaldson West (Raglan) (Table 2.9).

Table 2.9 Mineralogy of komatiite-associated Ni-Cu-(PGE) mineralization at Kambalda and Donaldson West (Hudson & Donaldson, 1984; Dillon-Leitch *et al.*, 1986; Lesher and Keays, 2002)

Mineral	Formula[§]	Kambalda	Donaldson West
Altaite	PbTe	+	
Arsenic	As	+	
Arsenopyrite	FeAsS	+	+
Bismuth	Bi	+	
Breithauptite	NiSb	+	
Bunsenite	NiO	+	
Calaverite	$AuTe_2$	+	
Chalcopyrite	$CuFeS_2$	++	++
Chromite	$Fe^{2+}Cr_2^{3+}O_4$	++	++
Cobaltite	CoAsS	+	+
Electrum	Au, Ag		+
Frohbergite	$FeTe_2$	+	
Gahnite	$ZnAl_2O_4$	+	
Galena	PbS	+	
Gersdorffite	NiAsS	+	
Gold	Au	+	
Heazlewoodite	Ni_3S_2	+	
Hedleyite	Bi_7Te_3	+	
Hematite	Fe_2O_3	+	
Hessite	Ag_2Te	+	+
Ilmenite	$Fe^{2+}Ti_2^{3+}O_4$	+	+
Magnetite	$Fe^{2+}Fe_2^{3+}O_4$	++	++
Melonite	$NiTe_2$	+	+
Merenskyite	$(Pd, Pt)(Te, Bi)_2$		+

Continued

Mineral	Formula§	Kambalda	Donaldson West
Millerite	NiS	+	
Michenerite	(Pd, Pt)BiTe	+	
Molybdenite	MoS_2	+	
Moncheite	(Pt, Pd)(Te, Bi)$_2$	+	
Nickeline	NiAs	+	
Palladoarsenide	Pd_2(As, Sb)	+	
Parkerite	Ni_3(Bi, Pb)$_2S_2$	+	
Pentlandite	(Fe, Ni)$_9S_8$	+ + +	+ + +
Petzite	Ag_3AuTe_2	+	
Pyrite	FeS_2	+ +	+ +
Pyrrhotite	$Fe_{1-x}S$	+ + +	+ + +
Rammelsbergite	$NiAs_2$	+	
Rucklidgeite	(Bi, Pb)$_3Te_4$	+	
Sperrylite	$PtAs_2$	+	+
Sphalerite	ZnS	+	+
Stibiopalladinite	Pd_5Sb_2	+	
Sudburyite	(Pd, Ni)Sb	+	+
Tellurobismuthite	Bi_2Te_3	+	
Testibiopalladite	PdTe(Sb, Te)	+	+
Titanomaghemite	Fe(Fe, Ti)$_2O_4$		+
Ullmannite	NiSbS		
Unknown Pd Sb phase		+	
Unknown Pd As phase		+	
Unknown Pd Sb Te phase	$Pd_3Sb_2Te_2$?		+
Violarite	$Fe^{2+}Ni_2^{3+}S_4$	+	
Volynskite	AgBiTe$_2$	+	

§ showing common substitutions for some minerals. Abundance: major + + +, minor + +, trace +. Other minerals in Kambalda ore concentrates, most likely derived from felsic dikes and hydrothermal veins, include: scheelite [$CaWO_4$], tantalite [(Fe, Mn)Ta_2O_6], cassiterite [SnO_2], rutile [TiO_2], barite [$BaSO_4$], monazite [(La, Ce, Nd)PO_4], zircon [$ZrSiO_4$], quartz [SiO_2], and andradite [$Ca_3Fe_2^{3+}(SiO_4)_3$]. The ultramafic host rocks contain serpentine, calcic pyroxene, calcic amphibole, chlorite, talc, magnesite, dolomite, magnetite, and Fe-chromite.

Ferrichromites are normally concentrated at the margins of massive ore layers (e.g., Ewers and Hudson, 1972; Groves *et al*., 1977; Frost and Groves, 1989; Lesher, 1989; Dowling *et al*., 2004). They are normally coarse-grained (0.5 – 2.0 mm) and euhedral to skeletal, some contain inclusions of Fe-Nu-Cu sulfides and/or silicates (see below) and most exhibit narrow Cr-magnetite rims. Compositionally, they are Al-poor Fe-chromites with 20 – 30 mole% $R^{2+}Fe_2O_4$, similar to spinels crystallized experimentally by Ewers *et al*. (1976) and Woolrich *et al*. (1981). They are interpreted to have crystallized at the magmatic stage on interfaces between layers of different sulfide content in response to gradients in fo_2 and limitations in the ability of Cr to diffuse from silicate rocks (Marston and Kay, 1980; Woolrich *et al*., 1981; Dowling *et al*., 2004; Da Fonseca *et al*., 2008).

Finely disseminated Type Ⅱ sulfides are mineralogically more variable and generally more Ni-rich, as a result of reactions with host rocks during metamorphism (Eckstrand, 1975; Groves *et al*., 1974; Groves and Keays, 1979; Donaldson, 1981; Grguric, 2003; Grguric *et al*., 2006). Typical sulfide assemblages for progressively altered dunites are pentlandite in dunite, pentlandite-heazlewoodite-magnetite in partially serpentinized dunite, pyrrhotite-pentlandite ± pyrite in lizardite serpentinite, pyrrhotite-pentlandite or pentlandite-millerite in antigorite serpentinite, and pyrrhotite-pyrite-pentlandite or pyrite-millerite-polydymite in talc-car-

bonate rock. Chromite and chalcopyrite are ubiquitous accessory phase. Additional phases include godlevskite, vaesite, awaruite, bravoite, cobaltite, nickeliferous linnaeite, and cubanite.

2.5.4 Ore chemistry

Because of the desirability of comparing analyses of whole-rock ore samples containing different amounts of gangue phases, it is customary to selectively leach sulfides and oxides (Davis, 1972) or to recalculate analyses to 100% sulfides (e.g., Ross and Keays, 1979; Naldrett *et al*., 1979; Kerr, 2001) or 100% sulfides plus oxides (Cowden *et al*., 1986; Cowden and Woolrich, 1987). Each method involves assumptions regarding the siting of Fe, Ni, and PGE in the rock, and each introduces systematic errors into the analysis. A good example of this is evident in Fig. 2.53C below where Cowden *et al*. (1986) recalculated their data to 100% sulfides + oxides, whereas Stone *et al*. (2004) recalculated their data to 100% sulfides, producing systematic offsets in what appears to have been identical data. As different workers have used different analytical/recalculation methods, care is required when comparing data from different studies.

Average ore compositions from many of these deposits have been compiled by Marston *et al*. (1984), Naldrett (1981, 2004), Lesher and Keays (2002), and Barnes and Lightfoot (2005). When plotted within the system Fe-Ni-S, most bulk compositions fall within the field of *mss* at 600℃, consistent with a magmatic origin. Individual samples, however, exhibit considerable scatter owing to variable degrees of magmatic fractionation and metamorphic alteration (see below). Some representative ore compositions are given in Table 2.10.

Komatiite-associated ores are characterized by high Ni/Cu and low Pd/Ir ratios that distinguish them from most other magmatic sulfide ores (Naldrett, 1981, 2004; Barnes *et al*., 1988) and from hydrothermal and volcanic-exhalative sulfides (Keays *et al*., 1982). Sulfides hosted by high-Mg komatiites (e.g., Kambalda, Dundonald, Langmuir, Trojan) contain near-chondritic abundances of PGE and exhibit slightly fractionated chondrite-normalized PGE distribution patterns (Pd/Ir = ~10), whereas those associated with komatiitic basaltic komatiites (e.g., Raglan), or believed to have equilibrated with fractionated komatiites (e.g., Alexo, possibly Shangani), exhibit more fractionated PGE patterns (Pd/Ir = ~30) (Barnes *et al*., 1985; Barnes and Naldrett, 1987). Ores associated with high-Mg komatiites, low-Mg komatiites, and komatiitic basalts exhibit complementary patterns at 0.001 – 0.01 × chondritic abundances, consistent with high degree partial melting of a mantle source, minor retention of Ir-group PGE (Os > Ir > Ru) in restite (Barnes *et al*., 1995; Barnes and Fiorentini, 2008), and strong partitioning of all PGE into sulfide (Barnes *et al*., 1985).

Most chalcophile elements (Ni, Cu, Co, Pt, Pd, Os, Ir, Rh, and Ru) correlate negatively with Fe, and chalcophile element abundances vary systematically with Ni content (Ross and Keays, 1979; Keays *et al*., 1981; Barnes and Naldrett, 1987; Cowden *et al*., 1986; Cowden and Woolrich, 1987; Lesher and Campbell, 1993). Footwall stringers and hydrothermal sulfide veins are enriched in Cu and PGE (Almeida *et al*., 2007; Ross and Keays, 1979; Lesher and Keays, 1984; Dillon-Leitch *et al*., 1986).

2.5.5 Ore tenor variations

Between type variations

Variations in the compositions of the different ore types formed from similar parental magmas can be attributed to differences the degree of fractional crystallization prior to sulfide segregation, differences in magma: sulfide ratio (*R* factor), and, in some cases, to the addition of external metals. For example, the high PGE tenors of most Type Ⅲ mineralization can be attributed to high *R* factors. The greater degree of fractionation of Type Ⅲ and Ib mineralization can be attributed to them forming from more fractionated magmas (Type Ⅲ) or via fractional crystallization of *mss* (Type Ib). The depletion of Cr in Type IVa ores can be attributed to the lower diffusion rate of Cr in sulfides compared to the chalcophile metals. The depletion of Cr and Ir in Type IVb ores can be attributed to the lower solubilities of those elements in hydrothermal fluids compared to the chalcophile metals.

Type Ⅱ ores appear to have formed at relatively low *R* factors. The average Pd content of Mount Keith sulfides may be estimated at ~1400 ppb (see Lesher and Keays, 2002). Assuming that the komatiitic magma contained ~10 ppb Pd (Keays, 1982) and the Pd partition coefficient was ~35000 (Peach and Mathez, 1993; Peach *et al*., 1990), the *R* factor can be calculated to be ~140 using the method of Campbell and Naldrett (1979). A similar calculation may be performed for Dumont. Using data reported by Brügmann *et al*. (1989), the average Pd content of Dumont sulfides may be estimated at ~3680 ppb. Making the same assumptions about the magma composition, which is also interpreted to be a high-Mg komatiite (Duke, 1986), yields an *R* factor of ~370. These values are within the mid-lower part of the 100 – 500 range calculated for Type I ores at Kambalda (Lesher and Campbell, 1993) and lower than the 300 – 1000 range calculated for Type I ores at Raglan (Barnes and Picard, 1993; Gillies, 1993; Lesher, 1999). Although Type Ⅱ sulfides might be expected to have formed under higher *R* conditions than Type I massive sulfides, their textures indicate that significant amounts of sulfide crystallized *in situ* (see below), so even though the abundance of sulfides was smaller, the effective *R* factor was relatively low. This interpretation is

Table 2.10 Representative compositions of komatiite-associated Ni-Cu-(PGE) ores recalculated to 100% sulfides

		1	2	3	4	5	6	7	8	9	10	11	12	13	14
		Kambalda	Kambalda	Kambalda	Kambalda	Kambalda	Kambalda	Pipe II	Thompson	Thompson	Thompson	Langmuir	Langmuir	Langmuir	Langmuir
		Range	STR	IPS	M $ -SED	Ni-SED	HQV	M $	M $	B $	Ni-SED	Po-rich	Py-rich	Ml-rich	Ni-SED
S	%	35 - 39	37.1	37.6	37.8	37.8	40.1	(39)	(39)	(39)	(39)	37.1	36.9	36.2	37.2
Fe	%	38 - 54	51.0	51.2	51.5	60.0	49.0	58.1	50.1	52.7	53.8	50.5	49.5	45.5	50.9
Ni	%	22 - 8	9.9	10.3	10.1	6.6	9.8	2.7	10.5	8.0	6.8	11.8	12.9	17.3	10.2
Cu	%	1.3 - 0.6	2.0	0.44	0.39	0.89	0.25	0.17	0.42	0.27	0.45	0.37	0.46	0.66	1.5
Co	%	0.3 - 0.2		0.22	0.21	0.15	0.27	0.12	0.14	0.14	0.10	0.24	0.24	0.31	0.11
Cr	%	0.4 - 0.2		0.18	0.03	0.11	0.02	0.17	0.17	0.16	0.02				
Zn	ppm	400 - 200		176	145	5732	90	170	607	481	395	39	33	59	
Pb	ppm	25 - 15										9	13	34	
Re	ppm							109	107	50	27				
Mo	ppm							11	8	12	43				
As	ppm	20 - 5			10	45		25	125	300	74	30	94	22	
Sb	ppm														
Bi	ppm	10 - 5													
Se	ppm	46 - 31		43	51	303	116	16	30	24	13	16	94	36	37
Te	ppm	20 - 10													
Ag	ppm	4 - 2			8	18									
Au	ppb	700 - 260	699	50	69	458	322	20	179	101	121	64	55	244	86
Pd	ppb	3460 - 1510	1373	794	914	2947	574	77	3224	1289	947	840	1105	2249	2004
Pt	ppb	2430 - 1000						29	431	482	52	586	402	1206	716
Rh	ppb	490 - 210						24	243	183	35	185	220	375	17
Ru	ppb	1560 - 710						140	376	320	28	534	910	575	229
Ir	ppb	350 - 160	185	151	201	9.1	0.5	30	184	137	10	199	250	197	3
Os	ppb	980 - 270						59	226	187	10	329	347	440	40
S/Se				8805	7435	1250	3469	23926	12800	16186	30659	22727	3917	10000	10000
n			3				3	3	6	7	14	18	8	12	4
Reference		CDNC86	KRW81	LK84	PDSLGBK84	PDSLGBK84	LK84	B90	B90	B90	B90	GN81	GN81	GN81	GN81

Continued

		15	16	17	18	19	20	21	22	23	24	25	26	27	28	29
		Persev-erance	Persev-erance	Persev-erance	Mount Keith	Dumont	Donaldson West	Donaldson West	Donaldson West	Donaldson West	Donaldson West	Namew Lake	Pechenga	Pechenga	Pechenga	Pechenga
		D $	N $	M $	D $	D $	D $	N $	RN $	M $	V $	D $	D $	M $	B $	V $
S	%	37.2	37.6	37.8	35.7	29.5	36.0	36.2	36.7	39.9	36.2	36.1	37.1	37.4	37.8	34.4
Fe	%	50.9	51.1	49.3	48.1	53.6	37.7	41.9		47.7	40.5	41.9	48.3	49.8	51.8	28.6
Ni	%	11.1	8.51	7.08	14.2	15.6	17	16.3	13.1	11.3	14.1	15.9	8.6	8.9	7.4	3.0
Cu	%	0.47	0.43	0.19	0.69	1.30	3.7	4.0	4.2	0.83	6.7	6.1	3.59	1.94	1.35	34.0
Co	%	0.28	0.19	0.17	0.43		0.43	0.22	0.20	0.13	0.18	0.27	0.25	0.20	0.18	0.04
Cr	%				0.93							0.68				
Zn	ppm				807							2344	573	179	261	1392
Pb	ppm											148				
Re	ppm											59				
Mo	ppm											23				
As	ppm						47	92		15.5	53	54	31	28	55	7
Sb	ppm						112	16		1.5	17	2.4	4	0.6	0.9	0.2
Bi	ppm						6	2		2	1	29				
Se	ppm				6.4	75	94	29		80.5	64	195	75	80	74	67
Te	ppm						1	2		1	1	18				
Ag	ppm						30	15		2	36		27	12	12	90
Au	ppb	109	43	24		614	200	122		25	956	1404	144	83	100	42
Pd	ppb	1818	850	448	1402	3677	25087	12688	16855	1105	15332	5320	867	386	379	51
Pt	ppb	1159	494	157	588	3125	36721	9383	8825	2676	5841	5198	810	359	398	223
Rh	ppb	74	44	100	206		1535	649		735	39	116	36	55	48	122
Ru	ppb	440	214	383	755		3070	840		1575	25	283	57	112	68	511
Ir	ppb	198	78	136	176	323	531	160		268	5	90	26	45	37	221
Os	ppb	253	102	171	512	258	649	202		340	9	104	26	64	44	442
S/Se					55781	3933	3834	12471		4957	5626	1851	4943	4669	5103	5139
n		13	12	39	105	8	14	12	9	3	11	18	20	31	21	2
Reference		BGH88	BGH88	BGH88	F95	BND90	D－LWC86	D－LWC86	D－LWC86	D－LWC86	D－LWC86	MLSPPH96	BMS01	BMS01	BMS01	BMS01

References are abbreviations of references in Table 2.3. Ore Types: D $: disseminated sulfides, N $: net-textured sulfides, M $: massive sulfides, IP $: interpillow sulfides, B $: breccia sulfides, Ni－SED: Ni－enriched sediments, V $: vein sulfides, HQV $: hydrothermal vein sulfides.

supported by the depletion of Ni in the olivines at Dumont (Duke, 1986) and Perseverance (Barnes *et al*., 1988a).

When performing calculations of this type it is important to use a highly chalcophile element ($D > 10 \times R$: see Campbell and Barnes, 1984) with a low olivine-sulfide partition coefficient. Ni, Co, and Ir partition strongly into olivine (or crystallize as labile phases with olivine), which has a significant effect on the mass balance calculations (Lesher and Burnham, 2001), but Pd, Pt, and Au do not partition into olivine.

Between deposit and between shoot variations

Like other Type I magmatic Ni-Cu-(PGE) deposits (e.g., Noril'sk, Sudbury), the compositions of the ores varies between different deposits within the same belt (e.g., Kamblada, Pechenga, Raglan, and Thompson) and between different shoots or zones within the same areas (Kambalda, Raglan, and Thompson). In many cases, ores with different compositions occur within the same tectonic and metamorphic settings, are hosted by similar rock types, and appear to have formed contemporaneously, suggesting a magmatic origin for the variations (Marston and Kay, 1980; Cowden and Woolrich, 1987; Lesher and Campbell, 1993). Although variations in the composition of the magma may be produced by varying the degree of partial melting (Naldrett and Barnes, 1986), by fractional crystallization (Duke, 1979; Duke and Naldrett, 1978), or by changing fo_2 and/or fs_2 among different magma batches (Woolrich *et al*., 1981), there is no evidence in the geochemical characteristics of the host rocks that these processes occurred to any significant degree (Lesher and Groves, 1984; Lesher and Campbell, 1993; Lesher and Stone, 1996).

Campbell and Naldrett (1979) showed that the partitioning behaviour of metals between sulfide and silicate liquids should be strongly influenced by the mass ratio (R) of the two phases. Sulfide melts that equilibrate with small amounts of magma (low R) should be depleted in PGE ≫ Cu > Ni > Co, resulting in lower tenor ores, whereas sulfide melts that equilibrate with large amounts of magma (high R) should retain nearly normal abundances of all chalcophile elements, resulting in higher tenor ores. Contrary to some misconceptions in the literature, variations in the R factor cannot increase the tenors of metals above the levels determined by sulfide:silicate partition coefficients, it can only decrease them. It is also important to appreciate that the partition coefficients between sulfide melt and silicate magma vary with magma composition and are generally lower in komatiitic magmas than in

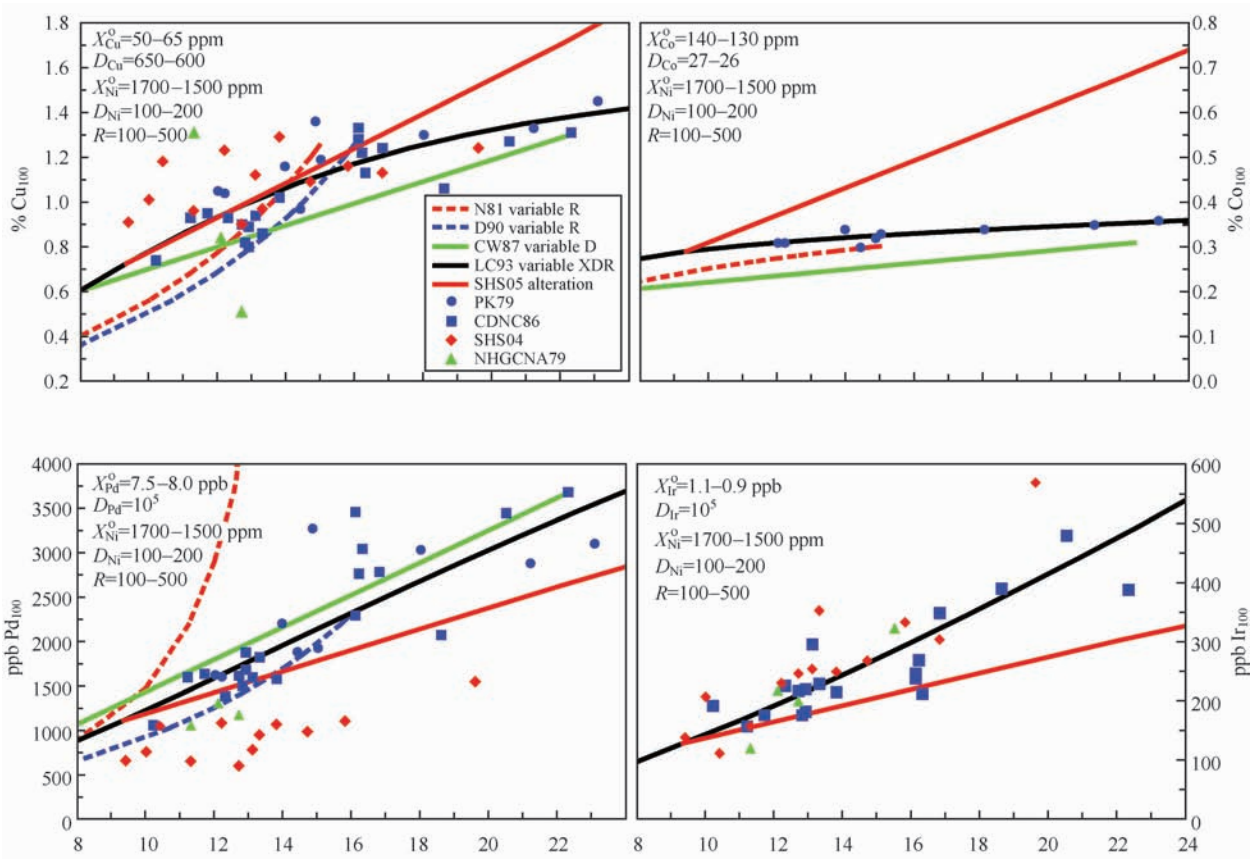

Fig. 2. 52 Variations in the Ni, Cu, Co, Pd, and Ir compositions of Western Australian komatiite-associated Ni-Cu-(PGE) deposits (modified after Lesher and Campbell, 1993). Data and models: N81 = Naldrett (1989), D90 = Duke (1990), CW87 = Cowden and Woolrich (1987), CDNC86 = Cowden *et al*. (1986), LC = Lesher and Campbell (1993), SHS05 = Stone *et al*. (2005).

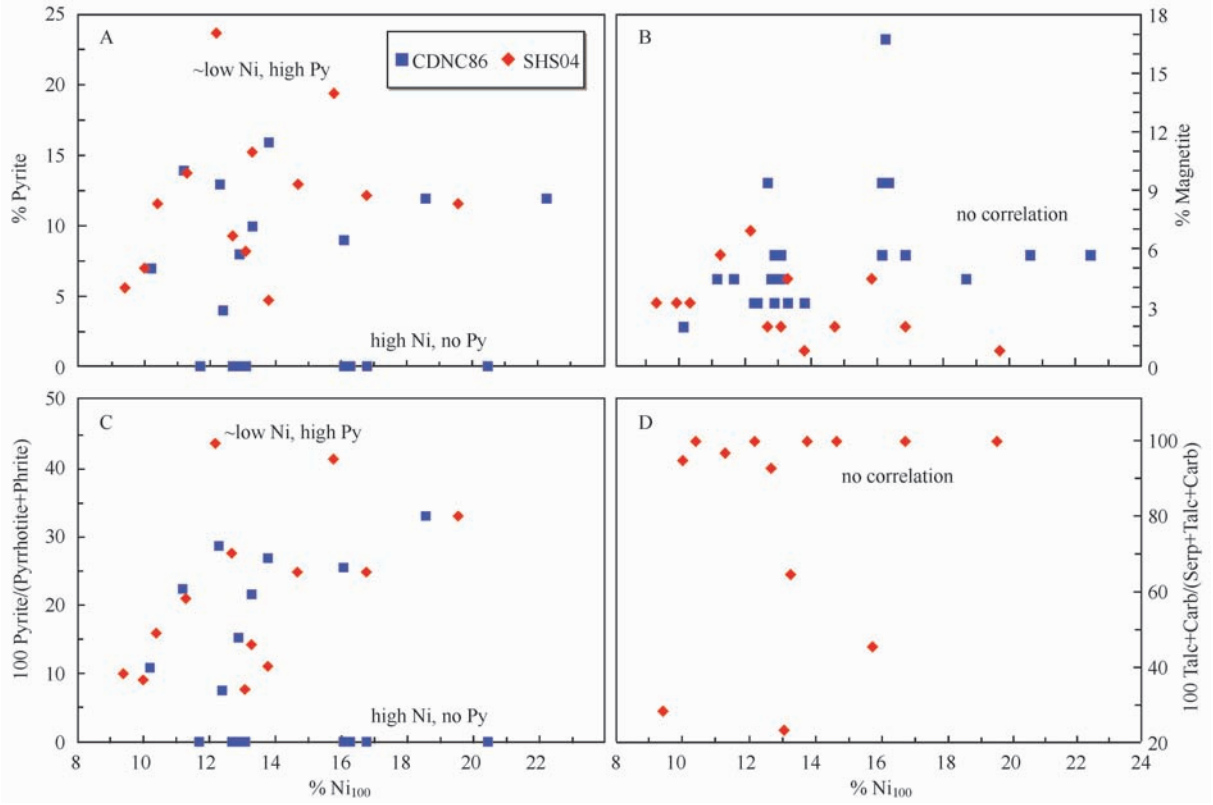

Fig. 2. 53 Ni tenor (Ni in 100% sulfides) with various alteration indices. (A) % pyrite, (B) % Magnetite, (C) Pyritization index, and (D) Talc-Carbonation Index. Data from Stone *et al.* (2004) with additional data in (A), (B), and (C) from Cowden *et al.* (1986).

basaltic magmas (see discussion by Lesher and Campbell, 1993). Variations in *R* factor have been used to model bulk compositional variations for different deposits and zones within individual deposits (Fig. 2. 52), yielding ranges of 20 – 400 for Type I deposits in the Thompson Nickel Belt (Burnham *et al.*, 2003; Naldrett *et al.*, 1979), 50 – 500 for deposits in the Abitibi Belt (Lesher, unpubl. data), 100 – 500 for Type I deposits in Western Australia (Lesher and Campbell, 1993), 300 – 1100 for Type I deposits in the Raglan belt (Barnes and Picard, 1993; Lesher *et al.*, 1999, 2007), and 250 – 1000 for Type I/Ⅱ deposits in the Pechenga Belt (Barnes *et al.*, 2001). Similar variations have been observed in other classes of magmatic Ni-Cu-PGE deposits, including Noril'sk and Sudbury (Naldrett, 2004). Lesher and Burnham (2001) noted that the magmatic systems invariably contained additional components, including xenomelts, residues/xenoliths, xenovolatiles, and crystalline silicates, all of which would influence mass balance calculations. The presence of olivine, which is abundant in Type Ⅱ deposits and which contains significant amounts of Ni, greatly influences the mass balance of Ni in the system.

Stone *et al.* (2004) argued that the ore tenor variations at Kambalda have been produced by metamorphic oxidation of pyrrhotite to pyrite and magnetite. However, contrary to their claims this model does not reproduce the observed metal variations (cf. SHS05 alteration model on Fig. 2. 52) and there are no statistically significant correlations between Ni tenor and pyrite content (Fig. 2. 53A), magnetite content (Fig. 2. 53B), pyritization index (Fig. 2. 53C), degree of talc-carbonation (Fig. 2. 53D), or with degree of deformation or degree of metamorphism (Table 2. 11).

This is evident by examining the reaction proposed by Stone *et al.* (2004):

$$12FeS + 6O_2 \rightarrow 3FeS_2 + 3Fe_3O_4 + S \qquad (1)$$

which is not balanced for mass or charge, but balancing it yields:

$$12FeS + 12O^{2-} \rightarrow 3FeS_2 + 3Fe_3O_4 + 6S^{2-} + 6e^- \qquad (2)$$

Obviously, this process adds only O and releases only S, so it cannot change metal ratios and, as such, cannot explain the observed variations in metal tenors in which the metal abundances decrease in relative terms in the order Pd ~ Ir ≫ Cu > Ni > Co, precisely the same order expected from variations in the *R* factor. Note that Co is a particularly critical element because it has a much lower partition coefficient than the other elements; if mobility of O and S were responsible, then it should be as enriched as the other elements.

The bulk variations are also inconsistent with a metamorphic process that involves mobilization of metals. Fe, Cu,

Table 2.11 Summary of Ni tenors vs. degree of deformation, metamorphism, and alteration. Data from Ross and Keays (1979), Gresham and Loftus-Hills (1981), Woolrich *et al.* (1981), Stone *et al.* (2004) and Cowden *et al.* (1986).

Ni Tenor*	High	Medium-high	Medium	Low-medium	Low
Deformation					
Undeformed to Weakly Deformed	Durkin, Victor, Scotia, *Katinniq C*	*Katinniq E*	*Katinniq Q*	*Katinniq K*	*Alexo*
Moderately to Strongly Deformed	Gibb, Edwards Lode, Ken, Jan, Wannaway N02, Carnilya Hill, *Bucko d $*	Lanfranchi, *Namew Lake*	Fisher, Gellatly, Hunt, Juan, McMahon, Foster, Mariners, Mt Edwards, Blair, *Thompson*	Long, Lunnon, Wannaway N01, *Birchtree*	Helmut, *Pipe 2*
Metamorphism					
Lower Greenschist	*Katinniq C*	*Katinniq E*	*Katinniq Q*	*Katinniq K*	*Alexo*
Middle Greenschist	Redstone, Langmuir #1	McWatters	Langmuir #2		*Hart*
Upper Greenschist	Durkin, Edwards, Lode, Ken, Jan	Lanfranchi	Fisher, Gellatly, Hunt, Juan, McMahon, Foster	Lunnon	Helmut
Lower Amphibolite	Gibb, Victor, Wannaway N02, Carnilya Hill, Scotia		Mariners Mt Edwards Blair	Long, Wannaway N01	
Middle Amphibolite					*Marbridge*
Upper Amphibolite	Nepean, Bucko d $	*Namew Lake*	*Thompson*	*Birchtree*	*Pipe 2*
Alteration**					
Partially Serpentinized	Scotia	*Namew Lake*			
Serpentinized	Durkin, Victor, *Katinniq C*, Bucko *d $*	*Katinniq E*	*Katinniq Q*, *Thompson*	Long, Lunnon, *Katinniq K*, *Birchtree*	*Pipe 2*
Mixed	Gibb		Hunt		
Talc-Carbonate	Edwards Lode, Ken, Jan, Wannaway N02, Carnilya Hill	Lanfranchi	Fisher, Gellatly, Juan, McMahon, Foster, Mariners, Mt Edwards, Blair	Wannaway N01	Helmut

*Ni tenor varies with the composition of the magma (higher Ni in high-Mg komatiite, intermediate Ni in low-Mg komatiite, and lower Ni in komatiitic basalt), sulfide/silicate partition coefficients (lower in high-Mg komatiites, higher in komatiitic basalts), and *R* factor (magma:sulfide ratio), so the assignments are relative to the maximum predicted values (~30 in high-Mg komatiitic systems and ~20 in komatiitic basaltic systems). ** Dominant alteration. Note that talc-carbonate alteration often appears to be superimposed on serpentinization.

Pd, Pt, and Rh are fairly soluble in metamorphic/hydrothermal fluids, Ni, Co, and Ru are less soluble, and Ir and Cr are essentially insoluble (see Keays *et al.*, 1982; Lesher and Keays, 1984, 2002; Wood and Mountain, 1991). If metamorphic fluids had mobilized metals, Cu should be decoupled from Ni and Pd should be decoupled from Ir. There is no doubt that deformation and metamorphism have locally affected the compositions of Ni-Cu-(PGE) mineralization (see below), but the majority of the variations in bulk ore deposit compositions appear to be quite easily explained by variations in *R* factor (a reasonable and predictable consequence of ore formation in variably dynamic magmatic systems) with dispersion in S, Cu, Pd, Au, and other mobile elements resulting from superimposed deformation and metamorphism (Lesher and Campbell, 1993). These are precisely the same elements that Burnham *et al.* (2003) showed had been mobilized outside the ore zones in the Thompson Nickel Belt, by comparing grab samples with mill feed composites and theoretical models.

Within shoot variations

Ewers and Hudson (1971), Keele and Nickel (1974), Ross and Keays (1979), Gresham and Loftus-Hills (1981), Keays *et al.* (1981), Woolrich *et al.* (1981), Cowden *et al.* (1986), Cowden and Woolrich (1987), Heath *et al.* (2001), Seat *et al.* (2004), and Stone *et al.* (2004) have shown that there are significant variations in the compositions of ores within individual ore shoots at Kambalda. Similar variations have been observed at Raglan (Dillon-Leitch *et al.*, 1986) and Thompson (Burnham *et al.*, 2003). Some of the variations at this scale are probably magmatic and some are probably metamorphic.

Because Cu and PPGE partition more strongly into the sulfide melt than *mss* (Li *et al.*, 1996; Fleet *et al.*, 1999b; Barnes *et al.*, 1997; Ebel and Naldrett, 1996; Ebel and

Naldrett, 1997), fractional crystallization of *mss* may produce a Cu and PPGE-enriched residual sulfide melt. Although this is observed on a small scale and may explain some of the observed differences in the compositions of net-textured and massive ores at Kambalda, rare Cu-PPGE-rich net-textured mineralization at Katinniq (Chisholm *et al.*, 1999) and Jinchuan (Tonnelier *et al.*, 2009), and some of the Cu-PPGE-rich footwall stringers in many Type I deposits (Keays *et al.*, 1981), most Type I deposits appear to have cooled relatively rapidly and did not undergo as much fractional crystallization as deposits like Sudbury or Noril'sk. An anomalous exception is Silver Swan, where variations of two orders of magnitude in IPGE contents entirely within the massive ore profile can be modeled by *mss* fractionation (Barnes, 2004).

Differences in the compositions of massive, net-textured, and disseminated sulfides within individual Type I ore profiles have be attributed to (1) variations in *R* factor during sulfide segregation (Lesher and Campbell, 1993), (2) fractionation of *mss* (Lunnon shoot: Keays and Davison, 1976; Alexo: Barnes and Naldrett, 1987; Pechenga: Barnes *et al.*, 2001; Silver Swan: Barnes, 2004), and (3) selective mobilization of metals from massive sulfides during deformation and metamorphism (Barrett *et al.*, 1977; Barrett *et al.*, 1976; Heath *et al.*, 2001; Keays *et al.*, 1981). The relative importance of these processes depends on the dynamics during ore emplacement, the rate of cooling, and the degree of post-magmatic modification, but these processes can normally be distinguished: *R* factor and fractional segregation processes will fractionate all PGE $\gg$ Cu > Ni > Co, crystallization of MSS will fractionate Au-Cu-PPGE from Ni-Co-IPGE, and interaction with metamorphic fluids will fractionate more soluble elements (e.g., As-Sb-Bi-Te-Ag-Au-Pd-Pt-Cu) from less soluble elements (e.g., Ru-Ni-Co-Ir-Cr).

Several studies have also noted compositional variations across the strike of individual ore shoots. There are clearly some magmatic variations (e.g., ferrichromite-rich ore pinchouts at some Kambalda shoots), but most of the variations across ore shoots are probably structural-metamorphic, especially if the ores were deformed at temperatures where pyrrhotite, pentlandite, and chalcopyrite existed as separate phases (see below). The ores at Otter shoot (Keele and Nickel, 1974) and Edwards Lode (Heath *et al.*, 2001) were among the most variable of the ores at Kambalda. Those at Otter shoot varied with the degree of alteration of the overlying host rock and the massive ores at Edwards Lode were strongly enriched in As and strongly depleted in Zn (relatively mobile) and Cr (relatively immobile) compared to normal Kambalda ores, suggesting that they were both metamorphically and tectonically modified.

These studies highlight the need to utilize multiple scales of sampling in order to understand variations in ore compositions. Grab samples, even if averaged, are the least reliable method, as they may not capture all of the small-medium scale variations and will miss metals mobilized into the wall rocks. Even large (2.5 kg) grab samples from ore stockpiles (e.g., Stone *et al.*, 2004) unless done randomly will also miss metals mobilized into wall rocks. Weighting grab samples from the various parts of individual ore profiles including footwall rocks (e.g., Ewers and Hudson, 1971; Cowden and Woolrich, 1981) will be more representative, but will miss along-strike variations. Channel sampling across individual ore horizons is better and when compared with bulk samples, will highlight which elements have been mobilized outside of the sampled area (e.g., Keays *et al.*, 1981). Compositing multiple large (50 kg) samples of carted ores (e.g., Ross and Keays, 1979; Woolrich *et al.*, 1981; Cowden *et al.*, 1986) or sampling mill feed composites (Burnham *et al.*, 2003) will best homogenize small-medium scale variations and will capture elements mobilized into the adjacent wall rocks, but may include materials from genetically separate ore systems if the mine or mill is extracting material from more than one ore system (see discussion by Lesher and Campbell, 1993).

Modification of ore tenors in Type II deposits

Because of the lower abundance of sulfide and the greater abundance of Ni and Ir accessible during serpentinization of olivine, Type Ⅱ mineralization can be significantly modified during alteration (Keele and Nickel, 1974; Eckstrand, 1975; Groves *et al.*, 1974; Groves and Keays, 1979), which makes it much more difficult to establish magmatic variations.

Partitioning of nickel between silicate and sulfide fractions is a sensitive function of the metamorphic mineral assemblage (Eckstrand, 1975; Frost, 1985). Under favorable circumstances, metamorphism can give rise to extreme nickel enrichment in sulfide, resulting in highly Ni-enriched concentrates. The economic viability of deposits such as the giant Mt. Keith deposit in the Agnew-Wiluna Belt of Western Australia rests on the high nickel tenor of the disseminated sulfide component of the ore (Grguric *et al.*, 2006).

The mineralogical and micro-textural features of Type Ⅱ disseminated sulfides in ultramafic rocks are complex, and have been studied in detail at a number of localities, including Black Swan (Groves *et al.*, 1974). These studies have emphasized distinctly different alteration paths and resulting sulfide assemblages in serpentinites on one hand and talc-carbonates on the other (Fig. 2.54).

In serpentinites, sulfide assemblages in Type Ⅱ ores are typically highly Ni-enriched, and are commonly dominated by pentlandite, or in some cases (Gole *et al.*, 1998) heazlewoodite or millerite. The interpretation of this effect has changed over the last two decades. Eckstrand (1975) and Donaldson (1981) considered it to be the result of release of originally olivine-hosted nickel during serpentinization in the

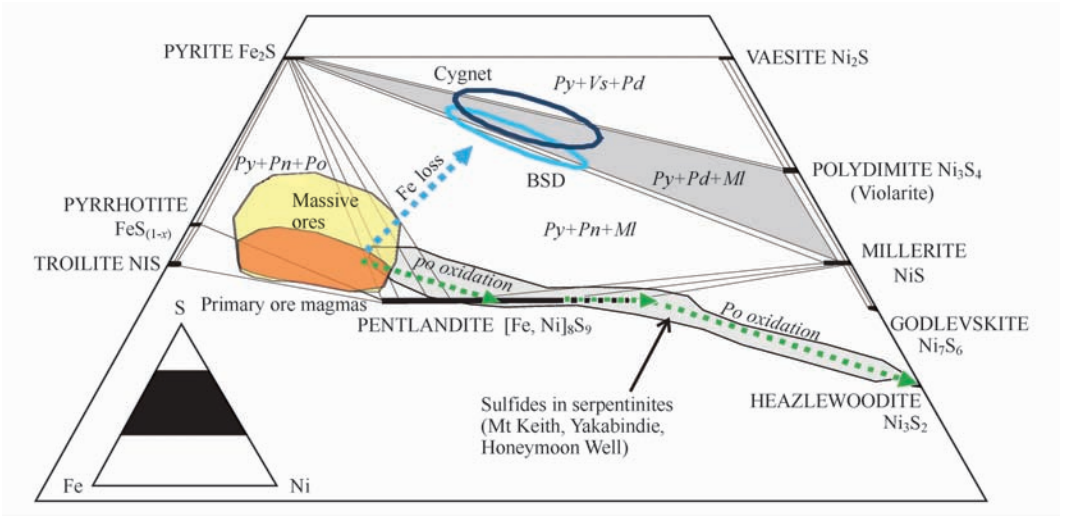

Fig. 2. 54 Phase equilibria in the Fe-Ni-S system below 350℃ (Craig, 1973; Craig and Kullerud, 1969; Hill, 1984). Fields for compositions of typical Western Australian sulfide ores from compilation of Barnes and Hill (2000). Paths of modification of sulfide mineralogy are shown corresponding to pyrrhotite oxidation in serpentinites, leading to pentlandite and heazlewoodite assembalges; and iron oxidation leading to millerite assemblages in serpentinites and talc carbonates (Barnes *et al*., 2009).

presence of reducing fluids. The uptake of this nickel into original pentlandite-pyrrhotite blebs produced an increase in Ni/Fe ratio and hence proportion of pentlandite. Grguric *et al*. (2006) concluded that a relatively small amount (if any) of the Ni originally in olivine is effectively released, much of it remaining in sub-micron sulfide inclusions in the serpentine pseudomorphs, and that upgrading of the sulfide tenor (i.e., the Ni content of the bulk sulfide fraction) is instead the result of oxidation of pyrrhotite to magnetite (and carbonation to ferroan magnesite in some cases). This is borne out by textural evidence for replacement of original sulfide blebs by magnetite and carbonate veinlets and coronas.

In talc-carbonates, sulfide mineralogy varies greatly between deposits, and also within deposits depending upon the abundance of sulfide in the rock. The effect is greatest, as in the case of serpentinization discussed above, for disseminated sulfides at low metamorphic grades. Disseminated sulfide assemblages in talc carbonates at Dumont (Eckstrand, 1975) and in the Cygnet orebody at Black Swan (Dowling *et al*., 2004) are dominated by millerite and pyrite, with minor polydimite (and vaesite at Cygnet). The assemblages have been interpreted by Eckstrand (1975) and Frost (1985) as the consequence of equilibration with oxidizing fluids during talc-carbonate formation. This oxidation is evident in parts of the Cygnet orebody from the presence of haematite-vaesite-pyrite assemblages. However, the distinction between assemblages in serpentinites and talc-carbonates is not straightforward, as millerite-pyrite assemblages have also been noted developing during early stages of serpentinization at Black Swan (Groves *et al*., 1974; Barnes *et al*., 2009).

2. 5. 6 S isotopes and S/Se ratios

$^{34}S/^{32}S$ ratios of sulfides in Type I ores and associated country rocks within an individual district are normally similar, but vary systematically between districts. For example, the ores at Langmuir and Windarra range from −2‰ to +2‰ $\delta^{34}S$ (Seccombe *et al*., 1981; Groves *et al*., 1979; Green and Naldrett, 1981), those at Kambalda and Widgiemooltha range from +1‰ to +4‰ $\delta^{34}S$ (Groves *et al*., 1979), those at Pechenga range from −3‰ to +8. 5‰ $\delta^{34}S$ (Green and Melezhik, 1999), those at Thompson range from +2. 5‰ to +6‰ $\delta^{34}S$ (Bleeker, 1990), those at Raglan range from +3‰ to +6‰ $\delta^{34}S$ (Lesher *et al*., 1999; Lesher, 2007), those at Alexo range from +4‰ to +6‰ $\delta^{34}S$ (Naldrett, 1966), and those at Fortaleza de Minas (a. k. a. O'Toole) range from +5‰ to +7‰ $\delta^{34}S$ (Choudhuri *et al*., 1997). Where the ores and country rocks have different S isotopic compositions, the values of the ores are typically between normal (depleted) mantle values (0 ± 1‰ $\delta^{34}S$) and the country rocks (Green and Naldrett, 1981; Eckstrand and Hulbert, 1987; Bleeker, 1990). At Pechenga the S isotopic compositions of the ores and sediments in the eastern part of the belt overlap but are different from those in the western part of the belt which also overlap (Green and Melezhik, 1999; Barnes *et al*., 2001). At Kambalda, S isotopic compositions of pyrrhotite from massive and matrix ores are identical and there is no apparent variation in isotopic composition with stratigraphic height through an ore profile (Seccombe *et al*., 1981). At Pechenga there are also no differences between ultramafic-hosted disseminated, massive, and breccia-

ted ores (Green and Melezhik, 1999).

S/Se ratios in Type I ores and metasedimentary rocks exhibit complementary variations (Groves *et al*., 1979; Green and Naldrett, 1981; Eckstrand and Hulbert, 1987; Bleeker, 1990). For example, S/Se ratios of Type I ores at Kambalda average 9430 ± 1870 (Groves *et al*., 1979), those at Thompson vary systematically between 8870 and 67240 (Bleeker, 1990), and those at Fortaleza de Minas range between 4810 and 17540 (Choudhuri *et al*., 1997). These values are higher than the mantle value of 3300 (McDonough and Sun, 1995) and are consistent with the interpretation that most of the S in these ores has been derived from associated sulfidic metasedimentary rocks (Groves *et al*., 1979; Green and Naldrett, 1981; Lesher and Groves, 1986; Bleeker, 1990; Fiorentini *et al*., 2006). S/Se ratios of Type Ⅱ ores at Mount Keith range 9300 – 43700, with S/Se ratio increasing with increasing S content (Groves and Keays, 1979). The high S/Se ratios were interpreted by Groves and Keays (1979) to be a product of addition of external S during serpentinization and talc-carbonation, but it is possible that the high S/Se ratios reflect addition of external S (Lesher and Keays, 2002). The correlation of S isotopic and S/Se data at Thompson (Bleeker, 1990), indicates that S and Se have not decoupled significantly during dynamic upper amphibolite facies metamorphism. Choudhuri *et al*. (1997) argued against derivation of S from country rocks at the deposits in the Morro de Ferro greenstone belt in Brazil for stratigraphic reasons, but the non-mantle $\delta^{34}S$ and S/Se ratios clearly indicate a crustal source. The S/Se ratios of Type Ⅳb sulfides at Kambalda ($(2-9)\times10^3$: Lesher and Keays, 1984) are slightly lower than the Type I ores at Kambalda ($(8-11)\times10^3$, Groves *et al*., 1979), suggesting that S and Se have decoupled slightly during hydrothermal transport.

In areas where $^{34}S/^{32}S$ are not fractionated or where there are multiple sources, more sophisticated methods are required. Fiorentini *et al*. (2006) measured $^{33}S/^{32}S$ and $^{34}S/^{32}S$ ratios in several ores from the Agnew-Wiluna belt (Western Australia) and the Abitibi Belt (Ontario). The inclusion of ^{33}S, an isotope that appears to have undergone photochemical mass-independent fractionation from ^{34}S in the ozone-absent Archean atmosphere, provides additional constraints on the source (s) of S because oxidized water-soluble ^{34}S species were preferentially incorporated into volcanic-associated massive sulfides, generating negative $\Delta^{33}S$ values (where $\Delta^{33}S$ refers to the degree of mass-independent fractionation of ^{33}S from ^{34}S), whereas reduced ^{33}S species were preferentially incorporated into sulfidic black shales and cherts, generating positive $\Delta^{33}S$ values. Fiorentini *et al*. (2006) found that volcanic-associated massive sulfides in these areas have consistently negative $\Delta^{33}S$ values as low as −0.7‰, whereas sulfidic black shales have 0 or positive $\Delta^{33}S$ values as high as +2.3‰. They also found that massive Fe-Ni-Cu sulfides have negative $\Delta^{33}S$ values as low as −0.8‰, whereas disseminated/matrix and coarse disseminated Fe-Ni-Cu sulfides have more variable but positive $\Delta^{33}S$ values ranging from 0.1‰ to 0.5‰. This suggests that the S in the massive ores came from assimilation or devolatilization of volcanic-associated massive sulfides, whereas the S in the disseminated/matrix sulfides came from sedimentary or mixed sedimentary-magmatic (mantle) S sources.

Finally, it is important to appreciate that S isotopes and S/Se of komatiite-associated Ni-Cu-(PGE) ores, regardless of whether derived from sources that have been fractionated by mass-dependent or mass-independent processes, will be strongly influenced by the amount of magma that equilibrates with the sulfides (Lesher and Stone, 1996; Lesher and Burnham, 1999, 2001). Sulfides that equilibrate with smaller amounts of magma will have $\delta^{34}S$, $\Delta^{33}S$, and S/Se ratios closer to that of S source, whereas sulfides that equilibrate with larger amounts of magma will have $\delta^{34}S$, $\Delta^{33}S$, and S/Se ratios closer to that of the magma.

2.6 Metamorphism

The metamorphism of komatiite-associated Ni-Cu-(PGE) deposits has been reviewed by Barrett *et al*. (1977), Marston *et al*. (1981), McQueen (1987), and Barnes and Hill (2000). Metamorphism ranges from lowermost greenschist facies at Alexo and Dundonald (Abitibi Belt) through middle-upper greenschist facies at Hart-Langmuir-McWatters-Redstone-Texmont-Sothman-Bannockburn (Abitibi), lower amphibolite facies at Kambalda, low to mid-amphibolite at Perseverance to upper amphibolite facies at Nepean, Forrestania, and Thompson. Petrofabric (Cowden and Woolrich, 1987) and experimental (McQueen, 1979; McQueen, 1987; Hill, 1984) studies indicate that most ores reverted to mixtures of *mss*, intermediate solid solution (*iss*), pentlandite, and/or pyrite, and relict spinels during peak metamorphism. The precise assemblage depends on temperature and composition, not only Fe-Ni-S contents, but also Cu content.

As a consequence of deformation and metamorphism, most massive ores exhibit metamorphic phase layering and tectonite fabrics. Ore fabrics at Kambalda mimic tectonite fabrics in adjacent silicate assemblages and preserve the total sequence of deformation (Cowden and Woolrich, 1987), indicating that the ores predate metamorphism and the earliest recognizable deformation. In higher grade, more complexly deformed areas, ore fabrics record only deformation or annealing events at lower metamorphic temperatures following unmixing of Fe-Ni-Cu sulfides from *mss* (Barrett *et al*., 1977). Stress-induced diffusion of Cu-PPGE accompanied the de-

formation of Type I ores (Barrett *et al*., 1977; Keays *et al*., 1981; Lesher and Keays, 1984; Bleeker, 1990; Paterson *et al*., 1984) and vapour-phase mobilization of S was common during waning metamorphism in some ores (Seccombe *et al*., 1981). However, there is no evidence that S isotopic compositions were substantially modified (Seccombe *et al*., 1981). Philpotts (1961), Dillon-Leitch *et al*. (1986), and Bazilevskaya and Lesher (unpubl. data) have described "reverse net-textured" sulfides that appear to represent pseudomorphous replacement of serpentinized olivine by sulfides.

As noted above, in more finely disseminated Type Ⅱ ores, oxidation, sulfidation, and carbonation reactions between sulfides, igneous silicates, and metamorphic fluids have substantially modified original sulfide compositions, as discussed above (Groves *et al*., 1974; Eckstrand, 1975; Nickel and Keele, 1975; Groves and Keays, 1979; Donaldson, 1981; Barnes *et al*., 2009) and possibly also S isotopic compositions (Seccombe *et al*., 1981).

All ore metals, except Ir and Cr, which appear to have very low solubilities in metamorphic/hydrothermal fluids, are potentially mobile during metamorphism. For example, Lesher and Keays (1984) demonstrated that Fe, Ni, Cu, Co, Cr, Zn, and especially Pd and Au were locally mobilized into post-tectonic Type Ⅳb quartz-sulfide ± carbonate veins in the footwall at Kambalda, but that the sulfides were strongly depleted in Ir and Cr. Paterson *et al*. (1984) and Bleeker (1990) showed that Ni-enriched metasediments at Kambalda and Thompson are enriched in many other ore metals, but strongly depleted in both Ir and Cr, suggesting mobilization of Ni into the metasedimentary rocks via high-temperature solid-state diffusion or magmatic-hydrothermal processes.

"Reverse-net" textures, where sulfides pseudomorph olivine, have been reported at Raglan. They have been attributed to replacement of unaltered portions of olivine and pyroxene (Philpotts, 1961), by replacement of serpentine (Barnes *et al*., 1982; Dillon-Leitch *et al*., 1986), and by replacement of magnetite produced during serpentinization of olivine (see discussion by Lesher, 2007). Olivine and sulfide co-exist in many other deposits and reverse-net textures occur in the lower parts of the host units where olivine is normally not preserved and not in the central parts of the host units were olivine is sometimes preserved, so replacement of olivine seems less likely.

2.7 Deformation

The deformation of komatiite-associated Ni-Cu-(PGE) deposits has been reviewed by Barrett *et al*. (1977) and McQueen (1987), and the deformation at specific deposits has been described by Marston and Kay (1980), Maiden *et al*. (1986), Bleeker (1990), Chisholm *et al*. (1999), Cowden and Archibald (1987), Stone and Archibald (2004), and Duuring *et al*. (2007).

Owing to the greater ductility of sulfides than silicate rocks, massive ore layers in Type I mineralization have been loci for penetrative deformation resulting in mobilization along fault planes and deformation in response to differential wall rock movements. Contacts between massive ores and more disseminated ores or wall rocks are often tectonic boundaries. Massive ores are commonly thickened in fold hinges, attenuated along faults, and tectonically displaced into wall rocks. Crosscutting relationships with late-metamorphic, largely post-tectonic dykes and hydrothermal quartz-carbonate veins indicate repeated episodes of ore deformation.

Tectonic breccia ores are common at Perseverance, Redross, Thompson, and Windarra, and are locally present at most other deposits. Lesher and Keays (1984), Paterson *et al*. (1984), and Bleeker (1990) have shown that tectonically-mobilized ores are compositionally similar to normal magmatic ores, but are slightly to strongly depleted in Cr, presumably reflecting the greater ductility of sulfides compared to chromite. Chalcopyrite stringers are present beneath many shoots at Kambalda, which Keays *et al*. (1981) showed by comparing samples of massive ores with samples of bulk mined ores at Kambalda to have been derived from massive sulfides during deformation. Similar stringers occur at Raglan (Dillon-Leitch *et al*., 1986; Chisholm *et al*., 1999). Many ores at Thompson are also depleted in Au > Cu > Pd, whereas other metals appear to have been only locally redistributed (Burnham *et al*., 2003).

Stone *et al*. (2005) suggested that mobilization of matrix (net-textured) sulfides at Kambalda could have generated massive sulfides, but no evidence of this process was found in the very detailed study of Barrett *et al*. (1977) that included the Lunnon and Juan shoots at Kambalda and the more-deformed ores at Nepean and Windarra. Barnes (2006) noted that the PGE chemistry of massive, matrix, and disseminated ores also preclude tectonic upgrading as an important process, even in areas of severe deformation such as Perseverance where it might be most likely. Simple mechanical deformation should result in tectonically-generated massive ores having the same composition as matrix ores or possibly being relatively enriched in Pd and Au owing to their greater hydrothermal mobility. There is no plausible mechanism that could concentrate IPGE in remobilized massive sulfides. Although massive ores may be tectonically mobilized, they cannot be formed from matrix ores.

Cowden and Archibald (1987), Stone and Archibald (2004), and Stone *et al*. (2005) have suggested that deformation and metamorphism at Kambalda have been so pervasive that they question the validity of observations and interpretations of primary magmatic and volcanological features. Not

only is this absolutely not true at Kambalda, but it is not true in most other deposits of this type. Sulfides are very ductile during deformation and metamorphism, so most of the strain partitions into sulfides, but they have been mobilized only very short distances (zero to tens of metres) at Alexo, Kambalda, and Raglan, only minor distances (tens of metres) at Fortaleza de Minas, Harmony, Nepean, Redross, and Windarra, and only moderate distances (tens to hundreds of metres) at Perseverance (1A shoot) and Thompson. We know the magnitudes of the displacements have been small because all except Thompson are still associated with their host rocks, most exhibit coherent ore segregation profiles, and many exhibit beautifully preserved magmatic contacts. The host rocks at Kambalda are orders of magnitude less deformed that those in the Thompson Nickel Belt, which also still retain well-preserved igneous textures and consistent stratigraphic locations (Layton-Matthews *et al*., 2007).

Volcanological models are absolutely essential in understanding and exploring for these deposits. Only in areas where the deformation have been intense enough to obscure the presence of anomalously-thick high-Mg host rocks, footwall embayments, and/or local S sources will such models fail. Even in the Thompson Nickel Belt, which is orders of magnitude more deformed and metamorphosed than Kambalda, analogous magmatic and stratigraphic models are successfully applied in exploration (Layton-Matthews *et al*., 2007). On the other hand, it would be impossible to explore for komatiite-associated Ni-Cu-(PGE) deposits (or any other type of magmatic Ni-Cu-(PGE) deposit) armed only with a structural model. Structural models are valuable in identifying magmatically and volcanologically prospective areas that have been uplifted to depths that can be drilled and they are valuable in finding dislocated portions of deformed ore shoots, but even these applications are limited if the all of the other information recorded in the rocks is ignored. 3D GIS studies of the type conducted by Stone *et al*. (2005) have their place, but as we have seen are quite clearly no replacement for detailed field mapping, petrographic studies, and geochemical work. We will undoubtedly see many improvements to the existing magmatic and volcanological models as more deposits are discovered, as the present models are too biased toward well-studied deposits like Kambalda, Raglan, Silver Swan, and Mt Keith, but they will come from studying the physical volcanology and trying to see through any superimposed deformation, not from ignoring the physical volcanology.

2.8 Ore genesis

A wide variety of geological, geochemical, and experimental evidence suggests an ultimate magmatic origin for the Ni-Cu-(PGE) mineralization in these deposits:

1) Type Ⅰ and Ⅱ mineralization are normally associated with the most magnesian, lowermost units in the host komatiite sequences and are spatially related to variations in the internal structure, physical volcanology, and stratigraphy of the overlying komatiite sequence that indicate a strong volcanic control on ore localization. These features are preserved in all but the most deformed and metamorphosed environments. Type Ⅲ mineralization occurs at levels in differentiated flows/sills where sulfide saturation is both predicted and observed to have been achieved.

2) Type Ⅰ mineralization exhibits graded massive/net-texured/disseminated ore segregation profiles often with well preserved magmatic net and disseminated textures. Type Ⅱ mineralization exhibits intercumulus textures indicative of igneous crystallization, and Type Ⅲ mineralization also exhibits textures consistent with magmatic crystallization.

3) The host units in those areas that have been studied exhibit systematic variations in degrees of crustal contamination and/or chalcophile element depletion that correlate with volcanic facies.

4) High Ni contents, high Ni/Cu ratios, relatively low Pd/Ir ratios, and low Zn and Pb contents of most Type Ⅰ, Ⅱ, and Ⅲ mineralization are consistent with known and inferred metal partitioning behaviour in mafic-ultramafic magmatic systems. Those that are not (e.g., Namew Lake) appear to have been contaminated by Cu-Zn-Pb-rich sulfides. Both Type Ⅰ and Type Ⅱ mineralization contain distinctive Al-poor, Fe-rich chromite, similar to those crystallized experimentally from sulfide-oxide liquids.

5) High Ir contents of Type Ⅲ mineralization and localization at specific lithological interfaces indicate an ultimate magmatic origin for this type of mineralization.

6) Type Ⅰ, Ⅱ, and Ⅲ mineralization predate deformation, metamorphism, and alteration of the host and wall rocks. Although some Type Ⅰ sulfides have been physically mobilized into veins and stringers during deformation and although some footwall rocks exhibit evidence of local volcanic or metamorphic interaction with the ores and host rocks, footwall rocks are otherwise unaltered and barren. There is no evidence that significant amounts of massive ores have been generated from disseminated or net-textured ores.

2.8.1 Type Ⅰ deposits

Type Ⅰ stratiform basal sulfides occur at or near the bases of the host units, indicating that sulfide saturation occurred early in their crystallization history. Type Ⅰb (magmatic vein) sulfides may form at an early stage, in which case they will contain normal magmatic sulfide compositions including high Cr contents, or at a late stage during fractional crystallization of *mss*, in which case they will be enriched in Cu-PPGE relative to Co-Ni-IPGE-Cr (Lesher and Keays, 1984;

Naldrett and Barnes, 1987; Barnes *et al*., 2004).

The source of the S deposits continues to be debated. Naldrett (1973), Naldrett and Cabri (1976), Naldrett and Turner (1977), and Malyuk (1985) proposed that the sulfides were transported and erupted directly from the mantle. Ross and Hopkins (1975) and Groves and Hudson (1981) suggested that they separated and segregated in a subsurface magma chamber prior to eruption, and Lesher *et al*. (1981) suggested that they separated during ascent. Although fluid dynamic calculations by Lesher and Groves (1986) and experiments by Bremond d'Ars *et al*. (2001) showed that finely dispersed sulfide droplets could be entrained during rapid ascent of low-viscosity komatiite magmas, Lesher and Groves (1986) noted several petrogenetic, thermodynamic, geochemical, and geological constraints that militate against transport of sulfides in the ascending komatiitic magmas, which are summarized and updated below.

Petrogenetic constraints

The extremely low abundances of highly incompatible lithophile elements (Th, U, Nb, Ta, LREE), highly positive ε_{Nd} signatures, very low abundances of moderately incompatible lithophile elements (MREE, Zr, HREE, Y), and very high abundances of highly compatible elements (Ni, Co, Mg) indicate that most mineralized komatiites were derived by very high degree partial melting of a long-term depleted mantle source (see Lesher and Stone, 1996; Sproule *et al*., 2002; Arndt *et al*., 2005). Because S was present in only very low abundances of 125 – 250 ppm in the mantle (McDonough and Sun, 1995; O'Neill *et al*., 1995) and is incompatible during melting, komatiites should have very low S contents (< 250 – 500 ppm: Lesher and Stone, 1996), which is significantly below the 2000 – 3000 ppm S capacity of komatiitic magmas at sulfide saturation (Shima and Naldrett 1975; Mavrogenes and O'Neill, 1999; Li and Ripley, 2005).

Thermodynamic constraints

Experimental studies by Helz (1982), Wendlandt (1982), Mavrogenes and O'Neill (1999) have shown that (i) there is a strong negative pressure dependence on sulfide solubility in basaltic melts and (ii) sulfide saturation isopleths are subparallel to anhydrous silicate liquidii. Thus, if sulfide-saturated at depth, magmas that ascend along liquidus paths should be sulfide-saturated during ascent and should exsolve an immiscible sulfide liquid during and after eruption. However, there is no evidence of significant intratelluric phenocryst contents in komatiites (see review by Arndt *et al*., 2008) and magmas of such low viscosity should ascend rapidly and lose little heat. Thus, komatiites should ascend along steeper P-T trajectories, nearer to an adiabatic gradient, and should arrive at the surface both superheated and undersaturated in sulfide (Lesher and Groves, 1986; Arndt *et al*., 2005).

Geochemical constraints

Because sulfide/melt partition coefficients for the PGE are of the order of 10^5 (see review by Naldrett, 2004), the high PGE abundances in most mineralized komatiites require that they were unsaturated in sulfide in the source region and during ascent (Keays, 1982, 1995; Lesher and Groves, 1986; Naldrett and Barnes, 1986; Lesher and Stone, 1996; Arndt *et al*., 2005). Most importantly, the presence of *local* chalcophile element depletion that is tied to stratigraphic location indicates that sulfide saturation was achieved locally, not prior to eruption (Lesher *et al*., 2001).

S isotopes and S/Se ratio

Differences in S isotopes and S/Se ratios between districts and significant deviations from chondritic values (see above) are not consistent with derivation from a homogeneous mantle source (Groves *et al*., 1979; Lesher and Groves, 1986; Ohmoto, 1986). It is unlikely that there was much oxidized S in the mantle, especially during the Archaean, and at such high temperatures fractionation of S isotopes between oxidized and reduced species would be insignificant (Ohmoto, 1986). In an attempt to reconcile the decoupling of S and Os isotopes at Kambalda, Foster *et al*. (1996) and Lambert *et al*. (1998) suggested that the S isotopic compositions might have been reset during metamorphism. However, the same mass balance constraints that favor resetting of Os isotopes at higher magma: sulfide ratios than S isotopes during magmatic processing (Lesher and Stone, 1996) also apply to resetting of Os isotopes at higher fluid: rock ratios than S isotopes during metamorphic alteration (see discussion by Lesher and Burnham, 2001). Although there is some evidence of sulfidation of Type I mineralization at Kambalda (Seccombe *et al*., 1981) and Type II mineralization at Katinniq (see Lesher, 2007), there is no evidence of widespread resetting of S isotopes (Groves *et al*., 1979; Seccombe *et al*., 1981; Lesher *et al*., 1999). The S isotope and S/Se variations in these deposits are best attributed to fractionation of S isotopes in a hydrothermal-exhalative environment with subsequent incorporation in and mixing with magmatic S in komatiitic magmas (Lesher and Groves, 1986; Lesher and Stone, 1996; Lesher and Burnham, 2001; Fiorentini *et al*., 2006).

Ore localization

Possibly the strongest argument that komatiites were not erupted containing entrained sulfides is the virtual absence of mineralization outside of the ore zones in many deposits. If magmas were erupted carrying sulfides, regardless of whether mantle-derived, exsolved during ascent, or produced by assimilation of lower crustal S, the entire host unit should contain ubiquitous disseminated mineralization: (i) sulfides should have been trapped in the chilled margins of host units; (ii) sulfides should have continued to exsolve throughout host units as the lavas cooled, oxidized, and crystallized after

emplacement; and (iii) fractional accumulation of sulfide-saturated komatiitic lavas should have resulted in significant enrichment of sulfide as well as olivine.

Field and stratigraphic relationships

The evidence for thermo-mechanical erosion of underlying S-rich footwall rocks has been summarized above. Xenoliths are only rarely preserved in deposits hosted by komatiites (e.g., Six Mile: Naldrett and Turner, 1977; Forrestania: Perring *et al*., 1996; Silver Swan: Dowling *et al*., 2004; Hunter's Road: Prendergast, 2001) or komatiitic basalts (e.g., Katinniq: Chisholm *et al*., 1999), presumably owing to the dynamics of the lava channel and dilution during lava replenishment (see discussion by Huppert and Sparks, 1985), however, they are ubiquitous in Ni-Cu-PGE deposits hosted by less magnesian magmas (e.g., Duluth, Chapter 5; Noril'sk, Chapter 4; Voisey's Bay, Chapter 6; Sudbury, see Naldrett, 2004). For the same reason, xenomelts are only locally preserved (e.g., Groves *et al*., 1986; McNaughton *et al*., 1988; Frost and Groves, 1989b; Dowling *et al*., 2004; (Houlé *et al*., 2002a; Houlé *et al*., 2002b).

Local contamination and local PGE depletion

The evidence for contamination and PGE depletion has been summarized above. A key point is that both are very localized. If all of the rocks exhibited uniform background contamination signatures or uniform background levels of PGE depletion, then it is possible that they came from a metasomatized source or became contaminated during ascent, or left sulfides in the source or became saturated in sulfide during ascent. However, many of the rocks are not contaminated or depleted in PGEs, indicating that contamination and sulfide saturation occurred *locally* (Sproule *et al*., 2005; Lesher *et al*., 2001; Barnes *et al*., 2007).

Sedimentary sulfur sources were proposed by Naldrett (1966), Prider (1970), Hudson (1972), Lusk (1976), and Hopwood (1981). Various aspects of those models were subsequently retracted or shown to be invalid, but those workers were the first to point out alternatives to the mantle-derived sulfide models. Subsequently, Groves *et al*. (1979) and Green and Naldrett (1981) proposed assimilation of sulfur from metasedimentary rocks during ascent through the crust, whereas more recent workers (e.g., Huppert and co-workers, 1984, 1985; Lesher *et al*., 1984; Lesher and Groves, 1986; Barnes *et al*., 1988; Bleeker, 1990; Perring *et al*., 1995, 1996; Lesher, 1999; Prendergast, 2003; Fiorentini *et al*., 2006) have favored assimilation of S from footwall or enclosing metasedimentary rocks during lava emplacement. Incorporation of crustal S is, of course, a fundamental aspect of most models for other types of Ni-Cu-PGE deposits (e.g., Ripley, 1986; Naldrett, 1989, 2004).

The restriction of Type I mineralization in many areas to embayments where sulfidic footwall rocks are locally thinned or locally absent, suggests that the metasedimentary rocks were thermo-mechanically eroded beneath thermally active lava conduits, melting sulfide that scavenged chalcophile elements from the komatiite lava to form Fe-Ni-Cu sulfide ores. Localities where sediments are partially to completely-preserved can be interpreted to be distal equivalents or less channelized lateral branches or breakouts (Fig. 2. 55). The absence of metasedimentary rocks adjacent to the ore zones ("barren void zone") at Kambalda suggests that some assimilation occurred in the proximal parts of the flanking sheet flow facies, and the presence of "chloritic" sediments (interpreted

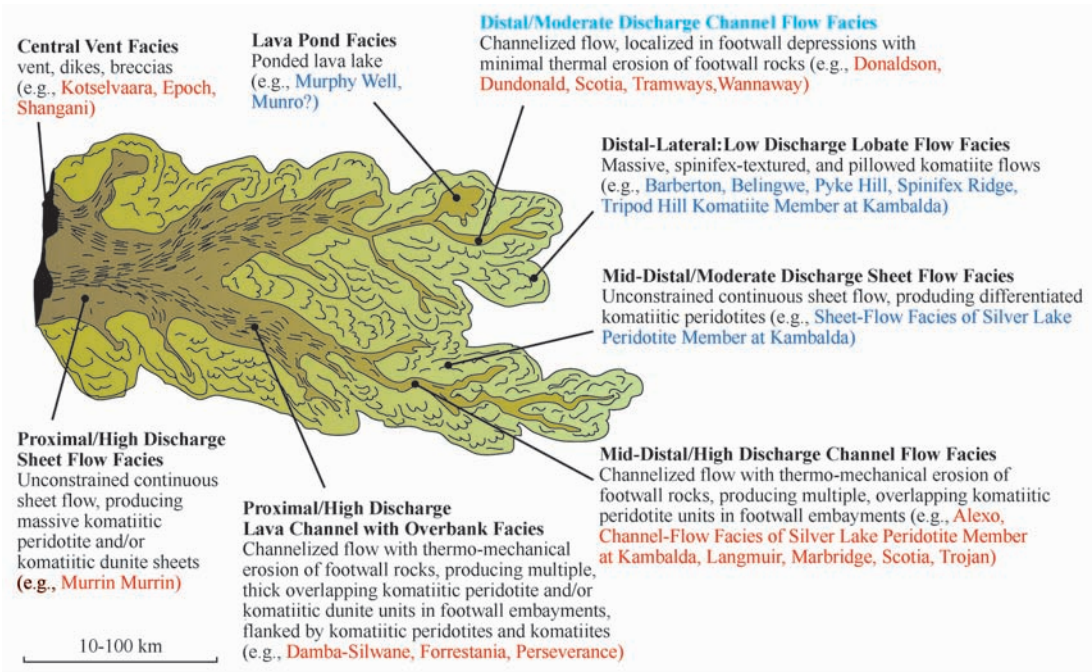

Fig. 2. 55 Komatiite flow field model (after Hill *et al*., 1995).

by Bavinton (1981) and Bavinton and Taylor (1980) as "chloritic" sediments, but which Lesher (1989) and Lesher and Burnham (1999, 2001) argued were partially decomposed based on their identical trace element composition between the void zone and sediment-covered contact suggests that some residues were preserved. The decoupling effect is evident in the geochemistry of the various components of the system (Fig. 2.31a-d): the compositions of the silicate xenomelts (ocellites), residues (chloritic sediments bordering the ore zone), and sulfide xenomelts (sulfide component of sediments) define an extract triangle that encloses the bulk composition of the sediment. Reaction of the sulfide xenomelt with the magma increased its metal content and reduced the metal content of the magma (upper parts of barren flanking units). The magmas above the channels were replenished, accounting for the lack of chalcophile element depletion (see discussion by Lesher and Burnham, 2001; Lesher *et al*., 2001).

Squire *et al*. (1998) found no evidence that sediments had been thermally eroded in their study of Foster shoot at Kambalda, and they and Cas and Beresford (2001) suggested that sediment was mechanically removed *via* burrowing and fluidization, as previously suggested by Bavinton (1981). Mechanical erosion of sediment is certainly possible, but it does not explain the presence of sediment xenomelts (Frost and Groves, 1989), the evidence for local contamination by sediment and local chalcophile element depletion (Lesher and Arndt, 1995; Lesher *et al*., 2001), and the need for external S and the similarity in the S isotopes of ores and sediments (Lesher and Groves, 1986; see below).

Stone and Archibald (2004) noted that ores overlie contact sediments in some locations without any evidence of faulting or erosion. This has been observed in several deposits at Kambalda, especially in the St. Ives and Tramways areas to the south (Gresham and Loftus-Hills, 1981), but also at Scotia, Mt Edwards, Blair, and Windarra (see Marston, 1984). Because the flanking sheet flows at Kambalda normally overlie sediments without any evidence of erosion (Bavinton, 1978, 1981; Lesher, 1989; Cowden and Roberts, 1990; Cas and Beresford, 2001), this likely reflect lower degrees of channelization in those units, either because they were more distal from the eruption site or simply less channelized at that point in the system (Lesher, 1989) and that the ores formed upstream (Lesher and Campbell, 1993).

Cas and Beresford (2001) argued against incorporation of sedimentary sulfur at Kambalda, proposing purely mechanical erosion of sediments to explain the absence of metasedimentary horizons in the ore zones. Many of their arguments are incorrect (e.g., S mass balance: Lesher and Burnham, 2001), or in the case of Os isotope arguments have been retracted (Lahaye *et al*., 2001), and does not explain any of the above problems in deriving sulfides from the magma. As noted by Lesher and Burnham (2001), any model for these deposits that does not involve incorporation of S from "local" sources must explain how a lava that was clearly undersaturated in sulfide and originally contained < 500 ppm S could have exsolved hundreds to millions of tonnes of sulfide ore without experiencing significant and widespread crystallization of the host rock, significant chalcophile element depletion in the ores or significant chalcophile element depletion in the host rocks. Some degree of thermomechanical erosion seems inevitable (Huppert *et al*., 1984; Huppert and Sparks, 1985; Williams *et al*., 1998, 1999, 2002; Williams *et al*., 1999; Kerr, 2001). The question that remains to be answered is the relative role this process played in individual parts of different deposits.

In summary, a ground melting model involving melting of S-rich rocks beneath lava channels appears to explain the geological, stratigraphic, mineralogical, geochemical, and isotopic data at most Type I deposits. It has also proven itself over time to be the most robust exploration model for deposits of this type.

2.8.2 Type II deposits

Type II strata-bound internal sulfides occur in the central parts of the host units and the presence of multiple ore horizons in some deposits indicate that sulfide saturation occurred during crystallization of the host rocks.

Type IIa

Coarse disseminated sulfides are too coarse (ave. ~1 cm diameter) to remain suspended in the magma except at very high flow rates and too abundant (up to 30% sulfide) to have exsolved *in situ*, so they must have formed during flow-through crystallization of the host unit (Lesher *et al*., 1984; Lesher and Groves, 1986) or as segregation vesicles (Beresford *et al*., 2000). Those at Kambalda (Beresford *et al*., 2000; Keele and Nickel, 1974) are commonly associated with amygdules and silicate blebs and occur in locations suggesting they represent a new pulse of lava and/or beheading of an underlying flow unit (Lesher *et al*., 1984; Cowden, 1988; Lesher, 1989). Either process could lead to the relatively uniform sizes. Inertial forces affect immiscible droplets during turbulent flow, resulting in coalescence of small droplets and break-up of large droplets, leading to a uniform droplet size (Lesher and Campbell, 1993), and vesicles commonly have relatively uniform sizes. Stone *et al*. (1987) suggested that the coarse disseminated sulfides that occur at the flow top of Fred's flow formed by degassing of S during emplacement, diffusion of metals into rising S-rich vapour bubbles, and subsequent crystallization of sulfides. They rejected an origin as immiscible sulfide droplets because of the association with amygdules, the high metal tenors of the blebs, and because of their high density relative to the silicate

lava. However, the metal tenors of the blebs (10% – 19% Ni) are not higher than could be achieved by transport during emplacement (Lesher and Campbell, 1993; Bremond d'Ars, 2001) and sulfide blebs are commonly trapped in the margins of MORB flows (Mathez, 1976). An alternative explanation, proposed for a similar occurrence at Dundonald (Eckstrand and Williamson, 1985), is that they are immiscible sulfide droplets that floated upwards attached to vapour bubbles. Regardless, the presence of a thin layer of chromites along the margins of the blebs (Stone *et al*., 1987) is more consistent with an origin as magmatic sulfide droplets or segregation vesicles than with crystallization from a vapour.

Type IIb

Type IIb mineralization is fine enough to have been carried in the magma, but a crustal source is supported by S/Se (Groves and Keays, 1979) and S isotope (Fiorentini *et al*., 2006) data, and in any case appears to be necessary from a geochemical and mass balance standpoint (Lesher and Keays, 2002). The magmas from which the very Fo-rich (up to Fo_{95}) adcumulate dunites formed must have had very high Mg contents, must have been emplaced at very high temperatures, and must have been strongly undersaturated in sulfide (Keays, 1982, 1995; Naldrett and Barnes, 1986). Furthermore, these magmas must have remained highly magnesian and very hot in order to have continued crystallizing essentially unzoned, essentially unfractionated high-Mg olivines at or near the liquidus (Lesher and Keays, 2002; Arndt *et al*., 2008). There is no geochemical evidence that the magmas fractionated anywhere near the point at which they would achieve sulfide saturation without the addition of external S (≤10% MgO; Lesher and Stone, 1996). This explains why most of the orthocumulate, porphyritic, and spinifex-textured rocks outside of the lava channels do not appear to have achieved sulfide saturation (see Lesher *et al*., 2001). If we assume that 30% MgO magmas derived by 50% partial melting of a depleted mantle source should contain less than 250 – 500 ppm S (Keays, 1995; Lesher and Stone, 1996), but should be able to dissolve ~2000 ppm S (based on the formulation of Li and Ripley, 2005), then the simplest and perhaps only way to bring them to sulfide saturation is to add 1% of a contaminant containing 11% – 13% S or 10% of a contaminant containing ~1.1% – 1.3% S. These amounts are consistent with the 2% – 10% contamination observed at Mt Keith (Fiorentini *et al*., 2007).

The amount of sulfide in Type IIb deposits (1% – 3% sulfide) is much less than in Type I deposits, but it still very much more than could have crystallized from the trapped liquid (0.6% based on the formulation of Li and Ripley, 2005). This and the similar grades of many deposits has led to suggestions that the sulfides may have segregated with olivine in cotectic proportions of ~60∶1 (Duke, 1986). Barnes (2007) noted that predicted cotectic ratios based on the formulation of Li and Ripley (2005) are more like 100∶1, and the proportions of olivine to sulfide in the ores at Mt Keith and Yakabindie range between 30∶1 to 40∶1, too low by a factor of 2.5 – 3 to be consistent with equilibrium cotectic precipitation of olivine and sulfide along the sulfide saturation surface. They suggested that this type of mineralization formed by mechanical transport and deposition of sulfide droplets, likely in a higher energy environment than that of Type I ores. Fiorentini *et al*. (2007) suggest that crustal assimilation may have continuously kept the Mt Keith system on the verge of sulfide supersaturation, but local change of intensive parameters other than crustal assimilation (e.g., T, fo_2, fs_2) best explain the observed variations in sulfide abundances and textures. A critical factor in the formation of Type IIb mineralization may be the stratigraphic architecture of the system. As discussed by Lesher and Arndt (1995) in terms of contamination, Lesher and Stone (1996) in terms of PGE depletion, and Lesher *et al*. (2001) in terms of fluid dynamics and R factor, if the S source is thin, the lava/magma channel will be replenished by sulfide-undersaturated lava/magma and will not form Type Ⅱ mineralization. However, if the S source is thick, the lava/magma in the channel may remain sulfide-saturated and may form Type Ⅱ mineralization.

Type IIc

Cloudy disseminated sulfides are present in amounts (<1%) that are small enough to have dissolved in the interstitial silicate liquid. They are subeconomic, but have important genetic and exploration implications. In deposits where the contaminant was very thin and where host rocks have been replenished (e.g., Kambalda), the magma may be driven away from sulfide saturation and the overlying rocks may contain negligible sulfides, but in areas where the contaminant was very thick (e.g., Raglan, Thompson), the magma will remain saturated in sulfides and will contain ubiquitous Type Ⅱ Ic mineralization.

2.8.3 Type III mineralization

Stone *et al*. (1993) attributed the present mineralogy and textures of the Type Ⅲ mineralization in the Boston Creek sill[1] to a "hydrothermal" process, but were not able to dis-

[1] Stone and colleagues (1993) interpreted the Boston Creek unit as a flow on the basis of the presence of a thick upper pyroxene spinifex-textured zone, but Houlé *et al*. (2001) have shown that it is transgressive to the upper contacts in several areas and that the upper chilled margin contains xenoliths of overlying rocks, indicating that it is a sill.

tinguish between a magmatic, magmatic-hydrothermal, or low-temperature hydrothermal origin. However, the "normal" fractionated Ir and Cr contents of the mineralization (Fig. 3E in Lesher and Stone, 1996) and the localization of the mineralization along the upper contacts of the lower cumulate zones in strongly differentiated mafic-ultramafic flows and sills are more consistent with a magmatic origin. The Boston Creek sill contains intercumulus igneous amphibole (Stone *et al*., 1997, 2003), which indicates that the *magma* contained minor amounts of water, and the geochemical trends in the data clearly indicate that it reached sulfide saturation at a late stage in the crystallization history of the host unit (Lesher and Stone, 1996), so it seems likely that the lava/magma also reach volatile saturation *late* in the crystallization history of the host unit. Thus, the textures and mineral associations probably represent precipitation from and/or modification by a volatile-rich, sulfide-saturated magmatic fluid that exsolved during the last stages of crystallization.

An external source of S is not required for Type Ⅲ mineralization. The abundance of S is relatively low and the common location of this type of mineralization at the top of the lower cumulate division and the base of the upper gabbro division indicates that it formed as a result of *in situ* fractional crystallization processes (Lesher and Stone, 1996). Unfortunately, because of the smaller size and less dynamic nature of these systems, this results in smaller abundances of sulfide and interaction with much smaller masses of magma than in large layered mafic-ultramafic intrusions (see Naldrett 2004; Maier *et al*., 2001). A critical factor in the formation of Type Ⅲ deposits is whether the magma experienced a previous history of sulfide saturation. If so, the metal tenor will be low. If not, the metal tenor will be higher.

The amount of sulfide is small enough to have been dissolved in the overlying differentiated silicate liquid, suggesting that the silicate liquid reached sulfide saturation as a consequence of normal fractional crystallization. The PGE variations in Fred's Flow and the Boston Creek sill, for example, show that the magma reached sulfide saturation at ~10% MgO (see discussion by Lesher and Stone, 1996), as the magma evolved from a komatiitic to basaltic (gabbroic) composition. Systematic vertical displacements of the peak abundances of different base, precious, and semi-metals through these zones may be attributed to decoupling of these elements owing to differences in sulfide/silicate partition coefficients (Fleet *et al*., 1999a; Peach and Mathez, 1993), to mixing of magmas that were filter-pressed from partially molten underlying cumulates with less evolved liquid at the temporary floor of the unit (Duke, 1986), and/or to hydrothermal mobilization (Ballhaus and Stumpfl, 1986; Boudreau *et al*., 1986), although it seems unlikely that Ir could be mobilized by the latter mechanism. Because the amount of S that can be dissolved in the magma is small and because these appear to have been relatively closed systems, unlike many continuously-replenished layered intrusions, ore tenors may be relatively high but ore grades are very low (see below). This latter point is very important. Unlike basaltic magmas, which may be emplaced at or near sulfide saturation, komatiites are normally strongly undersaturated in sulfide (Keays, 1982; Lesher and Groves, 1986; Lesher and Stone, 1996). This means that komatiites are much less likely to form significant PGE deposits than basalts unless they are able to fractionate significantly, but this can only occur in a relatively closed system, which restricts the amount of magma available to react with the sulfides.

2.8.4 Type Ⅳ deposits

Type Ⅳa sediment-hosted mineralization only occurs adjacent to Type I mineralization and appears to have formed by replacement of pre-existing sulfide-rich sediments. It occurs in environments ranging from lower greenschist (Langmuir) through lower amphibolite facies (Kambalda) to upper greenschist (Thompson). Paterson *et al*. (1984) evaluated all of the possible processes by which they could have formed and concluded that magmatic infiltration and tectonic mobilization were unlikely, and that they likely formed by mobilization of metals through a combination of hydrothermal transport and solid-state diffusion during metamorphism. Similar processes may have also operated at the magmatic stage.

2.9 Geological models

The geological model that best explains both Type I and Type Ⅱ mineralization involves voluminous eruption or intrusion of sulfide-undersaturated komatiitic lavas/magmas into rift-phase greenstone belts, forming moderately to deeply erosive lava/magma conduits (e.g., Zone 2, Zone 3, Katinniq, Zone 6, Zone 8, Boundary, and West Boundary at Raglan; parts of Pechenga; Mt. Keith and Perseverance), channelized sheet flows (e.g., most shoots at Kambalda; Cross Lake, Zone 5, and Zone 7 at Raglan), or feeder sills (e.g., Namew Lake, Thompson, and other parts of Pechenga) that incorporated variable amounts of S from country rocks during emplacement (Fig. 2.56 and Fig. 2.57A and B). The genetic model that best explains subseconomic Type Ⅲ mineralization is one that involves attainment of sulfide saturation *via* fractional crystallization (Fig. 2.57C).

The abundance and distribution of mineralization appears to be influenced by: (i) the volcanic setting and mode of emplacement of the host unit, (ii) the composition of the contaminant and mode and degree of S incorporation, (iii) the volume of lava/magma and its capacity to dissolve S, and

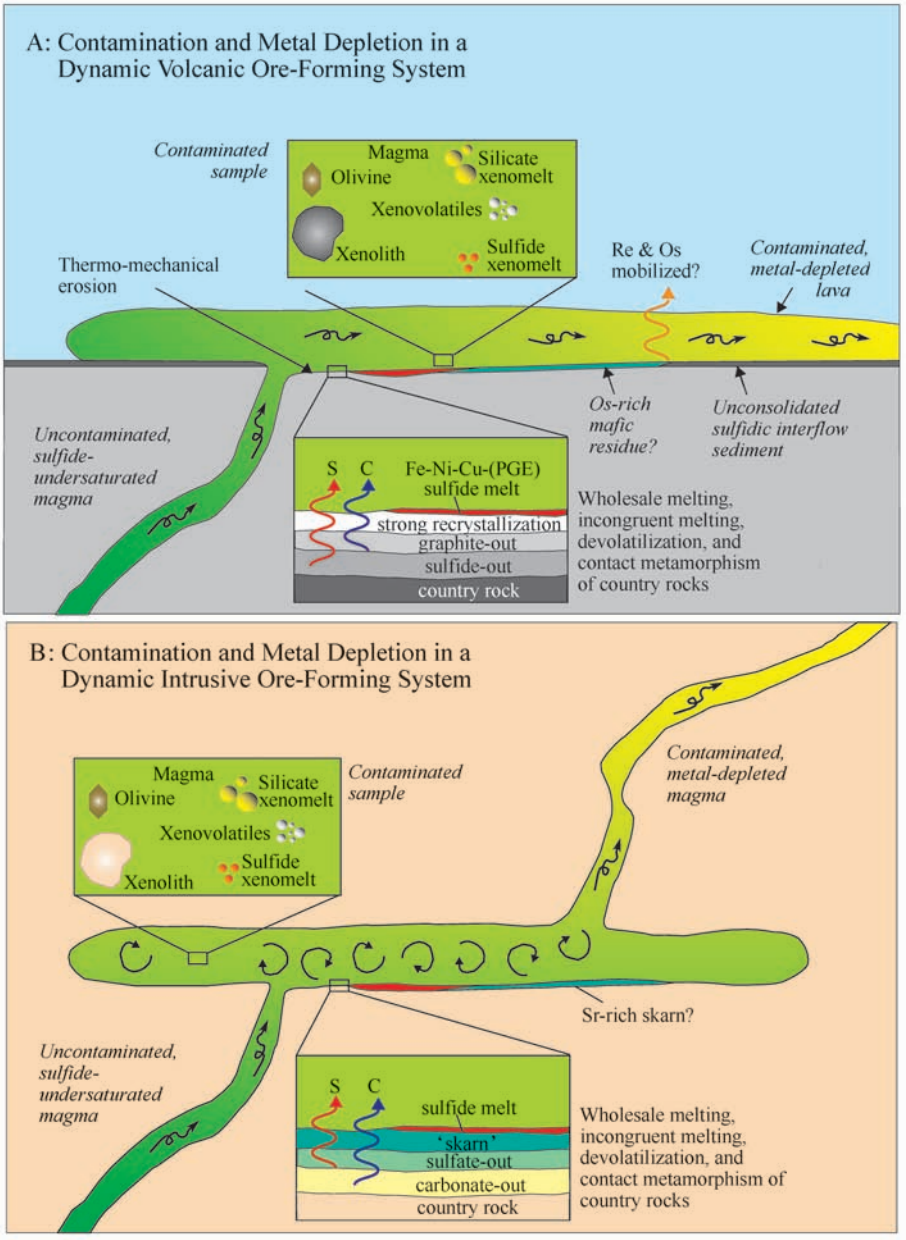

Fig. 2. 56 Geological model for the genesis of komatiite-associated volcanic and subvolcanic Type I/II mineralization (modified from Lesher *et al.* 2001).

(iv) the timing of sulfide saturation and opportunity for sulfide segregation (Lesher, 1989; Barnes *et al.*, 2001; Lesher *et al.*, 2001; Barnes, 2008). Units that incorporated proportionately larger amounts of external S achieved sulfide saturation early in their crystallization history and sulfides segregated rapidly, settling to the bases of the units, forming Type I sulfide ores. Units that incorporated proportionately smaller amounts of external S achieved sulfide saturation later in their crystallization history, forming Type II ores. Any S that could not be dissolved would have been transported in the flow as fine (<1 cm) droplets (Lesher and Groves, 1986) or along the base as a massive layer (Lesher and Campbell, 1993). Because the magma was being replenished in the channel, additional S would have to be melted and assimilated in order to maintain sulfide saturation; there would be a balance between the amount of magma and the amount of S being assimilated and if the magma was driven off of sulfide saturation (for example by exhaustion of the source upstream), sulfides may be dissolved (Kerr and Leitch, 2005; Lesher and Campbell, 1993). Units that incorporated little or no external S achieved sulfide saturation very late in their crystallization histories, only after substantial fractional crystallization, formed presently subeconomic Type III (stratiform "reef"-style) mineralization. Late-stage fractionation, metamorphism, deformation, and/or hydrothermal alteration form a wide range of other mineralization types.

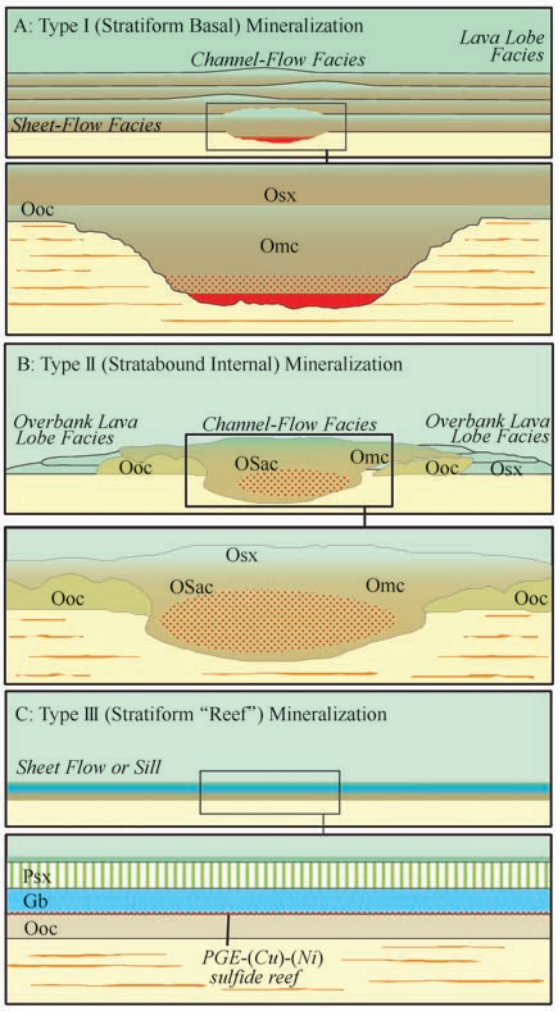

Fig. 2. 57 Geological models for the localization of Type I (A), Type II (B), and Type III (C) mineralization. Adapted from Lesher *et al.* (1984), Hill *et al.* (1995), and Lesher and Keays (2002).

Although the greatest degree of thermomechanical erosion and assimilation would occur beneath the lava/magma conduits, minor amounts may occur beneath flanking parts of the units, especially near the conduit (Lesher, 1989; Lesher *et al.*, 2001). This is consistent with the well-defined margins of the ore shoots, but absence of metasedimentary rocks along flanking contacts and minor amounts of mineralization in flanking areas at Kambalda, Raglan, and other deposits. Hangingwall ores at Kambalda and Raglan occur at the base of overlying units emplaced along the same volcanic pitchline (Lesher *et al.*, 1984; Lesher, 1999, 2007). The presence of thermally highly-conductive sulfides (~0. 05 cal/cm-s-℃: Williams *et al.*, 1972 vs. 0. 003 – 0. 006 cal/cm-s-℃ for komatiite: (Bickle, 1982) at the base of the flow may have enhanced thermomechanical erosion (Groves *et al.*, 1986), but accumulation of sulfides in areas with the greatest degree of thermomechanical erosion is attributable primarily to these being topographic lows that trapped dense sulfides (Lesher, 1989).

Thermomechanical erosion and S assimilation may occur along the entire length of the lava/magma conduit, but sulfide saturation may not occur until some intermediate point along the length of the conduit and sulfides may end up emplaced on sediment-bearing embayments in distal (or lateral) parts of the system (Lesher, 1989). All ores would have been above their liquidus at temperatures above the komatiite solidus, so low viscosity sulfides may have been mobilized subsequent to segregation. The intensity of mineralization at any location will be influenced by the topography of the footwall rocks and the fluid dynamics, which would trap dense sulfides and pond komatiite flows (Ross and Hopkins, 1975; Naldrett and Campbell, 1982; Lesher, 1989; Rice and Moore, 2001). This may explain, for example, why the ores in some deposits (e.g., Mickel, Silver Swan, parts of Katinniq) are not localized in the deepest parts of the embayments. There are two possible explanations for this: (1) they may have formed at a stage where the magma flow rate was high enough to have dissolved all of the sulfides, or (2) they may have formed at high enough flow rates that the sulfides were transported downstream. We must always remember that these are just parts of much larger (longer) systems.

The observed massive/matrix/disseminated ore profile in Type I deposits can be attributed to a combination of dynamic flow segregation (Hudson, 1972), static buoyancy ("billiard ball model": Naldrett, 1973), dynamic remelting (Lesher and Campbell, 1993), and capillary infiltration (Bazilevskaya and Lesher, unpubl.). Variations in the stratigraphic architecture and mode of emplacement of the host unit influenced the degree of assimilation and probably account for variations in ore tenor, intensity of mineralization, and stratigraphic relationships with S-rich rocks that are observed in different deposits (Lesher, 1989; Lesher and Stone, 1996; Lesher *et al.*, 2001). The compositions of the ores and the geochemical characteristics of the host rocks depend on the thickness of the assimilant, the fluid dynamic evolution of the system, and the *R* factor.

This model explains the general absence of deposits in areas that contain sulfidic metasedimentary rocks, but no lava channels, or in areas that contain lava channels, but no S source. Although barren cumulate sheet flows in one part of an area may be lateral facies equivalents of cumulate lava channels in another part and although sulfides may be mobilized from lava channels into sheet flow facies, most economic mineralization is localized in channels and they represent the most easily resolvable exploration target. Thus, this model not only explains why Ni-Cu-(PGE) mineralization is found almost exclusively in lava channels and magma conduits (Lesher *et al.*, 1984; Lesher, 1989; Naldrett, 1989, 2004; Barnes *et al.*, 1999; Prendergast, 2001, 2003; Lesher and Barnes, 2008), but it also explains why mineralization of

this type is not found as often in sheet flows or lava lobes or in large layered mafic-ultramafic intrusions (Maier *et al*., 2001).

Type Ⅱ mineralization, particularly that at Mt Keith and Yakabindie, has been considered to be genetically distinct from Type I, in that sulfide liquid deposition is held to have occurred essentially *in situ* through cotectic precipitation with olivine (Duke, 1986), as opposed to through physical transport and sedimentation of droplets formed by incorporation of sulfides upstream. This can be tested using recently developed quantitative models for S solubility as a function of magma composition and temperature (Li and Ripley, 2005) combined with numerical simulations of the fractional crystallization of olivine from komatiite magma, to predict the relative proportions of olivine and sulfide liquid that should segregate at equilibrium from a fractionating komatiite (Barnes, 2007). The predicted cotectic ratio of olivine to sulfide is higher and the S content of the cumulate assemblage is lower by a factor of 2 – 4, highest at Mt Keith and Six Mile but still higher at Goliath North than the values predicted from cotectic precipitation. This suggests that a purely cotectic precipitation model for this deposit type is incorrect for these deposits, and that much of the sulfide liquid was transported and mechanically deposited.

2.10 Exploration guides

The best exploration targets are presently large Type I deposits and clusters of smaller Type I deposits. Although Type Ⅱ deposits represent a very large Ni resource, most are presently subeconomic because of their low grade and the difficulty of extracting fine-grained disseminated sulfides from the host rocks, but will become more attractive with improvements in beneficiation. Some of the favorable geological and lithogeochemical features that may be used as guides in exploration for these deposits are summarized below (modified from Lesher, 1989; Lesher and Stone, 1996; Lesher and Keays, 2002; Barnes, 2006; and Arndt *et al*., 2008).

Province selection

1) Provinces where mafic-ultramafic magmas (komatiites, komatiitic basalts, picrites-ferropicrites, high-Mg basalts) were generated by high-degree partial melting of the mantle.

2) Tectonic settings exhibiting evidence of rifting during the volcanic stage and where magmas appear to have been emplaced onto continental crust or along continental margins.

3) Any type of komatiitic magma (i.e., Al-depleted, Al-undepleted, Al-enriched, Fe-rich).

Area selection

1) Crustal-scale faults that may focus ascent of magmas through the crust, although this is probably less critical in komatiite-associated deposits which may have formed further from eruptive sites because of their much lower viscosities.

2) Sequences that are thicker than other sequences in the same province and may represent loci for lava/magma channelization.

3) Sequences that contain a greater proportion of thicker, more olivine-rich, poorly differentiated units.

4) Sequences where lavas and/or intrusions are *locally* enriched in HILE relative to MILE and depleted in Nb relative to Th, indicating local contamination by upper crustal rocks.

5) Sequences where lavas and/or intrusions are *locally* depleted in PGE, indicating local segregation of sulfides.

6) Sequences where favorable host units have been uplifted by thrusting and/or folding.

Unit selection

1) Units containing abundant Mg-rich cumulus olivine (serpentinized units will contain abundant magnetite and will exhibit high magnetic susceptibilities, but talc-carbonated units will not).

2) Units that are poorly differentiated (normally more prospective) or differentiated (normally less prospective), depending on the physical volcanology.

3) Units that exhibit poor across-plunge continuity, but good down-plunge continuity, although establishing this will depend on the physical volcanology (e.g., lava conduit vs channelized sheet flow vs feeder sill), orientation, and deformation.

4) Units that appear to transgress sulfidic sediments, although this may occur "upstream" in the system.

5) Units that appear to have thermally-eroded footwall rocks and/or contain xenoliths or xenomelts.

6) Units that are enriched/depleted in chalcophile elements and/or contaminated/uncontaminated, relative to associated units, depending on the physical volcanology.

7) In the case of true komatiite systems (as opposed to komatiitc basalt systems), units which contain a substantial proportion of rocks with whole rock Ni > Cr (Barnes and Brand, 1999), and generally lacking chromite-enriched cumulates.

Peters (2006) has provided a comprehensive review of geophysical methods applied to komatiite-hosted deposits, with specific case studies from Western Australian deposits, and Butt *et al*. (2006) have done the same for geochemical exploration techniques. Electromagnetic (EM) methods have proved highly successful even in deeply weathered terrains, although the presence of conductive overburden in salt lake terrain is a major limitation. Geochemical prospecting is greatly complicated in weathered lateritic environments, but PGEs (and particularly Ir-Travis *et al*., 1976) are valuable discriminators of anomalies due to sulfide from those due to concentration of Ni in lateritic profiles. Surface geochemical and geophysical exploration methods used to further define prospec-

tive areas have also been described by Smith (1984), Pridmore *et al.* (1984) and Dentith *et al.* (1994).

Acknowledgements

We are very grateful to Chusi Li and Ed Ripley for inviting us to participate in the Xi'an short course and to Minwu Liu for logistical assistance. Our understanding of these deposits and their host rocks has developed over the past 30 years through collaborative research with Nick Arndt, Mike Bickle, Marcus Burnham, Ian Campbell, Mike Donaldson, Valeri Fedorenko, Cesar Ferreira-Filho, Marco Fiorentini, Martin Gole, David Groves, Robin Hill, Michel Houlé, Reid Keays, Ross Kerr, Caroline Perring, Rebecca Sproule, Thomas Menard, Harold Stowell, David Williams, and Mei-Fu Zhou, and with the many University of Alabama, Laurentian University, and University of Western Australia graduate students listed in the references. We have also benefited from discussions with many other colleagues, especially Sarah-Jane Barnes, Steve Beresford, Ray Cas, Tony Green, Jon Hronsky, Victor Melezhik, Tony Naldrett, and Martin Prendergast. Our research on komatiite-associated Ni-Cu-(PGE) deposits has been supported at various stages by grants from the US National Science Foundation, the Natural Sciences and Engineering Research Council of Canada, the Canadian Mining Industry Research Organization, Billiton Ltd. and WMC Ltd. (now BHP-Billiton Ltd.), Cominco Ltd. and Teck Ltd. (now Teck-Cominco), Falconbridge Ltd. (now Xstrata Ltd.), Hudson Bay Exploration & Development, Inco Ltd. (now Vale Inco Ltd.), Jinchuan Non-Ferrous Metal Co., and Outokumpu Ltd. to CML and by financial support from Outokumpu Oy, MPI Ltd., Independence Group NL, LionOre NL(now Norilsk Nickel Australia NL), and BHP-Billiton Ltd. to SJB. We are very grateful to the many mining company executives who encouraged and supported our work and the many mining company mining and exploration geologists who helped us in our work and with whom we had many beneficial and insightful discussions.

References

Almeida CM, Olivo GR, De Carvalho SG. 2007. The Ni-Cu-PGE sulfide ores of the Komatiite-hosted Fortaleza De Minas Deposit, Brazil: evidence of hydrothermal Remobilization. Can Mineral 45: 751 – 773

Arndt NT. 1977. Thick, layered peridotite-gabbro lava flows in Munro Township, Ontario. Can J Earth Sci 14: 2620 – 2637

Arndt NT. 1986. Thermal erosion by komatiites at Kambalda. Nature 324: 600

Arndt NT, Lesher CM, Barnes SJ. 2008. Komatiite. Cambridge University Press, Cambridge, p. 1 – 488

Arndt NT, Lesher CM, Czamanske GK. 2005. Mantle derived magmas and magmatic Ni-Cu-PGE deposits. Econ Geol 100th Anniversary Volume: 5 – 24

Arndt NT, Lesher CM, Houle MG, Lewin E, Lacaze Y. 2004. Intrusion and crystallization of a spinifex textured komatiite sill in Dundonald Township, Ontario. J Petrol 45: 2555 – 2571

Arndt NT, Naldrett AJ, Pyke DR. 1977. Komatiitic and iron-rich tholeiitic lavas of Munro Township, northeast Ontario. J Petrol 18: 319 – 369

Abzalov MZ, Both RA. 1997. The Pechenga Ni-Cu deposits, Russia: data on PGE and Au distribution and sulphur isotope compositions, Mineral Petrol 61: 119 – 143

Ballhaus C, Stumpfl EF. 1986. Sulfide and platinum mineralization in the Merensky Reef: evidence from hydrous silicates and fluid inclusions. Contrib Mineral Petrol 94: 193 – 204

Barley M, Krapez S, Kositcin N. 2008. Physical volcanology and geochemistry of a late Archaean volcanic arc; Kurnalpi and Gindalbie terranes, Eastern Goldfields Superterrane, Western Australia. Precam Res 161: 53 – 76

Barley ME, Brown SJA, Krapez B. 2006. Felsic volcanism in the eastern Yilgarn Craton, Western Australia: evolution of a Late Archean convergent margin. Geochim Cosmochim Acta 70: A35

Barnes S-J, Giovenazzo D. 1990. Platinum-group elements in the Bravo intrusion, Cape Smith Fold Belt, northern Quebec. Can Mineral 28: 431 – 449

Barnes S-J, Gorton MP, Naldrett AJ. 1983. A comparative study of olivine and clinopyroxene spinifex flows from Alexo, Abitibi greenstone belt, Ontario, Canada. Contrib Mineral Petrol 83: 292 – 308

Barnes S-J, Lightfoot PC. 2005. Formation of magmatic nickel sulfide deposits and processes affecting their copper and platinum group element contents. Econ Geol 100th Anniversary Volume: 179 – 214

Barnes S-J, Makovicky E, Makovicky M, Rose-Hansen J, Karupmoller S. 1997. Partition coefficients for Ni, Cu, Pd, Pt, Rh, and Ir between monosulfide solid solution and sulfide liquid and the formation of compositionally zoned Ni-Cu Sulfide bodies by fractional crystallization of sulfide liquid. Can J Earth Sci 34: 366 – 374

Barnes S-J, Melezhik VA, Sokolov SV. 2001. The composition and mode of formation of the Pechenga nickel deposits, Kola Peninsula, northwestern Russia. Can Mineral 39: 447 – 471

Barnes S-J, Naldrett AJ. 1986. Variations in platinum group element concentrations in the Alexo mine komatiite, Abitibi greenstone belt, northern Ontario. Geol Mag 123: 515 – 524

Barnes S-J, Naldrett AJ. 1987. Fractionation of the platinum-group elements and gold in some komatiites of the Abitibi Greenstone Belt, Northern Ontario. Econ Geol 82: 165 – 183

Barnes S-J, Naldrett AJ, Gorton MP. 1985. The origin of the fractionation of the platinum-group elements in terrestrial magmas. Chem Geol 53: 303 – 323

Barnes S-J, Picard CP. 1993. The behavior of platinum-group elements during partial melting, crystal fractionation, and sulphide segregation: an example from the Cape Smith Fold Belt, Northern Quebec. Geochim Cosmochim Acta 57: 79 – 87

Barnes SJ. 1998. Chromite in Komatiites, 1. Magmatic controls on

crystallization and composition. J Petrol 39：1689－1720

Barnes SJ. 2000. Chromite in komatiites, Ⅱ. Modification during greenschist to mid-amphibolite facies metamorphism. J Petrol 41：387－409

Barnes SJ. 2004. Komatiites and nickel sulfide ores of the Black Swan area, Yilgarn Craton, Western Australia. 4. Platinum Group Element distribution in the ores, and genetic implications. Mineral Deposita 39：752－765

Barnes SJ. 2006. Komatiite-hosted nickel sulfide deposits：geology, geochemistry, and genesis. Soc Econ Geologists Spec Pub 13：51－118

Barnes SJ, Barnes S-J. 1990. A new interpretation of the Katiniq nickel deposit, Ungava, Northern Quebec. Econ Geol 85：1269－1272

Barnes SJ, Brand NW. 1999. The distribution of Cr, Ni, and chromite in komatiites, and application to exploration for komatiite-hosted nickel sulfide deposits. Econ Geol 94：129－132

Barnes SJ, Coats CJA, Naldrett AJ. 1982. Petrogenesis of a Proterozoic nickel sulphide-komatiite association：the Katiniq Sill, Ungava, Quebec. Econ Geol 77：413－429

Barnes SJ, Fiorentini ML. 2008. Iridium, ruthenium and rhodium in komatiites：Evidence for iridium alloy saturation. Chem Geol 257：44－58

Barnes SJ, Fiorentini ML, Austin P, Gessner K, Hough R, Squelch A. 2008. Three-dimensional morphology of magmatic sulfides sheds light on ore formation and sulfide melt migration. Geology 36：655－658

Barnes SJ, Gole MJ, Hill RET. 1988a. The Agnew nickel deposit, Western Australia：part I. Stratigraphy and structure. Econ Geol 83：524－536

Barnes SJ, Gole MJ, Hill RET. 1988b. The Agnew nickel deposit, Western Australia：part Ⅱ. Sulfide geochemistry, with emphasis on the platinum-group elements. Econ Geol 83：537－550

Barnes SJ, Hill RET. 1995. Poikilitic chromite in komatiitic cumulates. Mineral Petrol 54：85－92

Barnes SJ, Hill RET. 2000. Metamorphism of komatiite hosted nickel sulfide deposits. In：Spry PG, Marshall B, Vokes FM (eds). Metamorphosed and Metamorphogenic Ore Deposits, Reviews in Economic Geology 11. Society of Economic Geologists, Boulder, p. 203－216

Barnes SJ, Hill RET, Gole MJ. 1988c. The Perseverance ultramafic complex, Western Australia：product of a komatiite lava river. J Petrol 29：305－331

Barnes SJ, Hill RET, Perring CS, Dowling SE. 2004. Lithogeochemical exploration for komatiite-associated Ni-sulfide deposits：strategies and limitations. Mineral Petrol 82：259－293

Barnes SJ, Lesher CM, Sproule RA. 2007. Geochemistry of komatiites in the Eastern Goldfields Superterrane, Western Australia and the Abitibi Greenstone Belt, Canada, and implications for the distribution of associated Ni-Cu-PGE deposits. App Earth Sci (Trans Inst Mining Metall Series B)116：167－187

Barnes SJ, Wells MA, Verrall MR. 2009. Effects of magmatic processes, serpentinization and talc carbonate alteration on sulfide mineralogy and ore textures in the Black Swan disseminated nickel sulfide deposit, Yilgarn Craton. Econ Geol (in press)

Barrett FM, Binns RA, Groves DI. 1977. Structural history and metamorphic modification of Archaean volcanic-type nickel deposits. Econ Geol 72：1195－1223

Barrett FM, Groves DI, Binns RA. 1976. Importance of metamorphic processes at the Nepean nickel deposit, Western Australia. Trans Institute Mining Metall, Section B 85：251－274

Barrie CT. 1999. Komatiite flows of the Kidd Creek footwall, Abitibi Subprovince, Canada. Econ Geol Monogs 10：143－161

Barrie CT, Corfu F, Davis P, Coutts AC, Maceachern D. 1999. Geochemistry of the Dundonald komatiite-basalt suite and genesis of Dundeal Ni deposit, Abitibi subprovince, Canada. Econ Geol 94：845－866

Bavinton OA. 1979. Interflow sedimentary rocks from the Kambalda ultramafic sequence：their geochemistry, metamorphism and genesis. PhD thesis, Australian National University, Canberra (unpubl)

Bavinton OA. 1981. The nature of sulfidic sediments at Kambalda and their broad relationships with associated ultramafic rocks and nickel ores. Econ Geol 76：1606－1628

Bavinton OA, Keays RR. 1978. Precious metal values from interflow sedimentary rocks from the komatiite sequence at Kambalda, Western Australia. Geochim Cosmochim Acta 42：1151－1163

Bavinton OA, Taylor SR. 1980. Rare earth element geochemistry of Archaean metasedimentary rock from Kambalda. Western Australia. Geochim Cosmochim Acta 44：639－648

Becker H, Horan M, Walker R, Gao S, Lorand J-P, Rudnick R. 2006. Highly siderophile element composition of the Earth's primitive mantle：constraints from new data on peridotite massifs and xenoliths. Geochim Cosmochim Acta 70：4528－4550

Beresford S, Cas R, Lahaye Y, Jane M. 2002. Facies architecture of an Archean komatiite-hosted Ni-sulphide ore deposit, Victor, Kambalda, Western Australia：implications for komatiite lava emplacement. J Volc Geothermal Res 118：57－75

Beresford S, Stone WE, Cas R, Lahaye Y, Jane M. 2005. Volcanological controls on the localization of the komatiite-hosted Ni-Cu-(PGE) Coronet deposit, Kambalda, Western Australia. Econ Geol 100：1457－1467

Beresford SW, Cas RAF. 2001. Komatiitic invasive lava flows, Kambalda, Western Australia. Can Mineral 39：525－535

Beresford SW, Cas RAF, Lambert DD, Stone WE. 2000. Vesicles in thick komatiite lava flows, Kambalda, Western Australia. J Geol Soc 157：11－14

Bickle MJ. 1982. The magnesium contents of komatiitic liquids. In：Arndt NT, Nisbet EG (eds). Komatiites. George Allen and Unwin, London, p. 477－494

Billington LG. 1984. Geological review of the Agnew nickel deposit, Western Australia. In：Buchanan DL, Jones MJ (eds). Sulphide deposits in mafic and ultramafic rocks. Institute of Mining and Metallurgy, London, pp 43－54

Binns RA, Groves DI. 1976. Iron-nickel partition in metamorphosed olivine-sulfide assemblages from Perseverance, Western Australia. Amer Mineral 61：782－787

Binns RA, Groves DI, Gunthorpe RJ. 1977. Nickel sulphides in Archaean ultramafic rocks of Western Australia. In：Siderenko

AV (ed). Correlation of the Precambrian, vol. 2. Nauka, Moscow, pp 349 – 380

Bleeker W. 1990. New structural-metamorphic constraints on early Proterozoic oblique collision along the Thompson Nickel Belt, northern Manitoba, Canada. In: Lewry JF, Stauffer MR (eds). The early Proterozoic Trans-Hudson Orogen of North America. Geological Association of Canada, pp 57 – 73

Boudreau AE, Mathez EA, McCallum IS. 1986. Halogen geochemistry of the Stillwater and Bushveld Complexes: evidence for transport of platinum group elements by Cl-rich fluids. J Petrol 27: 967 – 986

Brenner TL, Teixeira NA, Oliveira JAL, Franke ND, Thompson JFH. 1990. The O'Toole nickel deposit, Morro do Ferro greenstone belt, Brazilia. Econ Geol 85: 904 – 920

Brown MAN, Jolly RJH, Stone W, Coward MP. 1999. Nickel ore troughs in Archaean volcanic rocks, Kambalda, Western Australia; indicators of early extension. Geol Soc Spec Pubs 155: 197 – 211

Brügmann GE, Arndt NT, Hoffman AW, Tobschall HJ. 1987. Precious element abundances in komatiite suites from Alexo, Ontario, and Gorgona Island, Columbia. Geochim Cosmochim Acta 51: 2159 – 2169

Brugmann GE, Hanski EJ, Naldrett AJ, Smolkin VF. 2000. Sulphide segregation in ferropicrites from the Pechenga Complex, Kola Peninsula, Russia. J Petrol 41: 1721 – 1742

Brügmann GE, Naldrett AJ, Duke JM. 1989. Platinum-group element distribution in the komatiitic Dumont sill, northwestern Quebec, Canada. Bull Geol Soc Finland 61: 23

Buck PS, Vallance SA, Perring CS, Hill RET, Barnes SJ. 1998. Maggie Hays nickel deposit. In: Berkman DA, Mackenzie DH (eds). Geology of Australian and Papua New Guinean Mineral Deposits. Australian Institute of Mining and Metallurgy, Melbourne, pp 357 – 364

Burnham OM, Halden N, Layton-Matthews D, Lesher CM, Liwanag J, Heaman L, Hulbert L, Machado N, Michalak D, Pacey M, Peck D, Potrel A, Theyer P, Toope K, Zwanzig H (eds). 2003. Geology, Stratigraphy, Petrogenesis, and Metallogenesis of the Thompson Nickel Belt, Manitoba: Final Report for CAMIRO Project 97E-02. Mineral Exploration Research Centre, Sudbury

Butt CRM, Nickel EH, Brand NW. 2006. The weathering of nickel sulfide deposits and implications for geochemical exploration. Soc Econ Geologists Spec Pub 13: 139 – 165

Campbell IH, Barnes SJ. 1984. A model for the geochemistry of the platinum group elements in magmatic sulphide deposits. Can Mineral 22: 151 – 160

Campbell IH, Naldrett AJ. 1979. The influence of silicate: sulphide ratios on the geochemistry of magmatic sulphides. Econ Geol 74: 503 – 1505

Cas R, Self S, Beresford S. 1999. The behaviour of the fronts of komatiite lavas in medial to distal settings. Earth Planet Sci Letts 172: 127 – 139

Cas RAF, Beresford SW. 2001. Field characteristics and erosional processes associated with komatiitic lavas: Implications for flow behavior. Can Mineral 39: 505 – 524

Champion DC, Cassidy KF. 2007. An overview of the Yilgarn Craton and its crustal evolution. Proceedings of Geoconferences (WA) Inc Kalgoorlie'07 Conference, Geoscience Australia Record 2007/14: 8 – 12

Chauvel C, Dupre B, Jenner GA. 1985. The Sm-Nd age of Kambalda volcanics is 500 Ma too old! Earth Planet Sci Letts 74: 315 – 324

Chimimba LR. 1989. Geology and mineralogy at Trojan Mine, Zimbabwe. In: Buchanan DL, Jones MJ (eds). Sulphide deposits in mafic and ultramafic rocks: proceedings of the third nickel sulphide field conference, Perth, Western Australia. Institution of Mining and Metallurgy, London, pp 147 – 155

Chisholm KM. 2002. Nature and origin of ore-localizing embayments at the Katinniq Ni-Cu-(PGE) sulfide Deposit, Cape Smith Belt, New Québec. Unpub. NSc Thesis, Laurentian University, Sudbury

Chisholm KM, Welch MJ, Nemcsok G, Lemery RG. 1999. Mine geology of the Katinniq and Zone 2 Ni-Cu-(PGE) deposits. In: Lesher CM (ed) Komatiitic Peridotite-Hosted Fe-Ni-Cu-(PGE) Sulphide Deposits in the Raglan Area, Cape Smith Belt, New Québec. Mineral Exploration Research Centre, Laurentian University, Sudbury, pp 150 – 158

Choudhuri A, Iyer SS, Krouse HR. 1997. Sulfur isotopes in komatiite-hosted Ni-Cu sulfide deposits from the Morro de Ferro greenstone belt, southeastern Brazil. Internat Geol Rev 39: 230 – 238

Coad PR. 1979. Nickel sulphide deposits associated with ultramafic rocks of the Abitibi Belt and economic potential of mafic-ultramafic intrusions. Ontario Geol Surv Study 20: p. 84

Costa J, Carlos N, Ferreira-Filho CF, Osborne GA, Araujo SM, and Lopes RO. 1997. Geology and geochemistry of the Boa Vista nickel sulfide deposit, Crixas greenstone belt, central Brazil, Revista Brasileira de Geociencias 27: 365 – 376

Cowden A, Archibald NJ. 1987. Massive-sulfide fabrics at Kambalda and their relevance to the inferred stability of monosulfide solid-solution. Can Mineral 25: 37 – 50

Cowden A, Donaldson MJ, Naldrett AJ, Campbell IH. 1986. Platinum group elements and gold in the komatiite-hosted Fe-Ni-Cu sulphide deposits at Kambalda, Western Australia. Econ Geol 81: 1226 – 1235

Cowden A, Roberts DE. 1990. Komatiite hosted nickel sulphide deposits, Kambalda. In: Hughes FE (ed). Economic Geology of Australia and Papua New Guinea. Australian Institute of Mining and Metallurgy, Melbourne, p. 567 – 581

Cowden A, Woolrich P. 1987. Geochemistry of the Kambalda iron-nickel sulfides: Implications for models of sulfide-silicate partitioning. Can Mineral 25: 21 – 36

Craig JR. 1973. Pyrite-pentlandite assemblages and other low-temperature phase relations in the Fe-Ni-S system. Amer J Sci 273A: 496 – 510

Craig JR, Kullerud G. 1969. Phase relations in the Cu-Fe-Ni-S system and their application to magmatic ore deposits. Econ Geol Monog 4: 344 – 358

Crocket JH, MacRae WE. 1986. Platinum-group element distribution in komatiitic and tholeiitic volcanic rocks from Munro

Township, Ontario. Econ Geol 81: 1242 - 1251

Da Fonseca ROC, Campbell IH, O'Neill HSC, Fitzgerald JD. 2008. Oxygen solubility and speciation in sulphide-rich mattes. Geochim Cosmochim Acta 72: 2619 - 2635

Dann JC. 2001. Vesicular komatiites, 3.5-Ga Komati Formation, Barberton Greenstone Belt, South Africa: inflation of submarine lavas and origin of spinifex zones. Bull Volc 63: 462 - 481

Davis CES. 1972. Analytical methods used in the study of an ore intersection from Lunnon Shoot, Kambalda, Western Australia. Econ Geol 67: 1075 - 1092

Davis PC. 1999. Classic komatiite localities and magmatic Fe-Ni-Cu-(PGE) sulphide deposits of the Abitibi Greenstone Belt, Ontario-Quebec. Guidebook Series 1. Laurentian University, Sudbury, Canada

De-Vitry C, Libby JW, Langworthy PJ. 1998. Rocky's Reward Nickel Deposit. In: Berkman DA, Mackenzie DH (eds). Geology of Australian and Papua New Guinean Mineral Deposits. Australian Institute of Mining and Metallurgy, Carlton, pp 315 - 320

de Bremond d'Ars J, Arndt NT, Hallot E. 2001. Analog experimental insights into the formation of magmatic sulfide deposits. Earth Planet Sci Letts 186: 371 - 381

Dillon-Leitch HCH, Watkinson DH, Coats CJA. 1986. Distribution of platinum-group elements in the Donaldson West deposit, Cape Smith Belt, Quebec. Econ Geol 81: 1147 - 1158

Donaldson MJ. 1981. Redistribution of ore elements during serpentinisation and talc-carbonate alteration of some Archaean dunites, Western Australia. Econ Geol 76: 1698 - 1713

Donaldson MJ. 1983. Progressive alteration of barren and weakly mineralised Archaean dunites from Western Australia: a petrological, mineralogical and geochemical study of some komatiitic dunites from the Eastern Goldfields Province. PhD Thesis, University of Western Australia, Nedlands, WA, 345 pp

Donaldson MJ, Bromley GJ. 1981. The Honeymoon well nickel sulfide deposits, Western Australia. Econ Geol 76: 1550 - 1564

Donaldson MJ, Lesher CM, Groves DI, Gresham JJ. 1986. Comparison of Archaean dunites and komatiites associated with nickel mineralization in Western Australia: implications for dunite genesis. Mineral Deposita 21: 296 - 305

Dostal J, Mueller WU. 1997. Komatiite flooding of a rifted archean rhyolitic arc complex-geochemical signature and tectonic significance of the Stoughton-Roquemaure Group, Abitibi Greenstone Belt, Canada. J Geol 105: 545 - 563

Dowling SE, Barnes SJ, Hill RET, Hicks J. 2004. Komatiites and nickel sulfide ores of the Black Swan area, Yilgarn Craton, Western Australia. 2. Geology and genesis of the orebodies. Mineral Deposita 39: 707 - 728

Duke JM. 1979. Computer simulation of the fractionation of olivine and sulfide from mafic and ultramafic magmas. Can Mineral 76: 507 - 514

Duke JM. 1986. The Dumont nickel deposit: a genetic model for disseminated magmatic sulphide deposits of komatiitic affinity. In: Gallacher MJ, Ixer RA, Neary CR, Prichard HM (eds). Metallogeny of Basic and Ultrabasic Rocks. The Institute of Mining and Metallurgy, London, pp 151 - 160

Duke JM, Naldrett AJ. 1978. A numerical model of the fractionation of olivine and molten sulphide from komatiitic magma. Earth Planet Sci Letts 39: 255 - 266

Duuring P, Bleeker W, Beresford SW. 2007. Structural modification of the komatiite-associated Harmony nickel sulfide deposit, Leinster, Western Australia. Econ Geol 102: 277 - 297

Ebel DS, Naldrett AJ. 1996. Fractional crystallization of sulfide ore liquids at high temperature. Econ Geol 91: 607 - 621

Ebel DS, Naldrett AJ. 1997. Crystallization of sulfide liquids and the interpretation of ore composition. Can J Earth Sci 34: 352 - 365

Eckstrand OR. 1975. The Dumont serpentinite: a model for control of nickeliferous opaque assemblages by alteration products in ultramafic rocks. Econ Geol 70: 83 - 201

Eckstrand RO, Williamson BL. 1985. Vesicles in the Dundonald komatiites. Program and abstracts, Geological Association of Canada-Mineralogical Association of Canada annual meeting 10: A - 16

Evans DM, Cowden A, Barrett RM. 1989. Deformation and thermal erosion at the Foster nickel deposit, Kambalda St. Ives, Western Australia. In: M. D. Prendergast MD, Jones MJ (eds). Magmatic sulphides-the Zimbabwe Volume. Institute of Mining and Metallurgy, London, pp 215 - 219

Ewers WE, Graham J, Hudson DR, Rolls JM. 1976. Crystallisation of chromite from nickel-iron sulphide melts. Contrib Mineral Petrol 54: 61 - 64

Ferreira-Filho CF, Lesher CM. 2001. The komatiite-associated Ni-sulfide deposit of Boa Vista, Brazil. In: Cassidy KF, Dunphy JM, Van Kranendonk MJ (eds). 4th International Archean symposium Extended Abstracts, A GSO Record 2001/37, p. 429 - 431

Fiorentini ML, Bekker A, Rumble D, Barley ME, Beresford SW. 2006. Multiple S isotope study indicates footwall hydrothermal exhalative massive sulfides were the major sulfur source for Archean komatiite-hosted magmatic nickel-sulfides from Western Australia and Canada (abstract). Geochim Cosmochim Acta 70: A174

Fiorentini ML, Rosengren N, Beresford SW, Grguric B, Barley ME. 2007. Controls on the emplacement and genesis of the MKD5 and Sarah's Find Ni-Cu-PGE deposits, Mount Keith, Agnew-Wiluna Greenstone Belt, Western Australia. Mineral Deposita 126: 847 - 877

Fleet ME, Crocket JH, Liu MH, Stone WE. 1999a. Laboratory partitioning of platinum-group elements (PGE) and gold with application to magmatic sulfide-PGE deposits. Lithos 47: 127 - 142

Fleet ME, Liu MH, Crocket JH. 1999b. Partitioning of trace amounts of highly siderophile elements in the Fe-Ni-S system and their fractionation in nature. Geochim Cosmochim Acta 63: 2611 - 2622

Fornari DJ. 1986. Submarine lava tubes and channels. Bull Volc 48: 291 - 298

Foster JG, Lambert DD, Frick LR, Maas R. 1996. Re-Os isotopic evidence for genesis of Archaean nickel ores from uncontaminated komatiites. Nature 382: 703 - 705

Frost BR. 1985. On the stability of sulfides, oxides and native metals in serpentinite. J Petrol 26: 31 - 63

Frost KM, Groves DI. 1989a. Magmatic contacts between immiscible sulfide and komatiitic melts; implications for genesis of Kambalda sulfide ores. Econ Geol 84: 1697 - 1704

Frost KM, Groves DI. 1989b. Ocellar units at Kambalda: evidence for sediment assimilation by komatiite lavas. In: Prendergast MD, Jones MJ (eds). Magmatic sulphides-the Zimbabwe Volume. Institute of Mining and Metallurgy, London, pp 207 - 214

Frost KM, Woodhouse M, Pitkajarvi JT. 1998. Forrestania nickel deposits. In: Berkman DA, Mackenzie DH (eds). Australian Institute of Mining and Metallurgy, Melbourne, pp 365 - 370

Gillies SL. 1993. Physical volcanology of the Katinniq peridotite complex and associated Fe-Ni-Cu-(PGE) mineralization, Cape Smith Belt, Northern Quebec. Unpub. MSc Thesis, University of Alabama, Tuscaloosa

Giovenazzo D, Picard C, Guha J. 1989. Tectonic setting of Ni-Cu-PGE deposits in the central part of the Cape Smith Belt. Geoscience Canada 16: 134 - 136

Glotov AI, Polyakov GV, Hoa TT, Balykin PA, Akimtsev VA, Krivenko AP, Tolstykh ND, Phuong NT, Thanh HH, Hung TQ, Petrova TE. 2001. The Ban Phuc Ni-Cu-PGE deposit related to the phanerozoic komatiite-basalt association in the Song Da Rift, nortwestern Vietnam. Can Mineral 39: 573 - 589

Gole MJ, Andrews DL, Drew GJ, Woodhouse M. 1998. Honeymoon Well nickel deposits. In: Berkman DA, Mackenzie DH (eds). Geology of Australian and Papua New Guinean Mineral Deposits. Australian Institute of Mining and Metallurgy, Melbourne, pp 297 - 306

Gole MJ, Barnes SJ, Hill RET. 1987. The role of fluids in the metamorphism of komatiites, Agnew nickel deposit, Western Australia. Contrib Mineral Petrol 96: 151 - 162

Greeley R, Fagents SA, Harris RS, Kadel SD, Williams DA, Guest JE. 1998. Erosion by flowing lava-field evidence. J Geophys Res-Solid Earth 103: 27325 - 27345

Green AH, Melezhik VA. 1999. Geology of the Pechenga ore deposits; a review with comments on ore forming processes. Short Course Notes-Geological Association of Canada 13: 287 - 328

Green AH, Naldrett AJ. 1981. The Langmuir volcanic peridotite-associated nickel sulphide deposits: Canadian equivalents of the Western Australian occurrences. Econ Geol 76: 1503 - 1523

Gresham JJ. 1986. Depositional environments of volcanic peridotite-associated nickel deposits with special reference to the Kambalda dome. In: Friedrich GH (ed). Geology and metallogeny of copper deposits. Springer Verlag, Berlin, pp 63 - 90

Gresham JJ, Loftus-Hills GD. 1981. The geology of the Kambalda nickel field, Western Australia. Econ Geol 76: 1373 - 1416

Grguric BA. 2003. Minerals of the MKD5 nickel deposit, Mount Keith, Western Australia Aust J Mineral 9: 55 - 71

Grguric BA, Rosengren NM, Fletcher CM, Hronsky JMA. 2006. Type 2 deposits: geology, mineralogy and processing of the Mount Keith and Yakabindie orebodies, Western Australia. Soc Econ Geologists Spec Pub 13: 119 - 138

Groves DI, Barrett FM, Binns RA, McQueen KG. 1977. Spinel phases associated with metamorphosed volcanic-type iron-nickel sulfide ores from Western Australia. Econ Geol 72: 1224 - 1244

Groves DI, Barrett FM, McQueen KG. 1979. The relative roles of magmatic segregation, volcanic exhalation and regional metamorphism in the generation of volcanic-associated nickel ores of Western Australia. Can Mineral 17: 319 - 336

Groves DI, Batt WD. 1984. Spatial and temporal variations of Archaean metallogenic associations in terms of evolution of granitoid-greenstone terrains with particular emphasis on the Western Australian shield. In: Kroner A, Hanson GN, Goodwin AM (eds). Springer Verlag, Berlin, pp 73 - 98

Groves DI, Hudson DR. 1981. The nature and origin of Archean strata-bound volcanic-associated nickel-iron-copper sulfide deposits. In: Wolf KH (ed). Handbook of Strata-bound and Stratiform Ore Deposits. Elsevier, Amsterdam, pp 305 - 410

Groves DI, Hudson DR, Hack TBC. 1974. Modification of iron-nickel sulphides during serpentinisation and talc-carbonate alteration at Black Swan, Western Australia. Econ Geol 69: 1265 - 1281

Groves DI, Keays RR. 1979. Mobilization of ore forming elements during alteration of dunites, Mt. Keith-Betheno, Western Australia. Can Mineral 17: 373 - 389

Groves DI, Korkiakoski EA, McNaughton NJ, Lesher CM, Cowden A. 1986. Thermal erosion by komatiites at Kambalda, Western Australia and the genesis of nickel ores. Nature 319: 136 - 139

Hammerbeck ECI. 1984. Aspects of nickel metallogeny of Southern Africa. In: Buchanan DL, Jones MJ (eds). Sulphide deposits in mafic and ultramafic rocks: proceedings of the third nickel sulphide field conference, Perth, Western Australia. Institution of Mining and Metallurgy, London, pp 130 - 140

Hanski EJ. 1992. Petrology of the Pechenga ferropicrites and cogenetic Ni-bearing gabbro-wehrlite intrusions, Kola Peninsula, Russia. Geol Surv Finland Bull 367, p. 1 - 192

Heath C, Lahaye Y, Stone WE, Lambert DD. 2001. Origin of variations in nickel tenor along the strike of the Edwards lode nickel sulfide orebody, Kambalda, Western Australia. Can Mineral 39: 655 - 671

Helz RT. 1982. Determination of the P-T dependence of the first appearance of Fe-S liquid in natural basalts to 20 kb. EOS 58: 523

Hicks JD, Balfe GD. 1998. Silver Swan, Cygnet and Black Swan nickel deposits. In: Berkman DA, Mackenzie DH (eds). Geology of Australian and Papua New Guinean Mineral Deposits. Australasian Institute of Mining and Metallurgy, Melbourne, pp 339 - 346

Hill RET. 1984. Experimental study of phase relations at 600℃ in a portion of the Fe-Ni-Cu-S system and its application to natural sulphide assemblages. In: Buchanan DL, Jones MJ (eds). Sulphide deposits in mafic and ultramafic rocks. Institute of Mining and Metallurgy, London, pp 14 - 21

Hill RET. 2001. Komatiite volcanology, volcanological setting and primary geochemical properties of komatiite-associated nickel

deposits. Geochemistry: Exploration, Environment, Analysis 1: 365 - 381

Hill RET, Barnes SJ, Dowling SE, Thordarson T. 2004. Komatiites and nickel sulfide orebodies of the Black Swan area, Yilgarn Craton, Western Australia. 1. Petrology and volcanology of host rocks. Mineral Deposita 39: 684 - 706

Hill RET, Barnes SJ, Gole MJ, Dowling SE (eds). 1990. The physical volcanology of komatiites in the Norseman-Wiluna belt, Western Australia. Geological Society of Australia, Western Australian Division, Perth, p. 1 - 100

Hill RET, Barnes SJ, Gole MJ, Dowling SE. 1995. The volcanology of komatiites as deduced from field relationships in the Norseman-Wiluna greenstone belt, Western Australia. Lithos 34: 159 - 188

Hill RET, Gole MJ, Barnes SJ. 1989. Olivine adcumulates in the Norseman-Wiluna greenstone belt Western Australia: implications for the volcanology of komatiites. In: Prendergast MD, Jones MJ (eds). Magmatic sulphides-the Zimbabwe Volume. Institute of Mining and Metallurgy, London, pp 189 - 206

Hoatson DM, Jaireth S, Jaques AL. 2006. Nickel sulfide deposits in Australia: characteristics, resources and potential. Ore Geol Rev 29: 177 - 241

Hopf S, Head DL. 1998. Mount Keith nickel deposit. In: Berkman DA, Mackenzie DH (eds). Geology of Australian and Papua New Guinean Mineral Deposits. Australian Institute of Mining and Metallurgy, Melbourne, pp 307 - 314

Hopwood T. 1981. The significance of pyritic black shales in the genesis of Archaean nickel sulphide deposits. In: Wolf KH (ed). Handbook of Strata-Bound and Stratiform Ore Deposits. Elsevier, Amsterdam, pp 412-467

Houlé MG, Davis PC, Lesher CM, Arndt NT. 2002a. Extrusive and intrusive komatiites and komatitic basalts, peperites and ore genesis at the Dundonald Ni-Cu-(PGE) deposit, Abitibi Greenstone Belt, Canada. Proceedings, 9th International Platinum Symposium

Houlé MG, Gibson HL, Lesher CM, Davis PC, Cas RAF, Beresford SW, Arndt NT. 2008. Komatiitic Sills and Multigenerational Peperite at Dundonald Beach, Abitibi Greenstone Belt, Ontario: Volcanic Architecture and Nickel Sulfide Distribution. Econ Geol 103: 1269 - 1284

Houlé MG, Lesher CM, Gibson HL, Sproule RA. 2002b. Recent advances in komatiite volcanology in the Abitibi Greenstone Belt, Ontario. Summary of Fieldwork and Other Activities 2002, Ontaruio Geological Survey Open File Report 6100-7: 1 - 19

Houlé MG, Lesher CM, Gibson HL, Fowler AD, Sproule RA. 2001. Physical volcanology of komatiites in the Abitibi greenstone belt, Superior Province, Canada (Project Unit 99 - 021). Summary of Field work and other Aetivities, Ontario Geological Survey Open File Report 6070, p. 13 - 1—13 - 16

Hudson DR. 1972. Evaluation of genetic models for Australian nickel sulphide deposits. Austrlian Institute of Mining and Metallurgy Conference, Perth, papers: 99 - 109

Hudson DR, Donaldson MJ. 1984. Mineralogy of platinum group elements in the Kambalda nickel deposits, Western Australia. In: Buchanan DL, Jones MJ (eds). Sulphide Deposits in Mafic and Ultramafic rocks. Institute of Mining and Metallurgy, London, pp 55 - 61

Hulbert LJ, Grégoire DC. 1993. Re-Os systematics of the Rankin Inlet Ni ores: An example of the application of ICP-MS to the investigation of Ni-Cu-PGE mineralization and the potential use of Os-isotopes in mineral exploration. Canad Mineral 31: 861 - 876

Hulbert LJ, Hamilton MA, Horan MF, Scoates RFJ. 2005. U-Pb Zircon and Re-Os Isotope Geochronology of Mineralized Ultramafic Intrusions and Associated Nickel Ores From the Thompson Nickel Belt, Manitoba, Canada. Econ Geol 100: 29 - 41

Huppert HE, Sparks RSJ. 1985. Komatiites I: Eruption and Flow. J Petrol 26: 694 - 725

Huppert HE, Sparks RSJ, Turner JS, Arndt NT. 1984. Emplacement and cooling of komatiite lavas. Nature 309: 19 - 22

Jarvis RA. 1995. On the cross-sectional geometry of thermal erosion channels formed by turbulent lava flows. J Geophys Res 100: 10127 - 10140

Jolly WT. 1982. Progressive metamorphism of komatiites and related Archaean lavas of the Abitibi area, Canada. In: Arndt NT, Nisbet EG (eds). Komatiites. George Allen and Unwin, London, p. 247 - 265

Kauahikaua J, Cashman KV, Mattox TN, Heliker CC, Hon KA, Mangan MT, Thornber CR. 1998. Observations on basaltic lava streams in tubes from Kilauea volcano, Island of Hawaii. J Geophys Res-Solid Earth 103: 27303 - 27323

Keays RR. 1982. Palladium and iridium in komatiites and associated rocks: application to petrogenetic problems. In: Arndt NT, Nisbet EG (eds). Komatiites. George Allen and Unwin, London, p. 435 - 458

Keays RR. 1995. The role of komatiitic and picritic magmatism and S-saturation in the formation of ore deposits. Lithos 34: 1 - 18

Keays RR, Davidson RM. 1976. Palladium, iridium and gold in the ores and host rocks of nickel sulphide deposits in Western Australia. Econ Geol 71: 214 - 228

Keays RR, Ross JR, Woolrich P. 1981. Precious metals in volcanic peridotite-associated nickel sulfide deposits in Western Australia, Ⅱ. Distribution within ores and host rocks at Kambalda. Econ Geol 76: 1645 - 1674

Keele RA, Nickel EH. 1974. The geology of a primary millerite-bearing sulfide assemblage and supergene alteration at the Otter Shoot, Kambalda, Western Australia. Econ Geol 69: 1102 - 1117

Kerr A, Leitch AM. 2005. Self-destructive sulfide segregation systems and the formation of high-grade magmatic ore deposits. Econ Geol 100: 311 - 332

Kerr AC, Arndt NT. 2001. A note on the IUGS reclassification of the high-Mg and picritic volcanic rocks. J Petrol 42: 2169 - 2171

Kerr RC. 2001. Thermal erosion by laminar lava flows. J Geophys Res-Solid Earth 106: 26453 - 26465

Kilburn LC, Wilson HDB, Graham AR, Ogura Y, Coats CJA, Scoates RFJ. 1969. Nickel sulfide ores related to ultrabasic intrusions in Canada. In: Wilson HDB (ed). Magmatic ore De-

posits Monograph 4. Economic Geology Publishing Company, Lancaster, p. 267 - 293

Krapez B, Eisenlohr B. 1998. Tectonic Settings Of Archaean (3325 - 2775 Ma) Crustal-Supracrustal Belts In the West Pilbara Block. Precamb Res 88: 173 - 205

Lahaye Y, Barnes SJ, Frick LR, Lambert DD. 2001. Re-Os isotopic study of komatiitic volcanism and magmatic sulfide formation in the southern Abitibi greenstone belt, Ontario, Canada. Can Mineral 39: 473 - 490

Lambert DD, Foster JG, Frick LR, Ripley EM, Zientek ML. 1998. Geodynamics of magmatic Cu-Ni-PGE sulfide deposits-new insights from the Re-Os isotope system. Econ Geol 93: 121 - 136

Layton-Matthews D, Lesher CM, Burnham OM, Liwanag J, Halden NM, Hulbert L, Peck DC. 2007. Magmatic Ni-Cu-platinum-group element deposits of the Thompson mickel belt. In: Goodfellow WD (ed) Mineral Deposits of Canada: A Synthesis of Major Deposit-Types, District Metallogeny, the Evolution of Geological Provinces, and Exploration Methods. Geological Association of Canada Special Publication 5: 409 - 432

Le Bas MJ. 2000. IUGS reclassification of the high-Mg and picritic volcanic rocks. J Petrol 41: 1467 - 1470

Lesher CM. 1983. Localisation and genesis of komatiite-associated Fe-Ni-Cu sulfide mineralization of Kambalda, Western Australia (PhO thesis). University of Western Australia, Nedlands, Australia, p. 1 - 318

Lesher CM. 1989. Komatiite-associated nickel sulfide deposits. In: Whitney JA, Naldrett AJ (eds) Ore Deposition Associated with Magmas. Economic Geology Publishing Company, El Paso, pp 44 - 101

Lesher CM (ed). 1999. Komatiite peridotite-hosted Fe-Ni-Cu-(PGE) sulfide deposits in the Raglan area, Cape Smith Belt, new Quebec. In: Guidebook Series v. 2, Mineral Exploration Centre, Laurentian University, Sudbury, p. 184

Lesher CM. 2007. Deposits in the Raglan Area, Cape Smith Belt, New Québec. In: Goodfellow WD (ed). Mineral Deposits of Canada: A Synthesis of Major Deposit-Types, District Metallogeny, the Evolution of Geological Provinces, and Exploration Methods. Geological Associaton of Canada Special Publication 5: 351 - 386

Lesher CM, Arndt NT. 1995. REE and Nd isotope geochemistry, petrogenesis and volcanic evolution of contaminated komatiites at Kambalda, Western Australia. Lithos 34: 127 - 157

Lesher CM, Arndt NT, Groves DI. 1984. Genesis of komatiite-associated nickel sulphide deposits at Kambalda, Western Australia: a distal volcanic model. In: Buchanan DL, Jones MJ (eds). Sulphide deposits in mafic and ultramafic rocks. Institute of Mining and Metallurgy, London, pp 70 - 80

Lesher CM, Barnes SJ. 2008. Komatiite-associated Ni-Cu-PGE deposits. In: Arndt NT, Lesher CM, Barnes SJ (eds). Komatiite. Cambridge University Press, Cambridge, pp 295 - 327

Lesher CM, Burnham OM, Keays RR, Barnes SJ, Hulbert L. 2001. Trace-element geochemistry and petrogenesis of barren and ore-associated komatiites. Can Mineral 39: 673 - 696

Lesher CM, Campbell IH. 1993. Geochemical and fluid dynamic modelling of compositional variations in Archean komatiite-hosted nickel sulfide ores in Western Australia. Econ Geol 88: 804 - 816

Lesher CM, Groves DI. 1986. Controls on the formation of komatiite-associated nickel-copper sulfide deposits. In: Friedrich GH (ed). Geology and Metallogeny of Copper Deposits. Springer Verlag, Berlin, pp 63 - 90

Lesher CM, Keays RR. 2002. Komatiite-associated Ni-Cu-PGE deposits: geology, mineralogy, geochemistry and genesis. In: Cabri LJ (ed). The Geology, Geochemistry Mineralogy and Mineral Beneficiation of Platinum Group Elements. Canadian Institute of Mining Metallurgy and Petroleum Special Volume 54, pp 579 - 617

Lesher CM, Stone WE. 1996. Exploration geochemistry of komatiites. In: Wyman DA (ed) Igneous trace element geochemistry applications for massive sulphide exploration. Geological Association of Canada, pp 153 - 204

Li C, Ripley EM. 2005. Empirical equations to predict the sulfur content of mafic magmas at sulfide saturation and applications to magmatic sulfide deposits. Mineral Deposita 40: 218 - 230

Li C, Barnes S-J, Makovicky E. 1996. Partitioning of Ni, Cu, Ir, Rh, Pt and Pd between monosulfide solid solution and sulfide liquid: Effects of temperature and composition. Geochim Cosmochim Acta 60: 1231 - 1238

Libby JW, Stockman PR, Cervoj KM, Muir MRK, Whittle M, Langworthy PJ. 1998. Perseverance Nickel Deposit. In: Berkman DA, Mackenzie DH (eds). Geology of Australian and Papua New Guinean Mineral Deposits. Australian Institute of Mining and Metallurgy, Carlton, pp 321 - 328

Lorand J-P, Alard O, Godard M. 2008a. Platinum-group element signature of the primitive mantle rejuvenated by melt-rock reactions: evidence from Sumailperidotites (Oman Ophiolite). Terra Nova 21: 35 - 40

Lorand J-P, Luguet A, Alard O, Bezos A, Meisel T. 2008b. Abundance and distribution of platinum-group elements in orogenic lherzolites: a case study in A Fontete Rouge Lherzolite (French Pyrenees). Chem Geol 248: 174 - 194

Lusk J. 1976. A possible volcanic-exhalative origin for lenticular nickel sulfide deposits of volcanic association with special reference to those in Western Australia. Can J Earth Sci 13: 451 - 458

Maiden KJ, Chimimba LR, Smalley TJ. 1986. Cuspate ore-wall rock interfaces, piercement structures, and the localization of some sulfide ores in deformed sulfide deposits. Econ Geol 81: 1464 - 1472

Maier WD, Li CS, Dewaal SA. 2001. Why are there no major Ni-Cu sulfide deposits in large layered mafic-ultramafic intrusions? Can Mineral 39: 547 - 556

Malyuk BI. 1985. The origin of komatiite magmas: petrochemical test of models: Geokhimiya No. 6, p. 785 - 795

Marston RJ. 1984. Nickel mineralization in Western Australia. Geol Surv Western Austral Mineral Resources Bull 14: 271

Marston RJ, Groves DI, Hudson DR, Ross JR. 1981. Nickel sulfide deposits in Western Australia: a review. Econ Geol 76: 1330 - 1363

Marston RJ, Kay BD. 1980. The distribution, petrology and genesis of nickel ores at the Juan complex, Kambalda, Western Australia. Econ Geol 75: 546 - 565

Mathez EA. 1976. Sulfur solubility and magmatic sulfides in submarine basalt glass. J Geophys Res 81: 4269 - 4276

Mavrogenes JA, O'Neill HSC. 1999. The relative effects of pressure, temperature and oxygen fugacity on the solubility of sulfide in mafic magmas. Geochim Cosmochim Acta 63: 1173 - 1180

McDonough WF, Sun S-S. 1995. The composition of the Earth. Chem Geol 120: 223 - 253

McNaughton NJ, Frost KM, Groves DI. 1988. Ground melting and ocellar komatiites: a lead isotopic study at Kambalda, Western Australia. Geol Mag 125: 285 - 295

McQueen KG. 1979. Experimental heating and diffusion effects in Fe-Ni sulphide ore from Redross, Western Australia. Econ Geol 74: 140 - 148

McQueen KG. 1981a. The nature and metamorphic history of the Wannaway nickel deposit, Western Australia. Econ Geol 76: 1444 - 1468

McQueen KG. 1981b. Volcanic-associated nickel deposits from around the Widgiemooltha Dome, Western Australia. Econ Geol 76: 1417 - 1443

McQueen KG. 1987. Deformation and remobilization in some Western Australian nickel ores. Ore Geol Rev 2: 269 - 286

Melezhik VA, Hudson-Edwards KA, Green AH, Grinenko LN. 1994. Pechenga area, Russia; Part 2, Nickel-copper deposits and related rocks. Trans Inst Mining Metall Section B App Earth Sci 103, August: B146 - B161

Menard T, Lesher CM, Stowell HH, Price DP, Pickell JR, Onstott TC, Hulbert L. 1996. Geology, genesis, and metamorphic history of the Namew Lake Ni-Cu deposit, Manitoba. Econ Geol 91: 1394 - 1413

Muir JE, Comba CDA. 1979. The Dundonald deposit: an example of volcanic-type nickel sulfide ore in ultramafic lavas. Can Mineral 17: 351 - 360

Mungall JE. 2007. Crustal contamination of picritic magmas during transport through dikes: the Expo intrusive suite, Cape Smith fold belt, New Quebec. J Petrol 48: 1021 - 1039

Mungall JE, Su S. 2005. Interfacial tension between magmatic sulfide and silicate liquids: constraints on the kinetics of sulfide liquation and sulfide migration through silicate rocks. Earth Planet Sci Letts 234: 135 - 149

Murck BW, Campbell IH. 1986. The effects of temperature, oxygen fugacity and melt composition on the behaviour of chromium in basic and ultrabasic melts. Geochim Cosmochim Acta 50: 1871 - 1888

Naldrett AJ. 1966. The role of sulphurization in the genesis of iron-nickel sulphide deposits of the Porcupine district, Ontario. Can Inst Mining Metall Trans 69: 147 - 155

Naldrett AJ. 1973. Nickel sulphide deposits: their classification and genesis, with special emphasis on deposits of volcanic association. Can Inst Mining Metall Bull 66: 45 - 63

Naldrett AJ. 1989. Ores associated with flood basalts. In: Whitney JA, Naldrett AJ (eds). Society of Economic Geologists, El Paso, pp 103 - 134

Naldrett AJ. 2004. Magmatic Sulfide Deposits: Geology, Geochemistry and Exploration. Springer, Heidelberg. 464 pp

Naldrett AJ, Cabri LJ. 1976. Ultramafic and related rocks: their classification and genesis with special reference to the concentration of nickel sulfides and platinum group elements. Econ Geol 71: 1131 - 1158

Naldrett AJ, Gasparrini EL. 1971. Archaean nickel sulphide deposits in Canada; their classification, geological setting and genesis with some suggestions as to exploration. Geol Soc Austral Spec Pub 3: 201 - 225

Naldrett AJ, Hoffman EL, Green AH, Chou C-L, Naldrett SR, Alcock RA. 1979. The composition of Ni-sulfide ores, with particular reference to their content of PGE and Au. Can Mineral 17: 403 - 416

Naldrett AJ, Turner AR. 1977. The geology and petrogenesis of a greenstone belt and related nickel sulfide mineralisation at Yakabindie, Western Australia. Precamb Res 3: 43 - 103

Nisbet EG. 1982. The tectonic setting and petrogenesis of komatiites. In: Arndt NT, Nisbet EG (eds). Komatiites. George Allen and Unwin, London, p. 501 - 520

Nisbet EG, Chinner GA. 1981. Controls on the eruption of mafic and ultramfic lava, Ruth Well Ni-Cu prospect, West Pilbara. Econ Geol 76: 1719 - 1735

O'Neill HSC, Dingwell D, Borisov A, Spettel B, Palme H. 1995. Experimental petrochemistry of some highly siderophile elements at high temperatures, and some implications for core formatation and the mantle's early history. Chem Geol 120: 255 - 273

Ohmoto H. 1986. Stable isotope geochemistry of ore deposits. In: Valley JW, Taylor HPJ, O'Neil JR (eds). Stable Isotopes in High Temperature Geological Processes. Mineralogical Society of America, Washington DC, pp 491 - 559

Osmond R, Watts T. 1999. 3D geophysical model of the Raglan belt. In: Lesher CM (ed). Komatiitic Peridotite-Hosted Fe-Ni-Cu-(PGE) Sulphide Deposits in the Raglan Area, Cape Smith Belt, New Québec. Mineral Exploration Research Centre, Laurentian University, pp 185 - 190

Page ML, Schmulian ML. 1981. The proximal volcanic environment of the Scotia nickel deposits. Econ Geol 76: 1469 - 1479

Paterson HL, Donaldson MJ, Smith RN, Lenard MF, Gresham JJ, Boyack DJ, Keays RR. 1984. Nickeliferous sediments and sediment-associated nickel ores at Kambalda, Western Australia. In: Buchanan DL, Jones MJ (eds). Sulphide deposits in mafic and ultramafic rocks. Institution of Mining and Metallurgy, London, pp 81 - 94

Peach CL, Mathez EA. 1993. Sulfide melt-silicate melt partition coefficients for nickel and iron and implications for partitioning of other chalcophile elements. Geochim Cosmochim Acta 57: 3013 - 3021

Peach CL, Mathez EA, Keays RR. 1990. Sulfide melt-silicate melt distribution coefficients for the noble metals as deduced from MORB: implications for partial melting. Geochim Cosmochim Acta 54: 3379 - 3389

Peck DC, Scoates RFJ, Theyer P, Desharnais G, Hulbert LJ,

Huminicki MAE. 2002. Stratiform and contact-type PGE-Cu-Ni mineralization in the Fox River Sill and the Bird River belt, Manitoba. In: Cabri LJ (ed). The Geology, Geochemistry, Mineralogy and Mineral Beneficiation of Platinum-Group Elements. Canadian Institute of Mining, Metallurgy and Petroleum, Ottawa, pp 367 - 387

Peredery WV. 1979. Relationship of ultramafic amphibolites to metavolcanic rocks and serpentinites in the Thompson belt, Manitoba. Can Mineral 17: 187 - 200

Peredery WV, staff G. 1982. Geology and nickel sulfide deposits of the Thompson belt, Manitoba. In: Hutchinson RW, Spence CD, Franklin JM (eds). Precambrian sulfide deposits, Special Paper 25. Geological Association of Canada, Waterloo, p. 165 - 210

Perring CS, Barnes SJ, Hill RET. 1995. The physical volcanology of komatiite sequences from Forrestania, Southern Cross Province, Western Australia. Lithos 34: 189 - 207

Perring CS, Barnes SJ, Hill RET. 1996. Geochemistry of Archaean komatiites from the Forrestania Greenstone Belt, Western Australia: evidence for supracrustal contamination. Lithos 37: 181 - 197

Peters WS. 2006. Geophysical exploration for nickel sulfide deposits in the Yilgarn Craton. Soc Econ Geologists Spec Pub 13: 167 - 193

Philpotts AR. 1961. Textures of the Ungava nickel ores. Can Mineral 6: 681 - 688

Porter DJ, McKay KG. 1981. The nickel sulphide mineralization and metamorphic setting of the Forrestania area, Western Australia. Econ Geol 76: 1524 - 1549

Prendergast MD. 2001. Komatiite-hosted Hunters Road nickel deposit, central Zimbabwe: physical volcanology and sulfide genesis. Aust J Earth Sci 48: 681 - 694

Prendergast MD. 2003. The nickeliferous Late Archean Reliance komatiitic event in the Zimbabwe craton-magmatic architecture, physical volcanology, and ore genesis. Econ Geol 98: 865 - 891

Prichard HM, Hutchinson D, Fisher PC. 2004. Petrology and crystallization history of multiphase sulfide droplets in a mafic dike from Uruguay: Implications for the origin of Cu-Ni-PGE sulfide deposits. Econ Geol 99: 365 - 376

Prider RT. 1970. Nickel in Western Australia. Nature 226: 691 - 693

Pridmore DF, Coggon JH, Esdale DJ, Lindeman FW. 1984. Geophysical exploration for nickel sulphide deposits in the Yilgarn block, Western Australia. In: Buchanan DL, Jones MJ (eds). Sulphide deposits in mafic and ultramafic rocks. Institution of Mining and Metallurgy, London, pp 22 - 34

Puchtel IS, Humayun M, Campbell AJ, Sproule RA, Lesher CM. 2004. Platinum group element geochemistry of komatiites from the Alexo and Pyke Hill areas, Ontario, Canada. Geochim Cosmochim Acta 68: 1361 - 1383

Rice A, Moore JM. 2001. Physical modeling of the formation of komatiite-hosted nickel deposits and a review of the thermal erosion paradigm. Can Mineral 39: 491 - 503

Robinson DJ, Huthchinson RW. 1982. Evidence for a volcanogenic-exhalative origin of a massive nickel sulphide deposit at Redstone, Timmins, Ontario. In: Hutchinson RW, Spence CD, Franklin JM (eds). Precambrian Sulfide Deposits GAC Special paper 25. Geological Association of Canada, Waterloo, pp 211 - 254

Rose LA, Brenan JM. 2001. Wetting properties of Fe-Ni-Co-Cu-O-S melts against olivine: implications for sulfide melt mobility. Econ Geol 96: 145 - 157

Rosengren NM, Beresford SW, Grguric BA, Cas RAF. 2005. An intrusive origin for the komatiitic-dunite hosted Mount Keith disseminated nickel sulphide deposit, Western Australia. Econ Geol 100: 149 - 156

Rosengren NM, Grguric BA, Beresford SW, Fiorentini ML, Cas RAF. 2007. Internal stratigraphic architecture of the komatiitic dunite-hosted MKD5 disseminated nickel sulphide deposit, Mount Keith Domain, Agnew-Wiluna Greenstone Belt, Western Australia. Mineral Deposita 126: 821 - 845

Ross JR, Hopkins GMF. 1975. Kambalda nickel sulfide deposits. In: Knight CL (ed). Economic Geology of Australia and Papua New Guinea. I. Metals. Austr Inst Min Metallur Monograph 5, pp 100 - 121

Ross JR, Keays RR. 1979. Precious metals in volcanic-type nickel sulphide deposits in Western Australia I. Relationship with the composition of the ores and their host rocks. Can Mineral 17: 417 - 435

Ross JR, Travis GA. 1981. The nickel sulfide deposits of Western Australia in global perspective. Econ Geol 76: 1291 - 1329

Sanders TS. 1982. Nepean nickel deposits. In: Groves DI, Lesher CM (eds). Regional Geology and Nickel Deposits of the Norseman-Wiluna Greenstone Belt, Western Australia. . University of Western Australia Department of Geology and Extension Service, Nedlands, pp 35 - 44

Schmulian ML. 1984. Windarra nickel deposits. In: Buchanan DL, Jones MJ (eds). Sulfide deposits in mafic and ultramafic rocks. Institution of Mining and Metallurgy, London, pp 95 - 102

Seabrook CL, Prichard HM, Fisher PC. 2004. Platinum-group minerals in the Raglan Ni-Cu-(PGE) sulfide deposit, Cape Smith, Quebec, Canada. Can Mineral 42: 485 - 497

Seat Z, Stone WE, Mapleson DB, Daddow BC. 2004. Tenor variation within komatiite-associated nickel sulphide deposits: insights from the Wannaway deposit, Widgiemooltha dome, Western Australia. Mineral Petrol 82: 317 - 339

Seccombe PK, Groves DI, Marston RJ, Barrett FM. 1981. Sulfide paragenesis and sulfur mobility in Fe-Cu-Ni sulfide ores at Lunnon and Juan Main Shoots, Kambalda: textural and sulfur isotopic evidence. Econ Geol 76: 1675 - 1685

Shima H, Naldrett AJ. 1975. Solubility of sulfur in an ultramafic melt and the relevance of the system Fe-S-O. Econ Geol 70: 960 - 967

Smith BH. 1984. Geochemical exploration for nickel sulphides in lateritic terrain in Western Australia. In: Buchanan DL, Jones MJ (eds). Sulphide deposits in mafic and ultramafic rocks. Institution of Mining and Metallurgy, London, pp 35 - 42

Soule SA, Fornari DJ, Perfit MR, Tivey MA, Ridley WI, Schouten H. 2005. Channelized lava flows at the East Pacific Rise crest 9 - 10 degrees N: The importance of off-axis lava

transport in developing the architecture of young oceanic crust. Geochemistry, Geophysics, Geosystems, doi: 101029/2008GC001954 6: Q08005

Sproule RA, Lesher CM, Ayer JA, Thurston PC, Herzberg CT. 2002. Spatial and temporal variations in the geochemistry of komatiites and komatiitic basalts in the Abitibi greenstone belt. Precam Res 115: 153 - 186

Sproule RA, Lesher CM, Houle M, Keays RR, Thurston PC, Ayer JA. 2005. Chalcophile element geochemistry and metallogenesis of komatiitic rocks in the Abitibi Greenstone Belt, Canada. Econ Geol 100: 1169 - 1190

Squire RJ, Cas RAF, Clout JMF, Behets R. 1998. Volcanology Of the Archaean Lunnon Basalt and Its Relevance to Nickel Sulfide-Bearing Trough Structures At Kambalda, Western Australia. Aust J Earth Sci 45: 695 - 715

St-Onge MR, Lucas SB. 1993. Controls on the regional distribution of iron-nickel-copper-platinum-group element mineralization in the eastern Cape Smith Belt, Québec. Can J Earth Sci 31: 206 - 218

Stolz GW, Nesbitt RW. 1981. The komatiite nickel sulfide association at Scotia: a petrochemical investigation of the ore environment. Econ Geol 76: 1480 - 1502

Stone MS, Stone WE. 2000. A crustally contaminated komatiitic dyke-sill-lava complex, Abitibi greenstone belt, Ontario. Precam Res 102: 21 - 46

Stone WE, Archibald NJ. 2004. Structural controls on nickel sulphide ore shoots in Archaean komatiite, Kambalda, WA: the volcanic trough controversy revisited. J Structural Geol 26: 1173 - 1194

Stone WE, Beresford SW, Archibald NJ. 2005. Structural Setting and Shape Analysis of Nickel Sulfide Shoots at the Kambalda Dome, Western Australia: Implications for Deformation and Remobilization. Econ Geol 100: 1441 - 1455

Stone WE, Crocket JH, Fleet ME. 1993. Sulfide-poor platinum-group mineralization in komatiitic system: Boston Creek Flow, layer basaltic komatiite, Abitibi belt, Ontario. Econ Geol 99: 817 - 836

Stone WE, Crocket JH, Fleet ME. 1993. Sulfide-poor platinum-group mineralization in komatiitic systems: Boston Creek flow, layered basaltic komatiite, Abitibi belt, Ontario. Econ Geol 88: 817 - 836

Stone WE, Crocket JH, Fleet ME. 1996. Platinum-group mineral occurrence associated with flow top amygdule sulfides in komatiitic basalt, Abitibi Greenstone Belt, Ontario. Mineral Petrol 56: 1 - 24

Stone WE, Deloule E, Larson MS, Lesher CM. 1997. Evidence for hydrous high MgO melts in the Archaean. Geology 25: 143 - 146

Stone WE, Deloule E, Stone MS. 2003. Hydromagmatic amphibole in komatiitic, tholeiitic and ferropicritic units, Abitibi greenstone belt, Ontario and Quebec: evidence for Archaean wet basic and ultrabasic melts. Mineral Petrol 77: 39 - 65

Stone WE, Heydari M, Seat Z. 2004. Nickel tenor variations between Archaean komatiite-associated nickel sulphide deposits, Kambalda ore field, Western Australia: the metamorphic modification model revisited. Mineral Petrol 82: 295 - 316

Stone WE, Jensen LS, Church WR. 1987. Petrography and geochemistry of an unusual Fe-rich basaltic komatiite from Boston Township, northeastern Ontario. Can J Earth Sci 24: 2537 - 2550

Stone WE, Masterman EE. 1998. Kambalda nickel deposits. In: Berkman DA, Mackenzie DH (eds). Economic geology of Australia and Papua New Guinea. Australian Institute of Mining and Metallargy, Melbourne, p. 347 - 356

Swager CP. 1997. Tectono-stratigraphy of late Archaean greenstone terranes in the southern eastern Goldfields, Western Australia. Precamb Res 83: 11 - 42

Swager CP, Goleby BR, Drummond BJ, Rattenbury MS, Williams PR. 1997. Crustal structure of granite-greenstone terranes in the eastern Goldfields, Yilgarn Craton, as revealed by seismic reflection profiling. Precamb Res 83: 43 - 56

Swager CP, Witt WK, Griffin TJ, Ahmat AL, Hunter WM, McGoldrick PJ, Wyche S. 1992. Late Archaean granite-greenstones of the Kalgoorlie Terrane, Yilgarn Craton, Western Australia. In: Glover JE, Ho SE (eds). Geology Dept. (Key Centre) and University Extension, University of Western Australia, Nedlands, pp 107 - 122

Taranovic V, Lesher CM, Houle MG, Bedard JH. 2008. Physical volcanology and metallogenesis of komatiite-associated Ni-Cu-(PGE) mineralization in the C-Zone, Bannockburn Township, Ontario Society of Economic Geologists and Geological Society of South Africa Joint Meeting. Johannesburg, South Africa

Thibert F, Picard C, Trzcienski W. 1989. Pétrologie des filons-couches différenciées Roméo 1 et 2 dans la partie centrale de la bande du Cap Smith. Geoscience Canada 16: 140 - 144

Tonnelier N, Lesher CM, Arndt NT. 2009. Petrology and geochemistry of the Jinuchan intrusion and asssociated Ni-Cu-(PGE) mineralization, Xi'an Ni-Cu Symposium, Xi'an, China. In: Xi'an Ni-Cu Symposium. Xi'an (China)

Travis GA, Keays RR, Davison RM. 1976. Palladium and iridium in the evaluation of nickel gossans in Western Australia. Econ Geol 71: 1229 - 1243

Trofimovs J, Tait MA, Cas RAF, McArthur A, Beresford SW. 2003. Can the role of thermal erosion in strongly deformed komatiite-Ni-Cu-(PGE) deposits be determined? Perseverance, Agnew-Wiluna Belt, Western Australia. Aust J Earth Sci 50: 199 - 214

Viljoen MJ, Bernasconi A. 1979. The geochemistry, regional setting and genesis of the Shangani-Damba nickel deposits, Rhodesia. In: Anhaeusser AR, Foster RP, Stratten T (eds). A Symposium on Mineral Deposits and the Transportation and Deposition of Metals, Special Publication 2. Geological Society of South Africa, pp 67 - 98

Viljoen MJ, Bernasconi A, Van Coller N, Kinloch E, Viloen RP. 1976. The geology of the Shangani nickel deposit, Rhodesia. Econ Geol 71: 76 - 95

Wendlandt RF. 1982. Sulfide saturation of basalt and andesite melts at high pressure. Amer Mineral 67: 877 - 885

Williams DA, Kerr RC, Lesher CM. 1998. Emplacement and erosion by Archean komatiite lava flows at Kambalda: revisi-

ted. J Geophys Res-Solid Earth 103：27533－27549

Williams DA，Kerr RC，Lesher CM. 1999. Thermal erosion modeling of lava channels in the Raglan block. In：Lesher CM（ed）. Komatiitic Peridotite-Hosted Fe-Ni-Cu-(PGE) Sulphide Deposits in the Raglan Area，Cape Smith Belt，New Québec. Mineral Exploration Research Centre，Laurentian University，Sudbury，pp 174－176

Williams DA，Kerr RC，Lesher CM，Barnes SJ. 2001. Analytical/numerical modeling of komatiite lava emplacement and thermal erosion at Perseverance，Western Australia. Journal of Volcanology and Geothermal Research 110：27－55

Williams DAC. 1979. The association of some nickel sulfide deposits with komatiitic volcanism in Rhodesia. Can Mineral 17：337－349

Wood SA，Mountain BW. 1991. Hydrothermal solubility of palladium in chloride solutions from 300℃ to 700℃：preliminary experimental results-a discussion. Econ Geol 86：1562－1563

Woodall R，Travis GA. 1970. The Kambalda Nickel deposits. Ninth Commonwealth Mining and Metallurgy Congress，1969，London 2：517－533

Woolrich P，Cowden A，Giorgetta NE. 1981. The chemical and mineralogical variations in the nickel mineralization associated with the Kambalda Dome. Econ Geol 76：1629－1644

Xinh L-T，Chu N-V. 1984. Ni-Cu sulphide deposits in Vietnam. In：Buchanan DL，Jones MJ（eds）. Sulphide Deposits in Mafic and Ultramafic Rocks. Institution of Mining and Metallurgy，London，pp 132－134

Zhou M-F，Yang Z-X，Song X-Y，Keays RR，Lesher CM. 2002. Magmatic Ni-Cu-(PGE) sulphide deposits in China. In：Cabri LJ（ed）. The Geology，Geochemistry，Mineralogy and Mineral Beneficiation of Platinum-Group Elements. Canadian Institute of Mining，Metallurgy and Petroleum，Ottawa，pp 619－636

Zwanzig HV，Macek JJ，McGregor CR. 2007. Lithostratigraphy and geochemistry of the high-grade metasedimentary rocks in the Thompson nickel belt and adjacent Kisseynew Domain，Manitoba；implications for nickel exploration. Econ Geol 102：1197－1216.